FLOW PATTERNS
ON SIEVE TRAYS

VOLUME II

A THESIS SUBMITTED

BY

SIMON CHAMBERS B.Sc Dip.Ind.

A candidate for the degree of

Doctor of Philosophy

DEPARTMENT OF CHEMICAL ENGINEERING
AND
APPLIED CHEMISTRY

UNIVERSITY OF ASTON IN BIRMINGHAM

MAY 1993

CERTIFICATE

TABLE OF CONTENTS

APPENDIX 1

Source Code For Plotting Temperature Profiles and The Coordinates of The RTDs on The Tray

Listed below is the Fortran 77 computer program, (codenamed 2D3DTEMP.FOR), written to generate the temperature contours and surfaces. The coding calls on routines from the UNIRAS suite of plotting routines.

```
      PROGRAM TEMPERATURE
C++++++++++++++++++++++++++++++++++++++++++++++++++++++++++++++++++++++
C
C     NOTE : THIS IS THE UNIVERSAL VERSION WITH PRT POSITION GIVEN
C            IN A SEPARATE DATA FILE. (01/03/1991)
C            REQUIRES: i) PRTCOORD.DAT
C                      ii)FOR014.DAT(DATA OUTPUT FILE FROM COLTEMP)
C
C++++++++++++++++++++++++++++++++++++++++++++++++++++++++++++++++++++++
C
C     2D PLOT
C
      INTEGER  I,J,K,NUM,LENY(6),LENX(7),IPLANE(3),LENGTH(6)
      REAL  AIRV,WEIRL,DEW,DIA,WEIR,HOW,GAP,FREE,TDOWN,HOLED
      REAL  TEMPIN(5),TEMP(108),AIR(4),X(108),Y(108)
      REAL  XPOS(108),YPOS(108),TPOS(108),TR(108),ZCL(39)
      REAL  ZEST(24,20),XEDGE(44),YEDGE(44)
      CHARACTER*2  ALPHA
      CHARACTER*4  LABY(6),LABX(7)
      CHARACTER*21  TEXT(6)
C
      PARAMETER(JMEMFX=10000,JMEMSZ=JMEMFX+400)
      COMMON /UNIMEM/ IDUM1,MEMMAX,IDUM2,ITEM(JMEMSZ)
      MEMMAX=JMEMFX
C
      DATA  ZCL / 0.025,0.050,0.075,0.100,0.125,0.150,0.175
     $,0.200,0.225,0.250,0.275,0.300,0.325,0.350,0.375,0.400
     $,0.425,0.450,0.475,0.500,0.525,0.550,0.575,0.600,0.625
     $,0.650,0.675,0.700,0.725,0.750,0.775,0.800,0.825,0.850
     $,0.875,0.900,0.925,0.950,0.975 /
      DATA  LENY /6*-1/
      DATA  LENX /7*-1/
      DATA  LABY /'2000','1600','1200','800','400','0'/
      DATA  LABX /' ','800','400',' 0','-400','-800',' '/
      DATA  IPLANE /1,1,1/,LENGTH /0,16,0,21,0,16/
      DATA  TEXT /' ','WEIR LENGTH - mm',' '
     #,'FLOW PATH LENGTH - mm',' ','REDUCED TEMP - '/
C
C*********************************************************
C     COLUMN WALL DATA
C*********************************************************
C
      RAD = 1200
      HS = 1925/20

      DO 1000 I=1,11
            YEDGE(I)=(1-I)*HS
            YEDGE(23-I)=YEDGE(I)
1000  CONTINUE
      DO 1100 I=1,10
```

```
            YEDGE(22+I)=I*HS
            YEDGE(43-I)=YEDGE(22+I)
1100  CONTINUE
            YEDGE(43)=YEDGE(1)
            YEDGE(44)=999.999
C
      DO 1200 I=1,11
            XEDGE(I)=-SQRT(RAD**2-YEDGE(I)**2)
            XEDGE(23-I)=-XEDGE(I)
1200  CONTINUE
      DO 1300 I=1,11
            XEDGE(I+22)=SQRT(RAD**2-YEDGE(I+22)**2)
            XEDGE(43-I)=-XEDGE(I+22)
1300  CONTINUE
            XEDGE(43)=YEDGE(1)
            XEDGE(44)=999.999
C
C*************************************************************
C     PRT POSITIONS ON TRAY AND INLET DOWNCOMER
C*************************************************************
      OPEN (UNIT=15,FILE='PRTCOORD.DAT',STATUS='OLD')
        DO 42 I=1,108
            READ (15,*) X(I),Y(I)
    42 CONTINUE
        CLOSE (UNIT=15)
C
C*************************************************************
C     READING IN TEMPERATURE DATA
C*************************************************************
C
      OPEN (UNIT=14,FILE='FOR014.DAT',STATUS='OLD')
      READ (14,300) AIRV
      READ (14,301) WEIRL
      READ (14,301) DEW
      READ (14,302) ALPHA
      READ (14,300) DIA
      READ (14,300) WEIR
      READ (14,301) FREE
      READ (14,300) HOW
      READ (14,300) GAP
      READ (14,300) HOLED
      READ (14,302) ALPHA
      READ (14,302) ALPHA
      READ (14,303) (TEMPIN(I),I=1,5)
      READ (14,304) (TEMP(I),I=1,8)
      READ (14,305) (TEMP(I),I=9,18)
      READ (14,306) (TEMP(I),I=19,30)
      READ (14,306) (TEMP(I),I=31,42)
      READ (14,306) (TEMP(I),I=43,54)
      READ (14,306) (TEMP(I),I=55,66)
      READ (14,306) (TEMP(I),I=67,78)
      READ (14,306) (TEMP(I),I=79,90)
      READ (14,305) (TEMP(I),I=91,100)
      READ (14,304) (TEMP(I),I=101,108)
      READ (14,307) TDOWN
      READ (14,308) (AIR(I),I=1,4)
      CLOSE (UNIT=14)
  300 FORMAT (27X,F5.3)
  301 FORMAT (27X,F4.1)
  302 FORMAT (4X,A2)
  303 FORMAT (43X,5(F6.2,4X))
  304 FORMAT (28X,8(F6.2,4X))
  305 FORMAT (18X,10(F6.2,4X))
```

```
  306 FORMAT (8X,12(F6.2,4X))
  307 FORMAT (63X,F6.2)
  308 FORMAT (19X,4(F6.2,4X))
C
C*************************************************************
C     SETTING UP IRREGULAR ARRAYS
C*************************************************************
C
      NUM=0
      DO 12 I=1,108
         IF (TEMP(I).NE.99.99) THEN
            NUM=NUM+1
            XPOS(NUM)=X(I)
            YPOS(NUM)=Y(I)
            TPOS(NUM)=TEMP(I)
         END IF
  12  CONTINUE
C
C*************************************************************
C     AVERAGING INLET WATER TEMPERATURE
C*************************************************************
C
      WINT=DEW
      DO 13 I=1,5
         IF (TEMPIN(I).NE.99.99) THEN
            IF (TEMPIN(I).GT.WINT) THEN
               WINT=TEMPIN(I)
            END IF
         END IF
  13  CONTINUE
C
C*************************************************************
C     WET BULB TEMPERATURE
C*************************************************************
C
      TWB=DEW
C
C*************************************************************
C     SETTING UP REDUCED TEMPERATURES
C*************************************************************
C
      DO 14 I=1,NUM
         TR(I)=(TPOS(I)-TWB)/(WINT-TWB)
  14  CONTINUE
C
C*************************************************************
C     ROUTINES TO COMMENCE PLOTTING
C*************************************************************
C
      CALL GROUTE ('S HPOSTA4;E')
      CALL GOPEN
      CALL RORIEN (2)
      CALL GLIMIT (-1200.0,1200.0,-1000.0,1000.0,0.0,1.0)
      CALL RUNDEF (999.999,9999)
      CALL GFAULT (XEDGE,YEDGE,44,0)
      CALL GINTPF (XPOS,YPOS,TR,NUM,ZEST,24,20)
      HFAC=118.0
      CALL GVPORT (50.0,(42.0+HFAC),80.0,80.0)
      CALL GWBOX (1.2,1.0,0.0)
      CALL RCLASS (0.0,15,4)
      CALL RSHADE (2,0)
      CALL GSMTH (-1)
      CALL GCONAA (-60,60)
```

```
      CALL GCONA (1.7,3,30.0,3)
      CALL GCNR2S (ZEST,24,20)
      CALL GCNR2V (ZEST,24,20)
      CALL GSCALE
      CALL GWICOL (0.4,2)
      CALL GVECT (XEDGE,YEDGE,44)
      CALL GSCAMM
      CALL RTXJUS (0,6)
      CALL RTXHEI (2.5)
      CALL RTX (-1,'Air Velocity',155.0,(105.0+HFAC))
      CALL RTXN (AIRV,3,155.0,(99.0+HFAC))
      CALL RTXC (-1,' m/s')
      CALL RTX (-1,'Weir Load',155.0,(91.0+HFAC))
      CALL RTX (-1,'Inlet Gap',155.0,(77.0+HFAC))
      CALL RTXN (GAP,3,155.0,(71.0+HFAC))
      CALL RTXC (-1,' m')
      CALL RTX (-1,'Outlet Weir',155.0,(63.0+HFAC))
      CALL RTXN (HOW,3,155.0,(57.0+HFAC))
      CALL RTXC (-1,' m')
      CALL RTX (-1,'Hole Diameter',155.0,(49.0+HFAC))
      CALL RTXN (HOLED,3,155.0,(43.0+HFAC))
      CALL RTXC (-1,' m')
      CALL RTXNBO (8,'T')
      CALL RTXN (WEIRL,3,155.0,(85.0+HFAC))
      CALL RTXC (-1,' cm3/cm.s')
C
      CALL GSCALE
      CALL RUXLOP (1)
      CALL RUXSTI (7)
      CALL RUXDIS (1,1,9999)
      CALL RUXDIS (2,1,9999)
      CALL RUXDIS (3,1,9999)
      CALL RUXDIS (4,1,9999)
      CALL RUXDIS (6,1,9999)
      CALL RUXDIS (7,0,9999)
      CALL RUXDIS (8,0,9999)
      CALL RUXTEX (6,-1,'FLOW PATH LENGTH - mm'
     #,999.999,999.999,2.4)
      CALL RUXIS (2,-1200.0,2.3,1,LENY,LABY,6)
      CALL RUXTEA (4,9999,9999,999.999,9999,9999,-90.0)
      CALL RUXTEX (6,-1,'FLOW PATH LENGTH - mm'
     #,999.999,999.999,2.4)
      CALL RUXIS (2,1200.0,2.3,2,LENY,LABY,6)
      CALL RUXTEA (4,9999,9999,999.999,9999,9999,0.0)
      CALL RUXTEX (6,-1,'OUTLET WEIR - mm'
     #,999.999,999.999,2.5)
      CALL RUXIS (1,-1000.0,2.3,1,LENX,LABX,7)
      CALL RUXTEX (6,-1,'INLET WEIR - mm'
     #,999.999,999.999,2.5)
      CALL RUXIS (1,1000.0,2.3,2,LENX,LABX,7)
C
C*************************************************************
C     3D PLOT
C*************************************************************
C     COLUMN WALL DATA
C*************************************************************
C
      RAD = 1200
      HS = 1925/20

      DO 2000 I=1,11
            YEDGE(I)=(1-I)*HS
            YEDGE(23-I)=YEDGE(I)
```

```
2000  CONTINUE
      DO 2100 I=1,10
            YEDGE(22+I)=I*HS
            YEDGE(43-I)=YEDGE(22+I)
2100  CONTINUE
            YEDGE(43)=YEDGE(1)
            YEDGE(44)=999.999
C
      DO 2200 I=1,11
            XEDGE(I)=-SQRT(RAD**2-YEDGE(I)**2)
            XEDGE(23-I)=-XEDGE(I)
2200  CONTINUE
      DO 2300 I=1,11
            XEDGE(I+22)=SQRT(RAD**2-YEDGE(I+22)**2)
            XEDGE(43-I)=-XEDGE(I+22)
2300  CONTINUE
            XEDGE(43)=YEDGE(1)
            XEDGE(44)=999.999
C
C*************************************************************
C     PRT POSITIONS ON TRAY AND INLET DOWNCOMER
C*************************************************************
C
      OPEN (UNIT=15,FILE='PRTCOORD.DAT',STATUS='OLD'
      DO 62 I=1,108
         READ (15,*) X(I),Y(I)
         Y(I)=1000.0-Y(I)
   62 CONTINUE
      CLOSE (UNIT=15)
C
C*************************************************************
C     READING IN TEMPERATURE DATA
C*************************************************************
C
      OPEN (UNIT=14,FILE='FOR014.DAT',STATUS='OLD')
      READ (15,300) AIRV
      READ (15,301) WEIRL
      READ (15,301) DEW
      READ (15,302) ALPHA
      READ (15,300) DIA
      READ (15,300) WEIR
      READ (15,301) FREE
      READ (15,300) HOW
      READ (15,300) GAP
      READ (15,300) HOLED
      READ (15,302) ALPHA
      READ (15,302) ALPHA
      READ (15,303) (TEMPIN(I),I=1,5)
      READ (15,304) (TEMP(I),I=1,8)
      READ (15,305) (TEMP(I),I=9,18)
      READ (15,306) (TEMP(I),I=19,30)
      READ (15,306) (TEMP(I),I=31,42)
      READ (15,306) (TEMP(I),I=43,54)
      READ (15,306) (TEMP(I),I=55,66)
      READ (15,306) (TEMP(I),I=67,78)
      READ (15,306) (TEMP(I),I=79,90)
      READ (15,305) (TEMP(I),I=91,100)
      READ (15,304) (TEMP(I),I=101,108)
      READ (15,307) TDOWN
      READ (15,308) (AIR(I),I=1,4)
      CLOSE (UNIT=14)
C
C*************************************************************
```

```
C     SETTING UP IRREGULAR ARRAYS
C*************************************************************
C
      NUM=0
      DO 20 I=1,108
         IF (TEMP(I).NE.99.99) THEN
            NUM=NUM+1
            XPOS(NUM)=X(I)
            YPOS(NUM)=Y(I)
            TPOS(NUM)=TEMP(I)
         END IF
  20  CONTINUE
C
C*************************************************************
C     AVERAGING INLET WATER TEMPERATURE
C*************************************************************
C
      WINT=DEW
      DO 21 I=1,5
         IF (TEMPIN(I).NE.99.99) THEN
            IF (TEMPIN(I).GT.WINT) THEN
               WINT=TEMPIN(I)
            END IF
         END IF
  21  CONTINUE
C
C*************************************************************
C     WET BULB TEMPERATURE
C*************************************************************
C
      TWB=DEW
C
C*************************************************************
C     SETTING UP REDUCED TEMPERATURES
C*************************************************************
C
      DO 22 I=1,NUM
         TR(I)=(TPOS(I)-TWB)/(WINT-TWB)
  22  CONTINUE
C
C*****************************************************************
C     ROUTINES TO COMMENCE PLOTTING
C*****************************************************************
C
      CALL GRESET
      CALL GLIMIT (-1200.0,1200.0,0.0,2000.0,0.0,1.0)
      CALL RUNDEF (999.999,9999)
      HFAC=0.0
      CALL GVPORT (50.0,(42.0+HFAC),80.0,80.0)
      CALL GWBOX (1.0,1.0,0.5)
      CALL GEYE (6.0,4.0,7.0)
      CALL GSCALE
      CALL GVPROJ(2)
      CALL RAXDIS (3,1,9999)
      CALL RAXDIS (7,1,9999)
      CALL RAXDIS (6,1,9999)
      CALL RAXLFO (0,0,1,0)
      CALL RAXBTI (9999,999.999,999.999,200.0)
      CALL RAXSTI (3)
      CALL RAXDIS (4,1,3)
      CALL RAXIS3 (1,3.0,IPLANE,LENGTH,TEXT)
      CALL RAXDIS (4,1,0)
      CALL RAXIS3 (2,3.0,IPLANE,LENGTH,TEXT)
```

```
CALL RAXBTI (9999,999.999,999.999,0.1)
CALL RAXSTI (1)
CALL RAXIS3 (3,3.0,IPLANE,LENGTH,TEXT)
CALL GFAULT (XEDGE,YEDGE,17,1)
CALL GINTPF (X,Y,TR,NUM,ZEST,24,20)
CALL GSMTH (-1)
CALL GCONWI (0.0,1)
CALL RSHADE (2,0)
CALL GCONR3 (ZEST,24,20)
CALL GRESET
CALL GSCAMM
CALL RTXJUS (0,6)
CALL RTXHEI (2.5)
CALL RTX (-1,'Air Velocity',155.0,(109.0+HFAC))
CALL RTXN (AIRV,3,155.0,(103.0+HFAC))
CALL RTXC (-1,' m/s')
CALL RTX (-1,'Weir Load',155.0,(95.0+HFAC))
CALL RTX (-1,'Inlet Gap',155.0,(81.0+HFAC))
CALL RTXN (GAP,3,155.0,(75.0+HFAC))
CALL RTX (-1,'Outlet Weir',155.0,(67.0+HFAC))
CALL RTXN (HOW,3,155.0,(61.0+HFAC))
CALL RTX (-1,'Hole Diameter',155.0,(53.0+HFAC))
CALL RTX (-1,HOLED,3,155.0,(47.0+HFAC))
CALL RTXC (-1,' m')
CALL RTXNBO (8,'T')
CALL RTXN (WEIRL,3,155.0,(89.0+HFAC))
CALL RTXC (-1,' cm3/cm.s')
CALL GCLOSE
END
```

Coordinates Of The 108 RTDs On The Tray

The centre of the tray is arbitrarily assigned the coordinates (0,0). The coordinates of the RTDs are listed according to the location of all 108 temperature probes on the tray starting from the top right-hand corner of Figure 5.6 in Chapter 5.

TRAY INLET

		(-700,900)	(-500,900)	(-300,900)	(-100,900)	(100,900)	(300,900)	(500,900)	(700,900)	
	(-900,700)	(-700,700)	(-500,700)	(-300,700)	(-100,700)	(100,700)	(300,700)	(500,700)	(700,700)	(900,700)
(-1000,500)	(-900,500)	(-700,500)	(-500,500)	(-300,500)	(-100,500)	(100,500)	(300,500)	(500,500)	(700,500)	(900,500)	(1000,500)
(-1100,300)	(-900,300)	(-700,300)	(-500,300)	(-300,300)	(-100,300)	(100,300)	(300,300)	(500,300)	(700,300)	(900,300)	(1100,300)
(-1150,100)	(-900,100)	(-700,100)	(-500,100)	(-300,100)	(-100,100)	(100,100)	(300,100)	(500,100)	(700,100)	(900,100)	(1150,100)
(-1150,-100)	(-900,-100)	(-700,-100)	(-500,-100)	(-300,-100)	(-100,-100)	(100,-100)	(300,-100)	(500,-100)	(700,-100)	(900,-100)	(1150,-100)
(-1100,-300)	(-900,-300)	(-700,-300)	(-500,-300)	(-300,-300)	(-100,-300)	(100,-300)	(300,-300)	(500,-300)	(700,-300)	(900,-300)	(1100,-300)
(-1000,-500)	(-900,-500)	(-700,-500)	(-500,-500)	(-300,-500)	(-100,-500)	(100,-500)	(300,-500)	(500,-500)	(700,-500)	(900,-500)	(1000,-500)
	(-900,-700)	(-700,-700)	(-500,-700)	(-300,-700)	(-100,-700)	(100,-700)	(300,-700)	(500,-700)	(700,-700)	(900,-700)	
		(-700,-900)	(-500,-900)	(-300,-900)	(-100,-900)	(100,-900)	(300,-900)	(500,-900)	(700,-900)	

TRAY OUTLET

APPENDIX 2

Source Code For The Calculation of Efficiencies

Listed below the Fortran 77 computer program written to calculate the point and tray efficiencies.

```
      PROGRAM EFFICIENCY
C
      INTEGER*2  I,J,K,NUM
      REAL  PAIR,PWATER,PI,CP,AIRV,WEIRL,DEW,DIA,WEIR,HOLED
      REAL  FREE,HOW,GAP,TEMPIN(5),TEMP(108),AIR(4),TDOWN
      REAL  T(108),SUM,TIN,TOUT,DRY,MG,ML,HUMIN,HIN,HOUT,HLOSS
      REAL  HUMEQ,HOUTEQ,EMV,HUM(108),H(108),EOG,RATIO,CF
      CHARACTER*2  ALPHA
C
      PAIR=1.22
      PWATER=1000.0
      PI=3.141593
      CP=4.18

      OPEN (UNIT=15,FILE='EFF.DAT',STATUS='NEW')
C
C*********************************************************
C     READING IN TEMPERATURE DATA
C*********************************************************
C
         OPEN (UNIT=14,FILE='FOR014.DAT',STATUS='OLD')
         READ (14,300) AIRV
         READ (14,301) WEIRL
         READ (14,302) DEW
         READ (14,303) ALPHA
         READ (14,304) DIA
         READ (14,305) WEIR
         READ (14,306) FREE
         READ (14,307) HOW
         READ (14,308) GAP
         READ (14,300) HOLED
         READ (14,303) ALPHA
         READ (14,303) ALPHA
         READ (14,309) (TEMPIN(I),I=1,5)
         READ (14,310) (TEMP(I),I=1,8)
         READ (14,311) (TEMP(I),I=9,18)
         READ (14,312) (TEMP(I),I=19,30)
         READ (14,312) (TEMP(I),I=31,42)
         READ (14,312) (TEMP(I),I=43,54)
         READ (14,312) (TEMP(I),I=55,66)
         READ (14,312) (TEMP(I),I=67,78)
         READ (14,312) (TEMP(I),I=79,90)
         READ (14,311) (TEMP(I),I=91,100)
         READ (14,310) (TEMP(I),I=101,108)
         READ (14,313) TDOWN
         READ (14,314) (AIR(I),I=1,4)
         CLOSE (UNIT=14)
C
  300    FORMAT (27X,F3.1)
  301    FORMAT (27X,F4.0)
  302    FORMAT (27X,F4.1)
  303    FORMAT (4X,A2)
  304    FORMAT (27X,F5.3)
```

```
  305    FORMAT (27X,F5.3)
  306    FORMAT (27X,F4.1)
  307    FORMAT (27X,F5.3)
  308    FORMAT (27X,F5.3)
  309    FORMAT (43X,5(F6.2,4X))
  310    FORMAT (28X,8(F6.2,4X))
  311    FORMAT (18X,10(F6.2,4X))
  312    FORMAT (8X,12(F6.2,4X))
  313    FORMAT (63X,F6.2)
  314    FORMAT (10X,3(F6.2,4X))
C
C*************************************************************
C     SCREENING OUT NULL TEMPERATURE VALUES
C*************************************************************
C
      NUM=0
      DO 10 I=1,108
         IF (TEMP(I).NE.99.99) THEN
            NUM=NUM+1
            T(NUM)=TEMP(I)
         END IF
  10  CONTINUE
C
C*************************************************************
C     AVERAGING INLET AND OUTLET MEASURED TEMPERATURES - C
C*************************************************************
C
      J=0
      SUM=0.0
      DO 11 I=1,5
         IF (TEMPIN(I).NE.99.99) THEN
            J=J+1
            SUM=SUM+TEMPIN(I)
            END IF
  11  CONTINUE
      TIN=SUM/J
      WRITE(15,400) TIN
C
      J=0
      SUM=0.0
      DO 12 I=101,108
         IF (TEMP(I).NE.99.99) THEN
            J=J+1
            SUM=SUM+TEMP(I)
         END IF
  12  CONTINUE
      TOUT=SUM/J
      WRITE(15,401) TOUT
      WRITE(15,402) TDOWN
      IF (TDOWN.NE.99.99) THEN
         IF (TDOWN.GT.TOUT) THEN
            TOUT=TDOWN
          END IF
      END IF
C
      J=0
      SUM=0.0
      DO 13 I=1,4
         IF (AIR(I).NE.99.99) THEN
            J=J+1
            SUM=SUM+AIR(I)
         END IF
  13  CONTINUE
```

```
      DRY=SUM/J
      WRITE(15,403) DRY
      WRITE(15,404) DEW

  400 FORMAT (4X,'TIN = ',F9.5)
  401 FORMAT (4X,'TOUT =',F9.5)
  402 FORMAT (4X,'TDOWN =',F9.5)
  403 FORMAT (4X,'DRY =',F9.5)
  404 FORMAT (4X,'DEW =',F9.5)
C
C*************************************************************
C     CALCULATING MASS FLOWRATES - KG/S
C*************************************************************
C
      MG=PAIR*AIRV*PI*(DIA**2)/4
      WRITE(15,405) MG
      ML=PWATER*WEIRL*WEIR/10000.0
      WRITE(15,406) ML

  405 FORMAT (4X,'MG =',F10.6)
  406 FORMAT (4X,'ML =',F10.6)
C
C*************************************************************
C     CALCULATING INLET AIR HUMIDITY AND ENTHALPY
C*************************************************************
C
      CALL PSYCHRO (DRY,DEW,HUMIN,HIN)
      WRITE(15,407) HUMIN
      WRITE(15,408) HIN
  407 FORMAT (4X,'HUMIN = ',E13.7)
  408 FORMAT (4X,'HIN = ',F9.5)
C
C*************************************************************
C     OVERALL HEAT BALANCE TO GIVE HOUT
C*************************************************************
C
      HOUT=((ML*CP/MG)*(TIN-TOUT))+HIN
      HLOSS =(ML*CP*(TIN-TOUT))

      WRITE(15,409) HLOSS
      WRITE(15,410) HOUT

  409 FORMAT (4X,'HEAT LOST FROM WATER = ',F9.4)
  410 FORMAT (4X,'HOUTAV = ',F9.5)
C
C*************************************************************
C     CALCULATING TRAY EFFICIENCY
C*************************************************************
C
      CALL PSYCHRO (TOUT,TOUT,HUMEQ,HOUTEQ)
      WRITE(15,412) HUMEQ
      WRITE(15,413) HOUTEQ
      EMV=(HOUT-HIN)/(HOUTEQ-HIN)
      WRITE(15,414) EMV

  412 FORMAT (4X,'HUMEQ = ',E13.7)
  413 FORMAT (4X,'HOUTEQ = ',F9.4)
  414 FORMAT (4X,'EMV = ',F9.7)
C
C*************************************************************
C     CALCULATING POINT EFFICIENCY
C*************************************************************
C
```

```
      SUM=0.0
      DO 14 I=1,NUM
         CALL PSYCHRO (T(I),T(I),HUM(I),H(I))
         WRITE(15,*) T(I),H(I)
         SUM=SUM+H(I)
   14 CONTINUE
      WRITE(15,*) SUM,NUM,SUM/NUM
      EOG=(ML*CP/MG)*(TIN-TOUT)*NUM/(SUM-(NUM*HIN))
      WRITE(15,415) EOG

  415 FORMAT (4X,'EOG = ',F9.7)
      SUMH2=0
      DO 15 I=1,NUM
         H2(I)=EOG*(H(I)-HIN)+HIN
         WRITE(15,*)H2(I)
         SUMH2=SUMH2+H2(I)
   15 CONTINUE
      CF=NUM*HOUT/SUMH2
      WRITE (15,*)SUMH2,SUMH2/NUM,HOUT,CF
      DO 16 I=1,NUM
         H2(I)=H2(I)*CF
         EOG1(I)=(H2(I)-HIN)/(H(I)-HIN)
         WRITE (15,*) H2(I),EOG1(I)
   16 CONTINUE
C
C*************************************************************
C     CALCULATING EMV/EOG
C*************************************************************
C
      RATIO=EMV/EOG
      WRITE(15,416) RATIO
  416 FORMAT (4X,'RATIO = ',F9.6)
      END
C
C*************************************************************
C     ROUTINE TO CALCULATE AIR HUMIDITY AND ENTHALPY
C*************************************************************
C
      SUBROUTINE PSYCHRO (TDB,TWB,HUM,ENTH)
      REAL  A,B,C,D,E,F,G,Z1,Z2,Z3,Z4,Z5
      REAL  TD1,TD2,M1,M2,C1,C2,C3,Y1,Y2
      REAL  LO,TWB,TDB,P0,PSS,HUM,ENTH
      A=-2948.997118, B=-2.1836674, C=-0.000150474, D=-0.0303738468
      E=0.00042873,F=4.76955, G=25.83220018
      TD1=273.15, TD2=273.16
      P0=101.325
      M1=18.01534
      M2=28.9645
      C1=0.000666, C2=1.00568, C3=1.84598
      LO=2500.84
      Z1=A/(TWB+TD1)
      Z2=B*LOG(TWB+TD1)
      Z3=C*(10**(D*(TWB-0.01)))
      Z4=E*(10**(F*(1.0-(TD2/(TWB+TD1)))))
      Z5=G
      PSS=10**(Z1+Z2+Z3+Z4+Z5)
      Y1=P0*C1*(TDB-TWB)
      HUM=(M1/M2)*(PSS-(1000.0*Y1))/((1000.0*P0)-PSS+(1000.0*Y1))
      ENTH=(C2*TDB)+(HUM*(LO+(C3*TDB)))
      RETURN
      END
```

APPENDIX 3

Source Code For Plotting Clear Liquid Height Profiles and The Coordinates of The Manometer Pressure Tappings on The Tray

Listed below is the Fortran 77 computer program written to generate three dimensional height of clear liquid surfaces. The coding calls on routines from the UNIRAS suite of plotting routines.

```
C+++++++++++++++++++++++++++++++++++++++++++++++++++++++++++++++
C
C  MODIFIED  27/11/90
C  CHANGES:  INPUT FILE LENGTH CAN VARY
C            DATUM FILE MUST CONTAIN ONE DATA SET FOR EACH INPUT SET
C            NEEDS FILE CONFIG.DAT CONTAINING INLET GAP ETC.
C            MANOM.DAT MUST CONTAIN MANOMETER READINGS AND
C            MCOORD.DAT THE MANOMETER COORDINATES
C            OUTPUT IS HCLOUT.DAT AND POST.DAT FILES
C
C+++++++++++++++++++++++++++++++++++++++++++++++++++++++++++++++
      PROGRAM HCLALL
C
      INTEGER  I,J,IPLANE(3),LENGTH(6),NDATA
C
      REAL  XEDGE(17),YEDGE(17),X(32),Y(32),MHCL(12,32)
      REAL  AIRV(12),WEIRL(12),WTDP(12),CORDP(12)
      REAL  DAIRV(12),DWEIRL(12),DWTDP(12),DCORDP(12)
      REAL  DMHCL(12,32),XED(17),YED(17),XPOS(32),YPOS(32)
      REAL  HCL(12,32),CMHCL(12,32),DCMHCL(12,32)
      REAL  ZEST(25,21),HFAC,HEIGHT(32)
      REAL  INGAP,INWEIR,OUTWEIR,HOLEDIA
      CHARACTER*21  TEXT(6)
C
      DATA  IPLANE /1,1,1/,LENGTH /0,16,0,21,0,17/
      DATA  TEXT /' ','WEIR LENGTH - mm',' '
     #,'FLOW PATH LENGTH - mm',' ','CLEAR LIQUID - mm'/
C
C*************************************************************
C     COLUMN WALL DATA
C*************************************************************
C
      XEDGE(1)=999.999
      XEDGE(2)=-1200.0
      XEDGE(3)=-1150.0
      XEDGE(4)=-1050.0
      XEDGE(5)=-720.0
      XEDGE(6)=720.0
      XEDGE(7)=1050.0
      XEDGE(8)=1150.0
      XEDGE(9)=1200.0
      XEDGE(10)=1150.0
      XEDGE(11)=1050.0
      XEDGE(12)=720.0
      XEDGE(13)=-720.0
      XEDGE(14)=-1050.0
      XEDGE(15)=-1150.0
      XEDGE(16)=-1200.0
      XEDGE(17)=999.999
      YEDGE(1)=999.999
```

```
      YEDGE(2)=1000.0
      YEDGE(3)=600.0
      YEDGE(4)=350.0
      YEDGE(5)=0.0
      YEDGE(6)=0.0
      YEDGE(7)=350.0
      YEDGE(8)=600.0
      YEDGE(9)=1000.0
      YEDGE(10)=1400.0
      YEDGE(11)=1650.0
      YEDGE(12)=2000.0
      YEDGE(13)=2000.0
      YEDGE(14)=1650.0
      YEDGE(15)=1400.0
      YEDGE(16)=1000.0
      YEDGE(17)=999.999
C
C*************************************************************
C     MANOMETER POSITIONS ON TRAY
C*************************************************************

      OPEN(15,FILE='MCOORD.DAT',STATUS='OLD')
      DO 99 I=1,32
       READ(15,*) X(I),Y(I)
  99  CONTINUE
      CLOSE(15)

C
C*************************************************************
C     READING IN MEASURED MANOMETER DATA
C*************************************************************
C
      OPEN(14,FILE='MANOM.DAT',STATUS='OLD')
      DO 11 I=1,100
         READ (14,500,END=999) AIRV(I),WEIRL(I)
 500     FORMAT (1X,F4.1,1X,F5.1)
         READ (14,501,END=999) WTDP(I),CORDP(I)
 501     FORMAT (1X,F4.1,1X,F4.1)
         READ (14,502,END=999) (MHCL(I,J),J=1,16)
 502     FORMAT (1X,16(F4.1,1X))
         READ (14,502,END=999) (MHCL(I,J),J=17,32)
  11  CONTINUE
999   NDATA=I-1
      CLOSE (14)
C
C*************************************************************
C     READING IN DATUM TUBE LEVELS
C*************************************************************
C
      OPEN (UNIT=15,FILE='DATUM.DAT',STATUS='UNKNOWN')
      DO 12 I=1,NDATA
         READ (15,503) DAIRV(I)
  503    FORMAT (1X,F4.1)
         READ (15,501) DWTDP(I),DCORDP(I)
         READ (15,502) (DMHCL(I,J),J=1,16)
         READ (15,502) (DMHCL(I,J),J=17,32)
  12  CONTINUE

C*************************************************************
C   READ INLET GAP & WEIR, OUTLET GAP AND HOLE DIAMETER IN
C  METRES
C*************************************************************
```

```
      OPEN (UNIT=15,FILE='CONFIG.DAT',STATUS='UNKNOWN')
      READ (15,*)INGAP,INWEIR,OUTWEIR,HOLEDIA
      CLOSE (15)
C
C
C*************************************************************
C     PROCEDURE TO CALCULATE HCL VALUES
C*************************************************************
C
      DO 19 I=1,NDATA
         DO 20 J=1,32
            CMHCL(I,J=MHCL(I,J)-CORDP(I)
            DCMHCL(I,J)=DMHCL(I,J)-DCORDP(I)
            HCL(I,J)=10*(CMHCL(I,J)-DCMHCL(I,J))
  20     CONTINUE
  19  CONTINUE
C
C*************************************************************
C     OUTPUT OF HCL DATA
C*************************************************************
C
      OPEN(18,FILE='HCLOUT.DAT',STATUS='NEW')

      DO 21 I=1,NDATA
         WRITE (18,200) AIRV(I),WEIRL(I)
 200     FORMAT (15X,'AIRV = ',F4.1,5X,'WEIRL = ',F5.1)
         WRITE (18,201)
 201     FORMAT 2X,' ')
         WRITE (18,201)
         WRITE (18,202) HCL(I,21),HCL(I,17),HCL(I,1),HCL(I,5)
 202     FORMAT (8X,F4.1,14X,F4.1,8X,F4.1,14X,F4.1)
         WRITE (18,201)
         WRITE (18,203) HCL(I,22),HCL(I,18),HCL(I,2),HCL(I,6)
 203     FORMAT (8X,F4.1,8X,F4.1,20X,F4.1,8X,F4.1)
         WRITE (18,201)
         WRITE (18,204) HCL(I,23),HCL(I,19),HCL(I,3),HCL(I,7)
 204     FORMAT (2X,F4.1,20X,F4.1,8X,F4.1,20X,F4.1)
         WRITE (18,201)
         WRITE (18,203) HCL(I,24),HCL(I,20),HCL(I,4),HCL(I,8)
         WRITE (18,201)
         WRITE (18,202) HCL(I,25),HCL(I,29),HCL(I,13),HCL(I,9)
         WRITE (18,201)
         WRITE (18,205) HCL(I,26),HCL(I,30),HCL(I,14),HCL(I,10)
 205     FORMAT (2X,F4.1,14X,F4.1,20X,F4.1,14X,F4.1)
         WRITE (18,201)
         WRITE (18,202) HCL(I,27),HCL(I,31),HCL(I,15),HCL(I,11)
         WRITE (18,201)
         WRITE (18,203) HCL(I,28),HCL(I,32),HCL(I,16),HCL(I,12)
         WRITE (18,201)
         WRITE (18,201)
  21  CONTINUE
      CLOSE(18)
C
C*************************************************************
C     READING IN DATA TO CONTROL PLOTTING
C*************************************************************
C
      DO 22 I=1,NDATA,2
         W=WEIRL(I)
         A=AIRV(I)
         DO 23 K=1,17
            XED(K)=XEDGE(K)
            YED(K)=YEDGE(K)
```

```
 23       CONTINUE
          DO 24 J=1,32
             HEIGHT(J)=HCL(I,J)
             XPOS(J)=X(J)
             YPOS(J)=Y(J)
 24       CONTINUE
C
C*************************************************************
C     ROUTINES TO COMMENCE PLOTTING
C*************************************************************
C
      CALL GROUTE ('S HPOSTA4;E ')
      CALL GOPEN
      CALL RORIEN (2)
      CALL GLIMIT (-1200.0,1200.0,0.0,2000.0,0.0,50.0)
      CALL RUNDEF (999.999,9999)
      HFAC=118.0
      CALL GVPORT (40.0,(42.0+HFAC),80.0,80.0)
      CALL GWBOX (1.0,1.0,0.5)
      CALL GEYE (6.0,4.0,7.0)
      CALL GSCALE
      CALL GVPROJ(2)

      CALL RAXDIS (3,1,9999)
      CALL RAXDIS (7,1,9999)
      CALL RAXDIS (6,1,9999)
      CALL RAXFLO (0,0,1,0)
      CALL RAXBTI (9999,999.999,999.999,200.0)
      CALL RAXSTI (3)
      CALL RAXDIS (4,1,3)
      CALL RAXIS3 (1,3.0,IPLANE,LENGTH,TEXT)
      CALL RAXDIS (4,1,0)
      CALL RAXIS3 (2,3.0,IPLANE,LENGTH,TEXT)
      CALL RAXBTI (9999,999.999,999.99,10.0)
      CALL RAXSTI (4)
      CALL RAXIS3 (3,3.0,IPLANE,LENGTH,TEXT)
C
      CALL GFAULT (XED,YED,17,1)
      CALL GINTPF (XPOS,YPOS,HEIGHT,32,ZEST,25,21)
      CALL GSMTH (-1)
      CALL GCONWI (0.0,1)
      CALL GSHADE (4,0)
      CALL GCONR3 (ZEST,25,21)
      CALL GRESET
C
      CALL GSCAMM
      CALL RTXJUS (0,6)
      CALL RTXHEI (2.5)
      CALL RTX (-1,'Air Velocity',145.0,(116.0+HFAC))
      CALL RTXN (A,3,145.0,(110.0+HFAC))
      CALL RTXC (-1,' m/s')
      CALL RTX (-1,'Weir Load',145.0,(102.0+HFAC))
      CALL RTX (-1,'Inlet Gap',145.0,(88.0+HFAC))
      CALL RTXN (INGAP,3,145.0,(82.0+HFAC))
      CALL RTXC (-1,' m')
      CALL RTX (-1,'Inlet Weir',145.0,(74.0+HFAC))
      CALL RTXN (INWEIR,3,145.0,(68.0+HFAC))
      CALL RTXC (-1,' m')
      CALL RTX (-1,'Outlet Weir',145.0,(60.0+HFAC))
      CALL RTXN (OUTWEIR,3,145.0,(54.0+HFAC))
      CALL RTXC (-1,' m')
      CALL RTX (-1,'Hole Diameter',145.0,(46.0+HFAC))
      CALL RTXN (HOLEDIA,3,145.0,(40.0+HFAC))
```

```
      CALL RTXC (-1,' m')
      CALL RTXNBO (8,'T')
      CALL RTXN (W,1,145.0,(96.0+HFAC))
      CALL RTXC (-1,' cm3/cm.s')
C
C*************************************************************
C
      IF ((I+1).LE.NDATA) THEN
       W=WEIRL(I+1)
       A=AIRV(I+1)
       DO 25 K=1,17
          XED(K)=XEDGE(K)
          YED(K)=YEDGE(K)
 25    CONTINUE
       DO 26 J=1,32
          XPOS(J)=X(J)
          YPOS(J)=Y(J)
          HEIGHT(J)=HCL((I+1),J)
 26    CONTINUE
C
C*************************************************************
C
      CALL GRESET
      CALL GLIMIT (-1200.0,1200.0,0.0,2000.0,0.0,50.0)
      CALL RUNDEF (999.999,9999)
      HFAC=0.0
      CALL GVPORT (40.0,(42.0+HFAC),80.0,80.0)
      CALL GWBOX (1.0,1.0,0.5)
      CALL GEYE (6.0,4.0,7.0)
      CALL GSCALE
      CALL GVPROJ(2)
C
      CALL RAXDIS (3,1,9999)
      CALL RAXDIS (7,1,9999)
      CALL RAXDIS (6,1,9999)
      CALL RAXFLO (0,0,1,0)
      CALL RAXBTI (9999,999.999,999.999,200.0)
      CALL RAXSTI (3)
      CALL RAXDIS (4,1,3)
      CALL RAXIS3 (1,3.0,IPLANE,LENGTH,TEXT)
      CALL RAXDIS (4,1,0)
      CALL RAXIS3 (2,3.0,IPLANE,LENGTH,TEXT)
      CALL RAXBTI (9999,999.999,999.999,10.0)
      CALL RAXSTI (4)
      CALL RAXIS3 (3,3.0,IPLANE,LENGTH,TEXT)
C
      CALL GFAULT (XED,YED,17,1)
      CALL GINTPF (XPOS,YPOS,HEIGHT,32,ZEST,25,21)
      CALL GSMTH (-1)
      CALL GCONWI (0.0,1)
      CALL GCNR3V (ZEST,25,21)
      CALL GRESET
C
      CALL GSCAMM
      CALL RTXJUS (0,6)
      CALL RTXHEI (2.5)
      CALL RTX (-1,'Air Velocity',145.0,(116.0+HFAC))
      CALL RTXN (A,3,145.0,(110.0+HFAC))
      CALL RTXC (-1,' m/s')
      CALL RTX (-1,'Weir Load',145.0,(102.0+HFAC))
      CALL RTX (-1,'Inlet Gap',145.0,(88.0+HFAC))
      CALL RTXN (INGAP,3,145.0,(82.0+HFAC))
      CALL RTXC (-1,' m')
```

```
      CALL RTX (-1,'Inlet Weir',145.0,(74.0+HFAC))
      CALL RTXN (INWEIR,3,145.0,(68.0+HFAC))
      CALL RTXC (-1,' m')
      CALL RTX (-1,'Outlet Weir',145.0,(60.0+HFAC))
      CALL RTXN (OUTWEIR,3,145.0,(54.0+HFAC))
      CALL RTXC (-1,' m')
      CALL RTX (-1,'Hole Diameter',145.0,(46.0+HFAC))
      CALL RTXN (HOLEDIA,3,145.0,(40.0+HFAC))
      CALL RTXC (-1,' m')
      CALL RTXNBO (8,'T')
      CALL RTXN (W,1,145.0,(96.0+HFAC))
      CALL RTXC (-1,' cm3/cm.s')
     ENDIF
    CALL GCLOSE
 22 CONTINUE
    END
```

Coordinates of The Manometer Pressure Tappings on The Tray

The centre of the inlet downcomer is arbitrarily assigned the coordinates (0,0). The coordinates are listed according to the location of all 32 pressure tappings on the tray starting from the top right-hand corner of Figure 5.16 in Chapter 5.

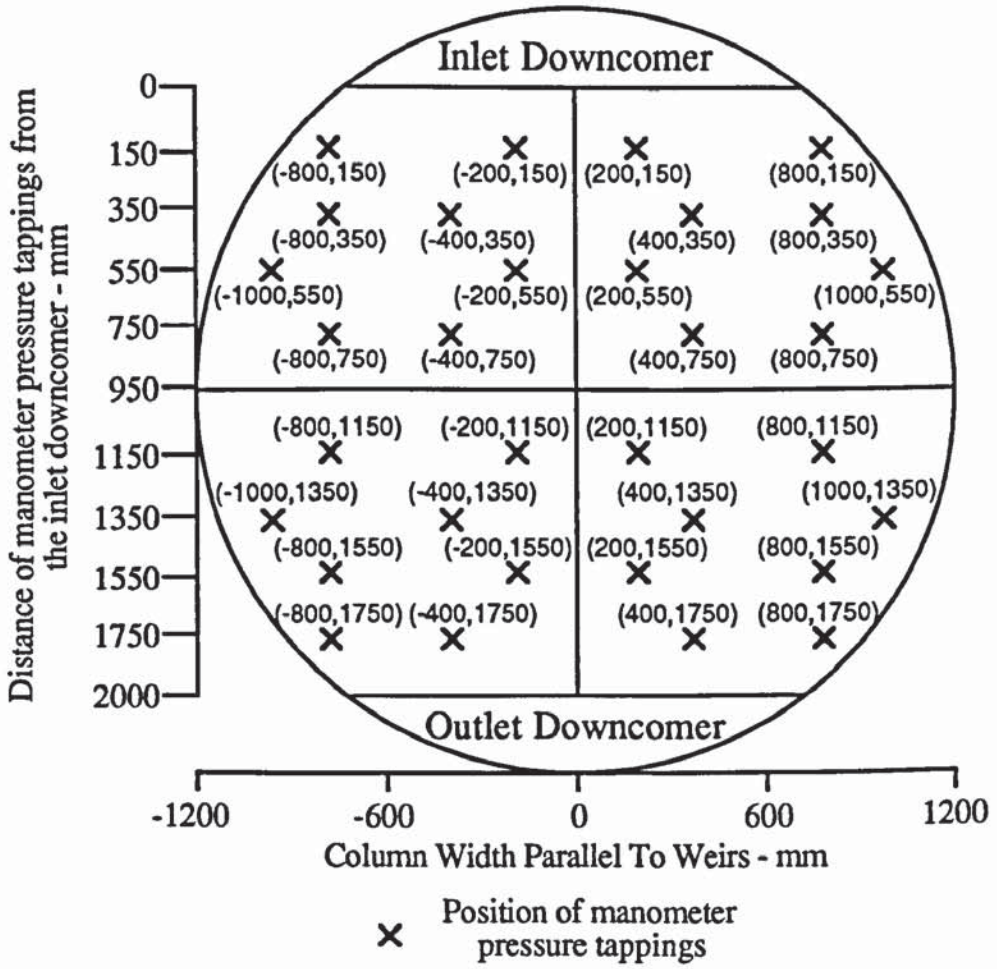

Figure A3.1 Coordinates of the manometer pressure tappings across the test tray

APPENDIX 4

Two-Dimensional Reduced Temperatue Isotherm Displays For The Effect of the Gas Flow Pattern on Liquid Flow Studies

The two-dimensional black and white displays presented below are a full set of reduced temperature profiles to complement the results of the water-cooling experiments in Chapter 6. Water-cooling was used to show the effect of gas influenced and non-gas influenced liquid flow patterns on mass transfer. In these experiments, the superficial air velocity was varied over a wide range for a fixed weir loading at the equal inlet gap-outlet weir settings of 10 mm, 10 mm; 20 mm, 20 mm; and 50 mm, 50 mm. The flow rate information is presented in Table A4.1.

Experimental Investigation	Air Velocity - ms^{-1}	Weir load - $10^4.m^3/m.s$	Inlet Gap - mm	Outlet Weir - mm
Heat transfer	1.243	27.78	10	10
by	1.523	37.04	20	20
water-cooling	1.760	46.30	50	50
	1.969	55.55		

Table A4.1 Summary of flow rates and downcomer settings used in the air - water contacting experiments.

Note the complex nature of the reduced temperature profiles in all of the experiments compared with the parallel or "U-shaped" isotherms produced in the separation of flow and pressure simulation experiments, (see Appendices 7 and 9).

In addition, the designations assigned to each temperature profile are included in the labelling of each diagram. A reminder of the temperature profile designations used in these studies are summarised below.

Temperature Profile	Designation
Straight and Parallel Isotherms	P
Distinctive "U-shaped" Isotherms	U
Mixed or Confused Isotherms	M
"U-shaped" or Closed Looped Isotherms	UC

Table A4.2 Summary of temperature profile designations.

PAGE
MISSING
IN
ORIGINAL

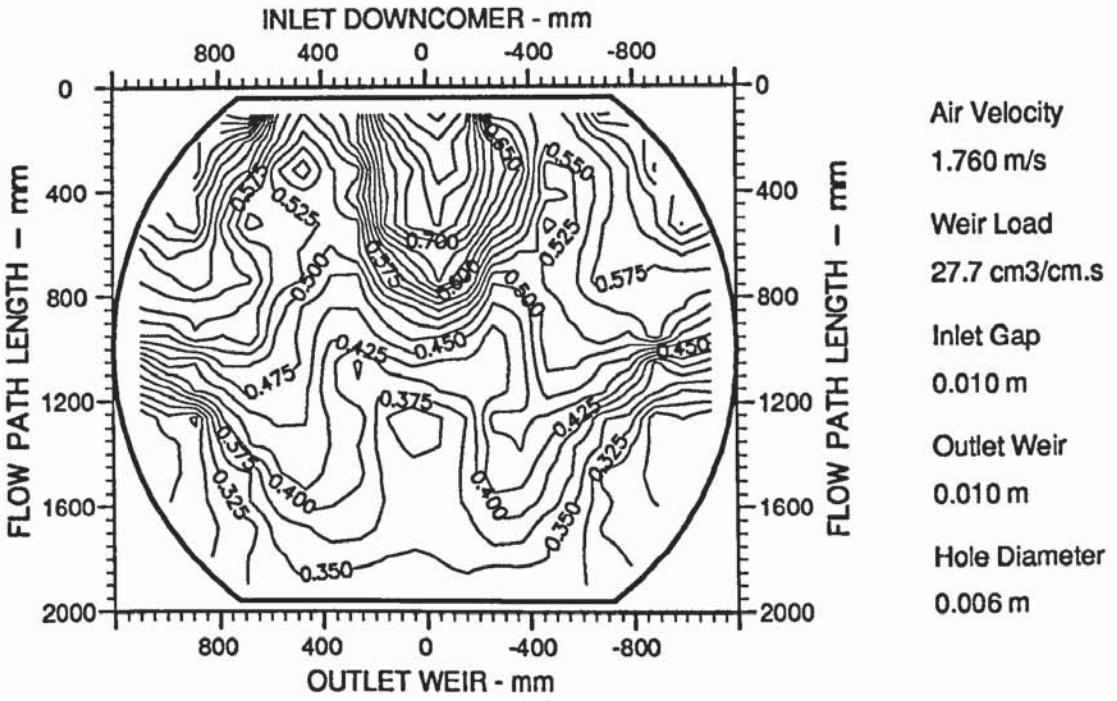

Figure A4.3 Two-dimensional reduced temperature profiles showing mixed or confused isotherms (designation M).

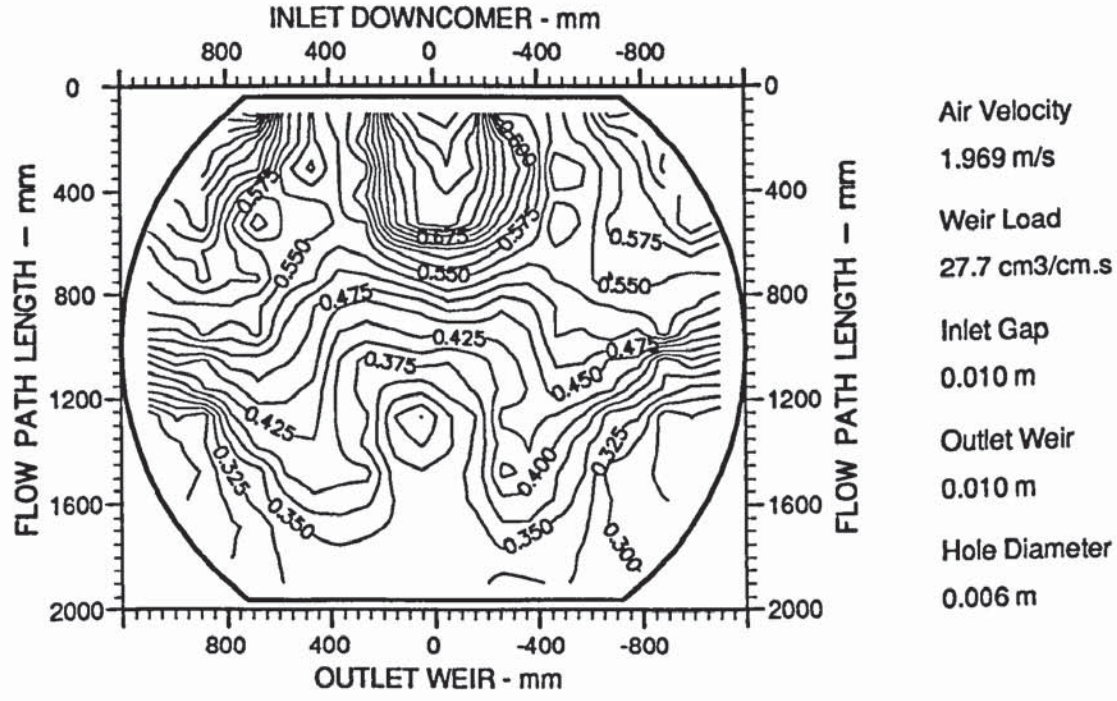

Figure A4.4 Two-dimensional reduced temperature profiles showing mixed or confused isotherms (designation M).

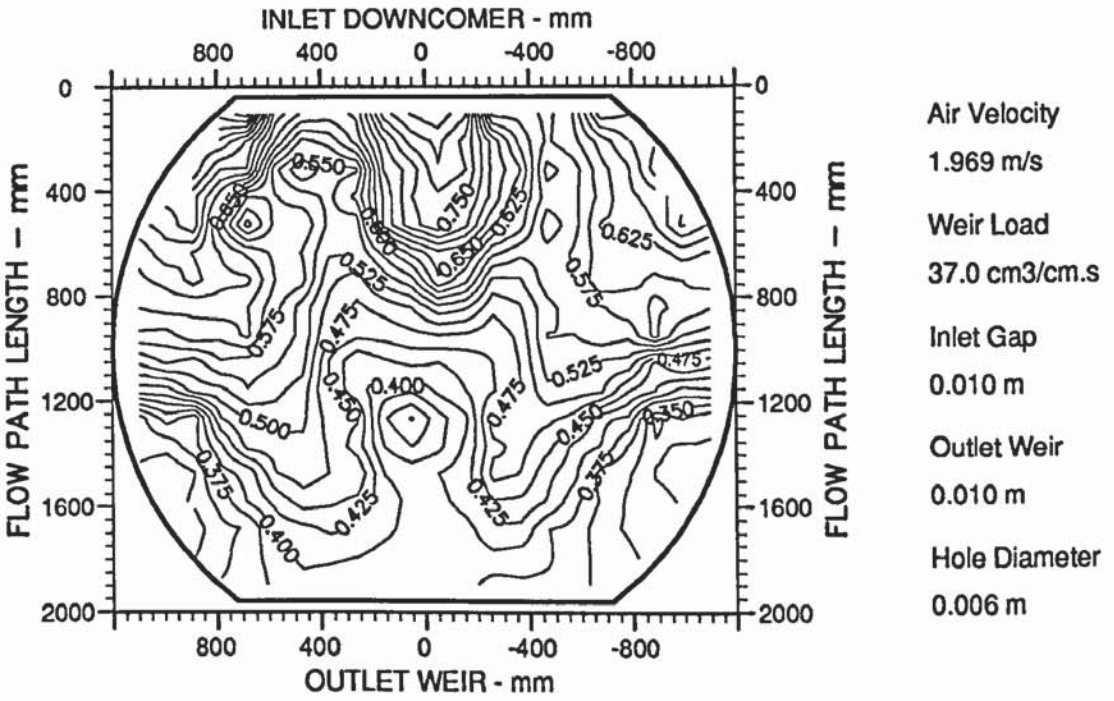

Figure A4.5 Two-dimensional reduced temperature profiles showing mixed or confused isotherms (designation M).

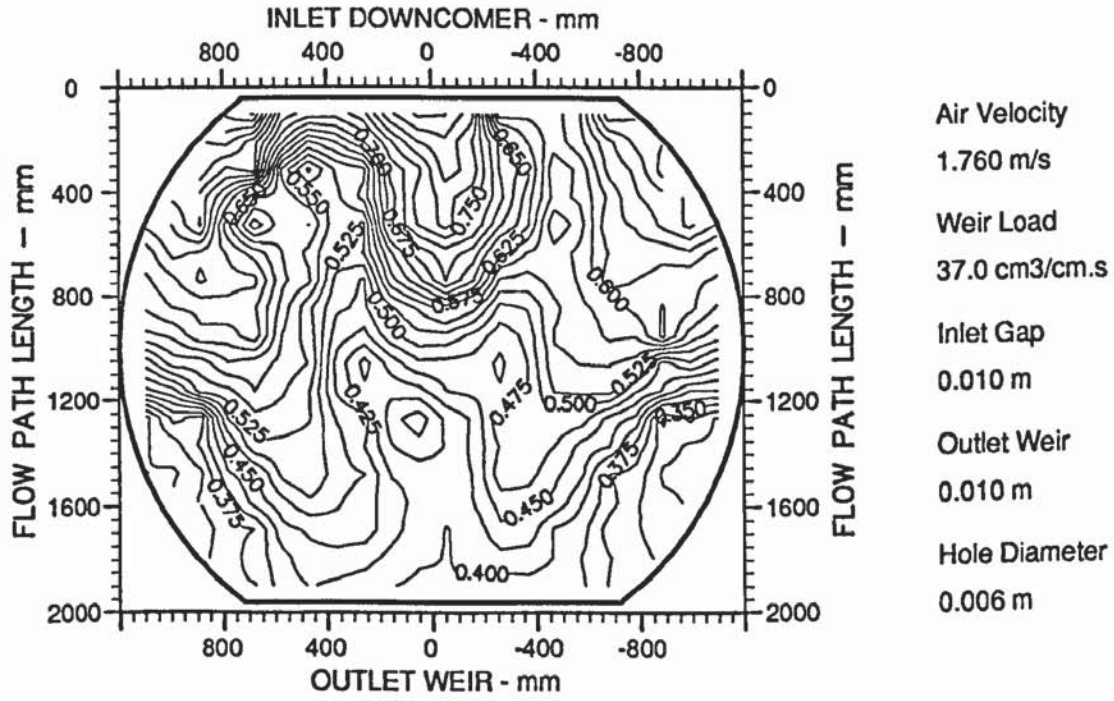

Figure A4.6 Two-dimensional reduced temperature profiles showing mixed or confused isotherms (designation M).

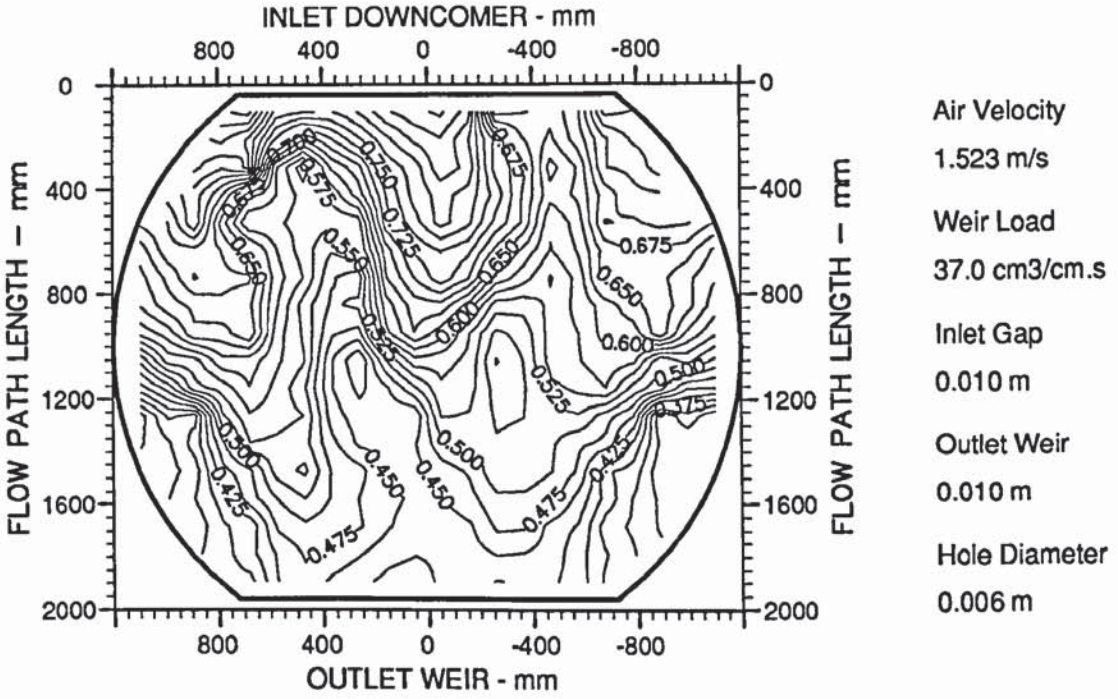

Figure A4.7 Two-dimensional reduced temperature profiles showing mixed or confused isotherms (designation M).

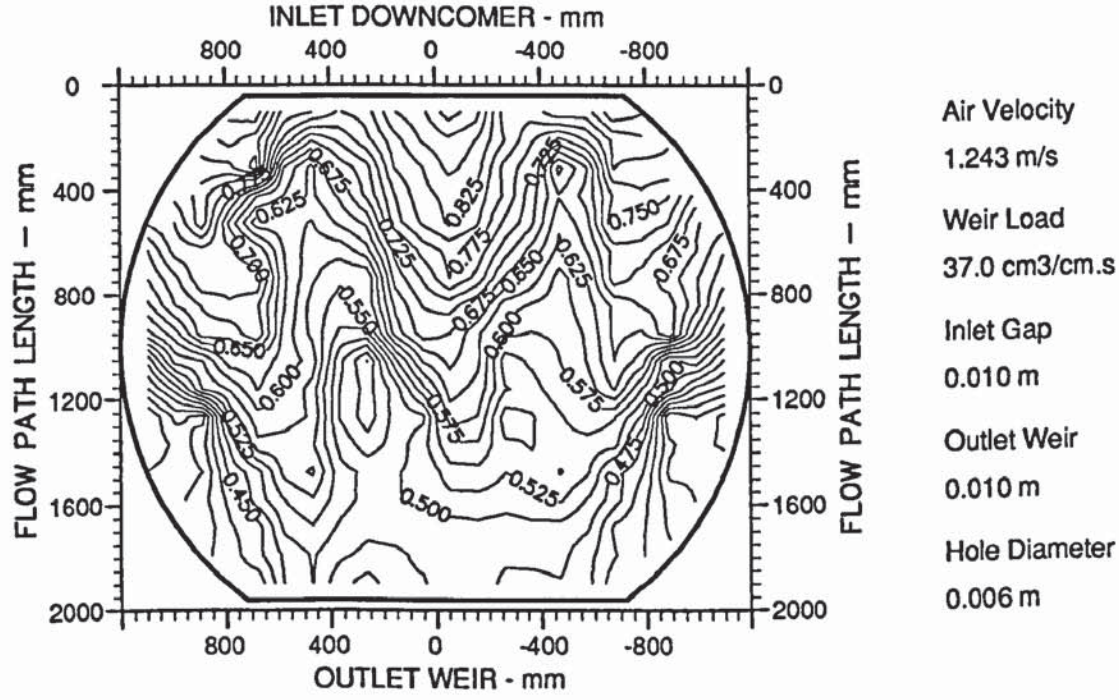

Figure A4.8 Two-dimensional reduced temperature profiles showing mixed or confused isotherms (designation M).

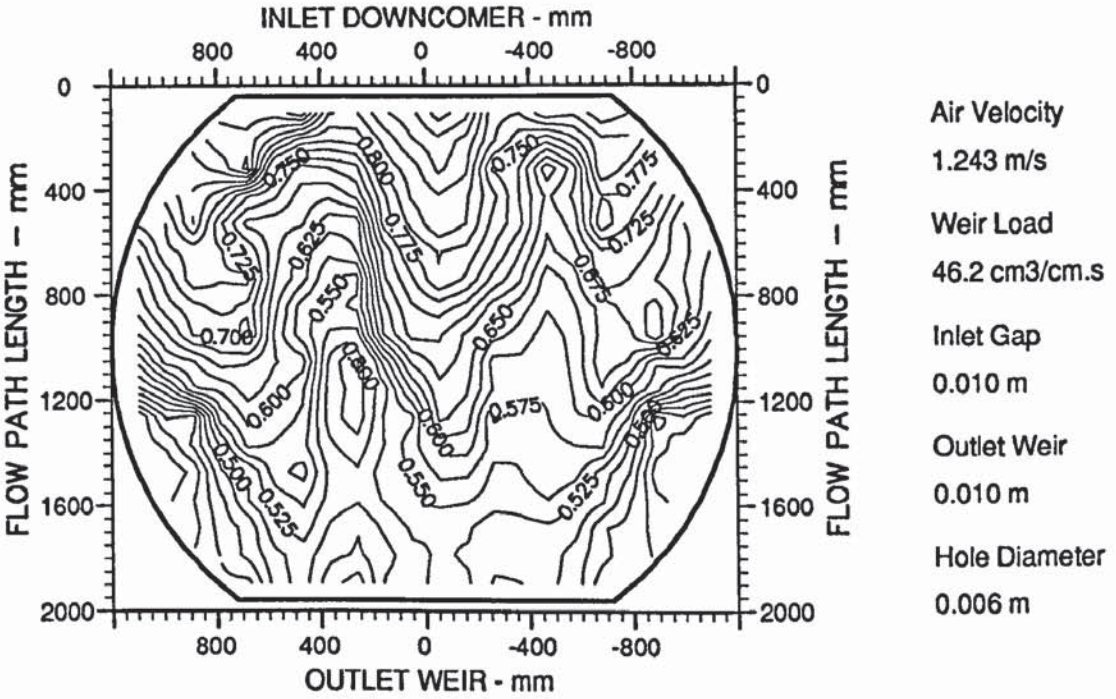

Figure A4.9 Two-dimensional reduced temperature profiles showing confused and "U-shaped" isotherms (designation M/U).

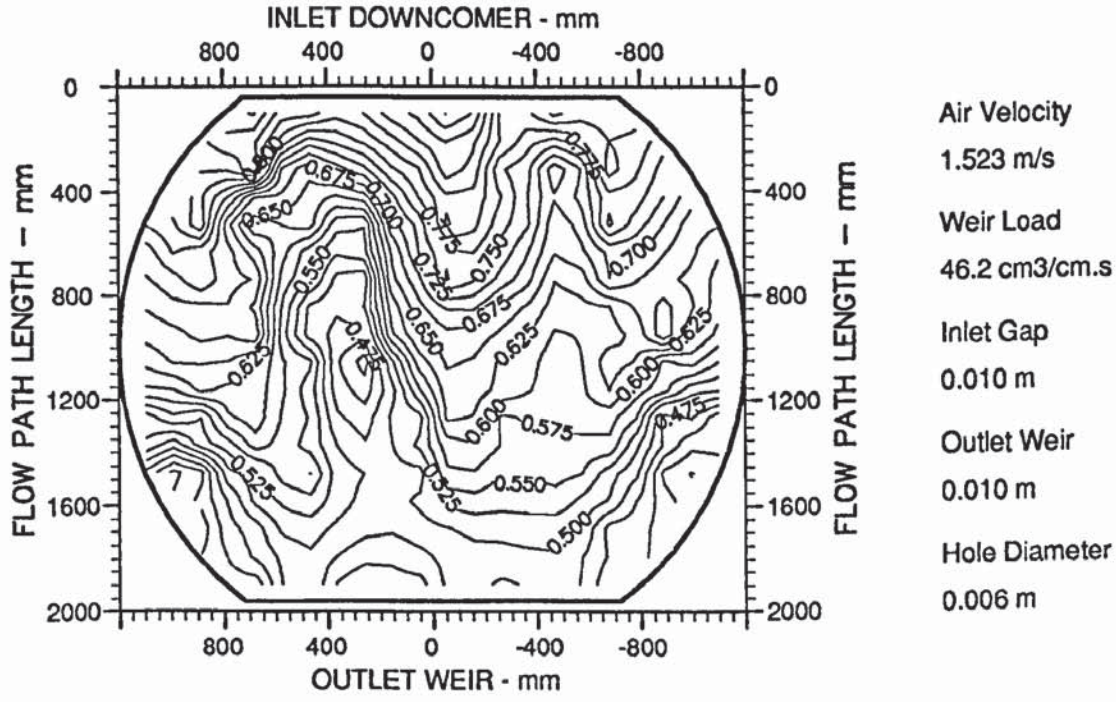

Figure A4.10 Two-dimensional reduced temperature profiles showing confused and "U-shaped" isotherms (designation M).

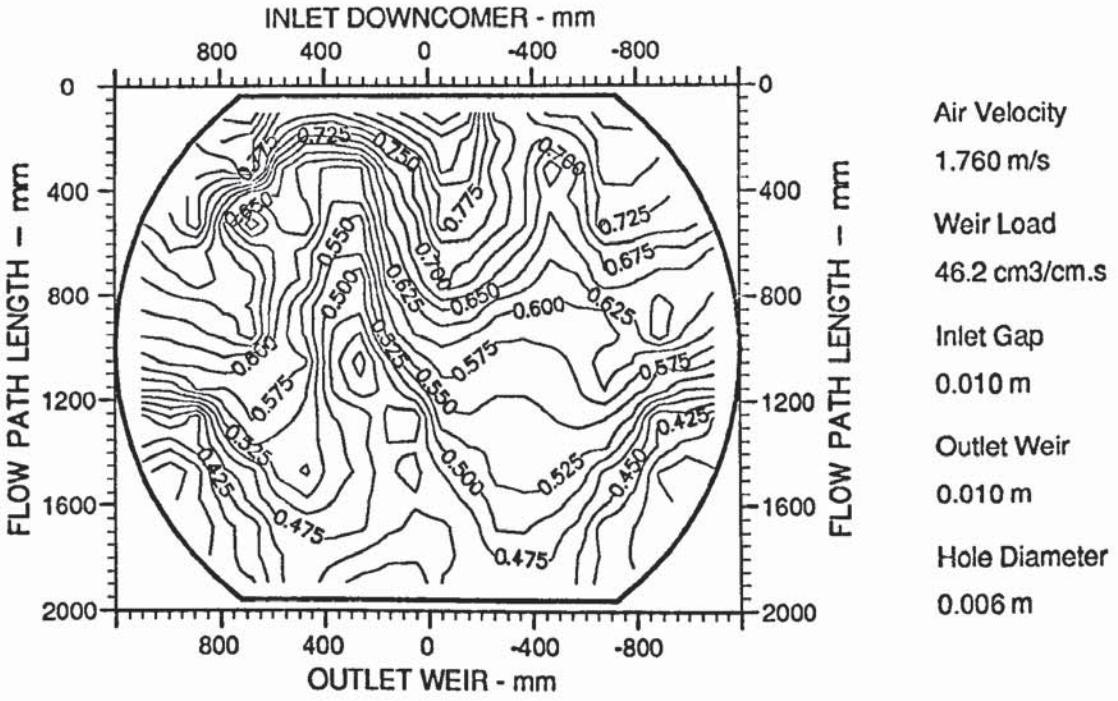

Figure A4.11 Two-dimensional reduced temperature profiles showing mixed or confused isotherms (designation M).

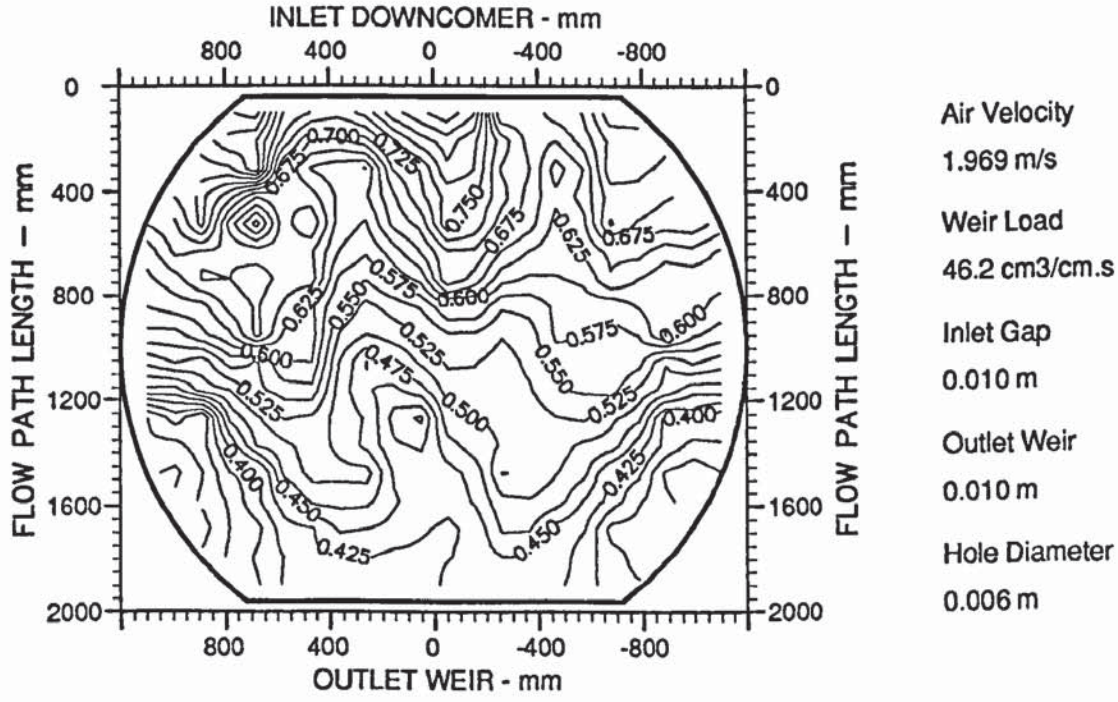

Figure A4.12 Two-dimensional reduced temperature profiles showing mixed or confused isotherms (designation M).

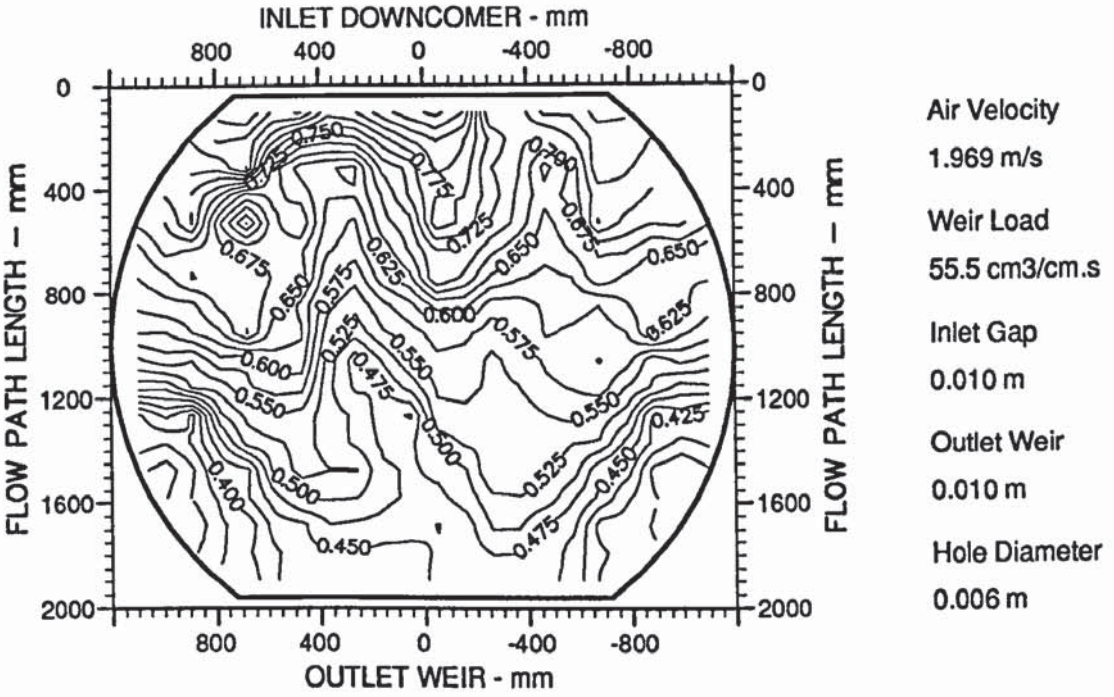

Figure A4.13 Two-dimensional reduced temperature profiles showing mixed or confused isotherms (designation M).

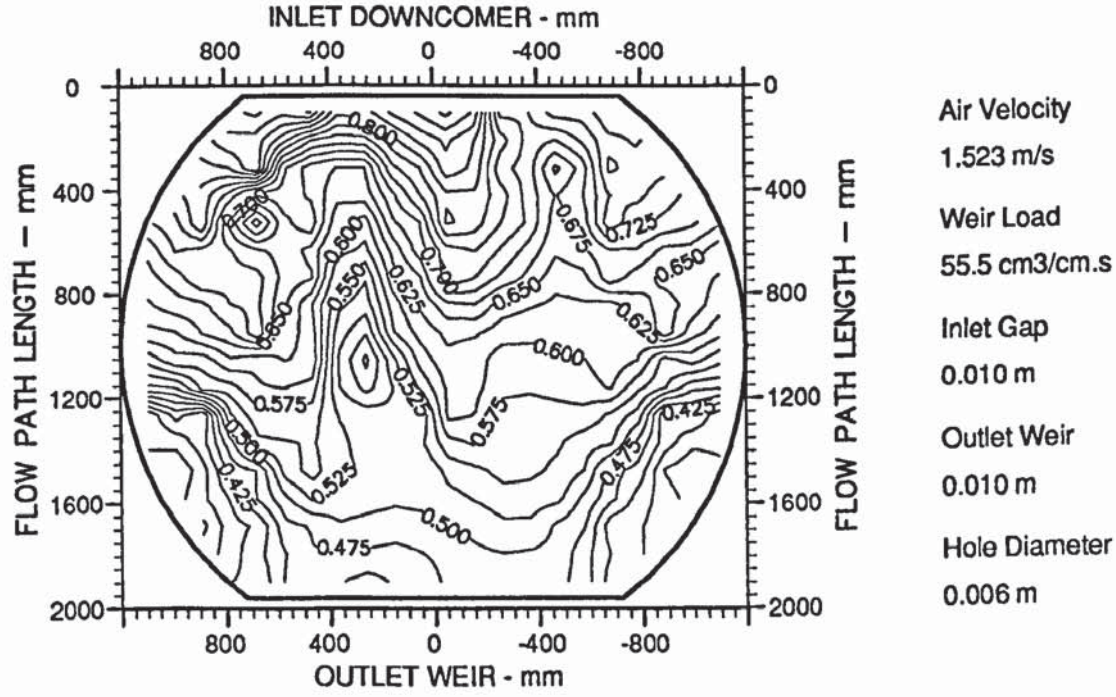

Figure A4.14 Two-dimensional reduced temperature profiles showing mixed or confused isotherms (designation M).

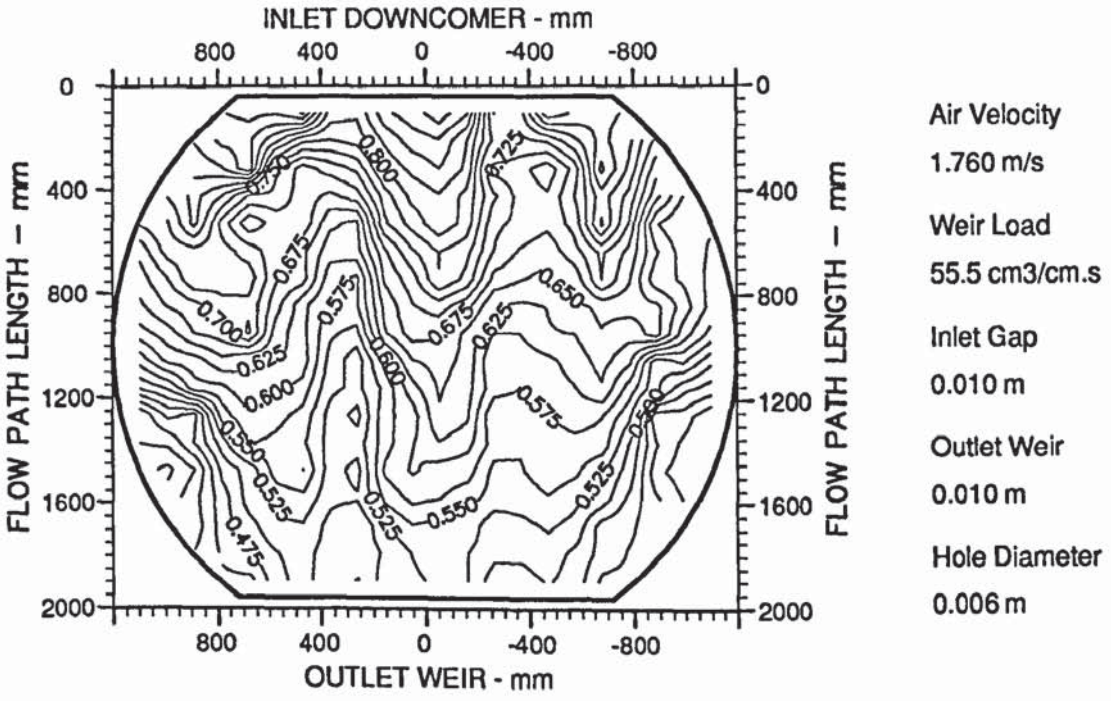

Figure A4.15 Two-dimensional reduced temperature profiles showing confused and "U-shaped" isotherms (designation M/U).

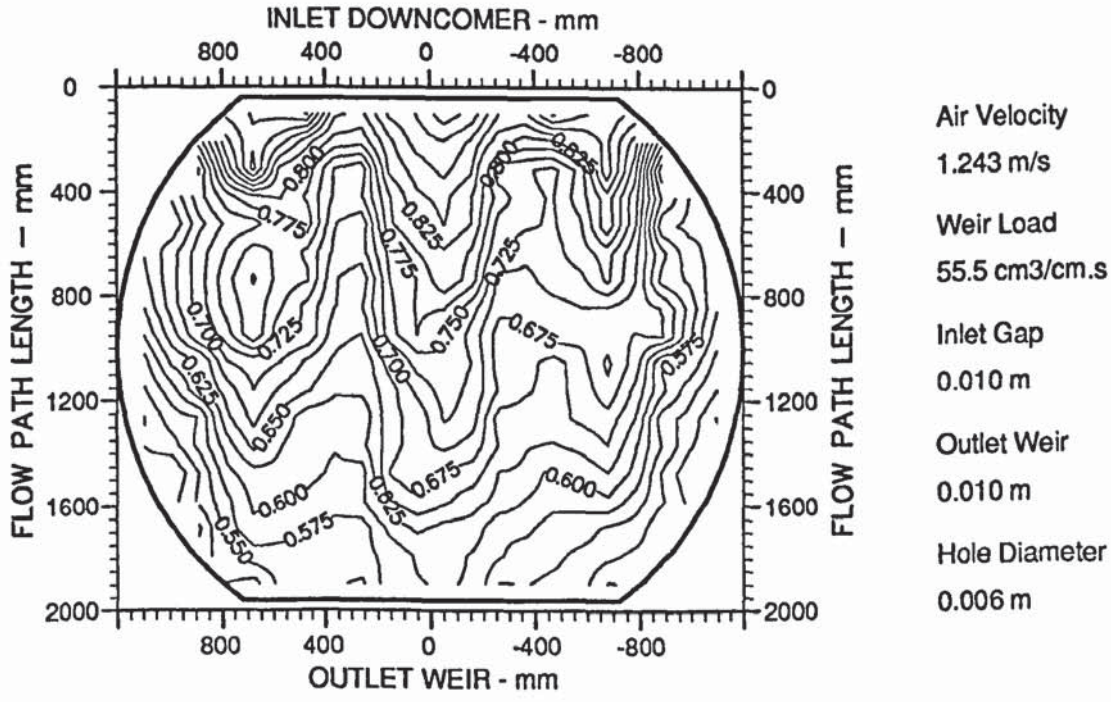

Figure A4.16 Two-dimensional reduced temperature profiles showing confused and "U-shaped" isotherms (designation M/U).

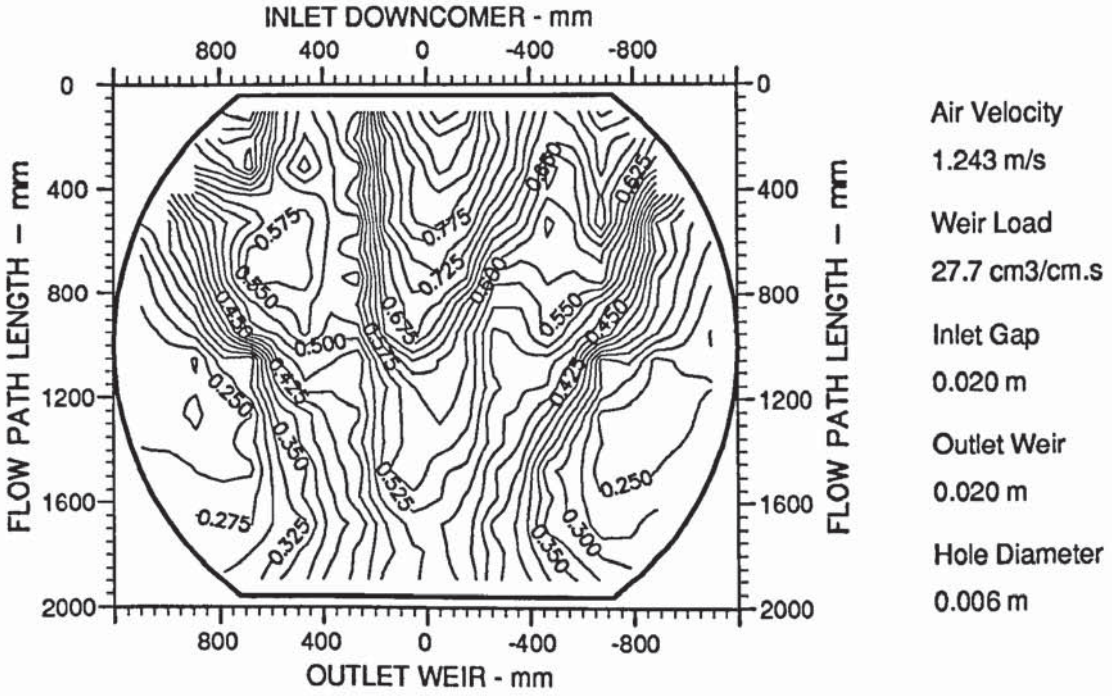

Figure A4.17 Two-dimensional reduced temperature profiles showing confused and "U-shaped" isotherms (designation M/U).

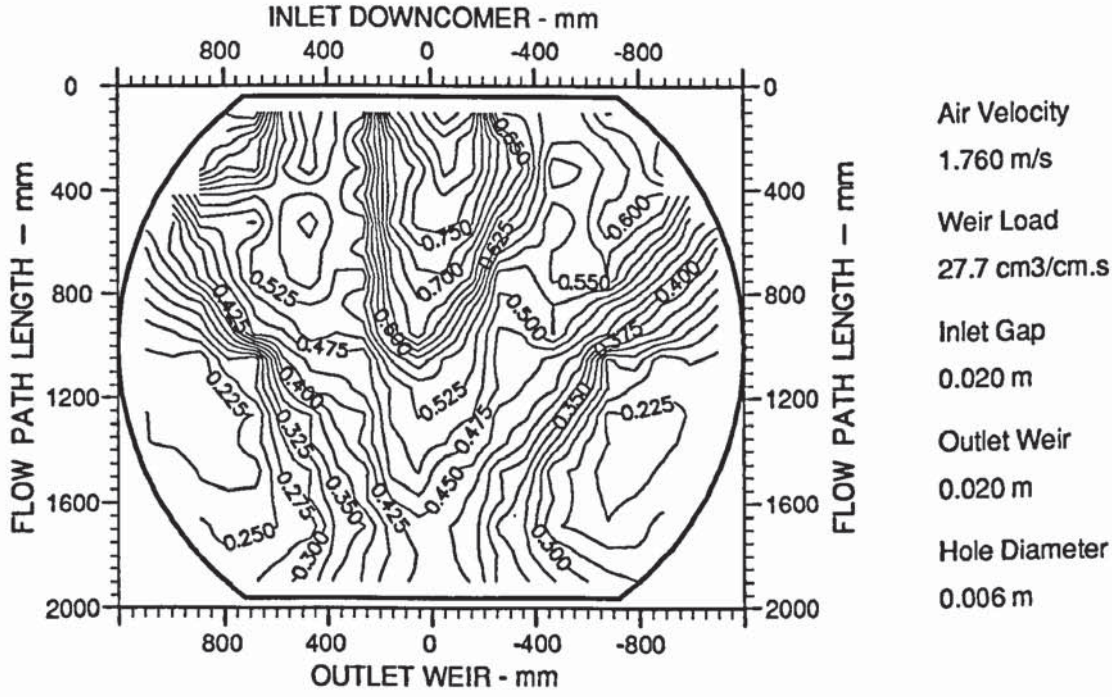

Figure A4.18 Two-dimensional reduced temperature profiles showing confused and "U-shaped" isotherms (designation M/U).

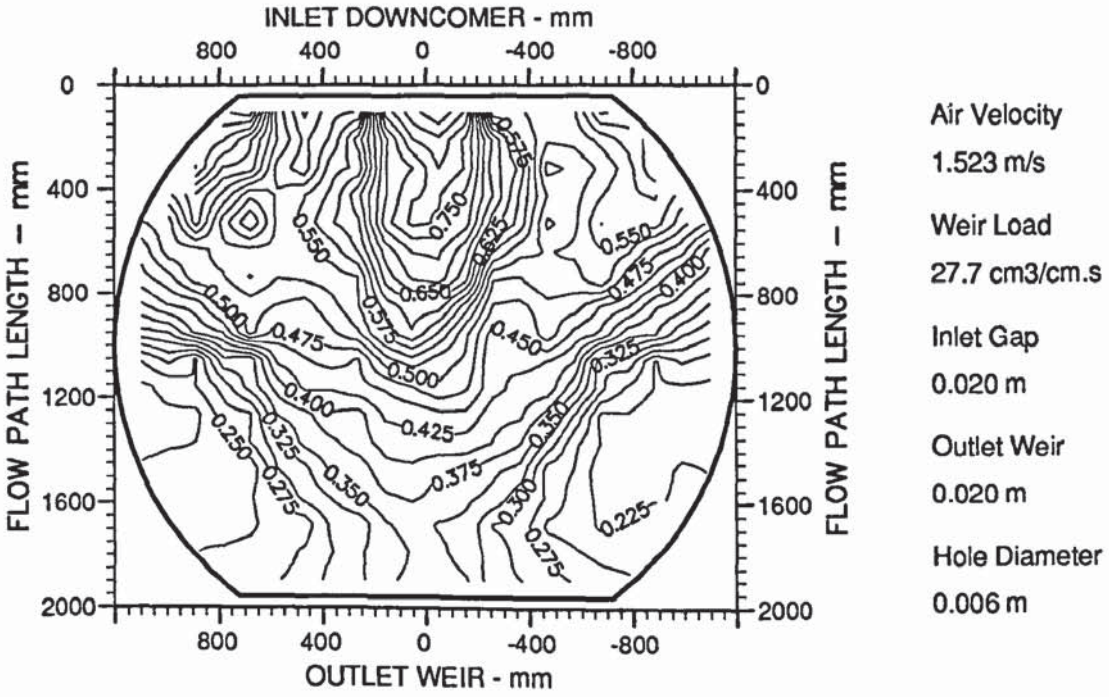

Figure A4.19 Two-dimensional reduced temperature profiles showing confused and "U-shaped" isotherms (designation M/U).

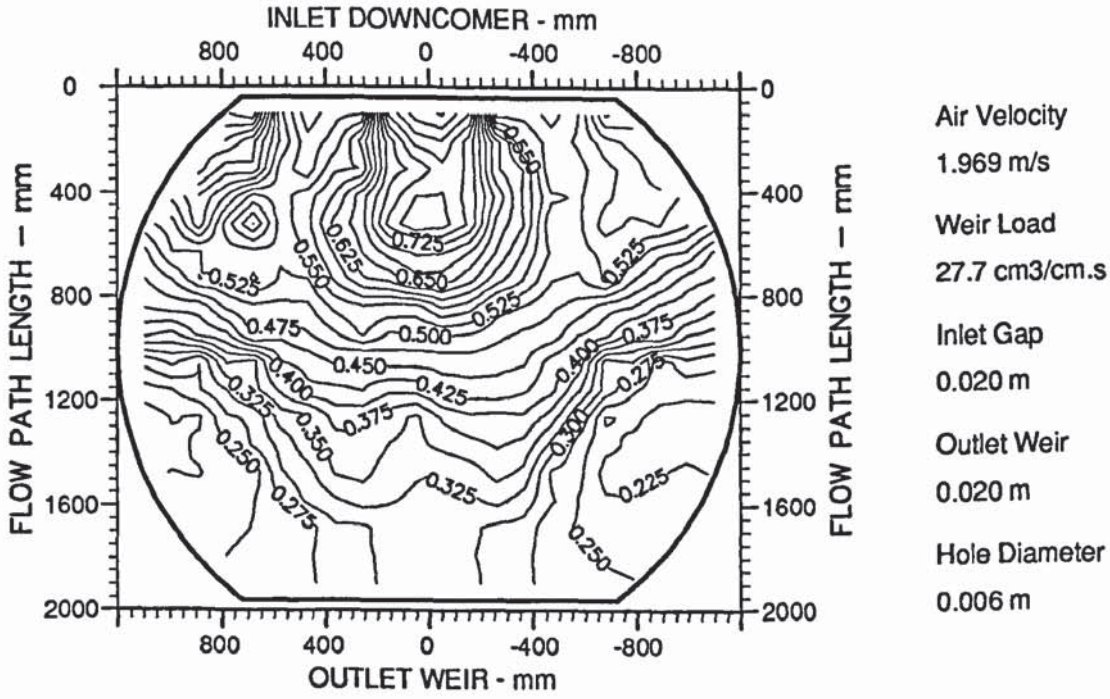

Figure A4.20 Two-dimensional reduced temperature profiles showing mixed or confused isotherms (designation M).

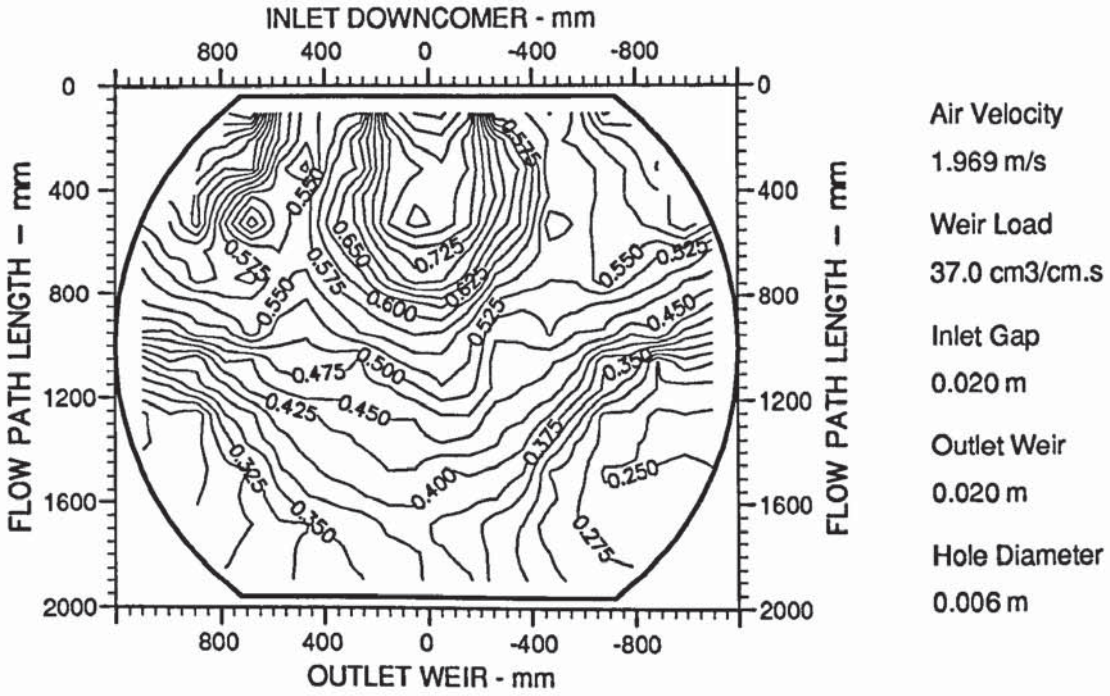

Figure A4.21 Two-dimensional reduced temperature profiles showing confused and "U-shaped" isotherms (designation M).

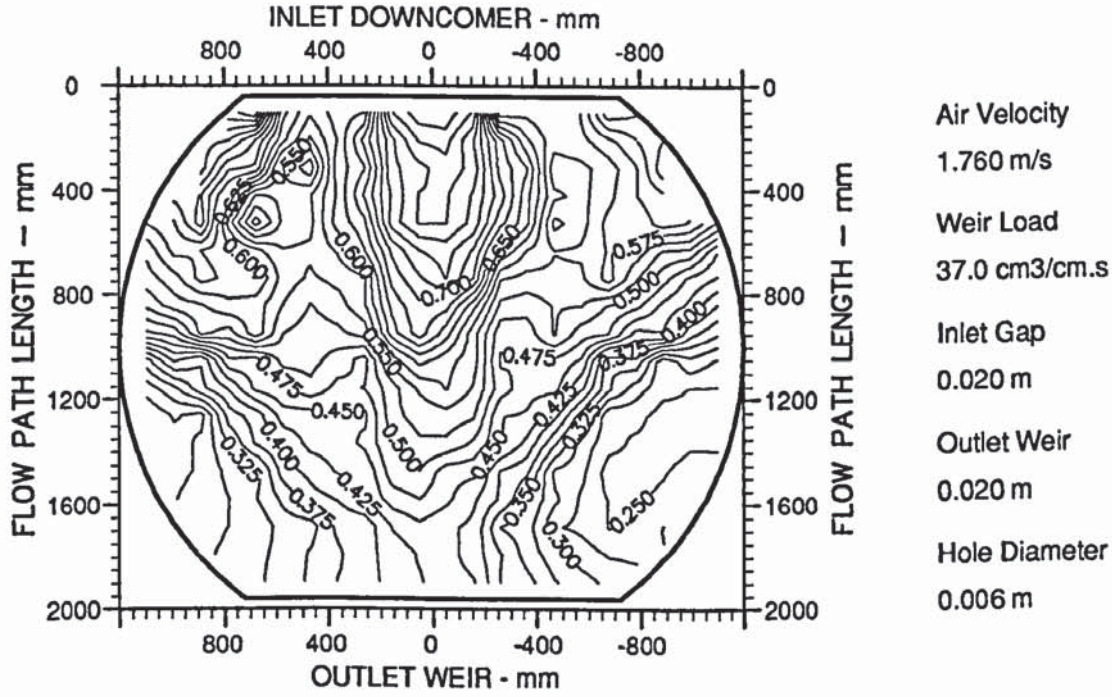

Figure A4.22 Two-dimensional reduced temperature profiles showing confused and "U-shaped" isotherms (designation M/U).

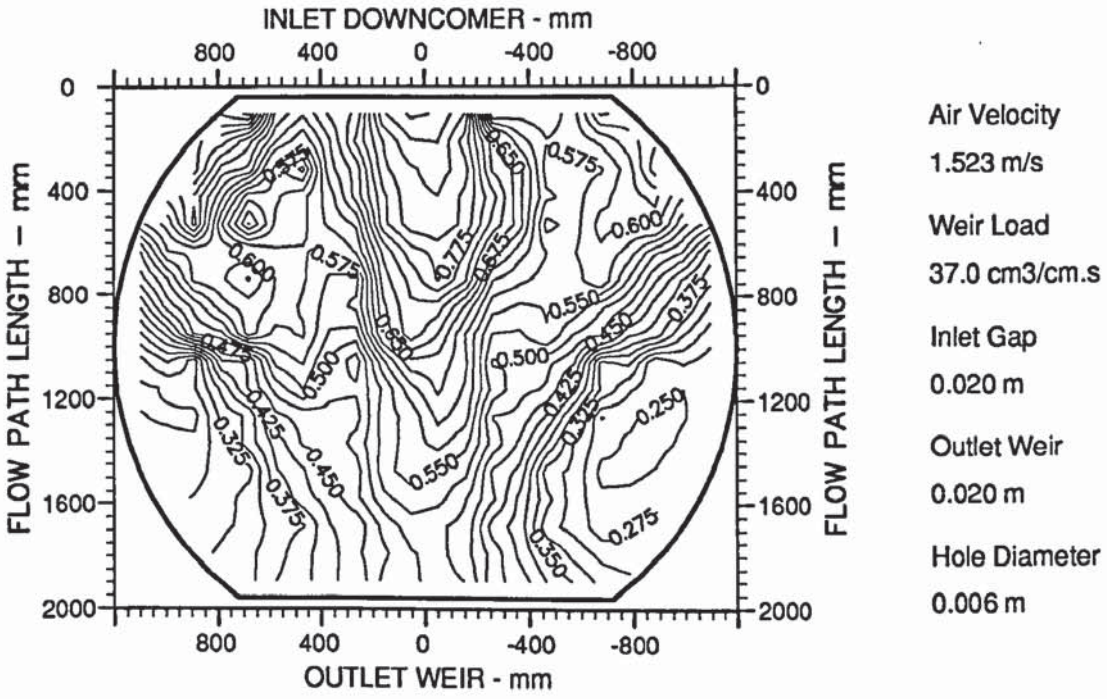

Figure A4.23 Two-dimensional reduced temperature profiles showing confused and "U-shaped" isotherms (designation M/U).

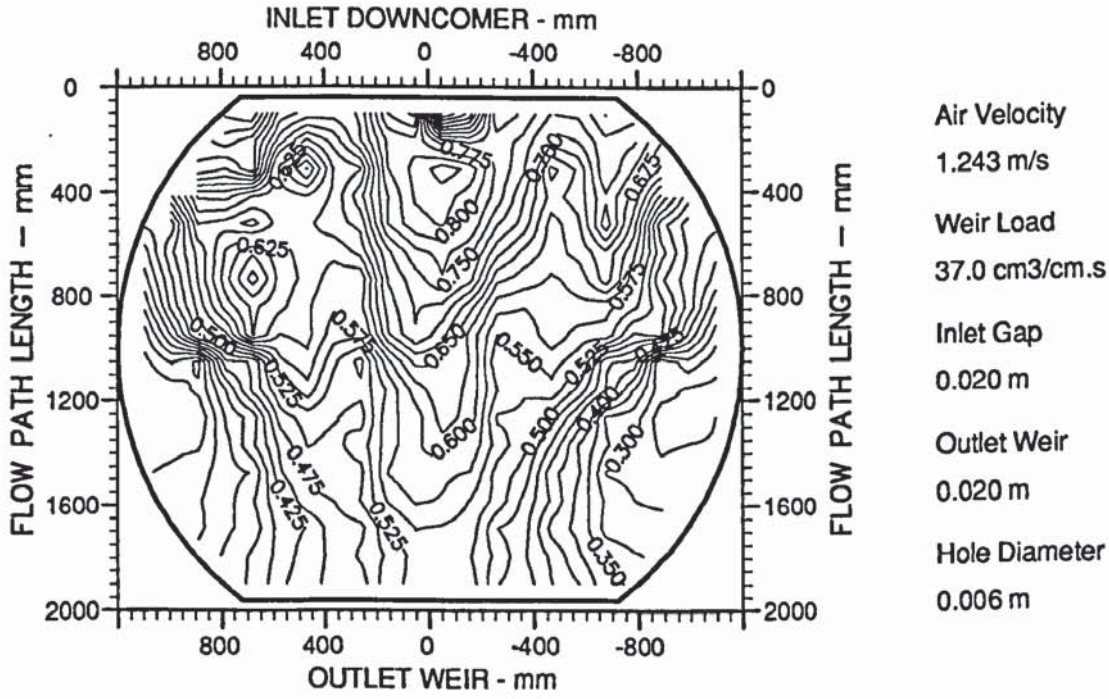

Figure A4.24 Two-dimensional reduced temperature profiles showing confused and "U-shaped" isotherms (designation M/U).

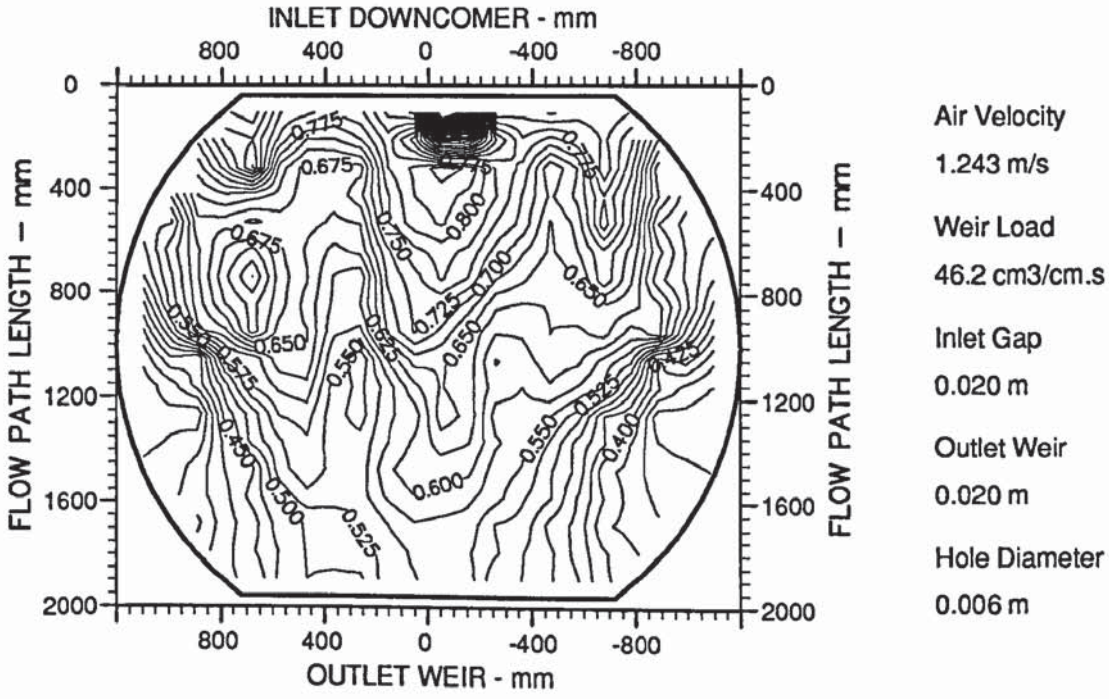

Figure A4.25 Two-dimensional reduced temperature profiles showing mixed or confused isotherms (designation M).

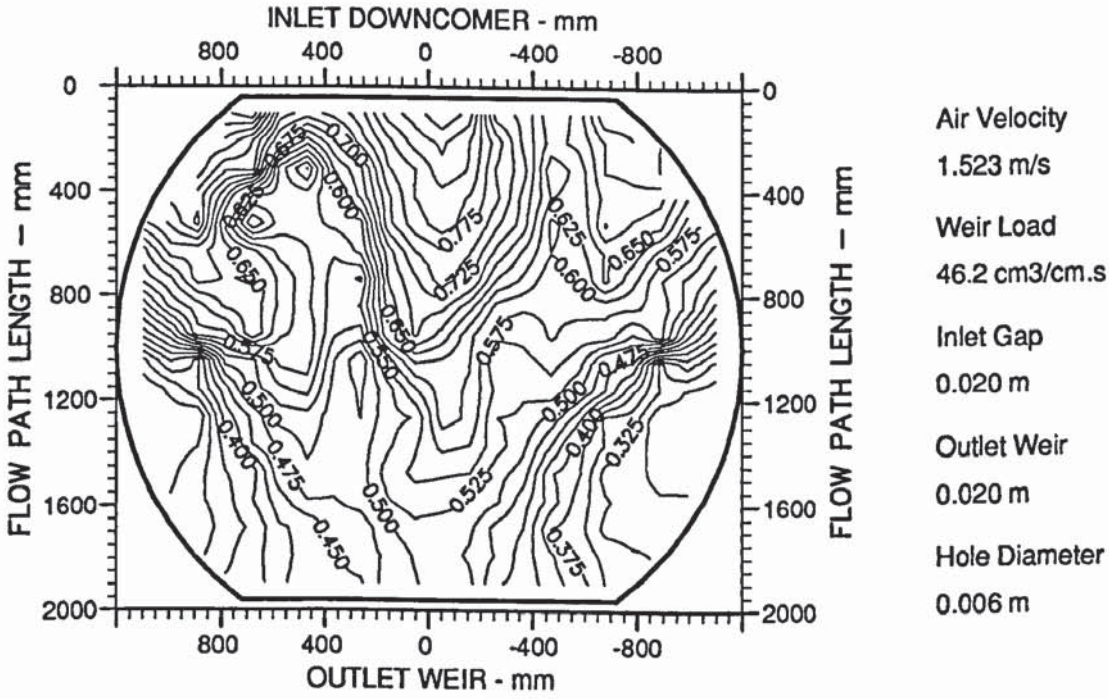

Figure A4.26 Two-dimensional reduced temperature profiles showing mixed or confused isotherms (designation M).

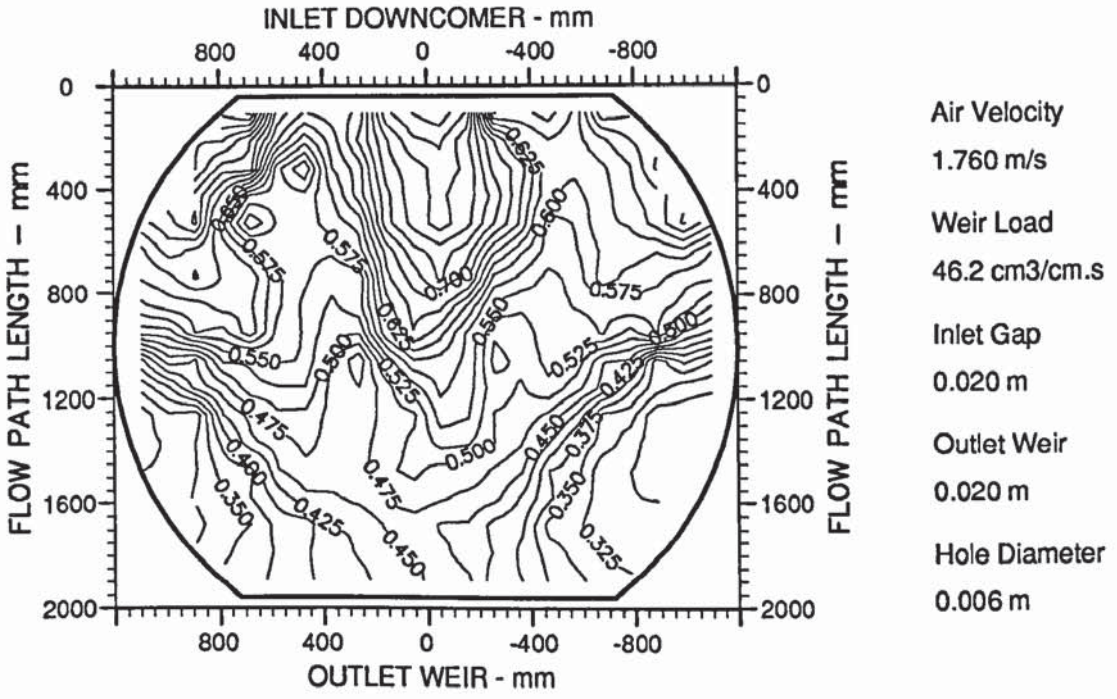

Figure A4.27 Two-dimensional reduced temperature profiles showing mixed or confused isotherms (designation M).

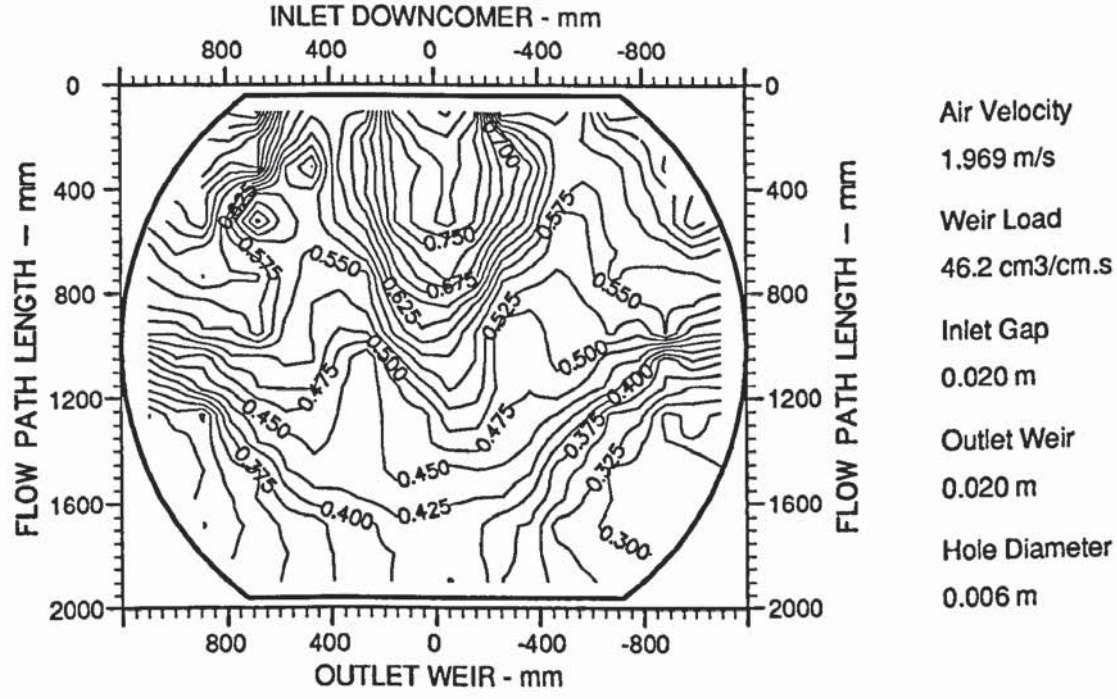

Figure A4.28 Two-dimensional reduced temperature profiles showing mixed or confused isotherms (designation M).

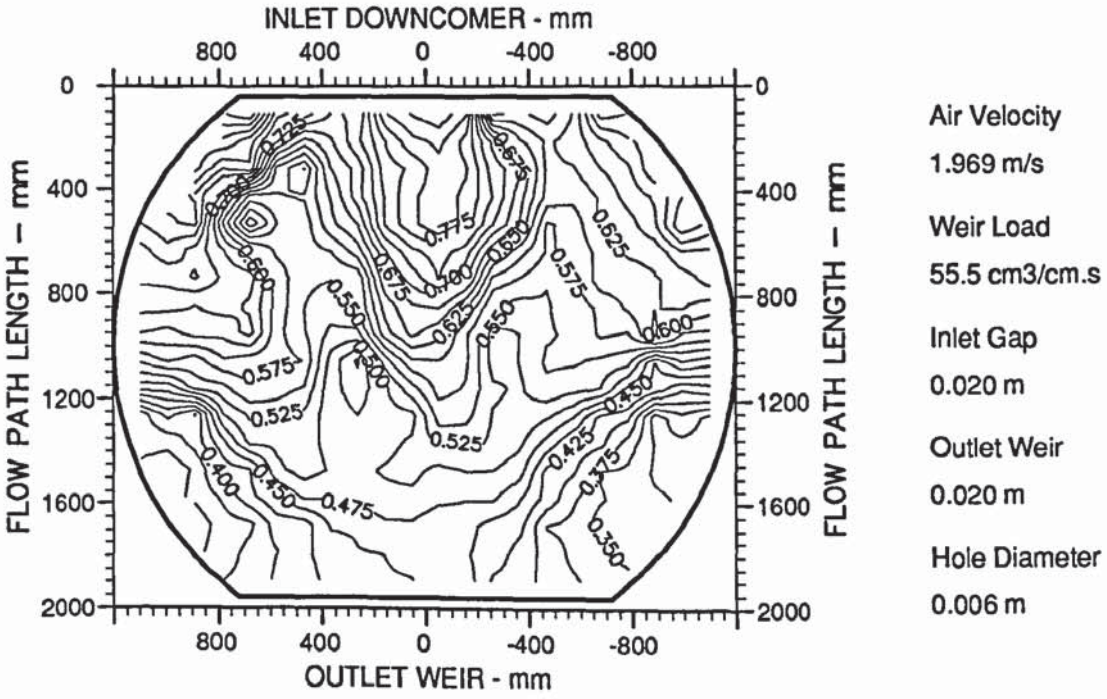

Figure A4.29 Two-dimensional reduced temperature profiles showing mixed or confused isotherms (designation M).

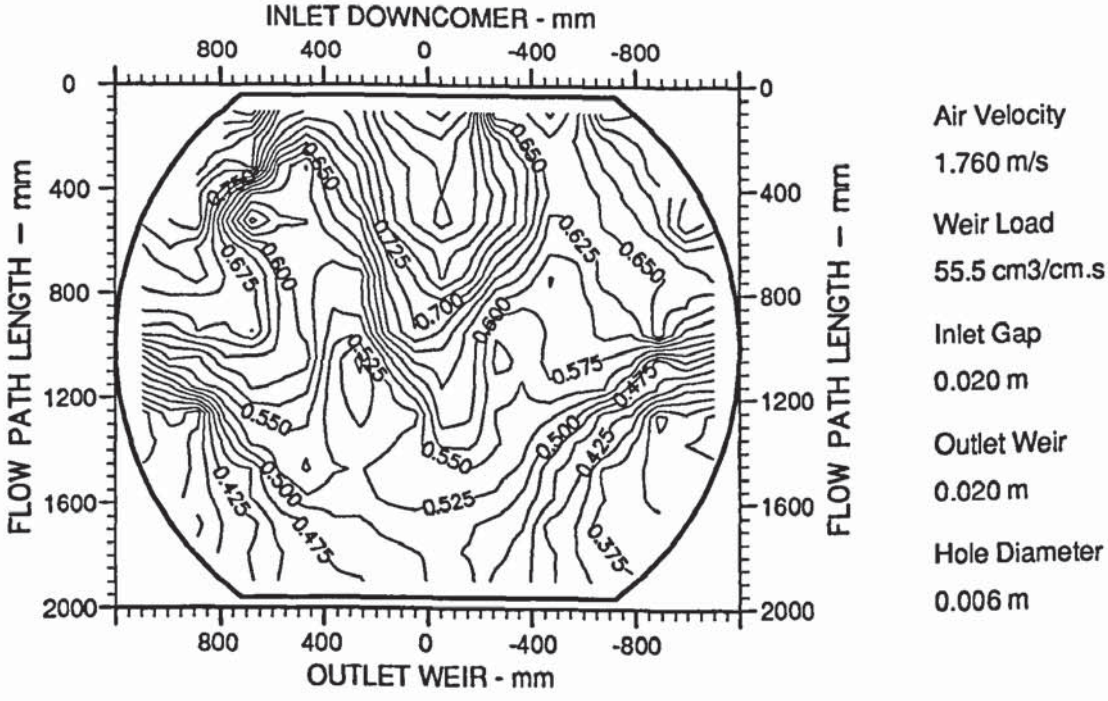

Figure A4.30 Two-dimensional reduced temperature profiles showing mixed or confused isotherms (designation M).

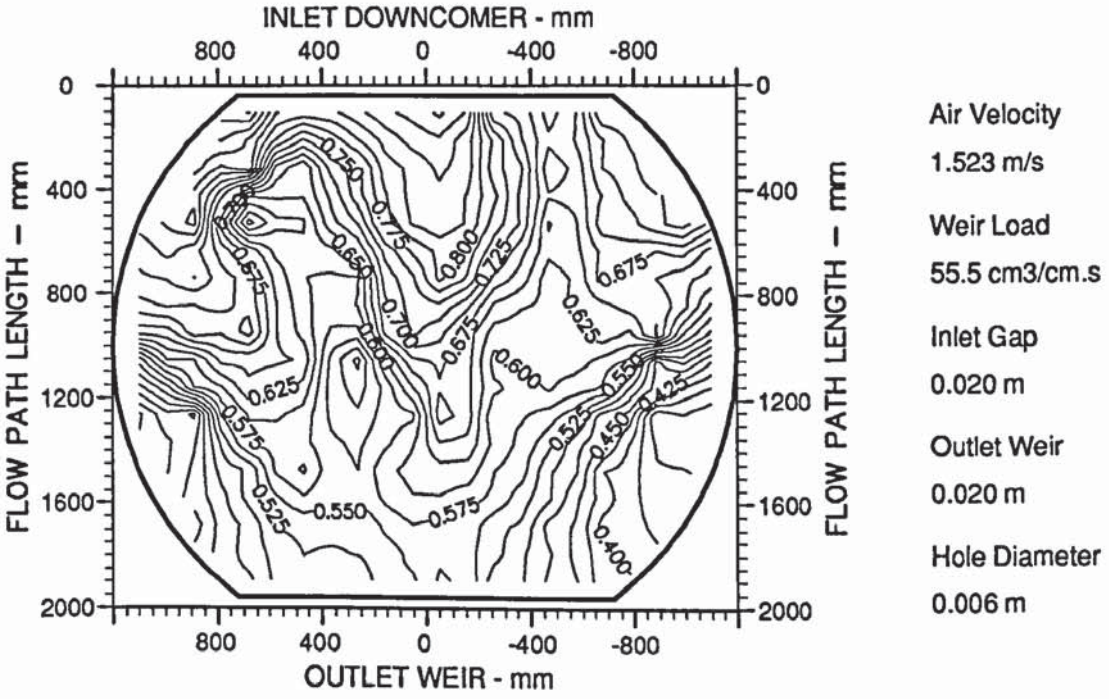

Figure A4.31 Two-dimensional reduced temperature profiles showing mixed or confused isotherms (designation M).

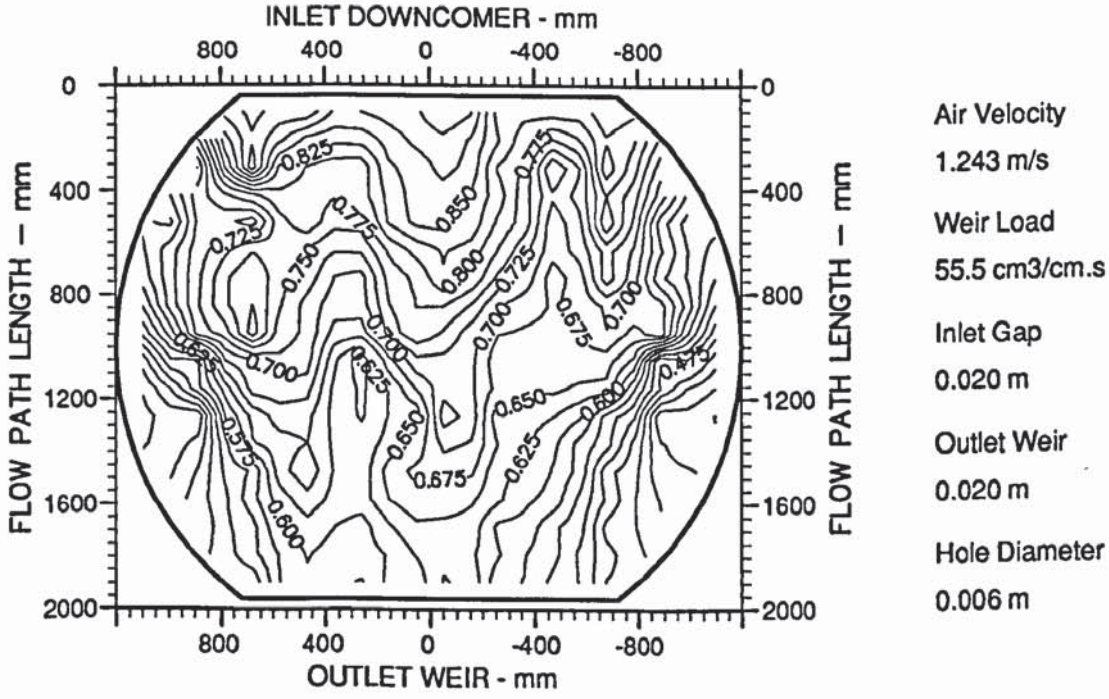

Figure A4.32 Two-dimensional reduced temperature profiles showing mixed or confused isotherms (designation M).

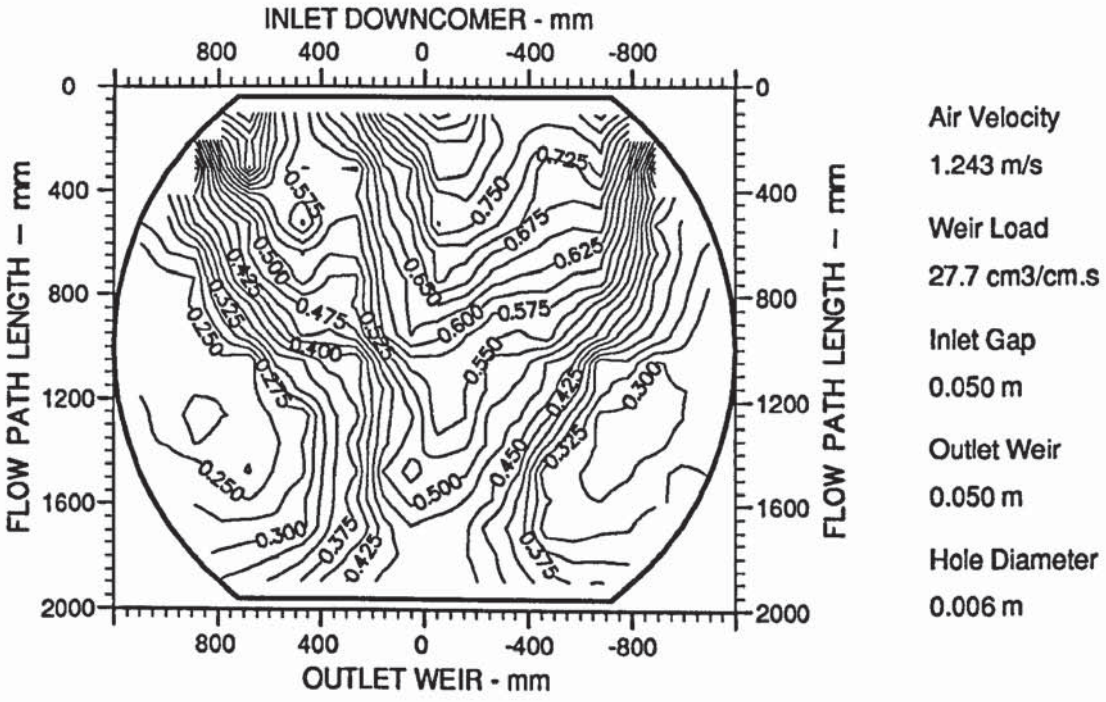

Figure A4.33 Two-dimensional reduced temperature profiles showing "U-shaped" and closed looped isotherms (designation UC).

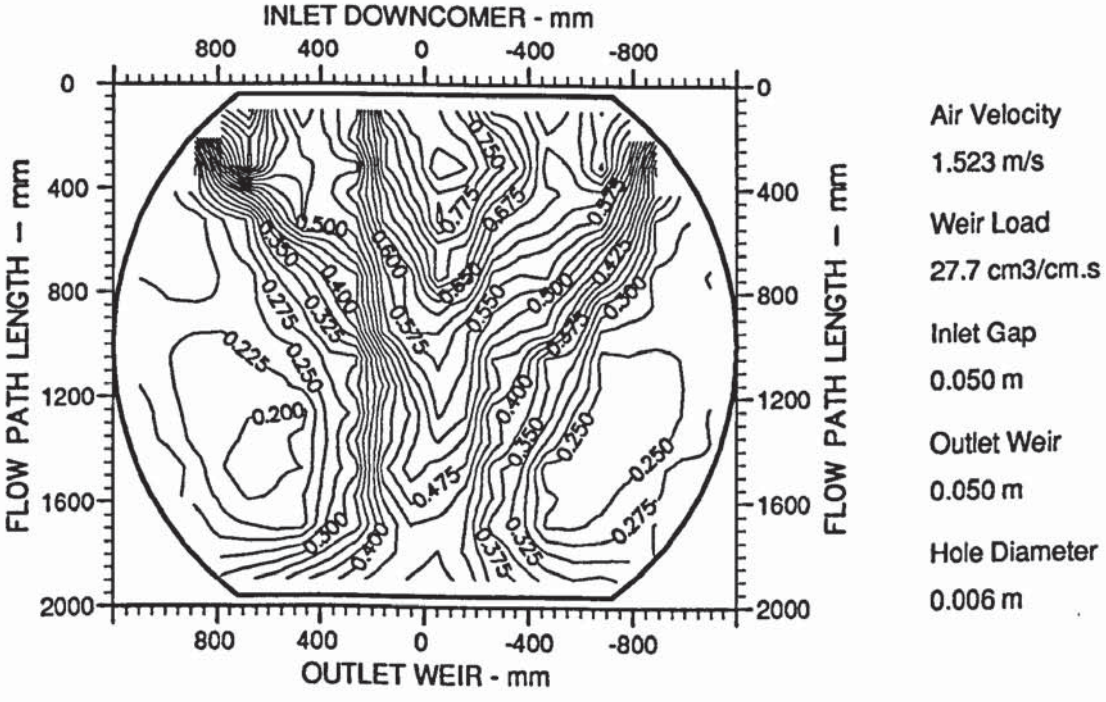

Figure A4.34 Two-dimensional reduced temperature profiles showing "U-shaped" and closed looped isotherms (designation UC).

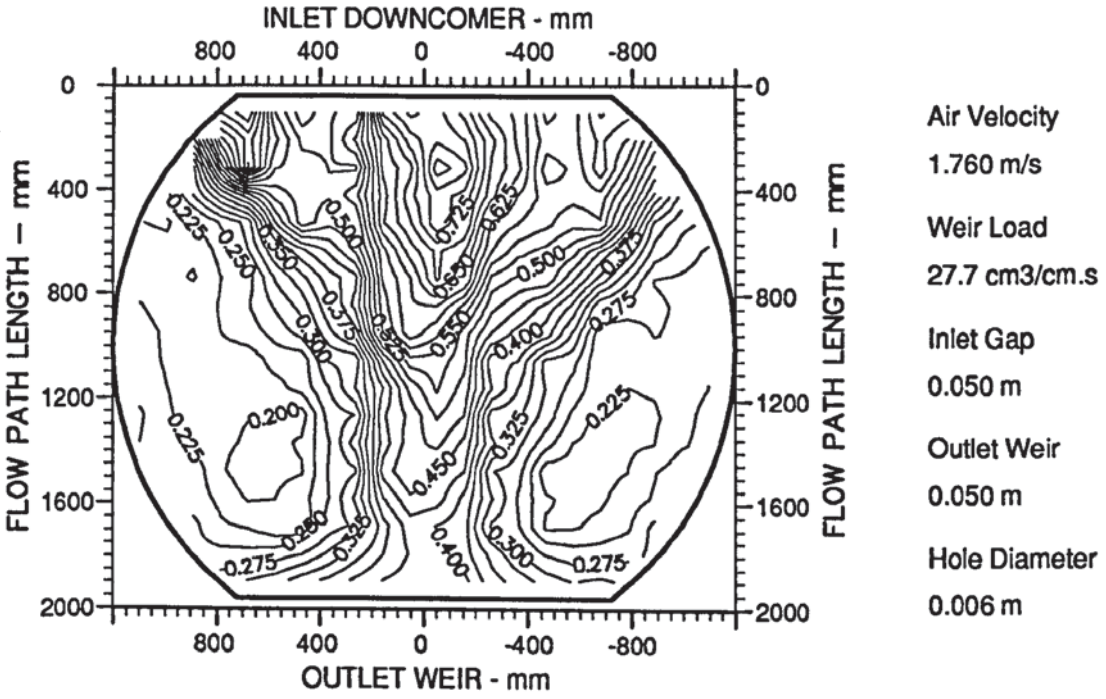

Figure A4.35 Two-dimensional reduced temperature profiles showing "U-shaped" and closed looped isotherms (designation UC).

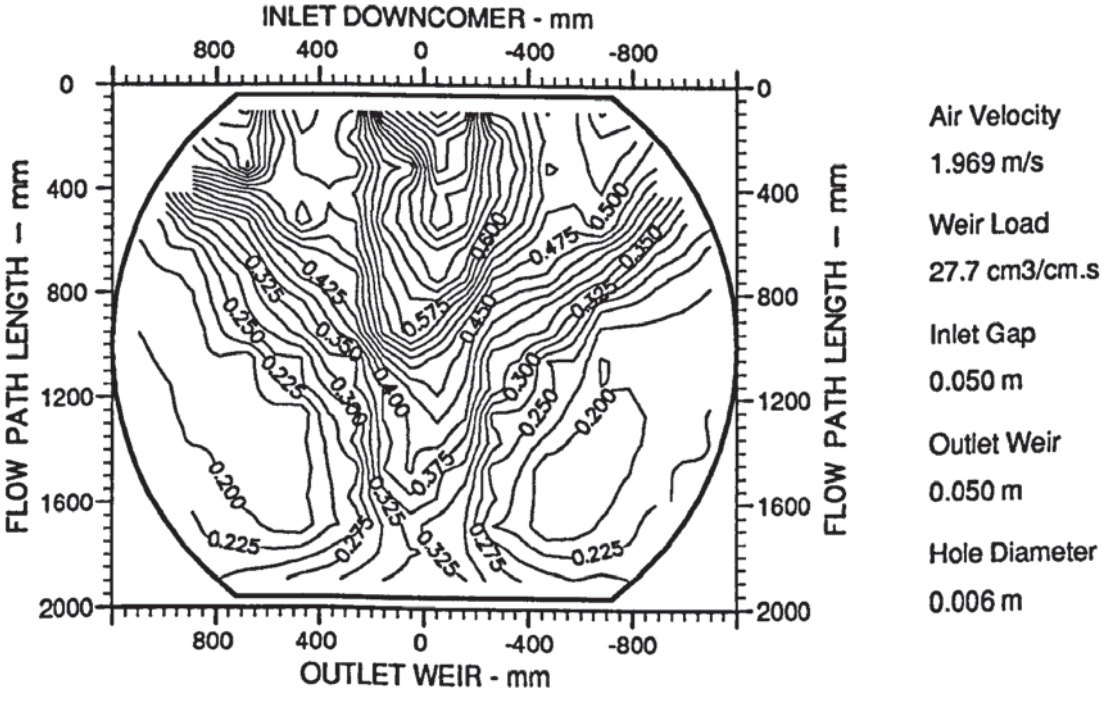

Figure A4.36 Two-dimensional reduced temperature profiles showing "U-shaped" and closed looped isotherms (designation UC).

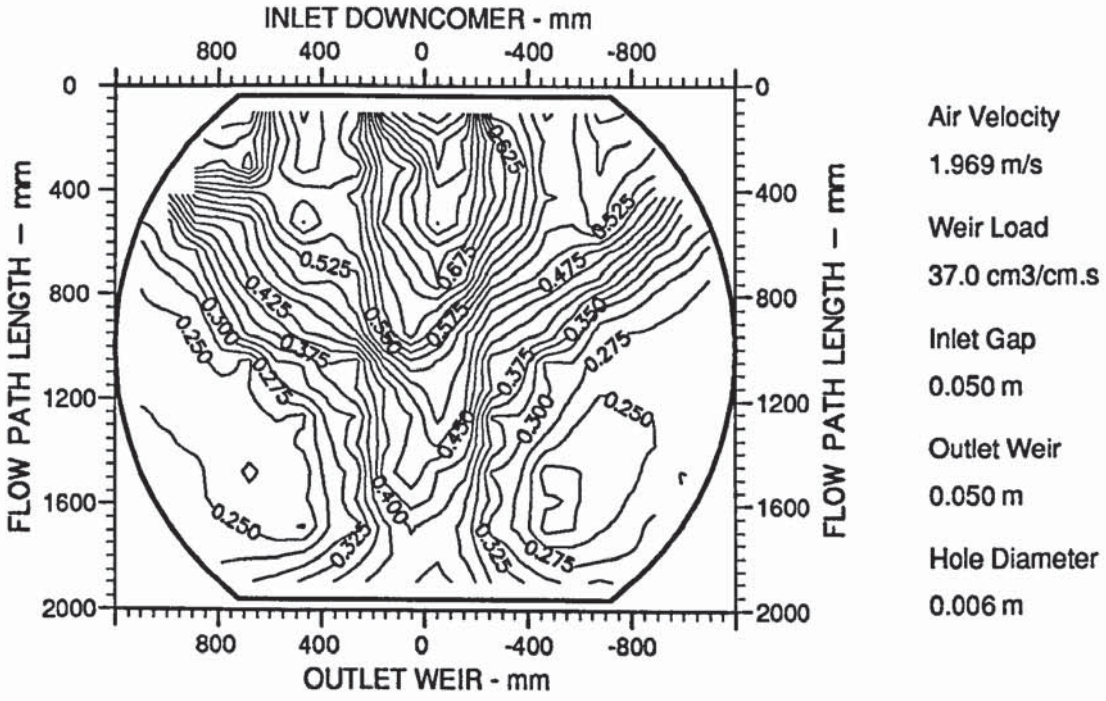

Figure A4.37 Two-dimensional reduced temperature profiles showing "U-shaped" and closed looped isotherms (designation UC).

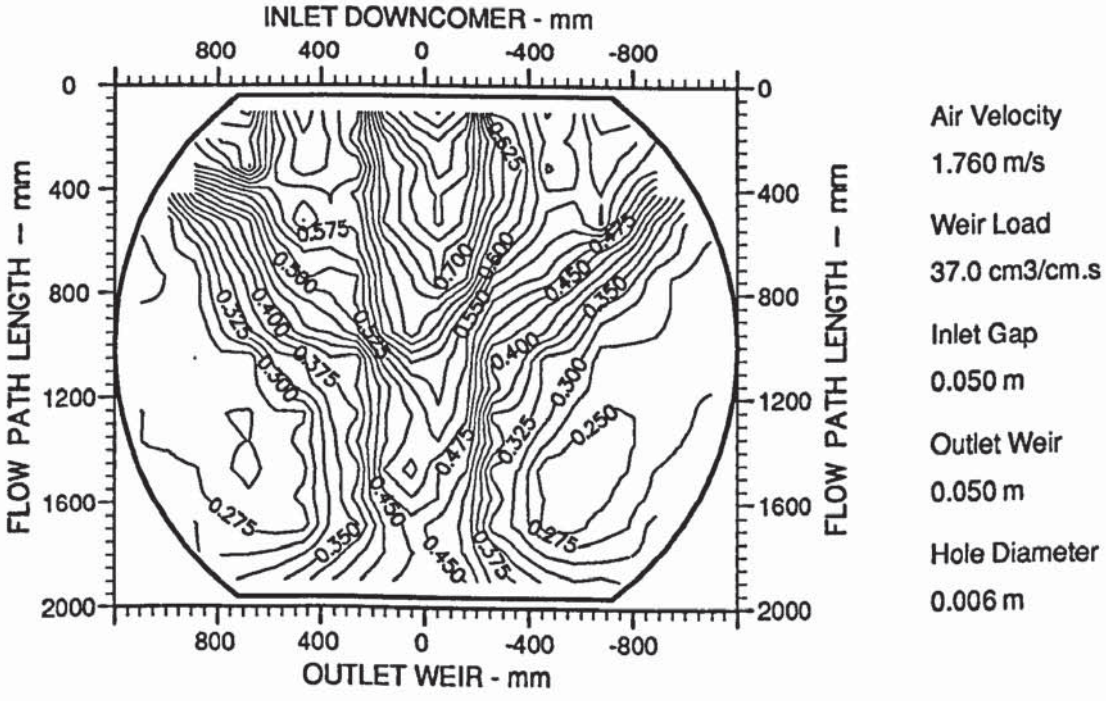

Figure A4.38 Two-dimensional reduced temperature profiles showing "U-shaped" and closed looped isotherms (designation UC).

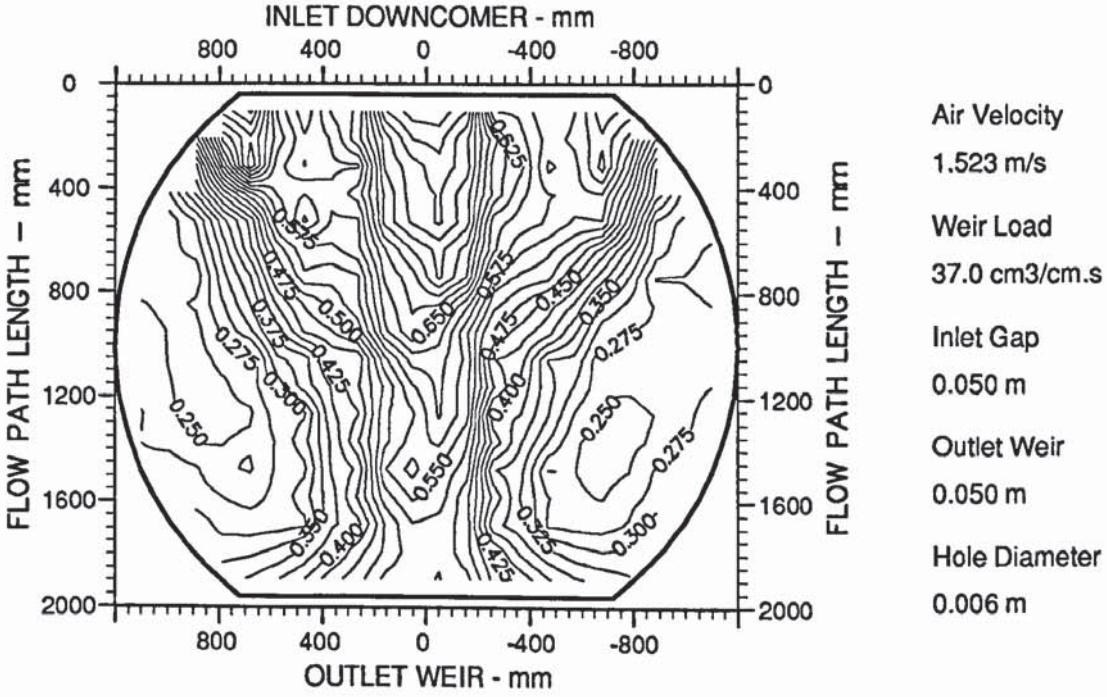

Figure A4.39 Two-dimensional reduced temperature profiles showing "U-shaped" and closed looped isotherms (designation UC).

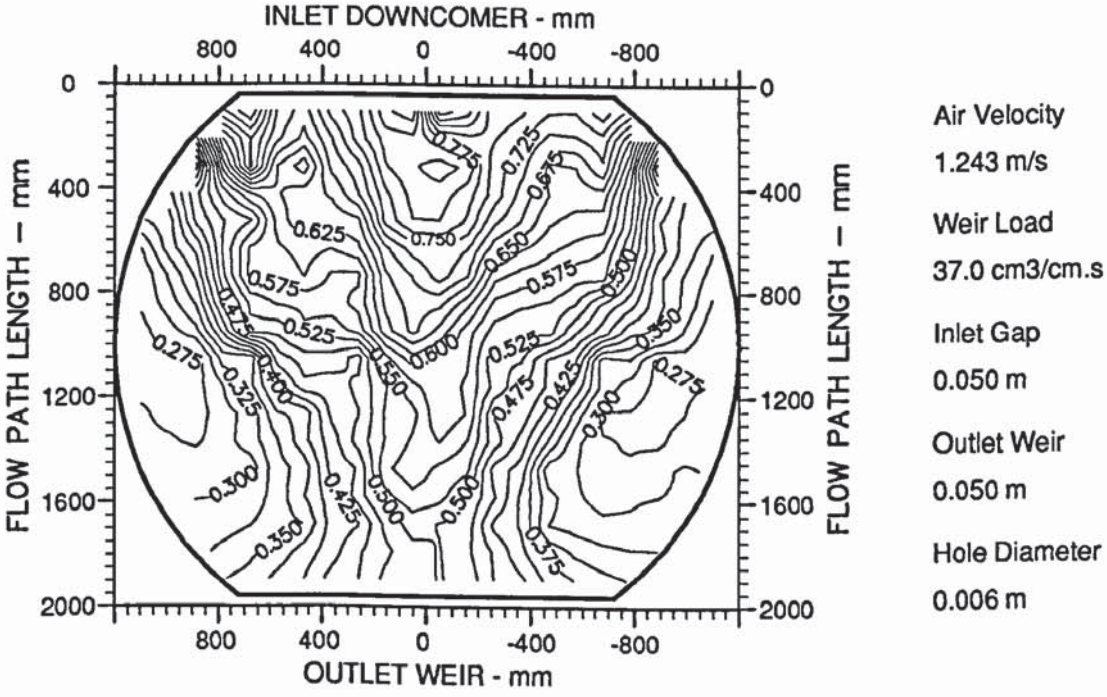

Figure A4.40 Two-dimensional reduced temperature profiles showing confused and "U-shaped" isotherms (designation M/U).

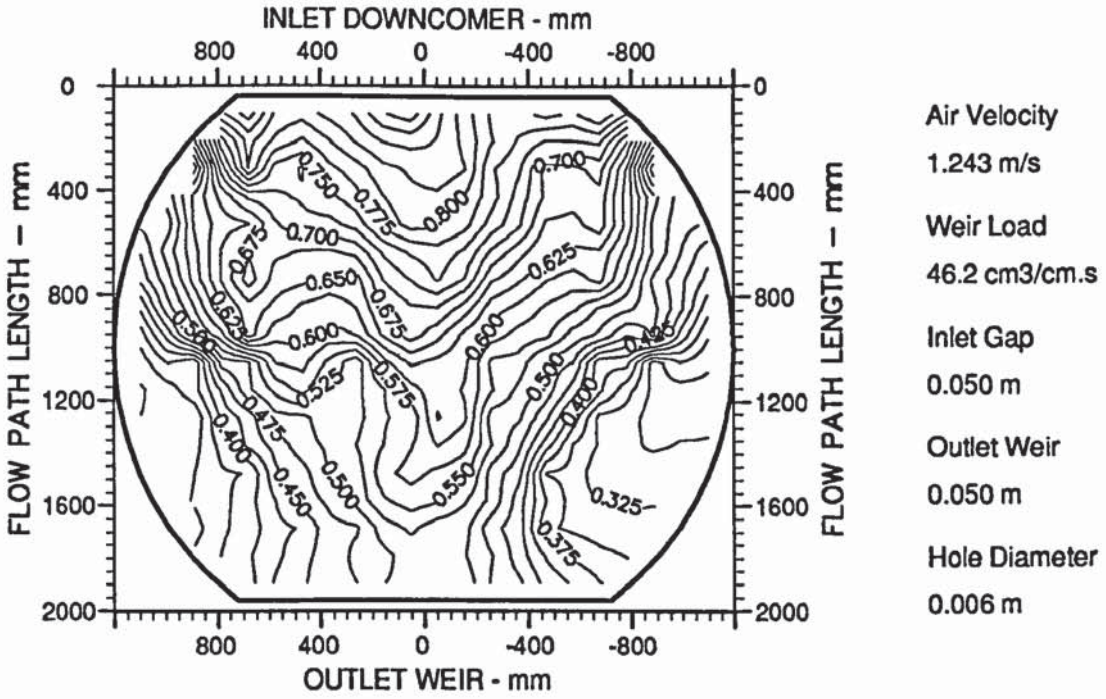

Figure A4.41 Two-dimensional reduced temperature profiles showing mixed or confused isotherms (designation M).

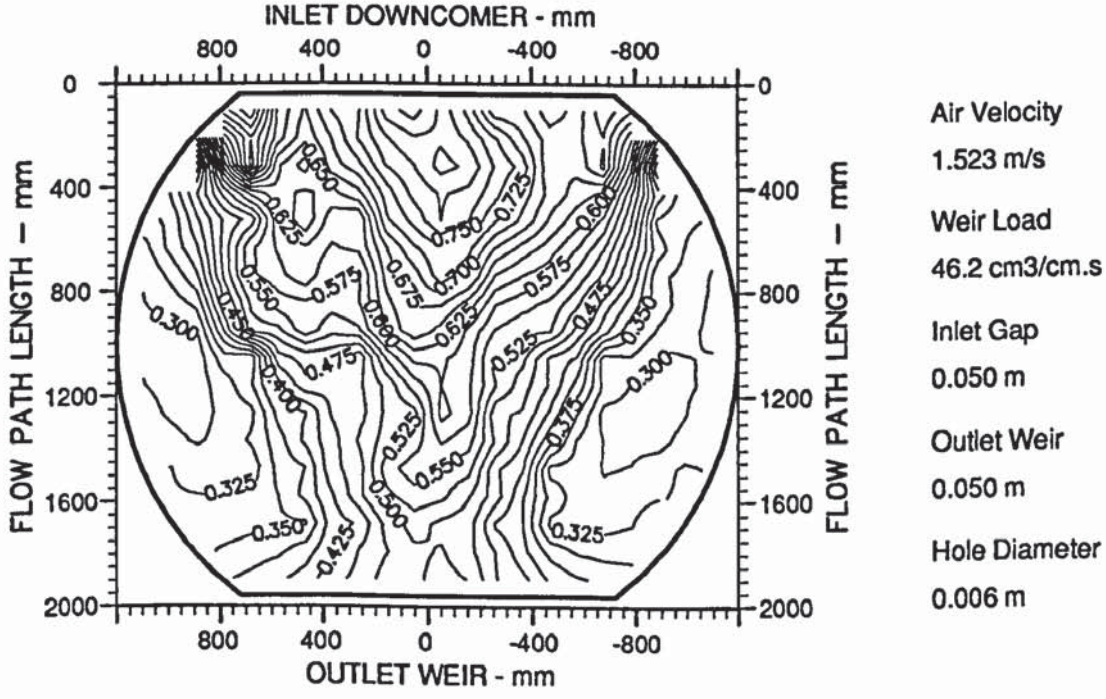

Figure A4.42 Two-dimensional reduced temperature profiles showing "U-shaped" and closed looped isotherms (designation UC).

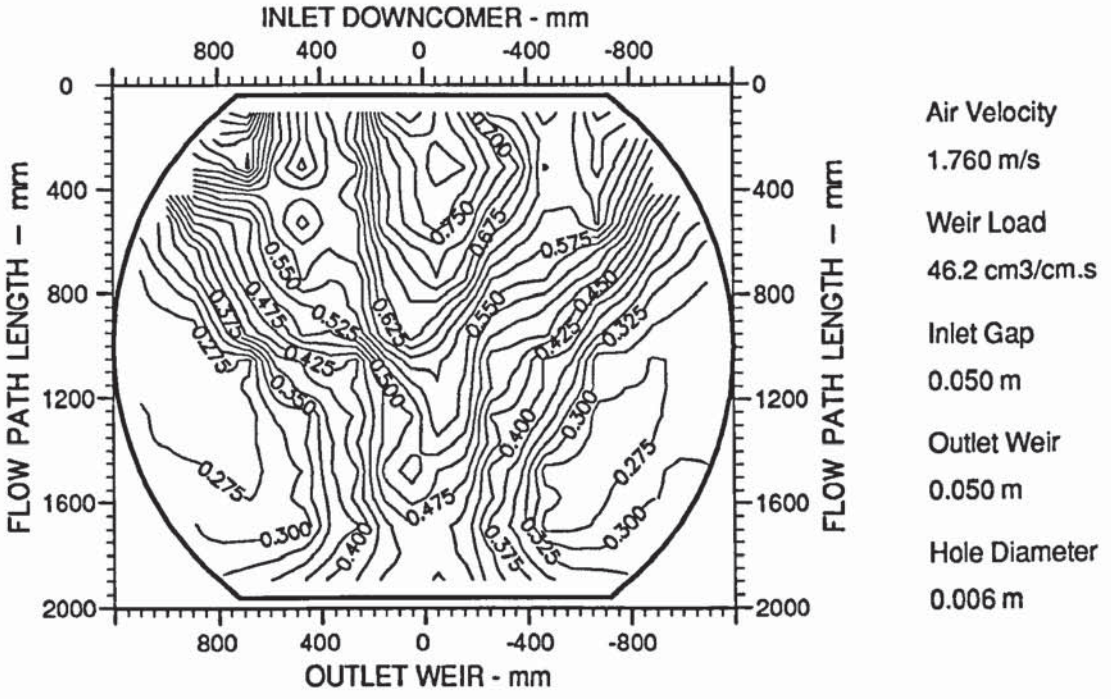

Figure A4.43 Two-dimensional reduced temperature profiles showing "U-shaped" and closed looped isotherms (designation UC).

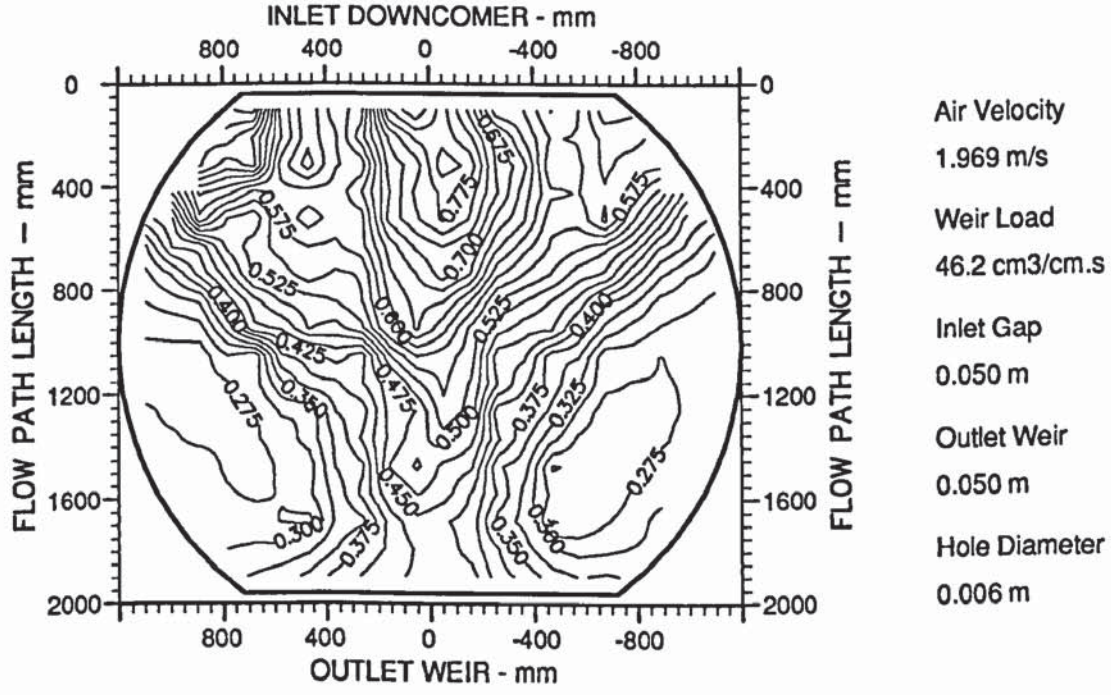

Figure A4.44 Two-dimensional reduced temperature profiles showing "U-shaped" and closed looped isotherms (designation UC).

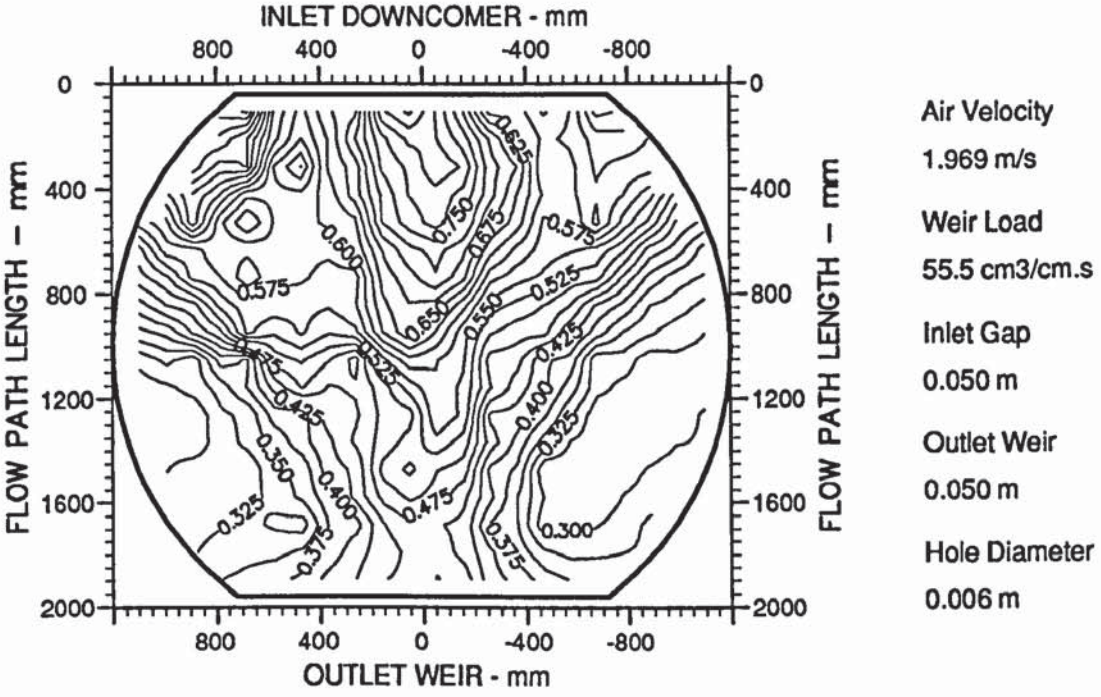

Figure A4.45 Two-dimensional reduced temperature profiles showing "U-shaped" and closed looped isotherms (designation UC).

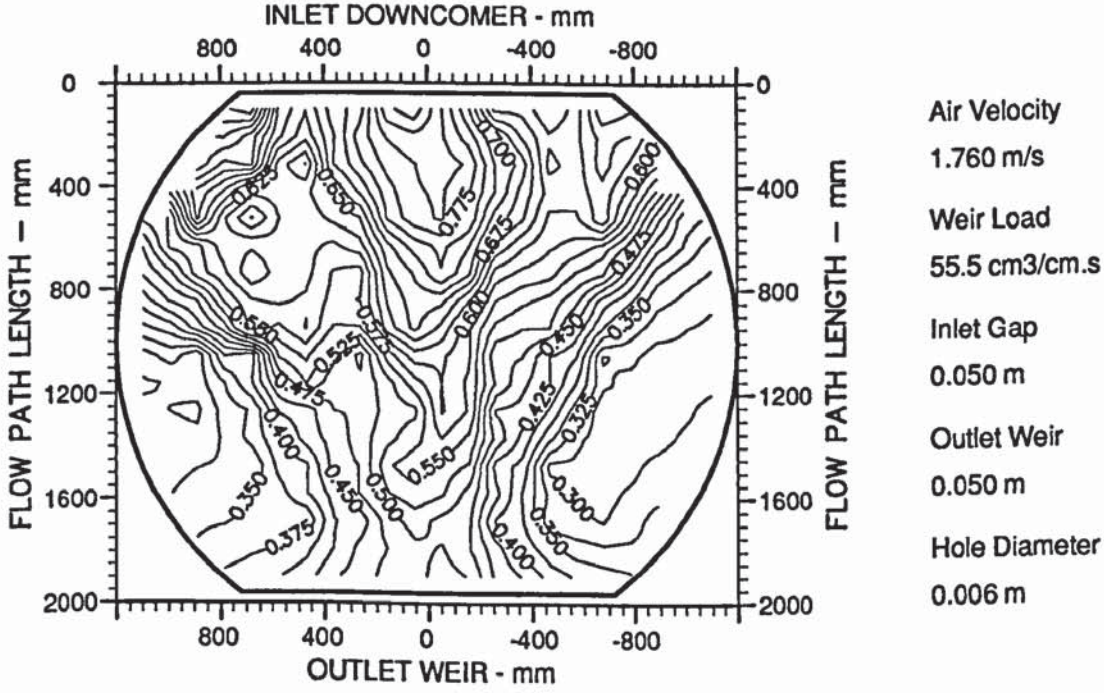

Figure A4.46 Two-dimensional reduced temperature profiles showing "U-shaped" and closed looped isotherms (designation UC).

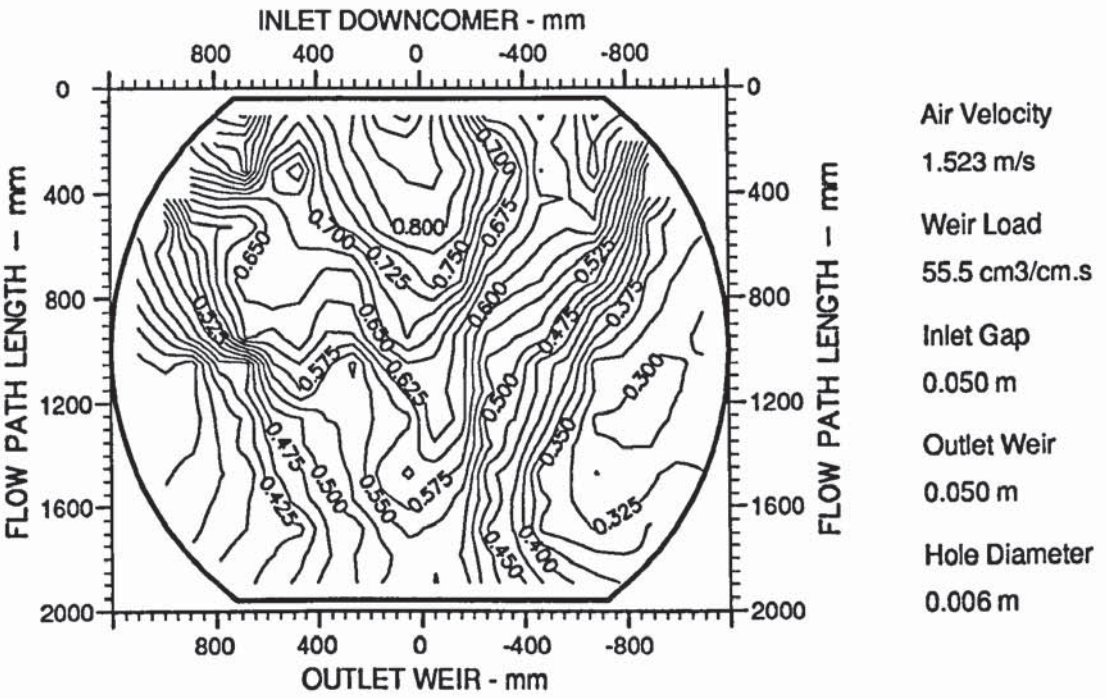

Figure A4.47 Two-dimensional reduced temperature profiles showing confused and "U-shaped" isotherms (designation M/U).

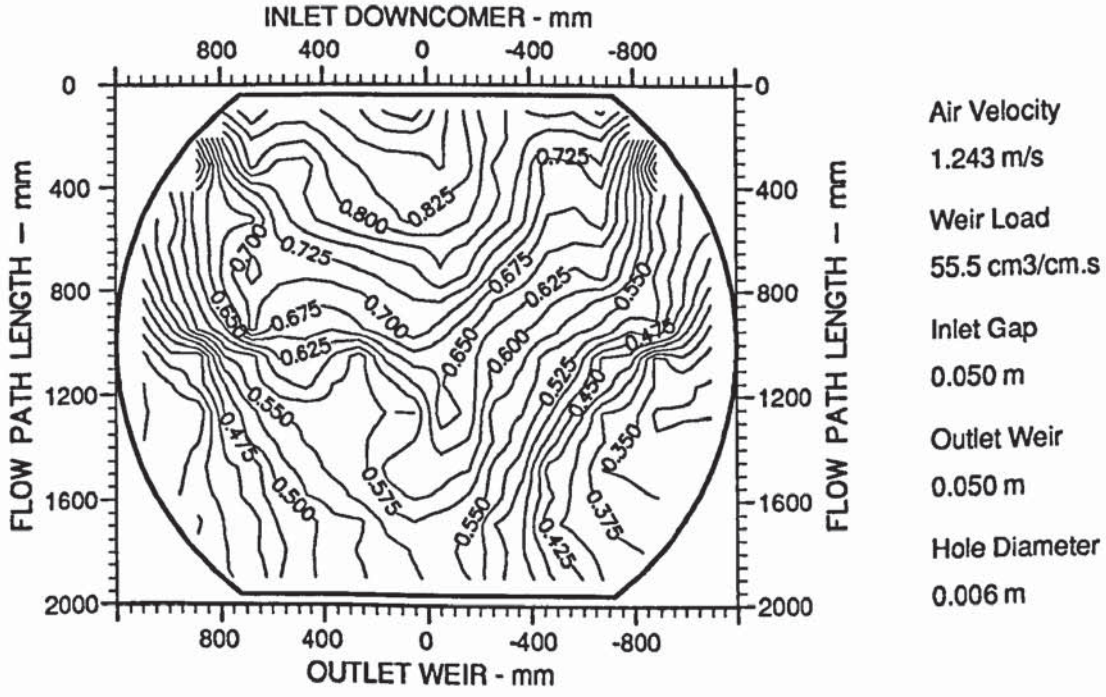

Figure A4.48 Two-dimensional reduced temperature profiles showing mixed or confused isotherms (designation M).

APPENDIX 5

Estimation of the Clearance Height Required To Raise The Chimney Distributor Tray Above The Air Flow Chamber

The procedure for calculating the height at which the chimney distributor tray was raised in order to maintain the same active, or free, area for the air flow, was as follows:-

The free or active hole area expressed as a percentage of the total distributor tray area is:

$$\% \text{ Free Area} = \frac{\text{Hole Area}}{\text{Total Area}} \times 100\ \% = \frac{130 \cdot \left[\frac{\pi\,(0.05)^2}{4}\right]}{\frac{\pi\,(2.0)^2}{4}} \times 100 = 8.125\%$$

The relation that is used to calculate both the height for raising the distributor tray and the the length of the perimeter segments adjacent to the downcomers which need to be blocked-off, is given by:

$$\left[\begin{array}{c}\text{Free Area of} \\ \text{Distributor}\end{array}\right] = \frac{\left[\begin{array}{c}\text{Total Area} \\ \text{of Risers}\end{array}\right] + \left[\begin{array}{c}\text{Effective Bubbling from the} \\ \text{Perimeter of the Raised Distributor}\end{array}\right]}{\text{Effective Bubbling Area in the Inter-tray Space}}$$

$$= \frac{\left[\begin{array}{c}\text{Total Area of Non-bubbling Perimeter} \\ \text{Segments of the Raised Distributor}\end{array}\right]}{\text{Total Downcomer Area}} \qquad \text{(A5.1)}$$

By referring to Figure A5.1 and defining terms mathematically, this equation may be rewritten as:

$$\frac{n \cdot \frac{\pi\, d_r^2}{4}}{\frac{\pi\, d_i^2}{4}} = \frac{n \cdot \frac{\pi\, d_r^2}{4} + (\pi\, d_i - 2a)t}{\frac{\pi\, d_o^2}{4} - 2A_D} = \frac{2at}{2A_D} \qquad \text{(A5.2)}$$

The total area of the non-bubbling perimeter segments of the raised distributor tray, adjacent to the downcomers, was evaluated from:

$$\frac{130\cdot(0.05)^2}{(1.84)^2} = \frac{2\cdot a\cdot t}{2\times 0.263}$$

$$\text{Thus} \quad at = 0.263\cdot\left[\frac{130\cdot(0.05)^2}{(1.82)^2}\right] = 0.0259 \qquad \text{(A5.3)}$$

To calculate the height at which the chimney distributor tray is raised in order to maintain the same active, or free, area for the air flow, the following procedure is used:-

$$\frac{n\cdot\frac{\pi d_r^2}{4} + \pi d_i t - 2at}{\frac{\pi d_o^2}{4} - 2A_D} = \frac{130\cdot(0.05)^2}{(1.84)^2}$$

$$\frac{\frac{130\cdot\pi (0.05)^2}{4} + \pi (1.84)\cdot t - 2(0.0253)}{\frac{\pi (2.44)^2}{4} - 0.526} = 0.0891$$

$$\text{hence} \quad t = \frac{0.0981\left(\frac{\pi (2.44)^2}{4} - 0.526\right) + 2(0.0253) - \frac{130\cdot\pi (0.05)^2}{4}}{\pi\cdot(1.84)}$$

$$= 0.036 \text{ m or } 36.0 \text{ mm} \qquad \text{(A5.4)}$$

The length of the perimeter segment blocked-off , both in the inlet and outlet regions, when the distributor tray is raised 36.0 mm, is:

$$a\cdot(0.036) = 0.0253 \quad \therefore\ a = \frac{0.0253}{0.036} = 0.703 \text{ m or } 703 \text{ mm}$$

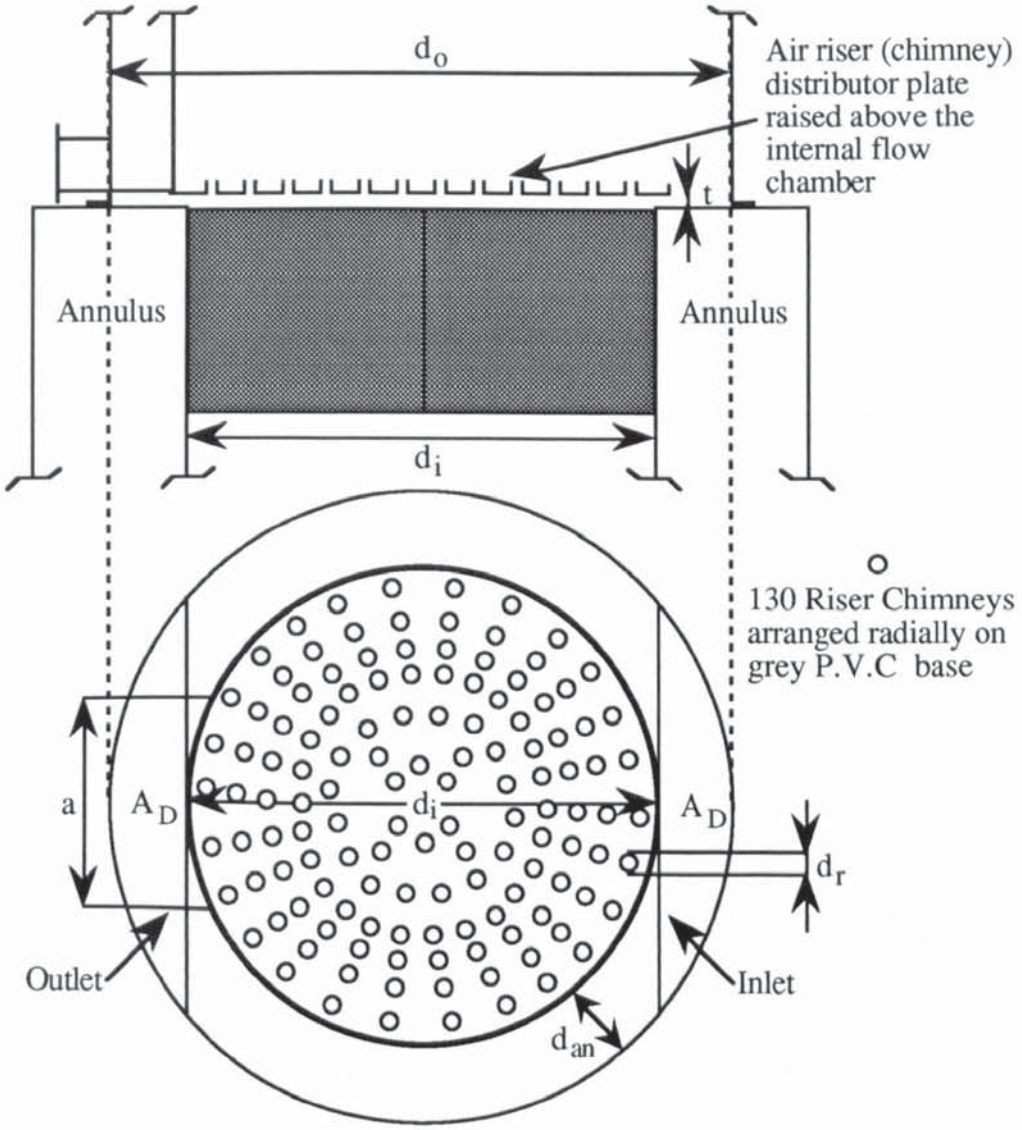

A_D = Downcomer area = 0.243 m^2

a = Length of perimeter section to be blocked when the dsitributor is raised

d_{an} = Diameter of the internal annulus inside the column wall = 220 mm

d_i = Diameter of the distributor tray = 2000 mm

d_o = Tray column diameter = 2440 mm

d_r = Diameter of chimney riser = 50 mm

n = Number of risers on the distributor tray = 130

t = height at which the distributor tray is raised

Figure A5.1 Simplified diagram of the chimney tray raised above the air flow chamber and the parameters required to estimate t.

APPENDIX 6

Three-Dimensional Air Velocity Surface Profiles Above The New Air Distributor Tray

Air velocity profiles were measured above the new 1.80 mm hole, 10 % free area, air distributor tray using a hot wire anemometer. Measurements were made at thirty two sample points, as shown in Figure A6.1, at a height of 233 mm above the tray deck.

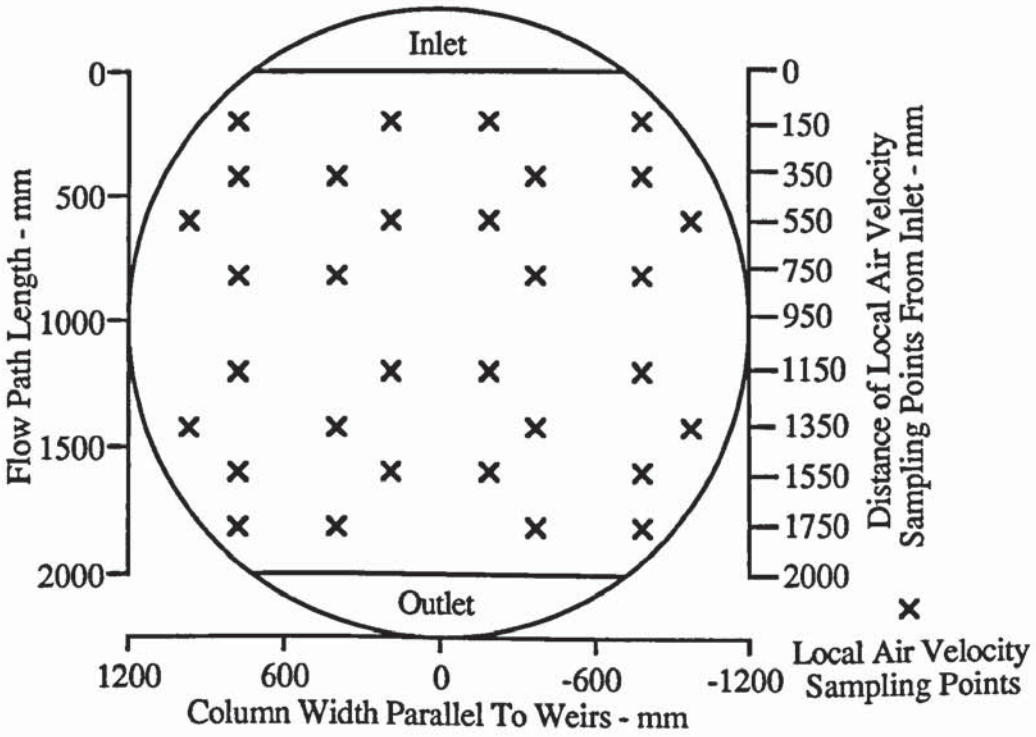

Figure A6.1 Position of air velocity sample points across the tray.

For each superficial air velocity setting of 1.00, 1.50, 2.00, and 2.50 ms^{-1}, thirty two point air velocity measurements were made and used as input in a computer program for generating three-dimensional response curves using the UNIRAS suite of plotting routines. In this appendix, the point to point air velocity results are presented in grids, the same shape as the distributor tray, followed by the corresponding three dimensional response curves.

Given the imperfections of the experimental technique, the air velocity response curves above the new distributor tray were similar to those of Ali (1984). (In these experiments, a comparatively uniform gas distribution was generated above a large diameter shallow packed bed using a sytem of annular and crossed baffles for an inlet tangential air feed).

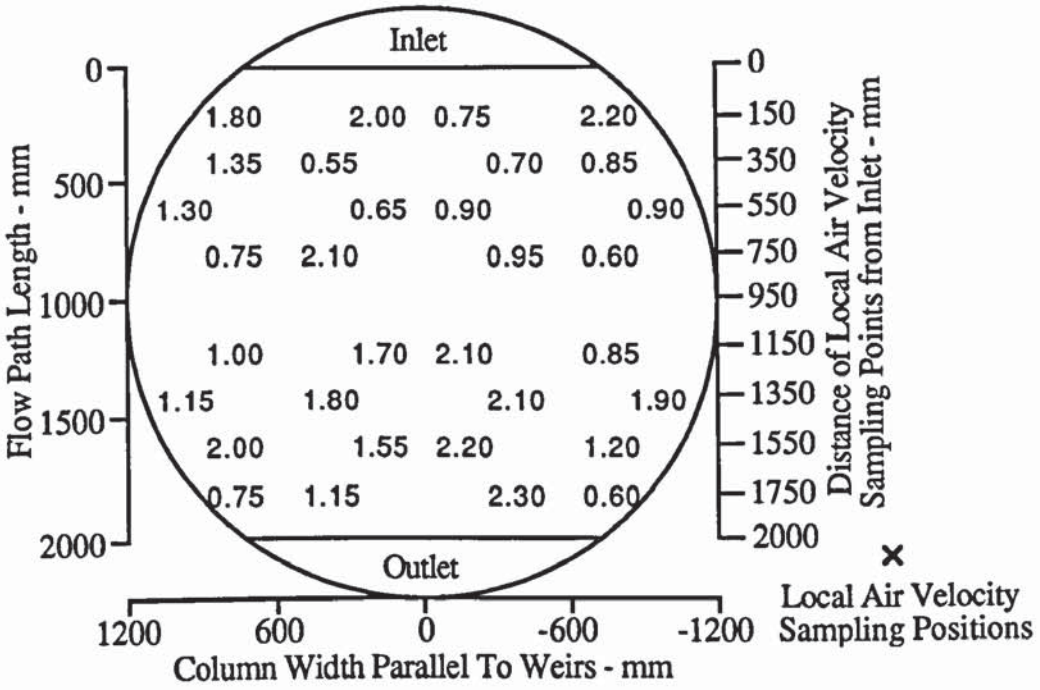

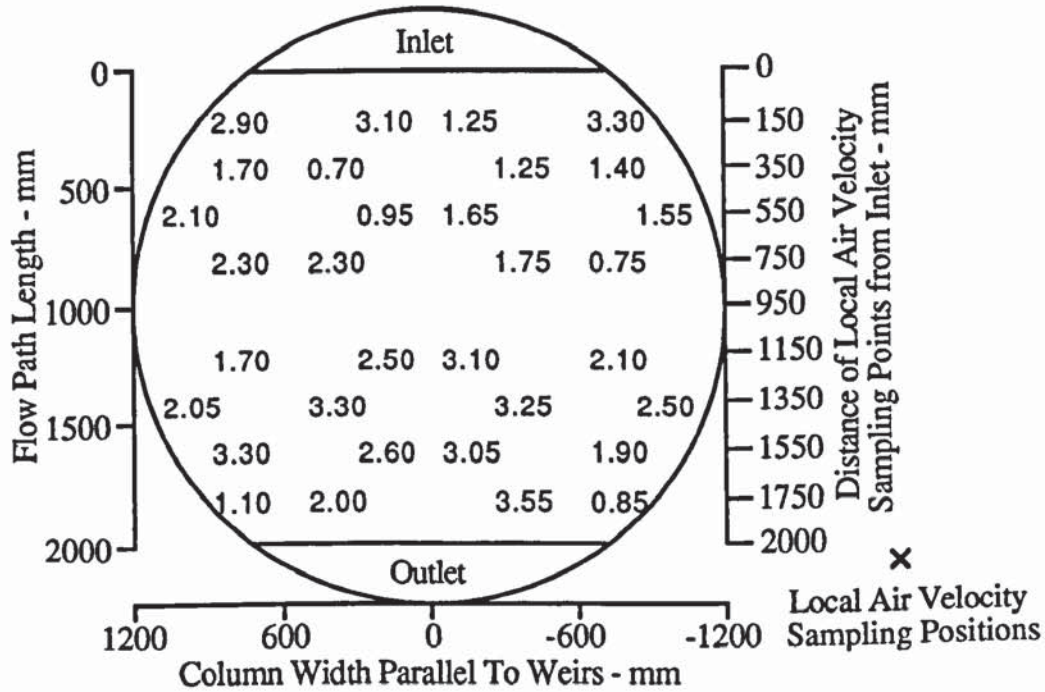

Sampling Height above Air Distributor Plate = 0.233m

Hole Diameter = 1.80mm Number of Points sampled = 32

Figure A6.2a Measured point air velocity profiles above the perforated air distributor tray at low air flowrates.

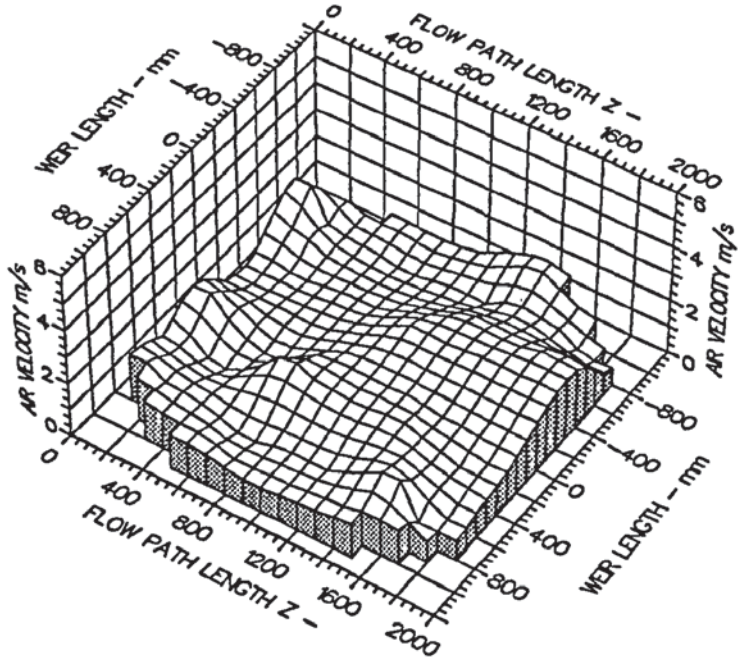

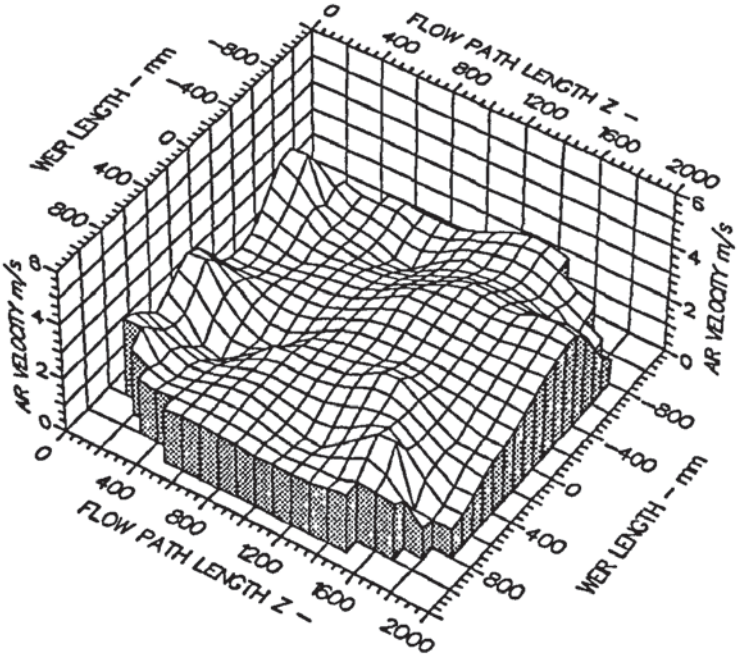

Figure A6.2b Three-dimensional air velocity response curves above the perforated air distributor tray at low air flowrates.

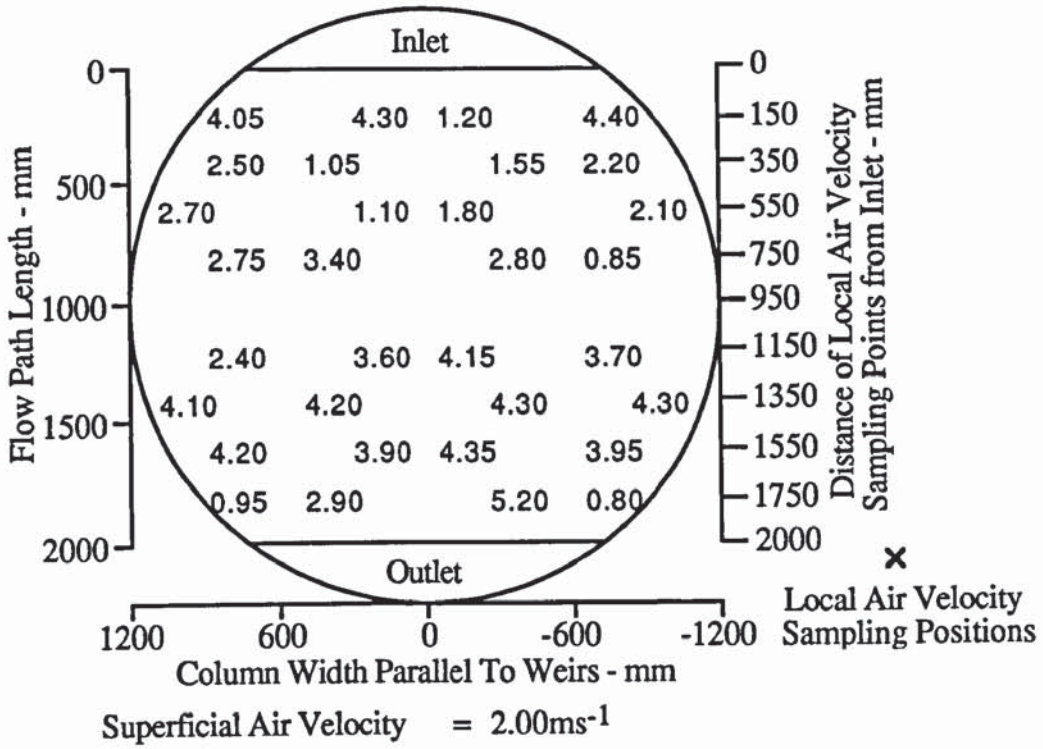

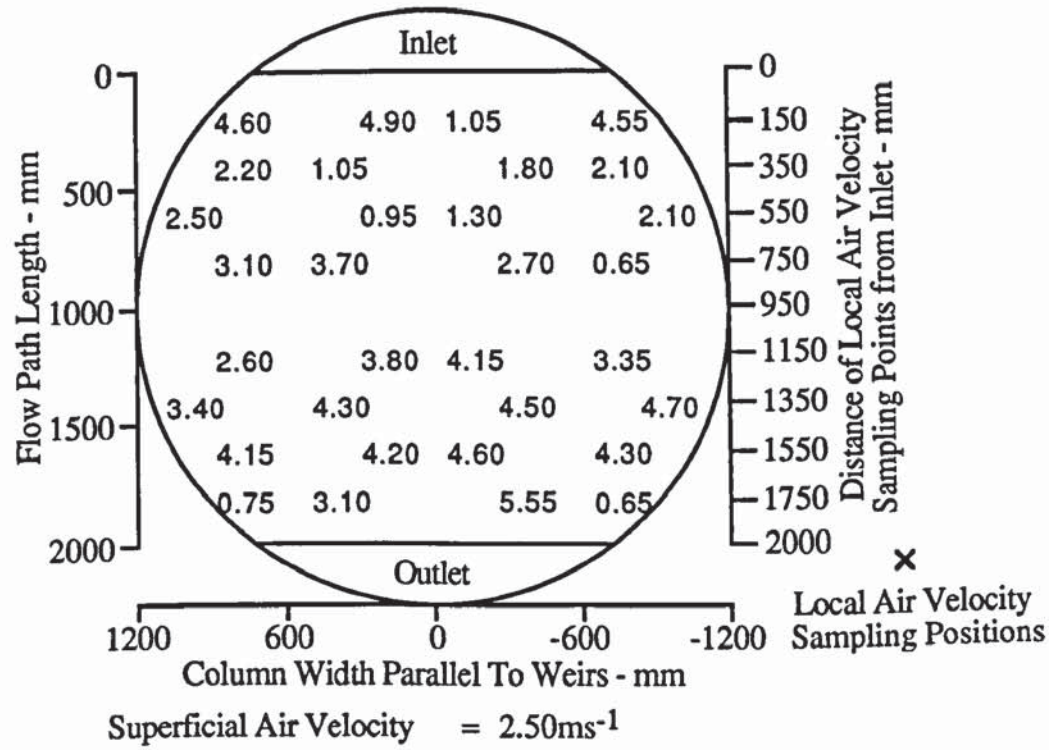

Sampling Height above Air Distributor Plate = 0.233m

Hole Diameter = 1.80mm Number of Points sampled = 32

Figure A6.3a Measured point air velocity profiles above the perforated air distributor tray at high air flowrates.

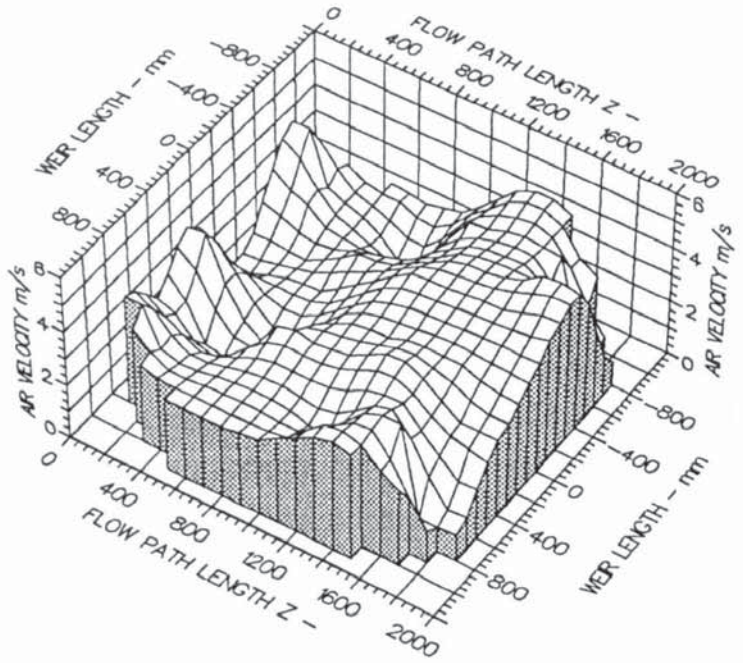

Air Velocity
2.000 m/s

Sample Height
0.233 m

Mean Air Velocity
2.990 m/s

Hole Diameter
0.0018 m

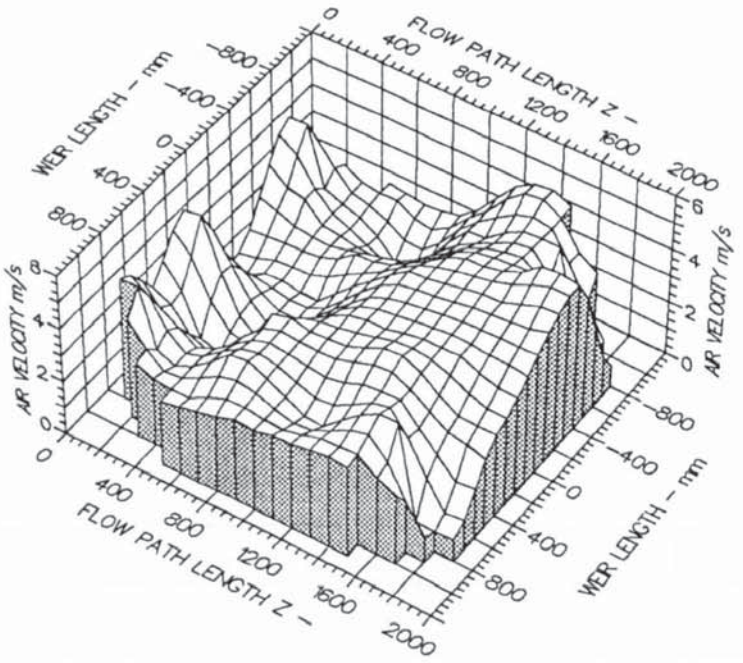

Air Velocity
2.500 m/s

Sample Height
0.233 m

Mean Air Velocity
3.061 m/s

Hole Diameter
0.0018 m

Figure A6.3b Three-dimensional air velocity response curves above the perforated air distributor tray at high air flowrates.

APPENDIX 7

Two-Dimensional Reduced Temperature Isotherm Displays For The Effect of the Gas Flow on the Separation of Liquid Flow

The two-dimensional black and white displays presented below are a full set of reduced temperature profiles to complement the results of the water-cooling experiments in Chapter 8. Water-cooling was used to show the effect of non-separated and separated liquid flow patterns on mass transfer. In these experiments, the water weir load was varied over a wide range for a fixed air velocity at the equal inlet gap-outlet weir settings of 10 mm, 10 mm; 20 mm, 20 mm; and 50 mm, 50 mm. The flow rate information is presented in Table A7.1.

Experimental Investigation	Air Velocity - ms^{-1}	Weir load - $10^4.m^3/m.s$	Inlet Gap - mm	Outlet Weir - mm
	1.00	25.0		
	1.25	50.0	10	10
Heat transfer by	1.50	100.0	20	20
water cooling	2.00	150.0	50	50
	2.50	200.0		
		250.0		

Table A7.1 Summary of flow rates and downcomer settings used in the separation of flow air - water contacting experiments.

Note that the reduced temperature profiles in all of the experiments are either parallel, "U-shaped", or a mixture of isotherms according to the level of flow separation produced on the tray.

In addition, the designations assigned to each temperature profile are included in the labelling of each diagram. A reminder of the temperature profile designations used in these studies are summarised below.

Temperature Profile	Designation
Straight and Parallel Isotherms	P
Shallow Transverse "U-shaped" Isotherms	hU
Severe Transverse "U-shaped" Isotherms	TU
Distinctive "U-shaped" Isotherms	U
Mixed or Confused Isotherms	M

Table A7.2 Summary of temperature profile designations.

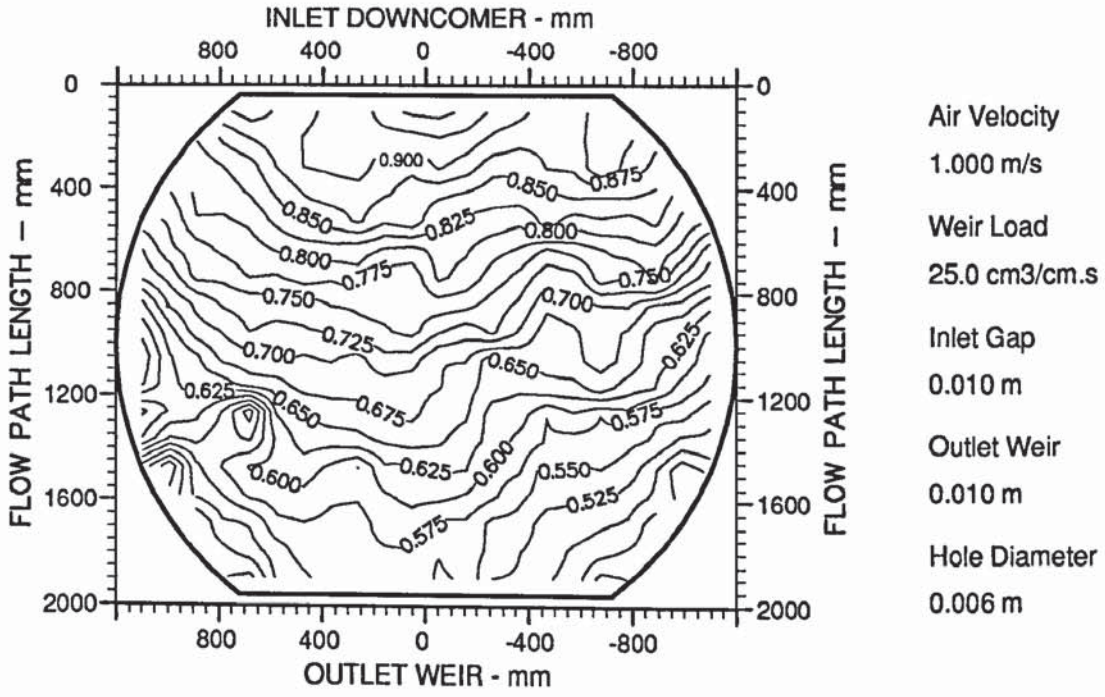

Figure A7.1 Two dimensional reduced temperature profiles showing a mixture of parallel isotherms and shallow "U-shapes" (designation P/hU).

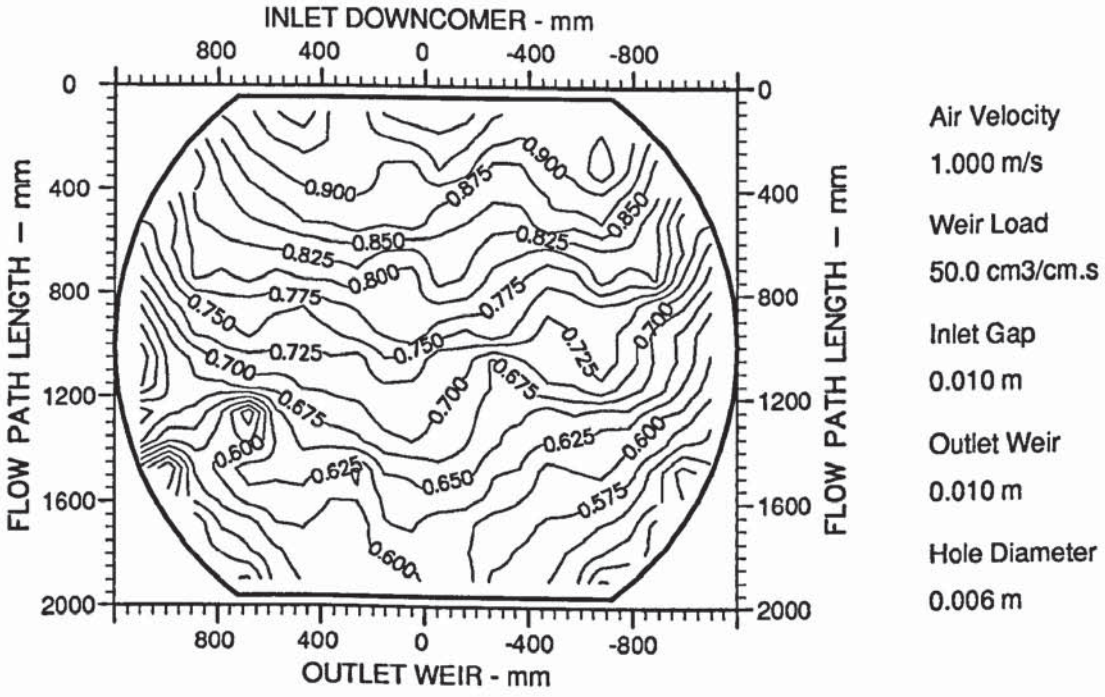

Figure A7.2 Two dimensional reduced temperature profiles showing straight and parallel isotherms (designation P).

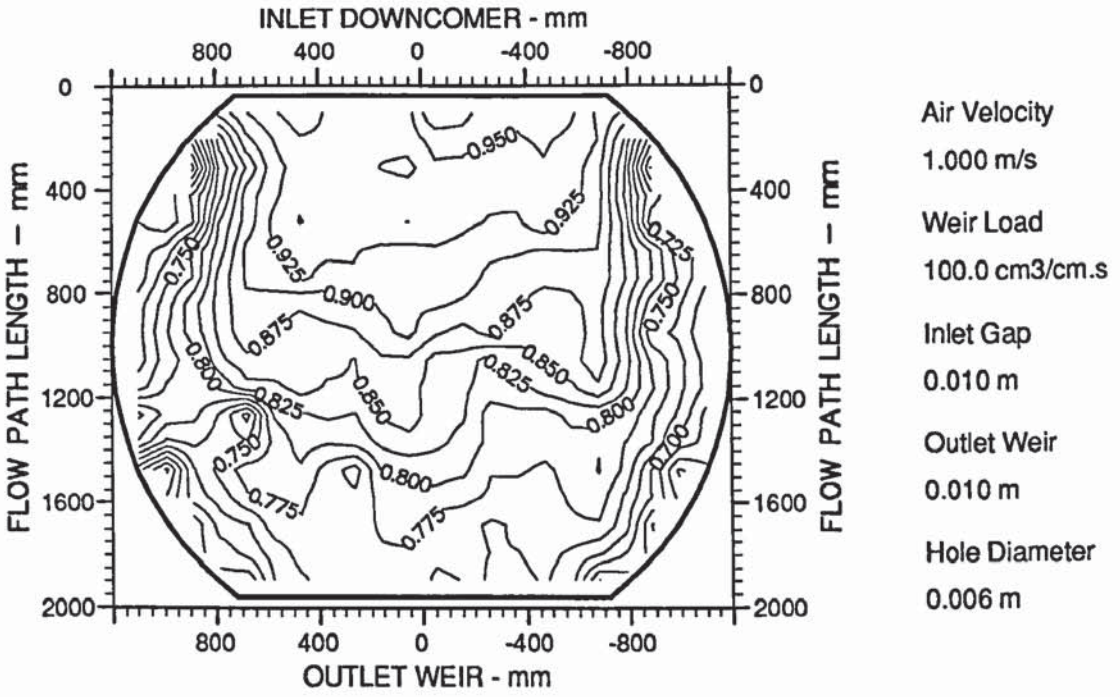

Figure A7.3 Two dimensional reduced temperature profiles showing straight and parallel isotherms (designation P).

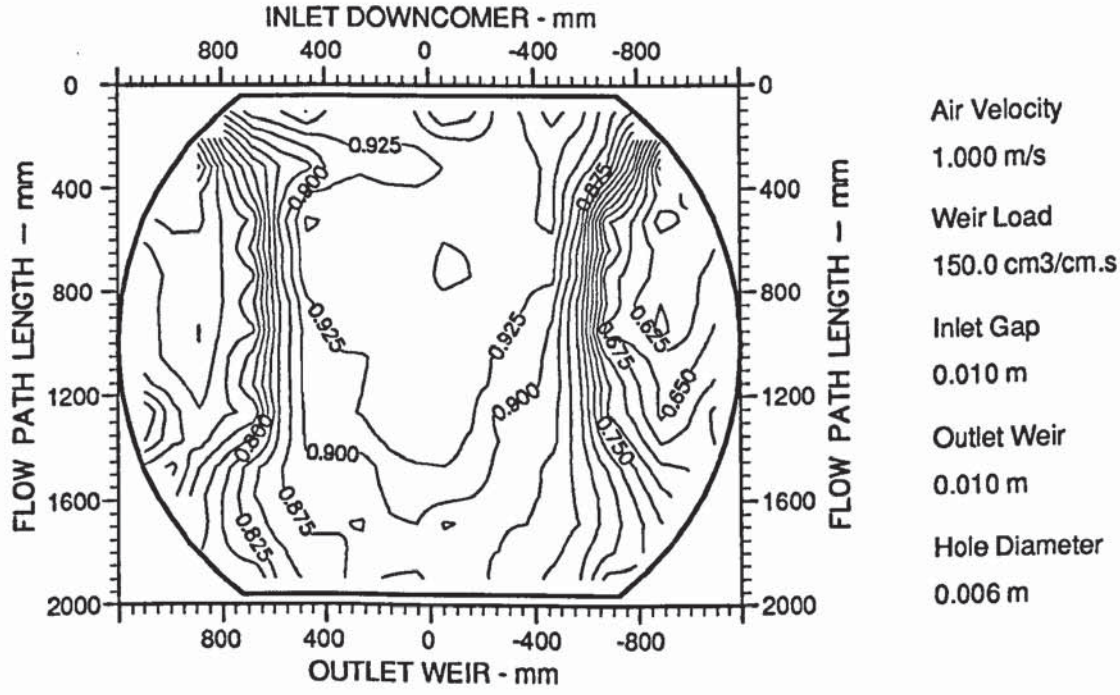

Figure A7.4 Two dimensional reduced temperature profiles showing straight and parallel isotherms (designation P).

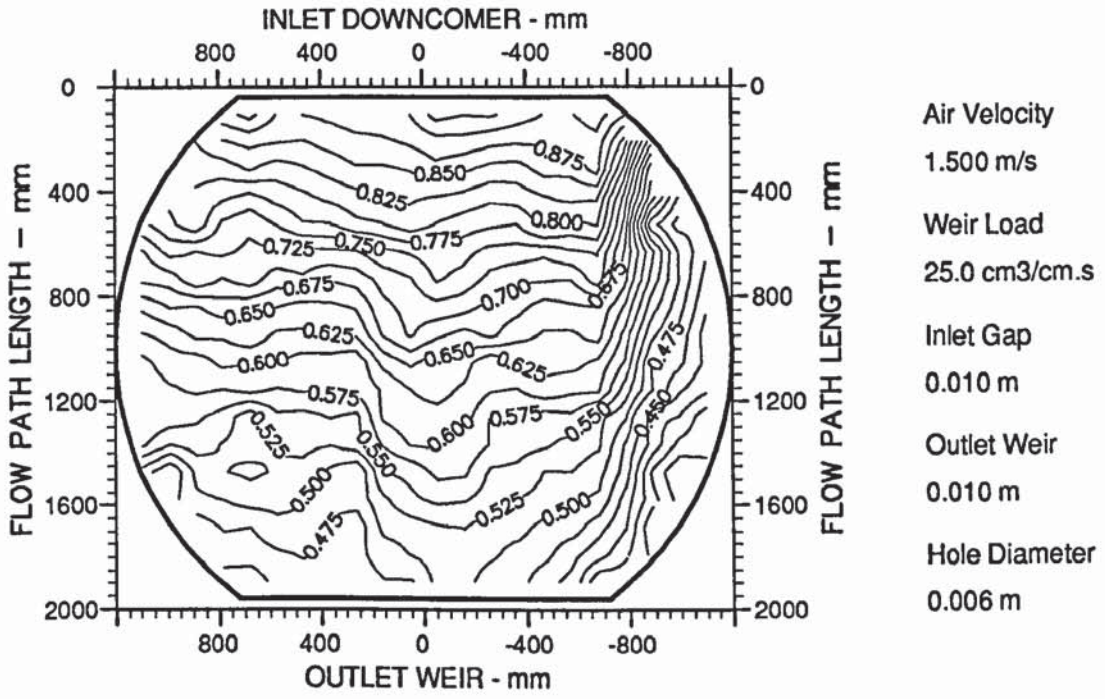

Figure A7.5 Two dimensional reduced temperature profiles showing shallow transverse "U-shaped" isotherms (designation hU).

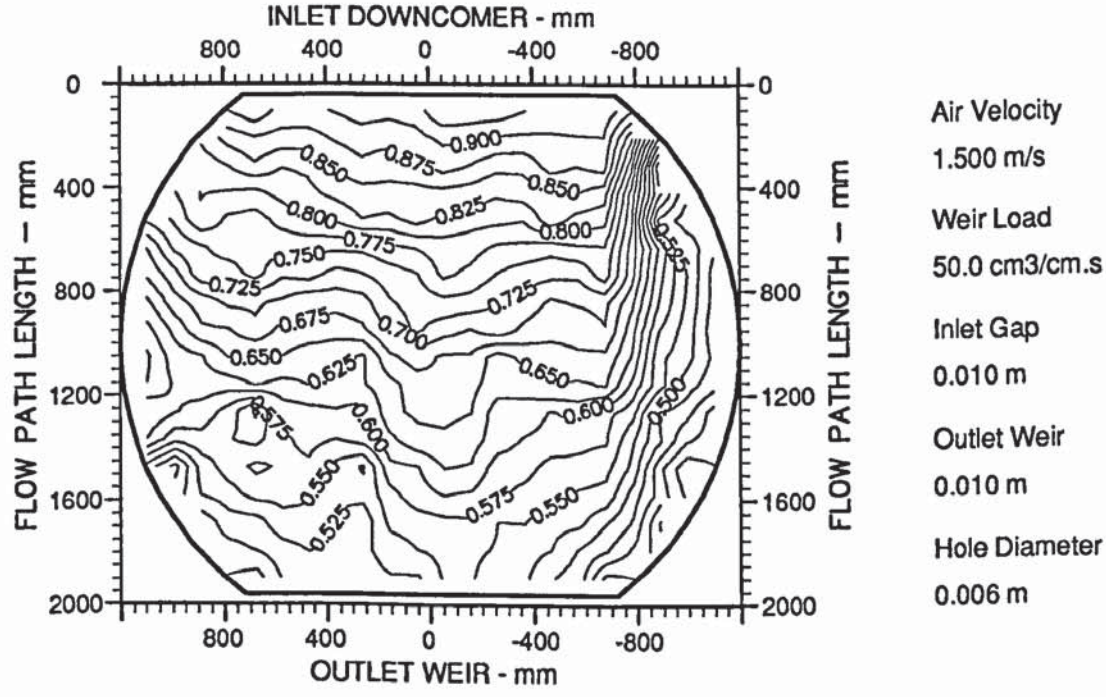

Figure A7.6 Two dimensional reduced temperature profiles showing shallow transverse "U-shaped" isotherms (designation hU).

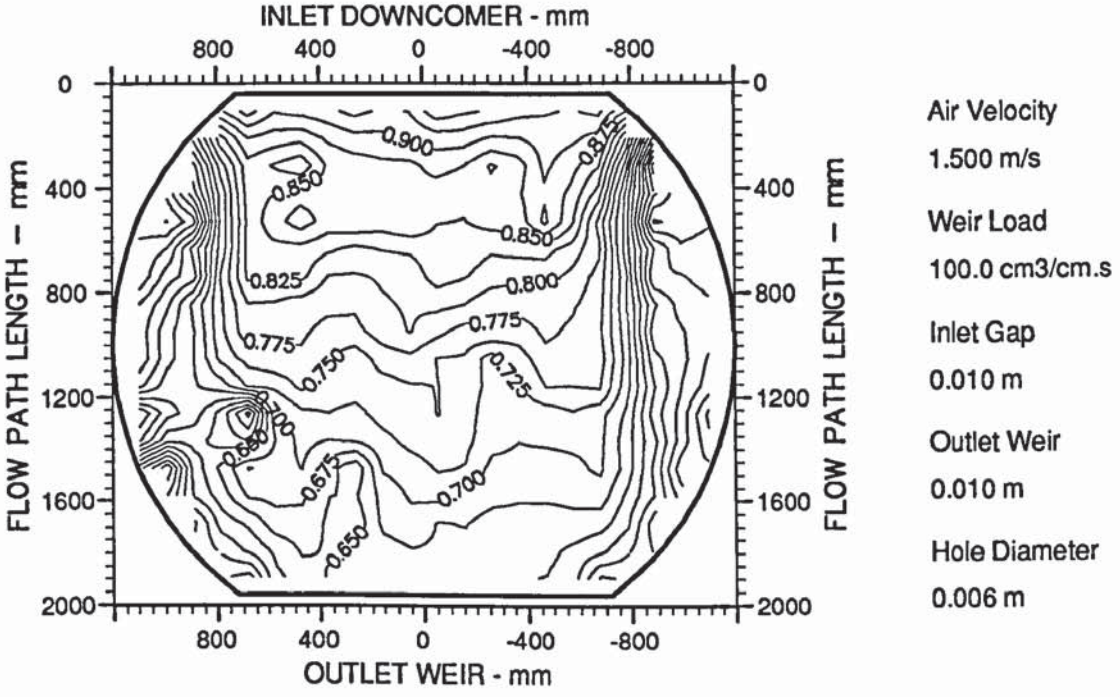

Figure A7.7 Two dimensional reduced temperature profiles showing straight and parallel isotherms (designation P).

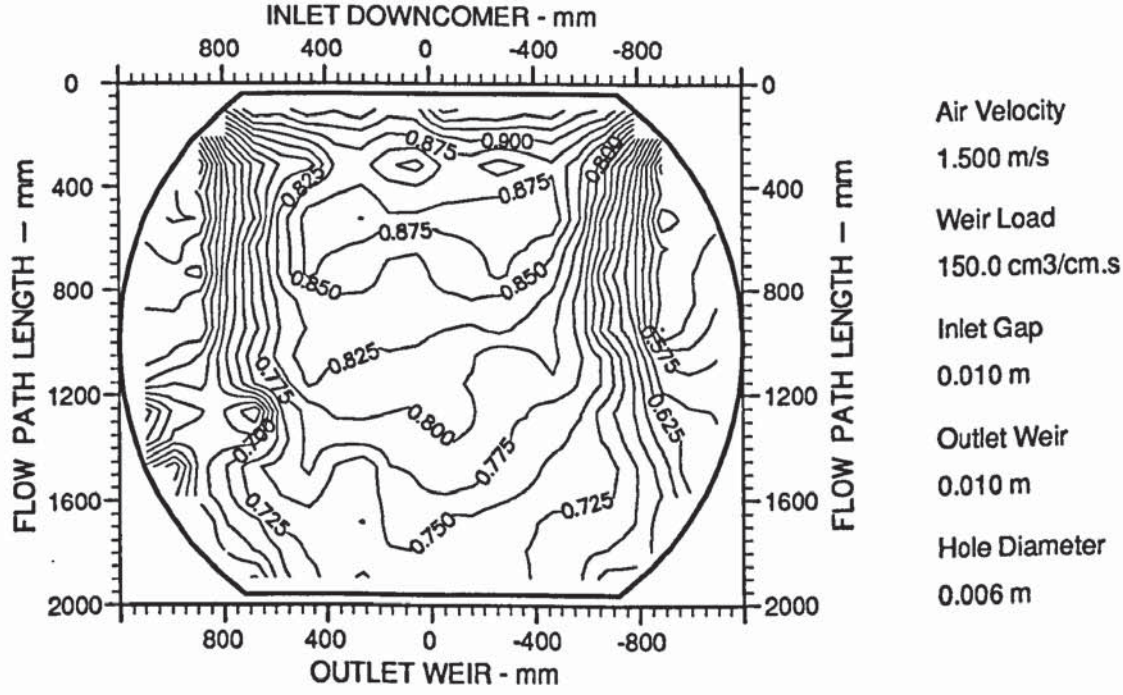

Figure A7.8 Two dimensional reduced temperature profiles showing straight and parallel isotherms (designation P).

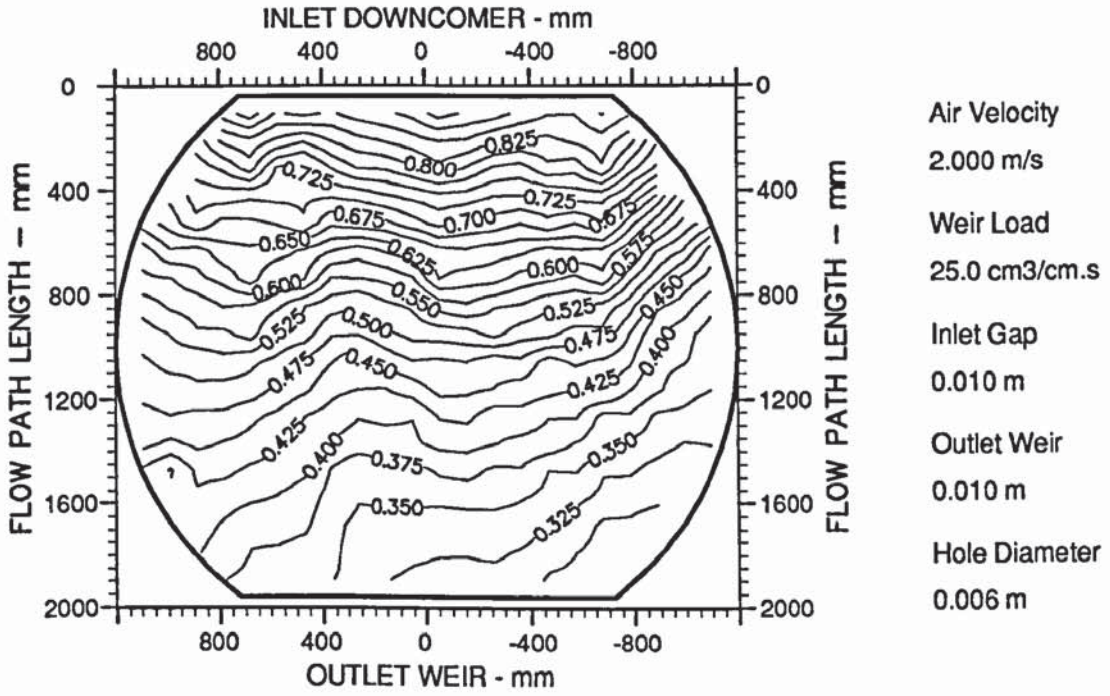

Figure A7.9 Two dimensional reduced temperature profiles showing severe transverse "U-shaped" isotherms (designation TU).

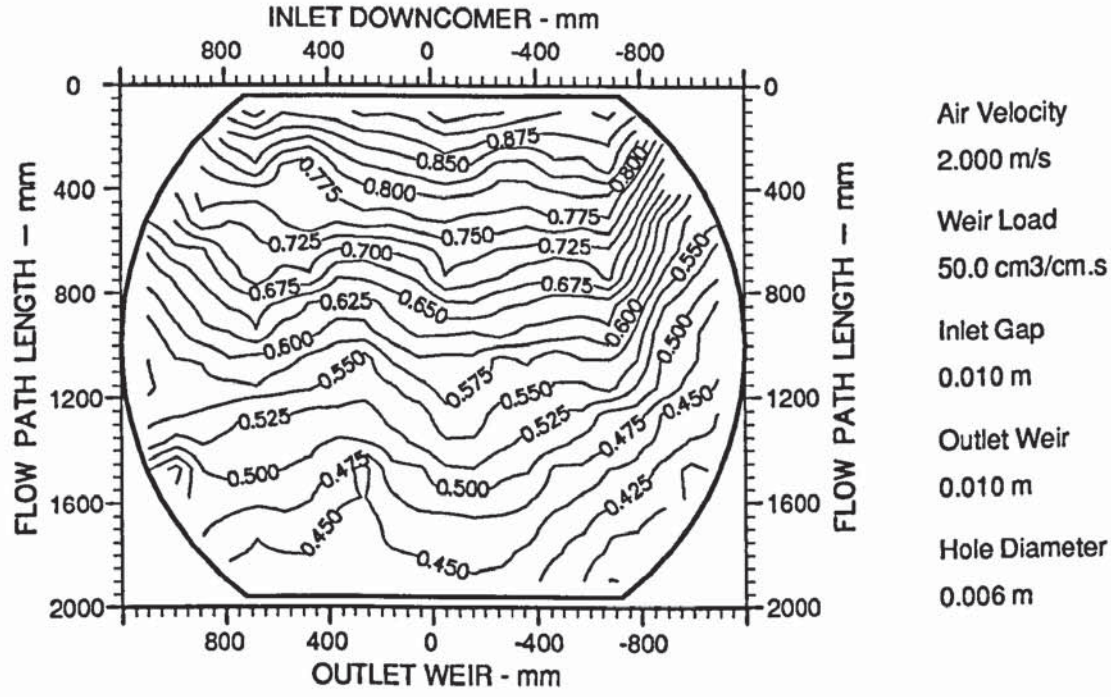

Figure A7.10 Two dimensional reduced temperature profiles showing severe transverse "U-shaped" isotherms (designation TU).

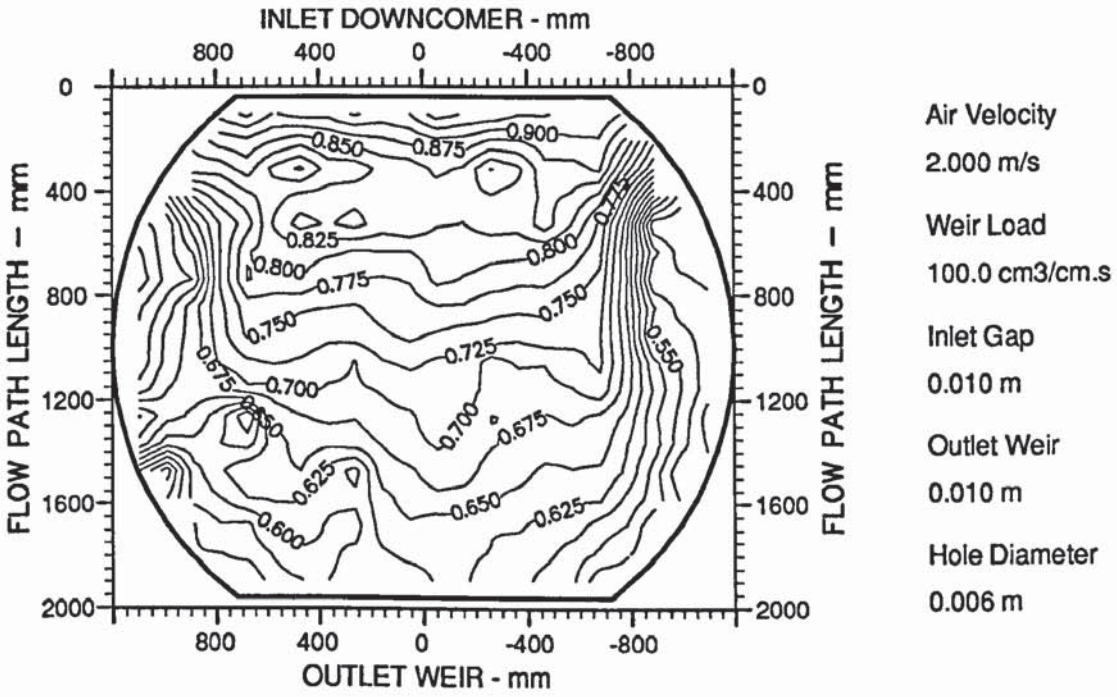

Figure A7.11 Two dimensional reduced temperature profiles showing severe transverse "U-shaped" isotherms (designation TU).

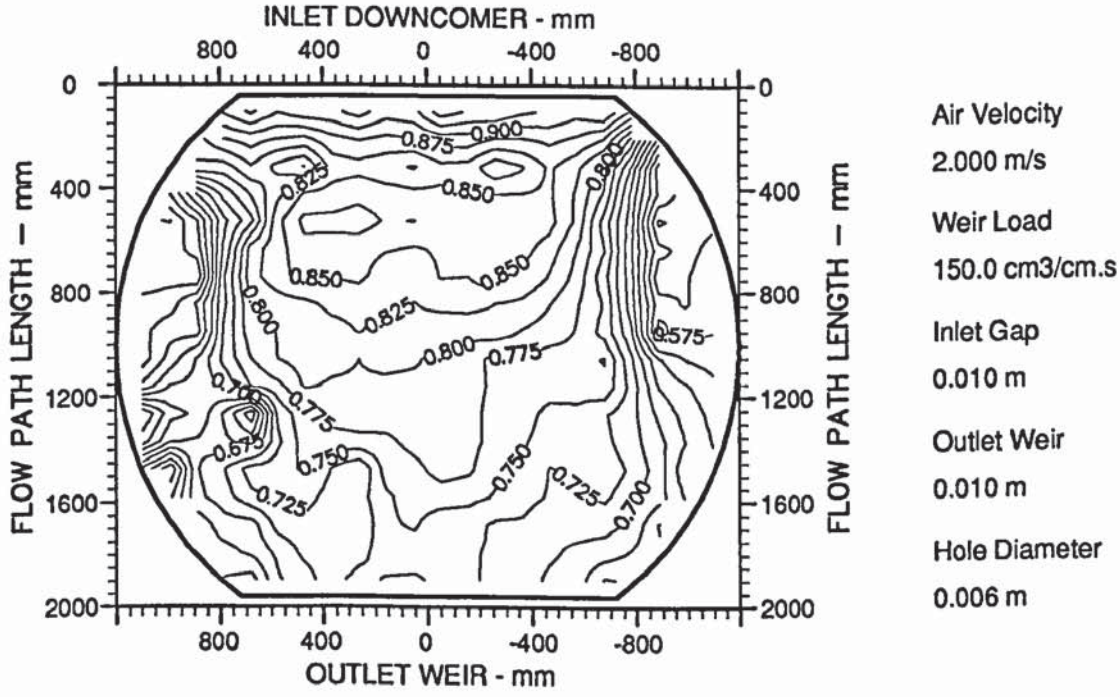

Figure A7.12 Two dimensional reduced temperature profiles showing shallow transverse "U-shaped" isotherms (designation hU).

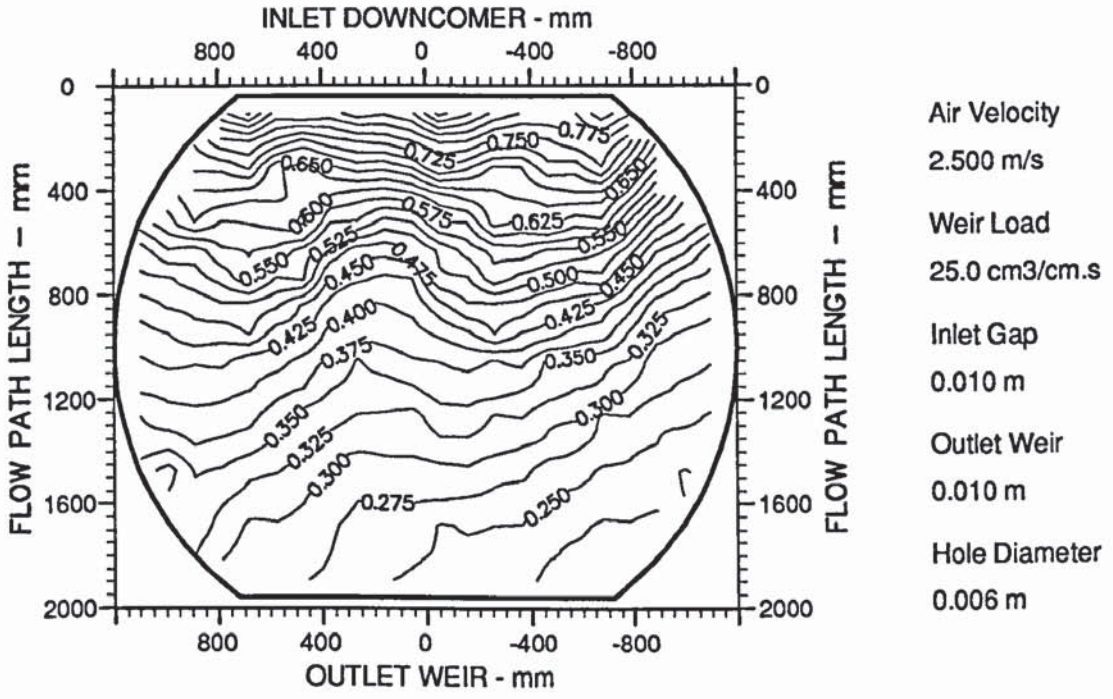

Figure A7.13 Two dimensional reduced temperature profiles showing severe transverse "U-shaped" isotherms (designation TU).

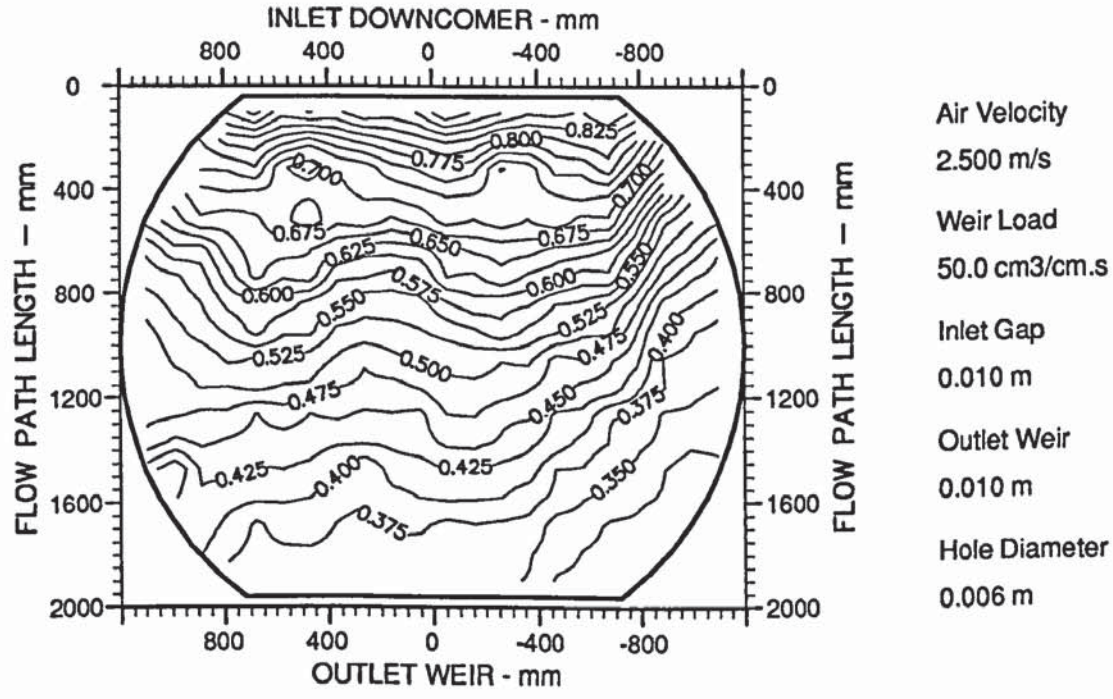

Figure A7.14 Two dimensional reduced temperature profiles showing severe transverse "U-shaped" isotherms (designation TU).

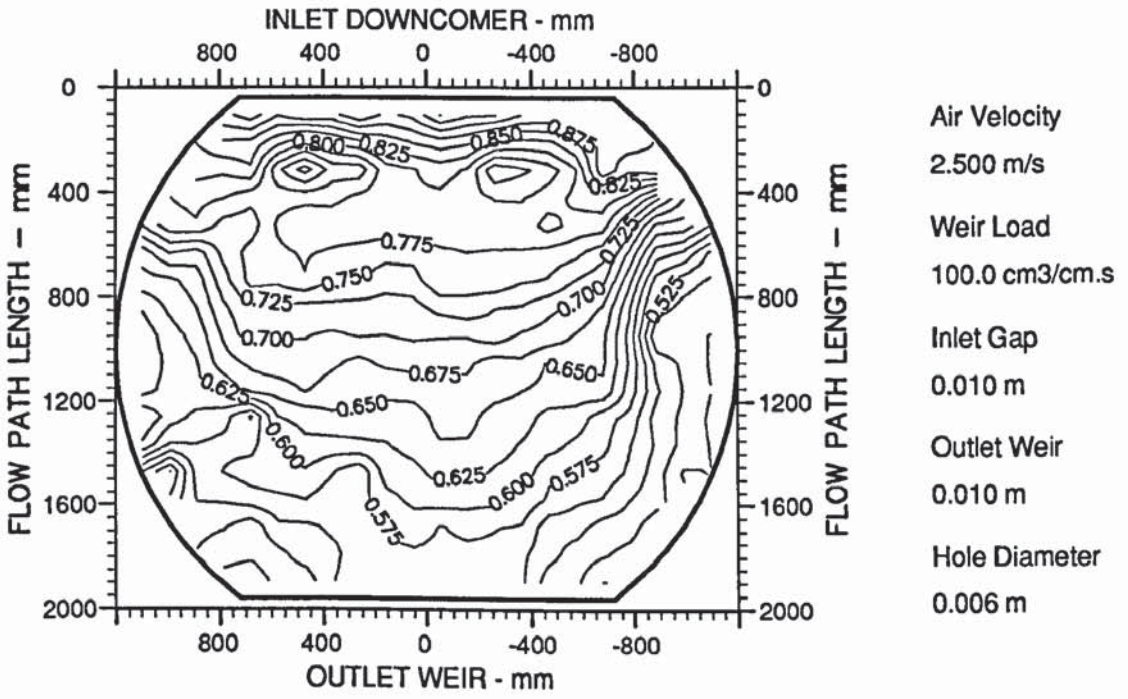

Figure A7.15 Two dimensional reduced temperature profiles showing severe transverse "U-shaped" isotherms (designation TU).

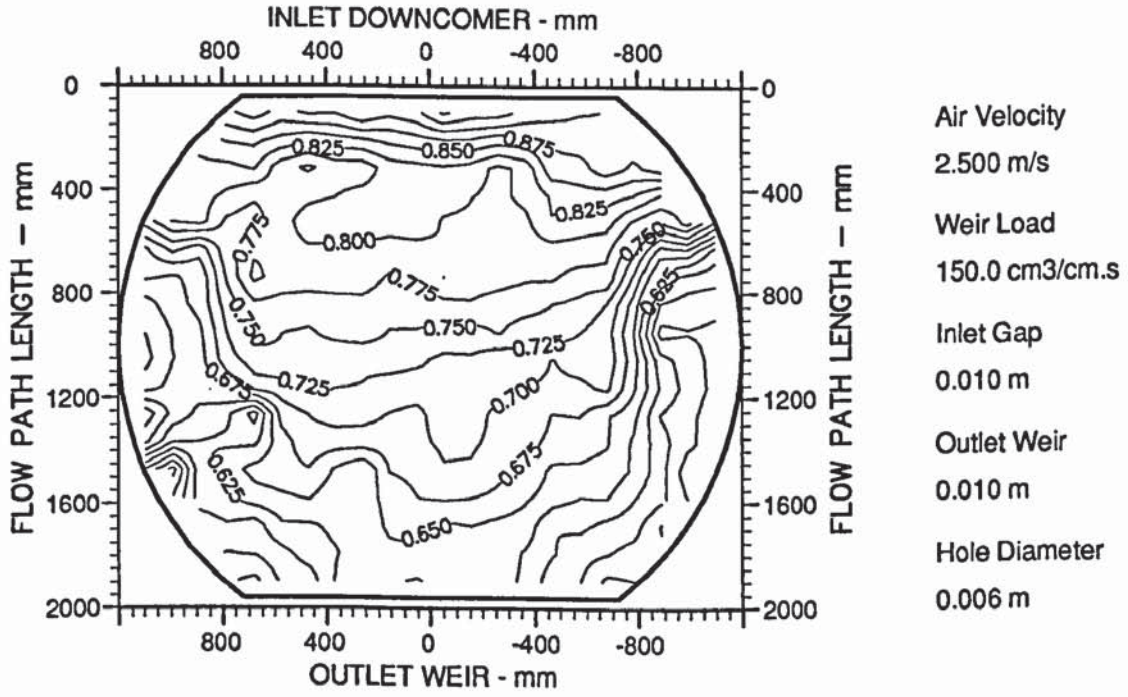

Figure A7.16 Two dimensional reduced temperature profiles showing severe transverse "U-shaped" isotherms (designation TU).

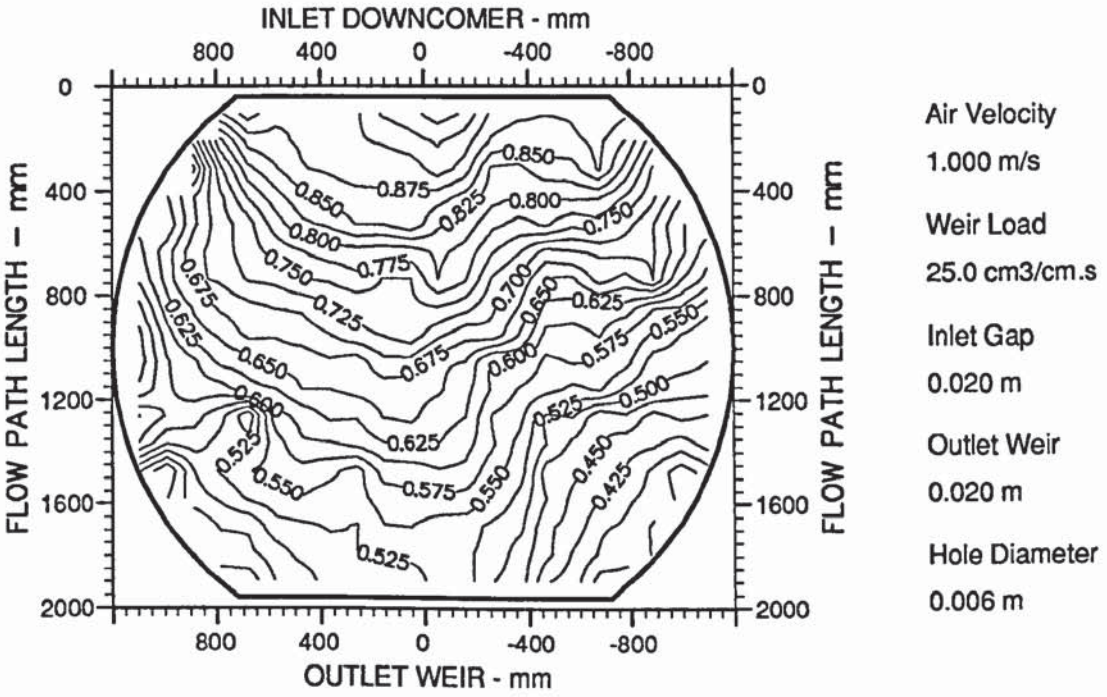

Figure A7.17 Two dimensional reduced temperature profiles showing a mixture of parallel isotherms and shallow "U-shapes" (designation P/hU).

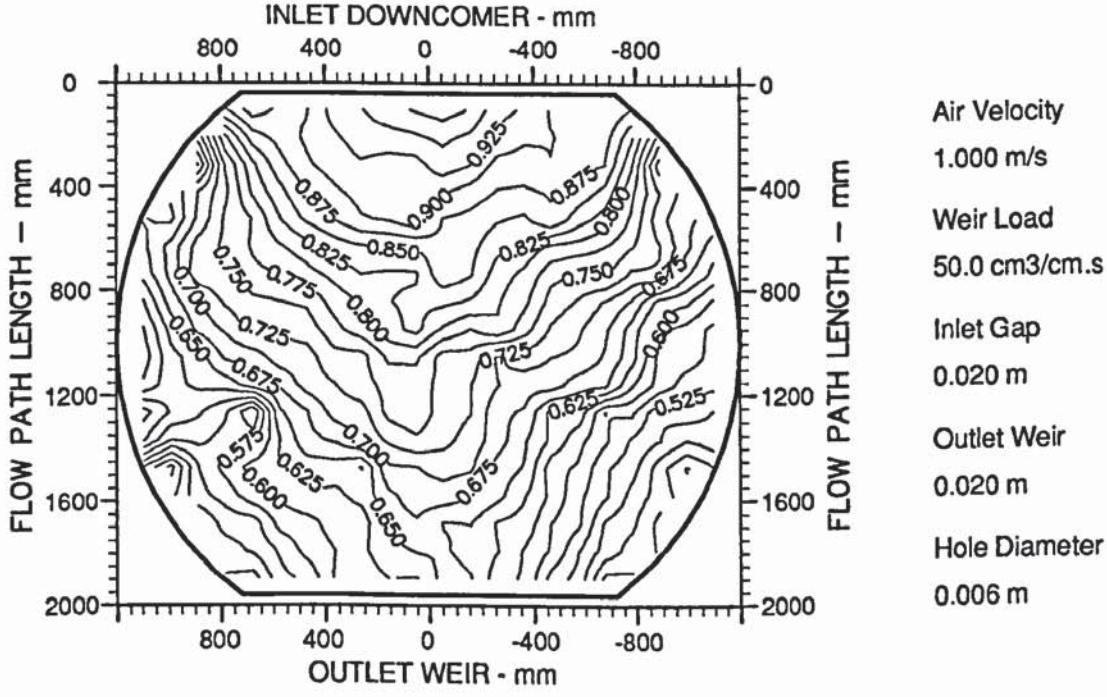

Figure A7.18 Two dimensional reduced temperature profiles showing a mixture of parallel isotherms and shallow "U-shapes" (designation P/hU).

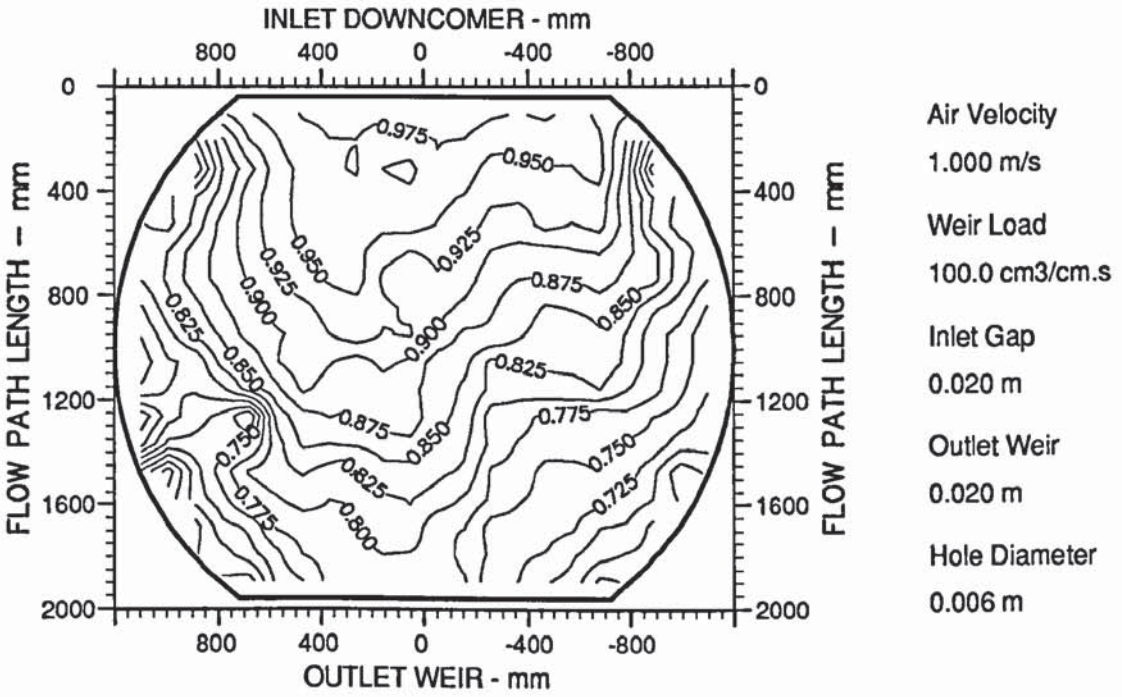

Figure A7.19 Two dimensional reduced temperature profiles showing straight and parallel isotherms (designation P).

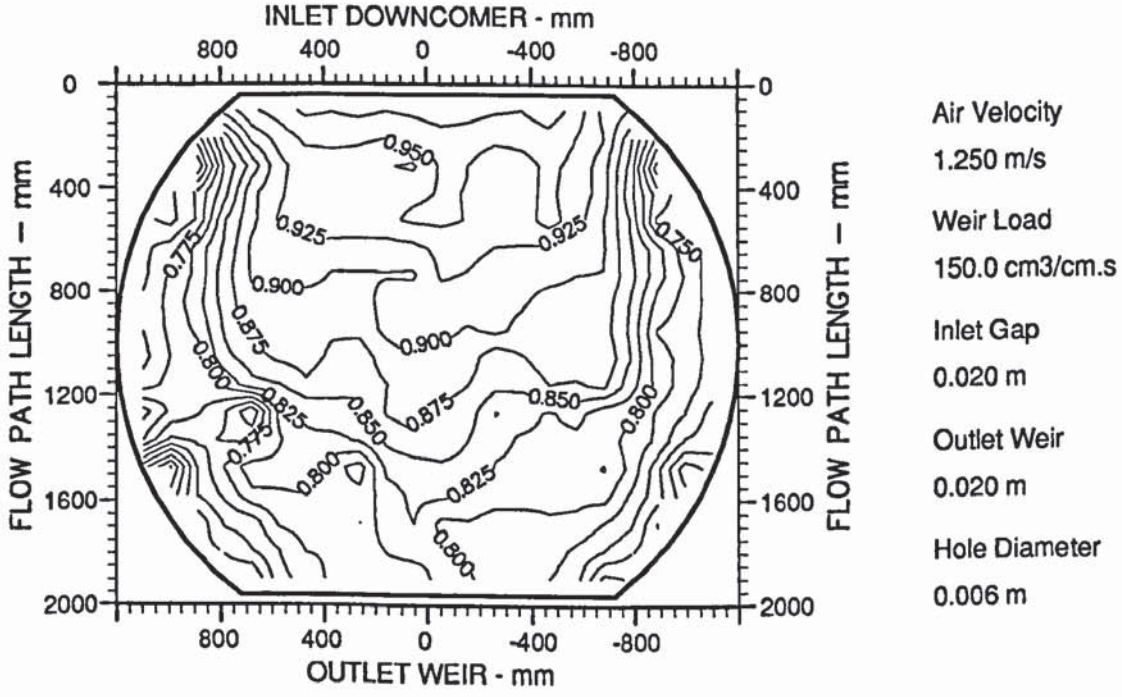

Figure A7.20 Two dimensional reduced temperature profiles showing straight and parallel isotherms (designation P).

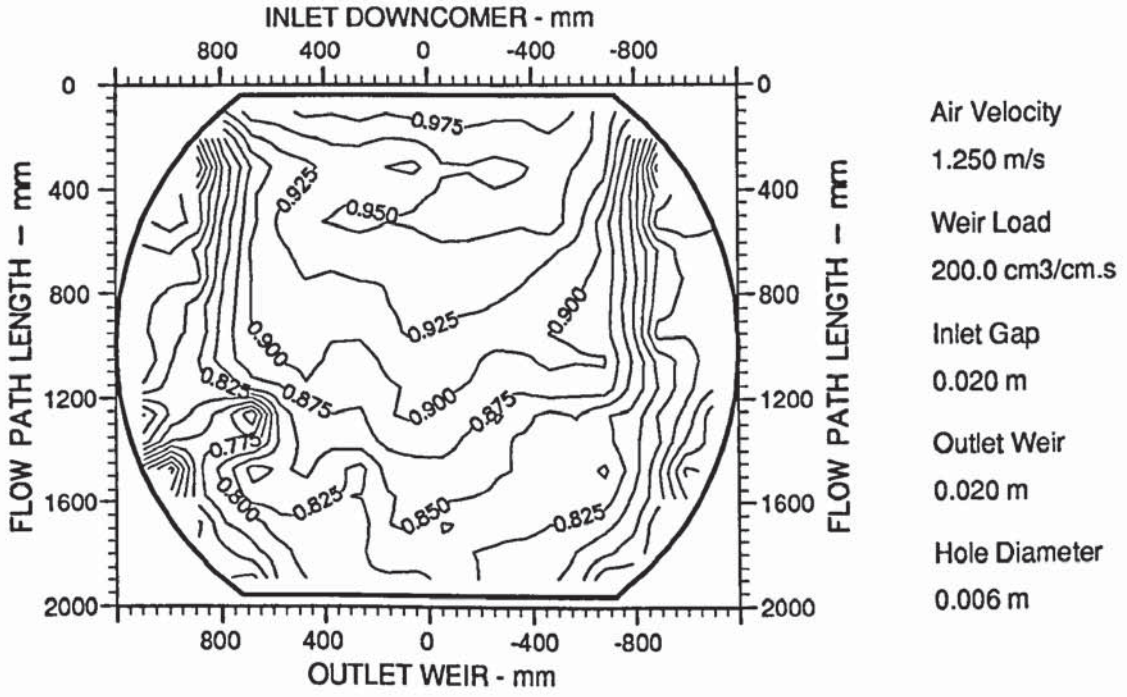

Figure A7.21 Two dimensional reduced temperature profiles showing distinctively "U-shaped" isotherms (designation U).

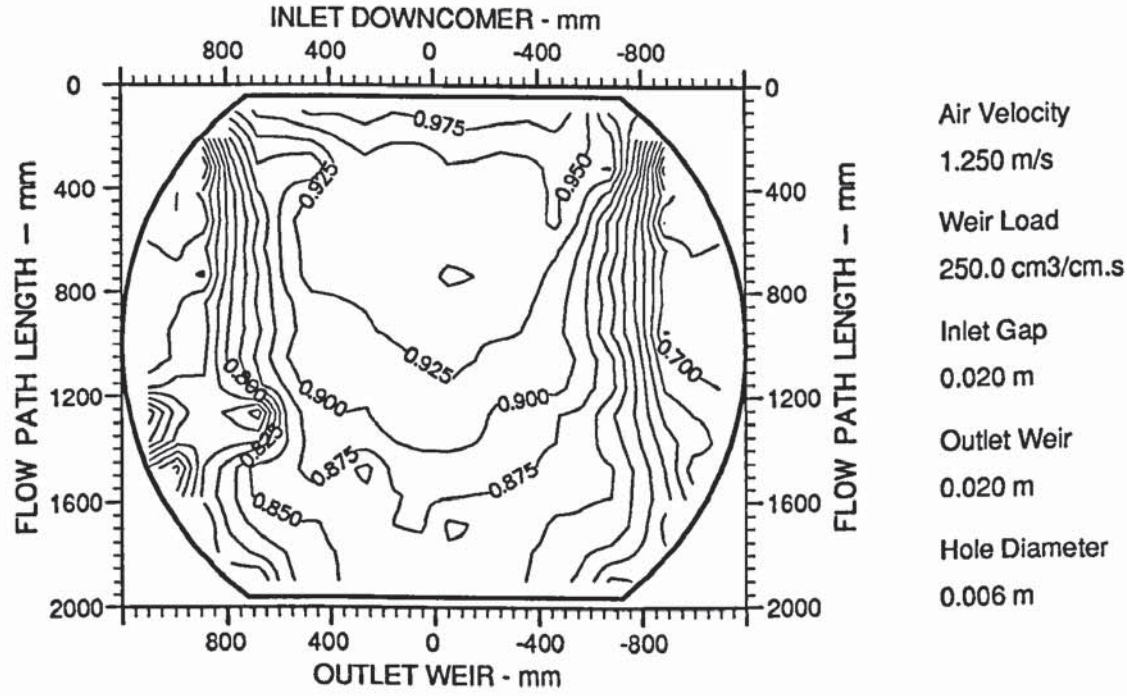

Figure A7.22 Two dimensional reduced temperature profiles showing distinctively "U-shaped" isotherms (designation U).

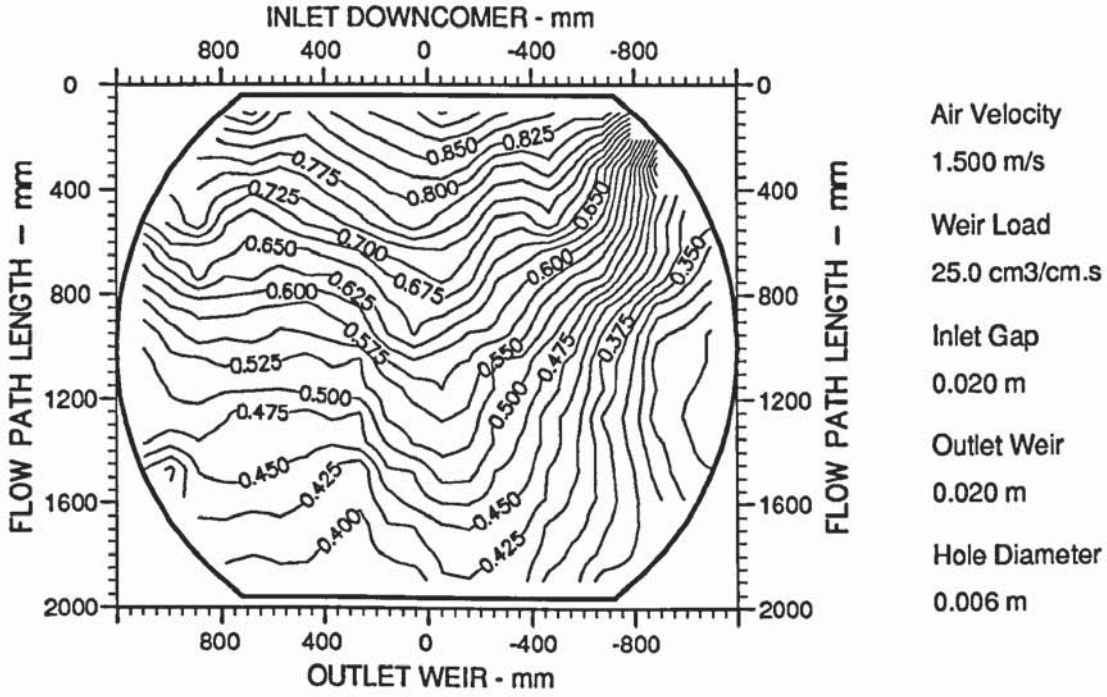

Figure A7.23 Two dimensional reduced temperature profiles showing shallow transverse "U-shaped" isotherms (designation hU).

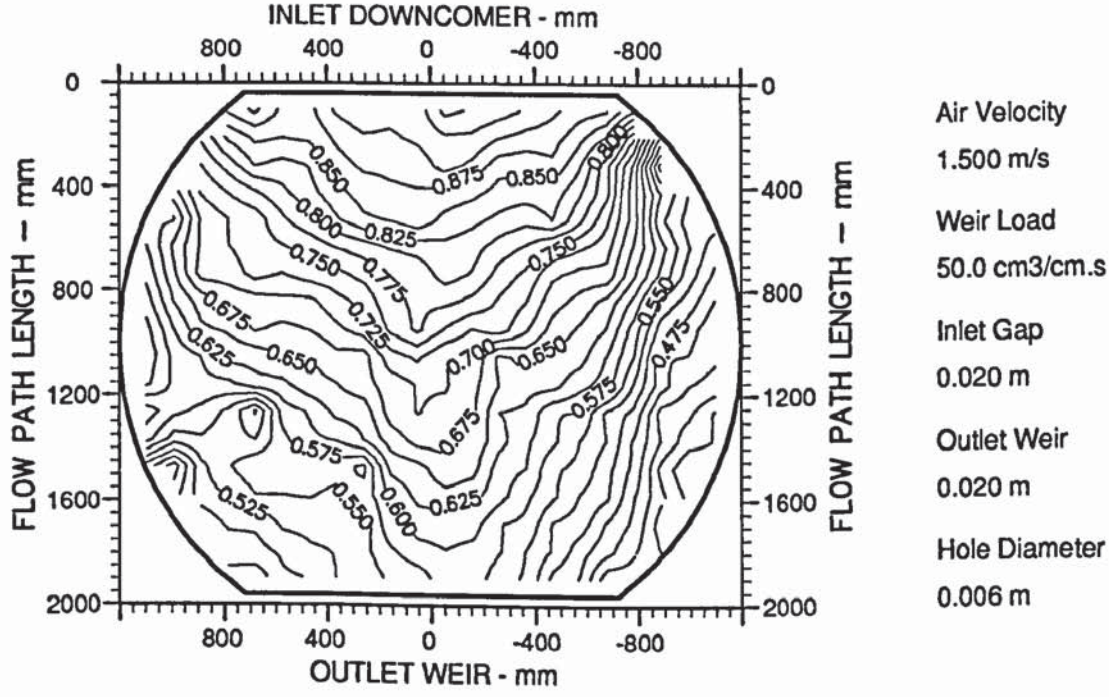

Figure A7.24 Two dimensional reduced temperature profiles showing straight and parallel isotherms (designation P).

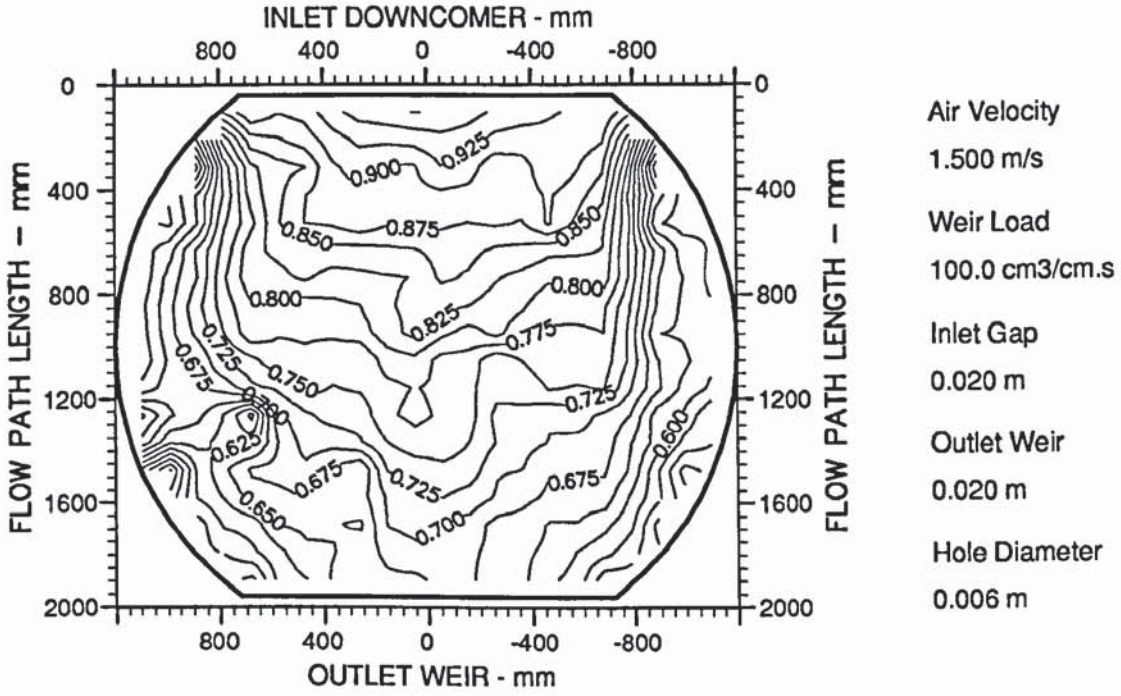

Figure A7.25 Two dimensional reduced temperature profiles showing distinctively "U-shaped" isotherms (designation U).

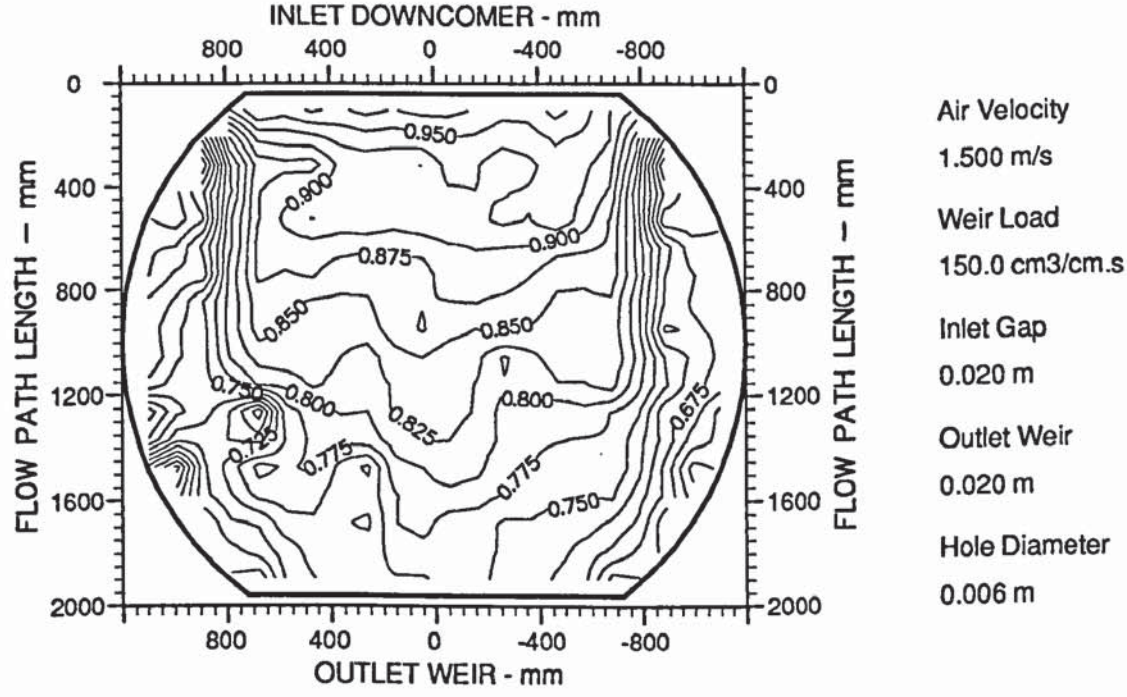

Figure A7.26 Two dimensional reduced temperature profiles showing distinctively "U-shaped" isotherms (designation U).

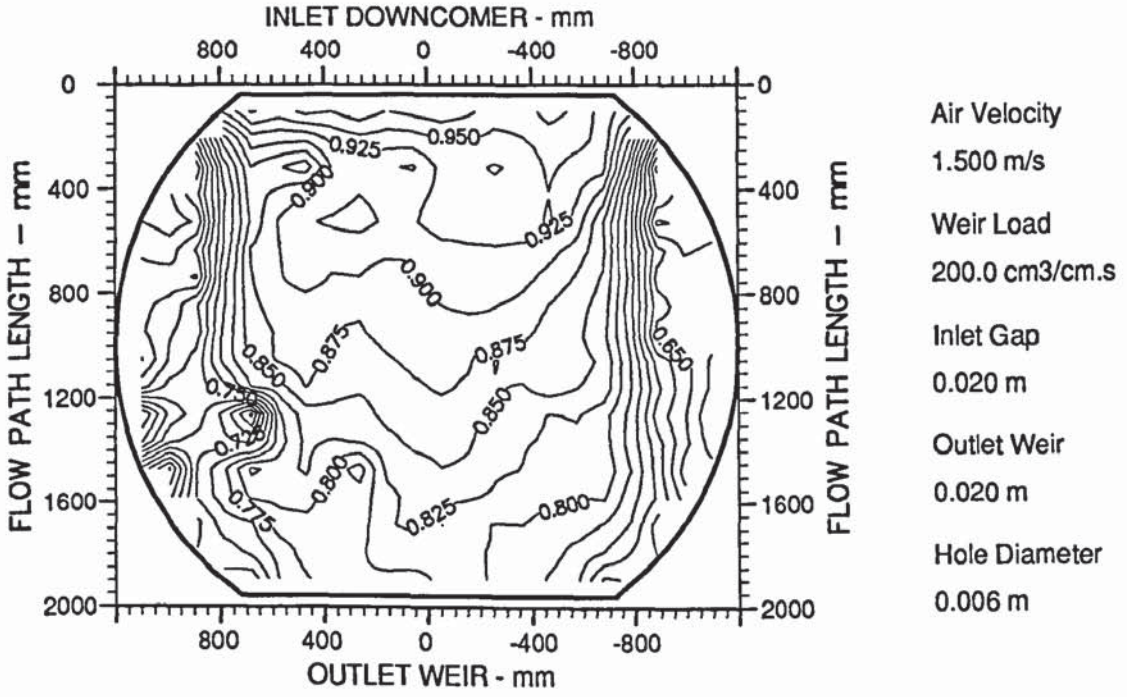

Figure A7.27 Two dimensional reduced temperature profiles showing shallow transverse "U-shaped" isotherms (designation hU).

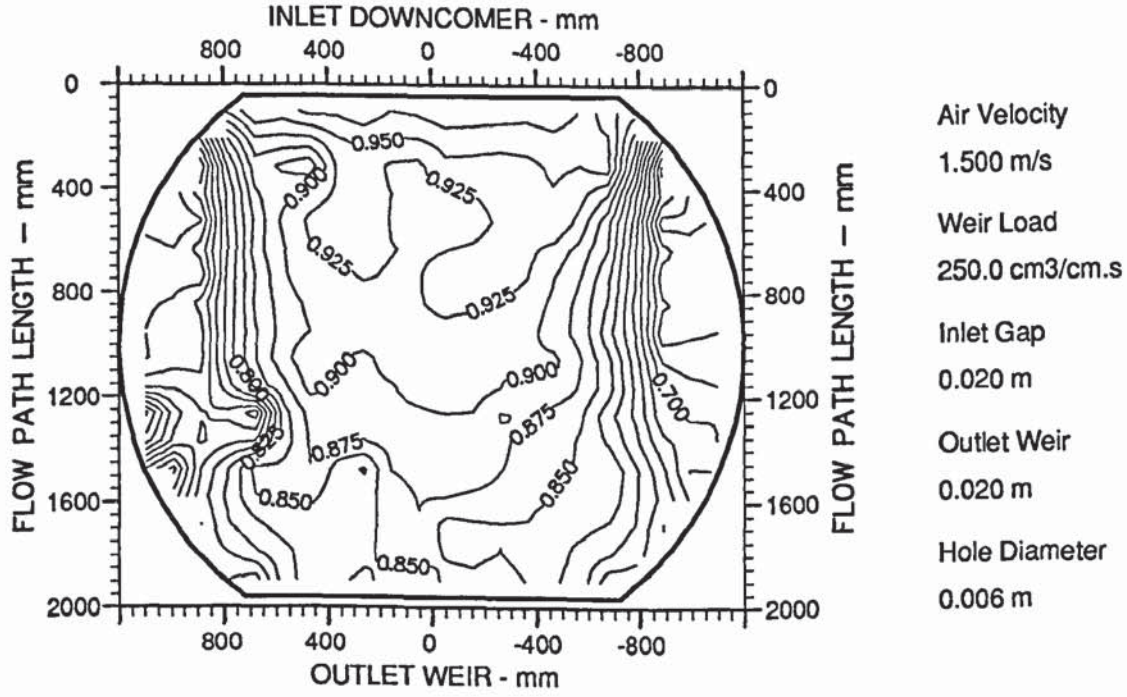

Figure A7.28 Two dimensional reduced temperature profiles showing a mixture of parallel isotherms and shallow "U-shapes" (designation P/hU).

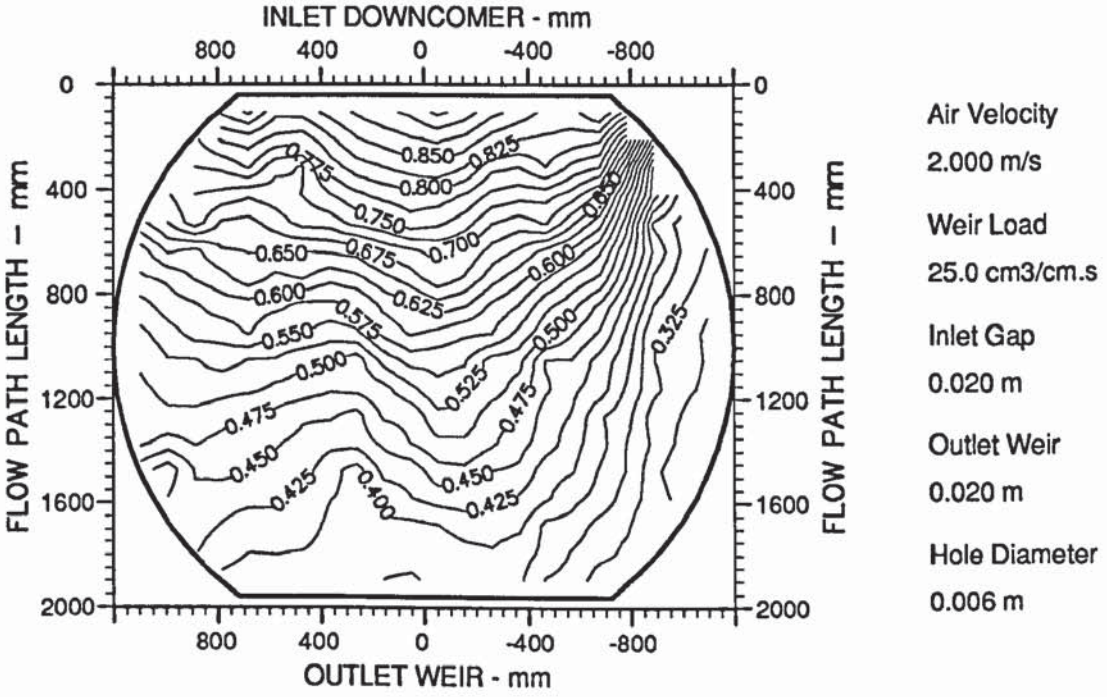

Figure A7.29 Two dimensional reduced temperature profiles showing severe transverse "U-shaped" isotherms (designation TU).

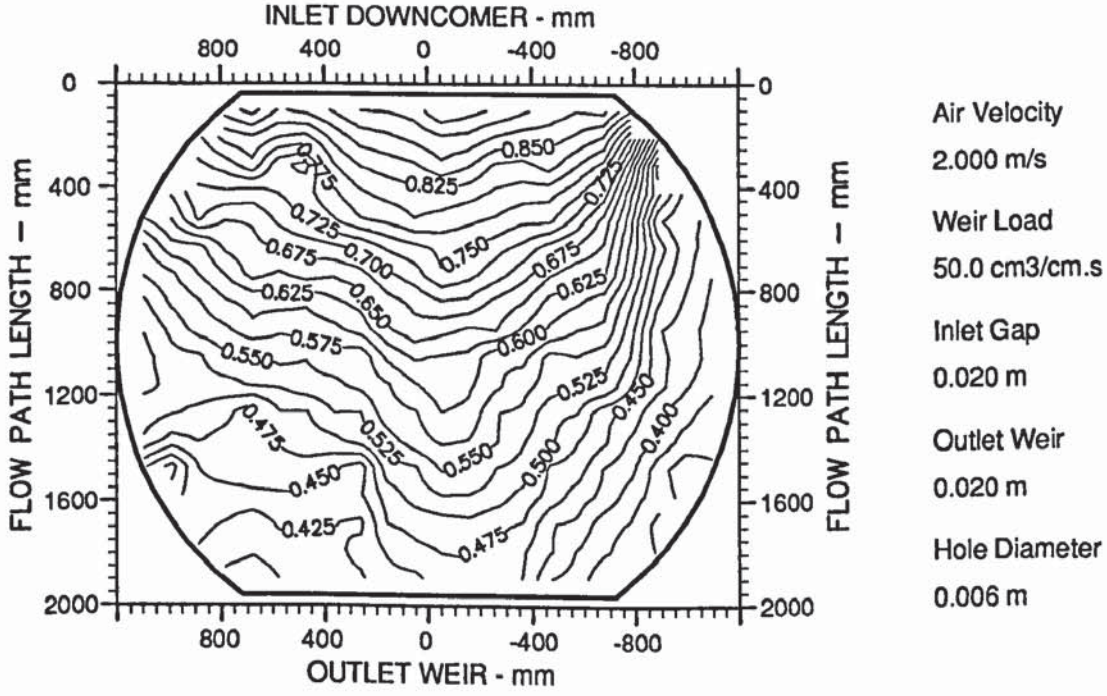

Figure A7.30 Two dimensional reduced temperature profiles showing severe transverse "U-shaped" isotherms (designation TU).

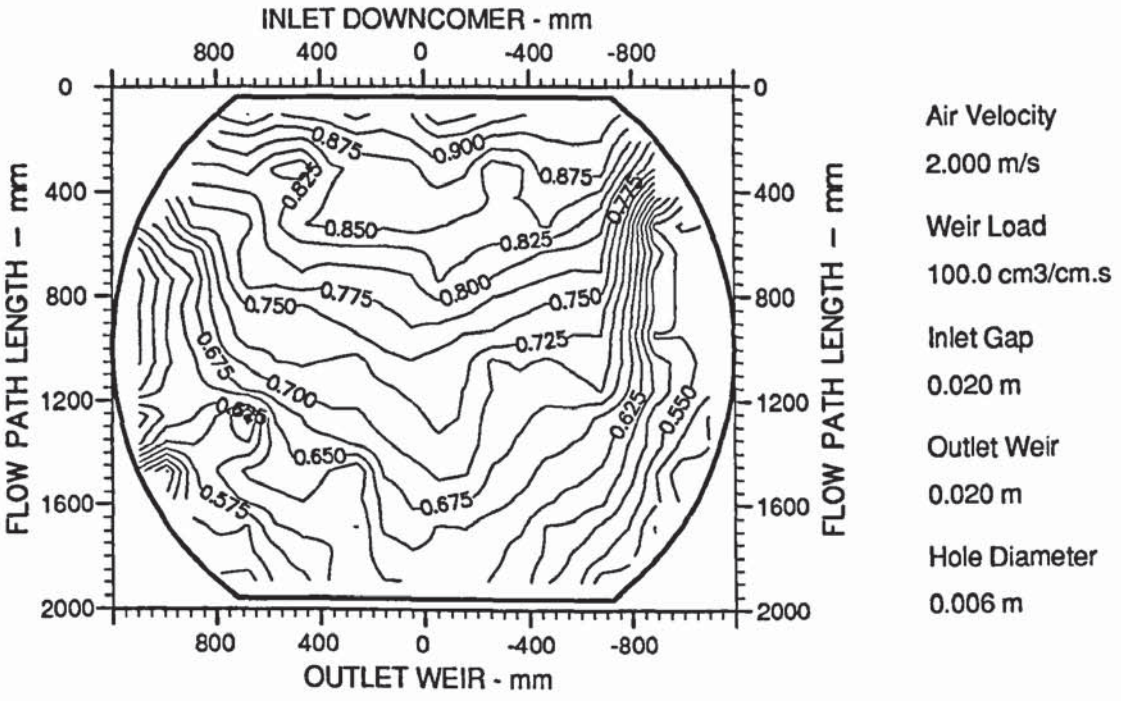

Figure A7.31 Two dimensional reduced temperature profiles showing shallow transverse "U-shaped" isotherms (designation hU).

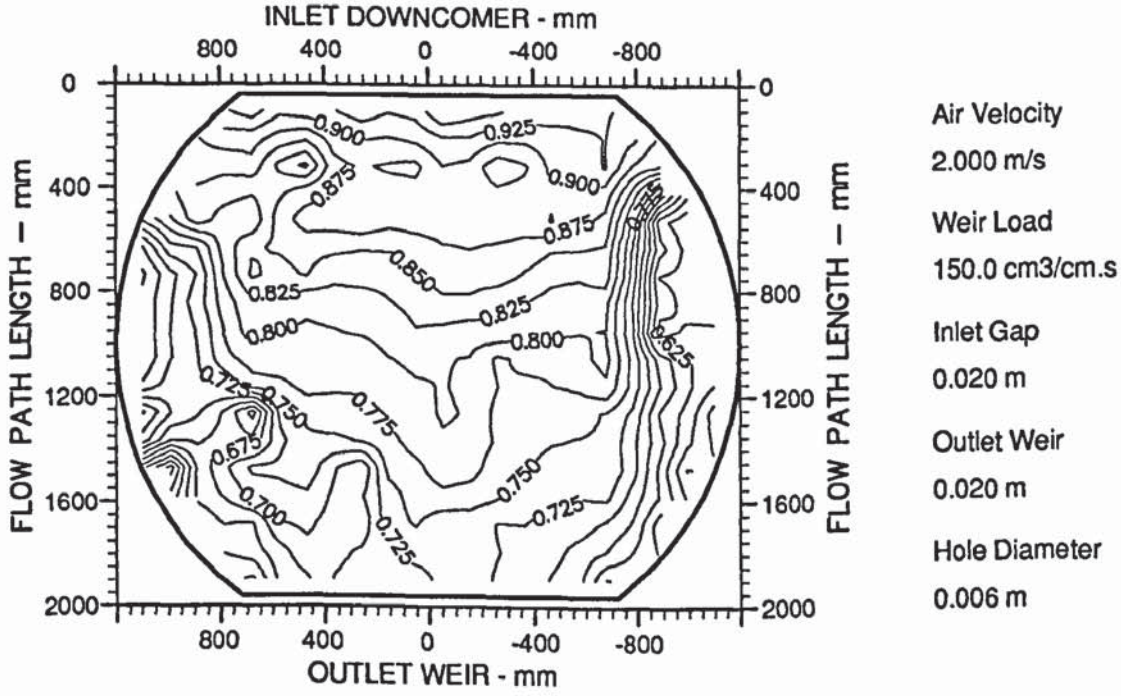

Figure A7.32 Two dimensional reduced temperature profiles showing shallow transverse "U-shaped" isotherms (designation hU).

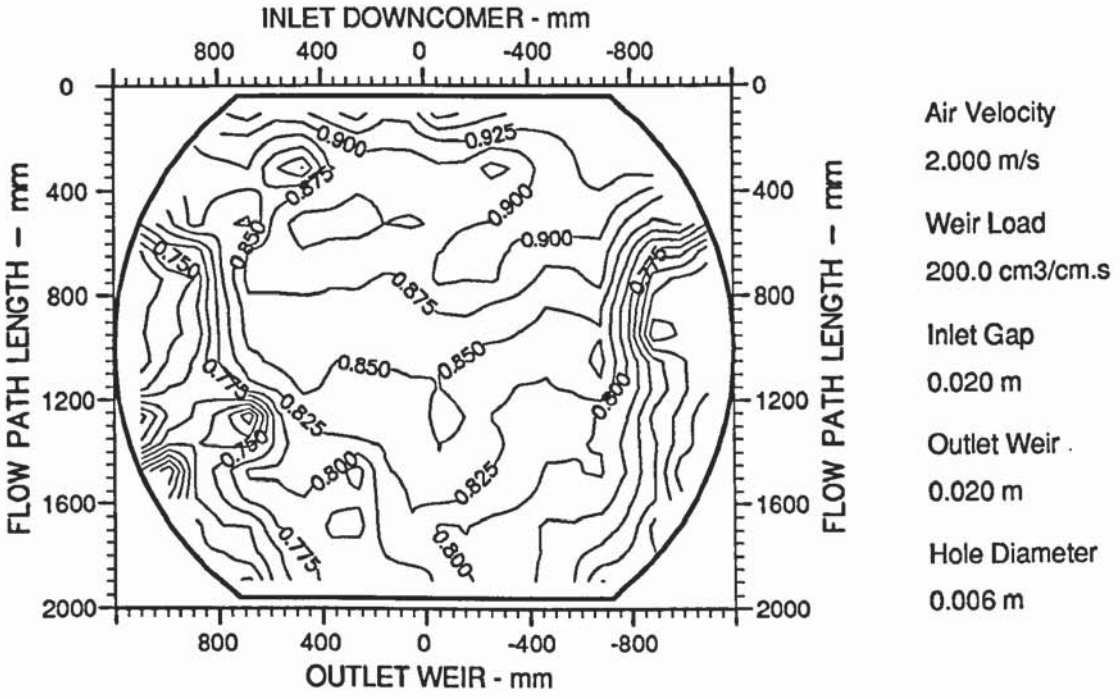

Figure A7.33 Two dimensional reduced temperature profiles showing severe transverse "U-shaped" isotherms (designation TU).

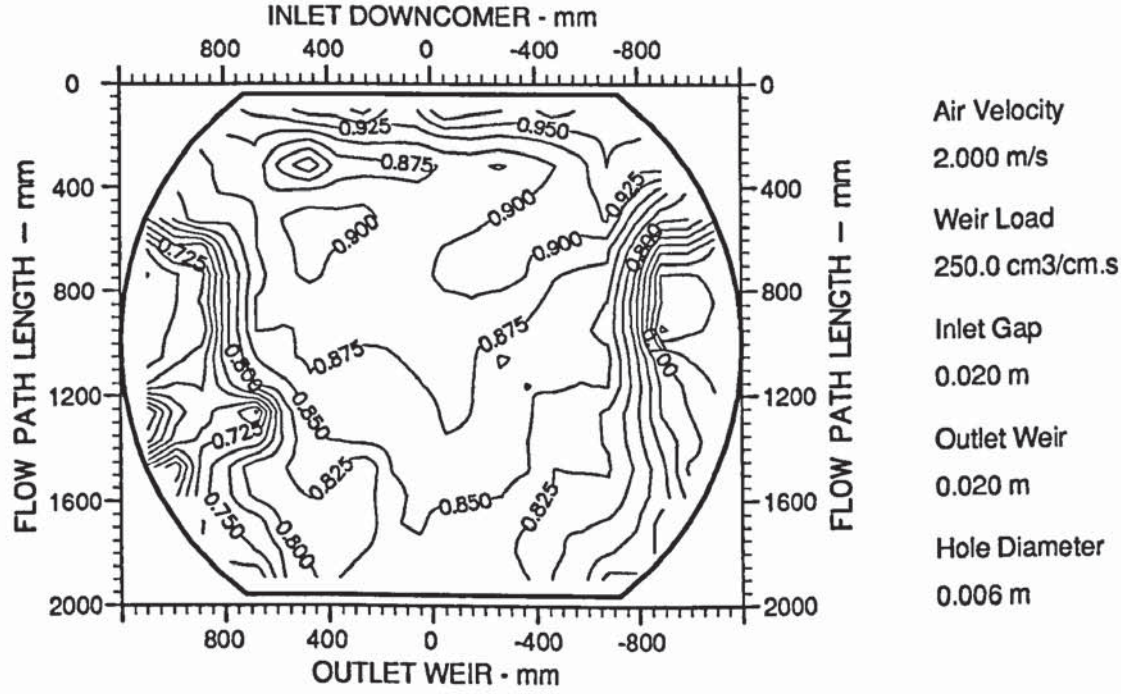

Figure A7.34 Two dimensional reduced temperature profiles showing severe transverse "U-shaped" isotherms (designation TU).

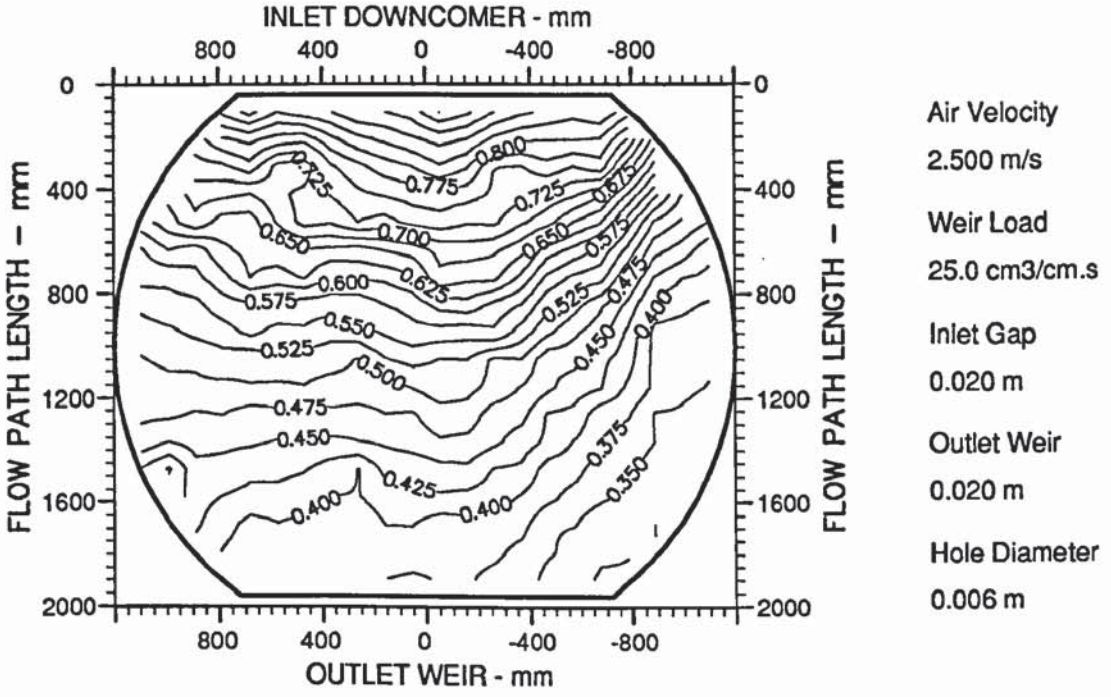

Figure A7.35 Two dimensional reduced temperature profiles showing confused and severe transverse "U-shaped" isotherms (designation M/TU).

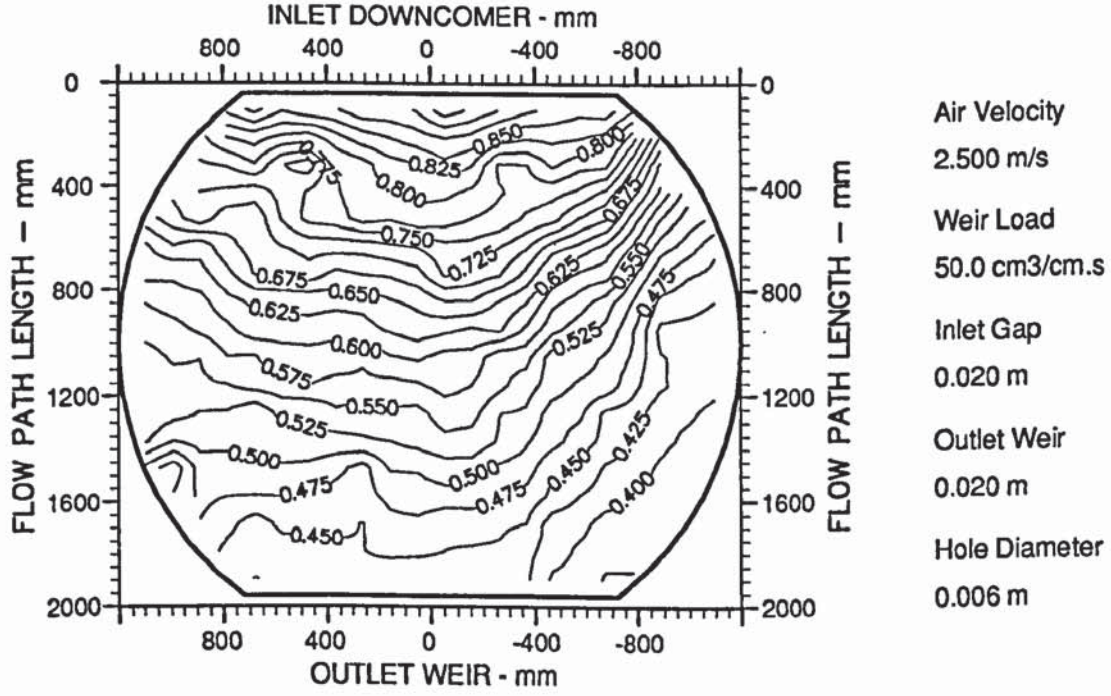

Figure A7.36 Two dimensional reduced temperature profiles showing confused and severe transverse "U-shaped" isotherms (designation M/TU).

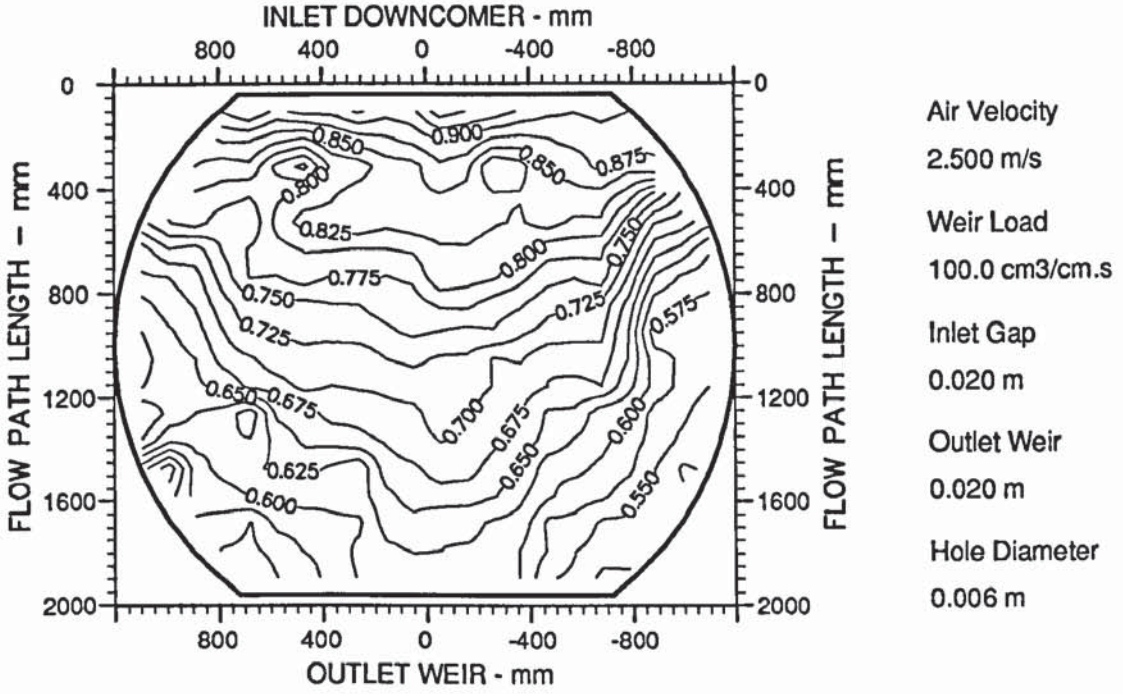

Figure A7.37 Two dimensional reduced temperature profiles showing severe transverse "U-shaped" isotherms (designation TU).

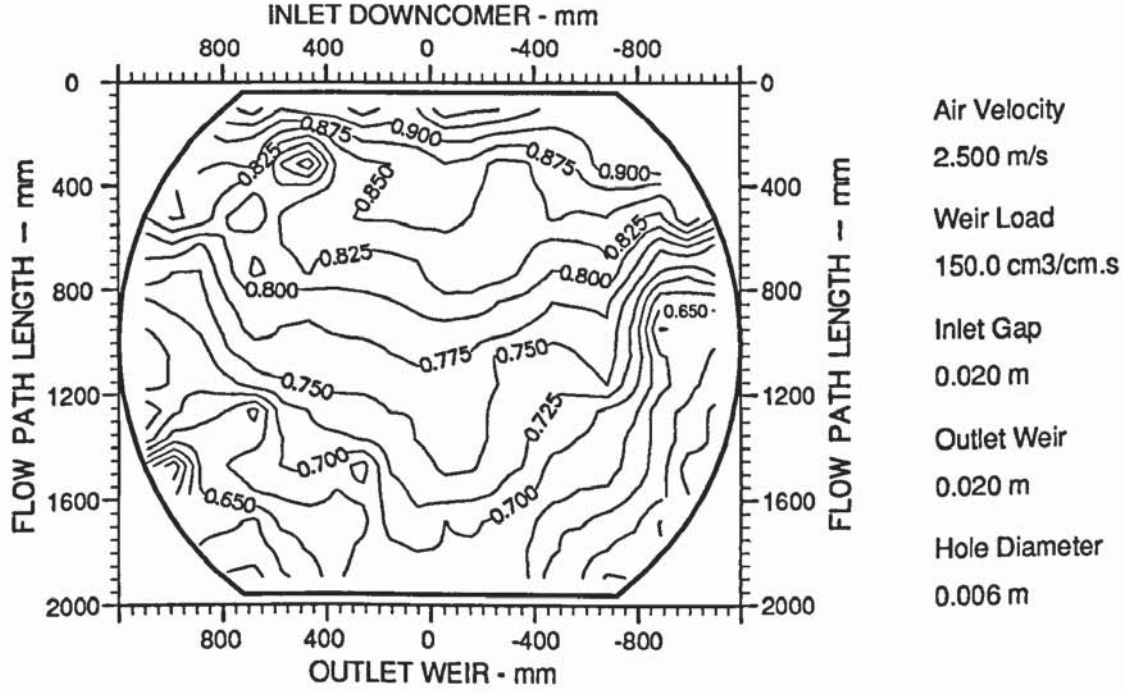

Figure A7.38 Two dimensional reduced temperature profiles showing severe transverse "U-shaped" isotherms (designation TU).

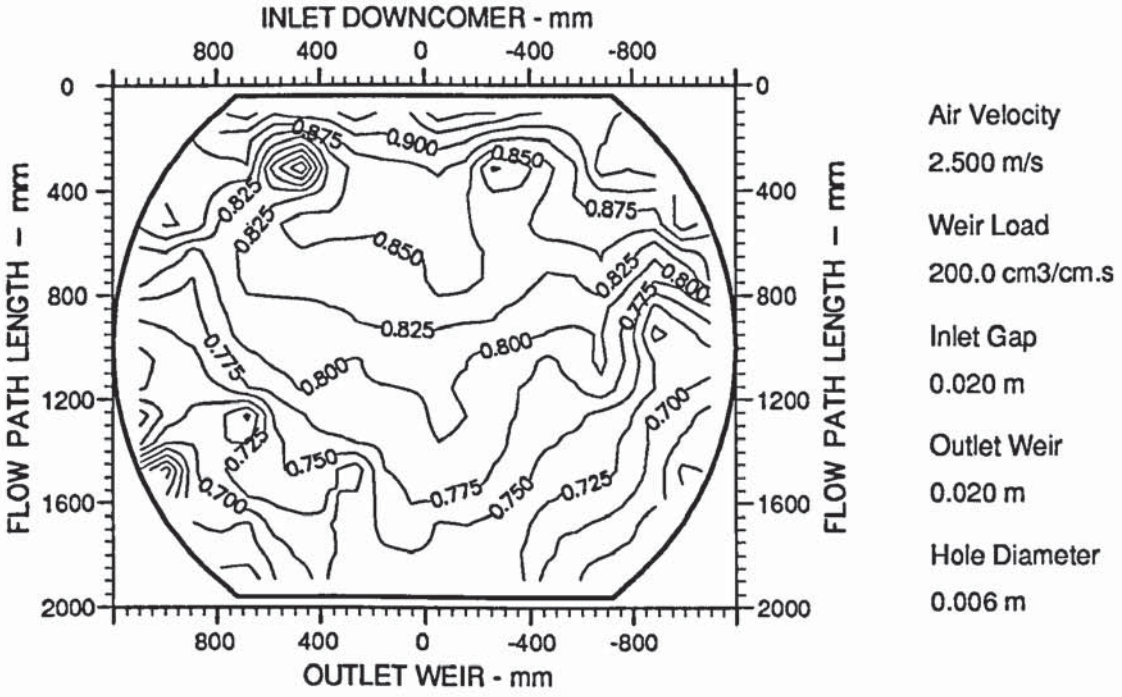

Figure A7.39 Two dimensional reduced temperature profiles showing confused and severe transverse "U-shaped" isotherms (designation M/TU).

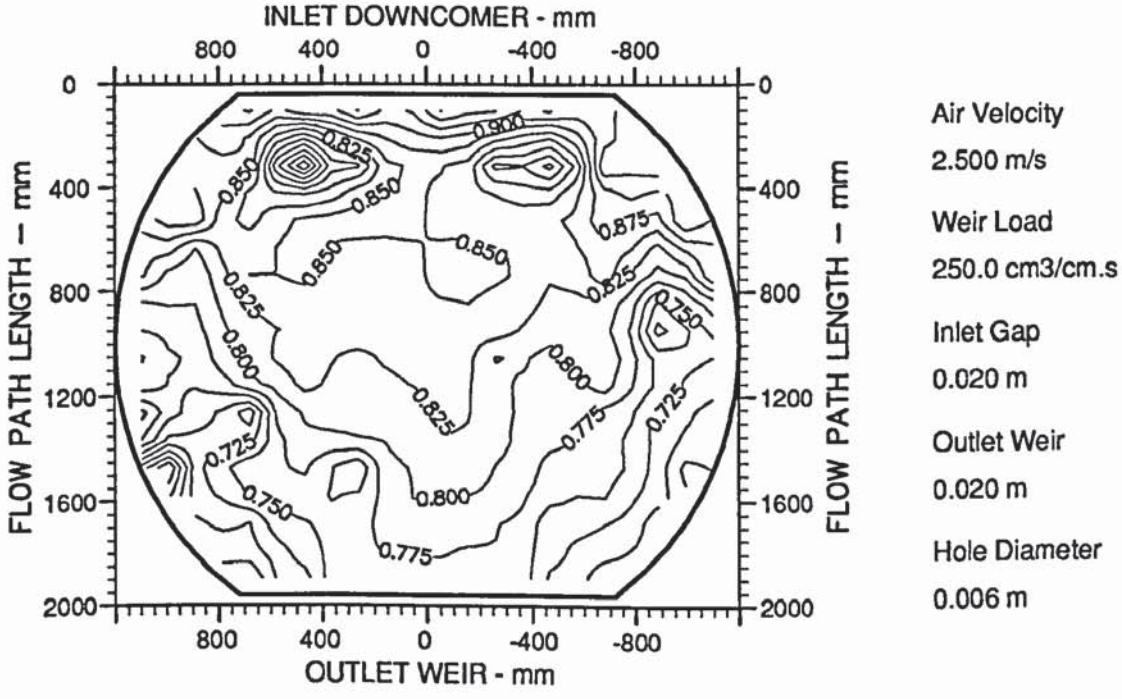

Figure A7.40 Two dimensional reduced temperature profiles showing mixed or confused isotherms (designation M).

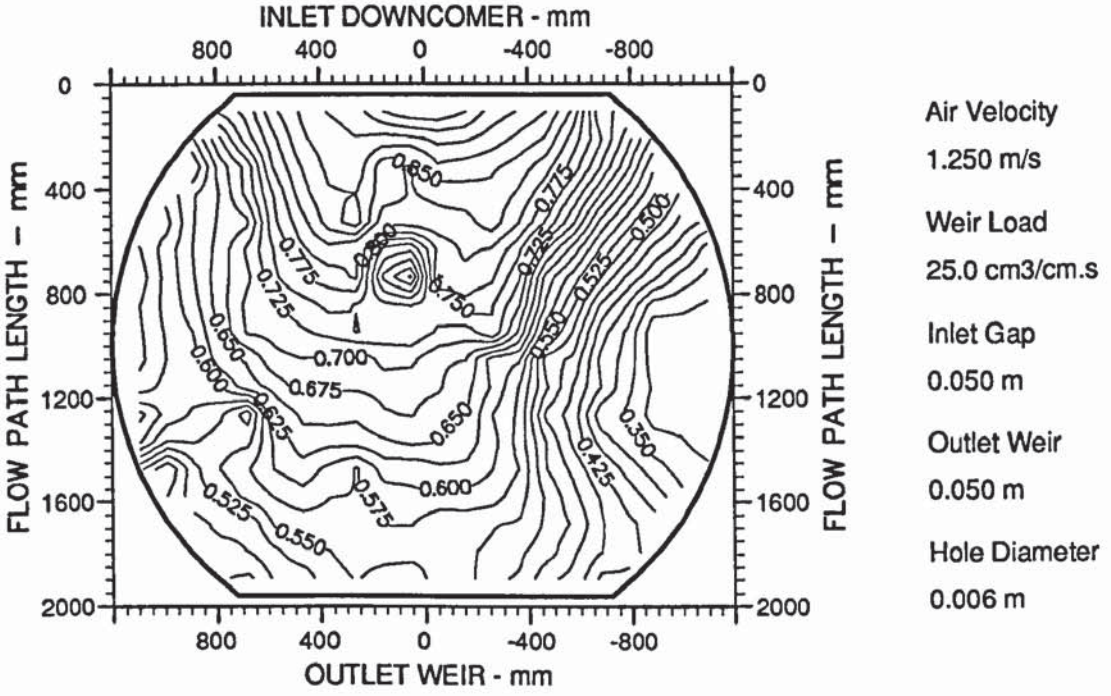

Figure A7.41 Two dimensional reduced temperature profiles showing a mixture of "U-shaped" and confused isotherms (designation U/M).

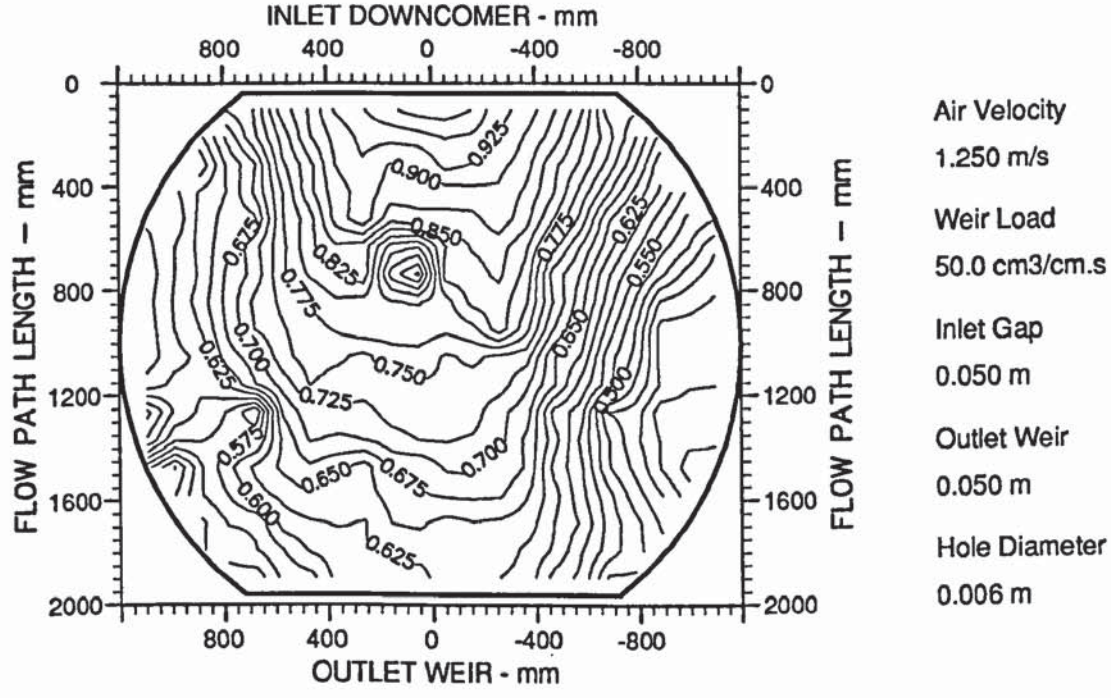

Figure A7.42 Two dimensional reduced temperature profiles showing a mixture of "U-shaped" and confused isotherms (designation U/M).

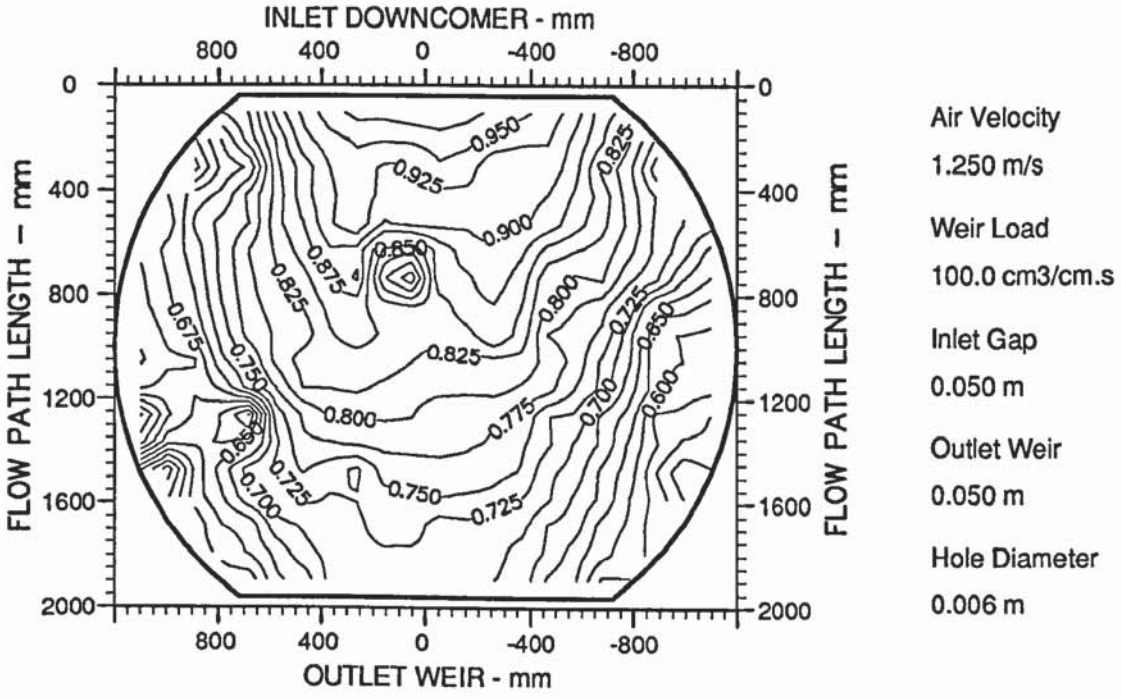

Figure A7.43 Two dimensional reduced temperature profiles showing straight and parallel isotherms (designation P).

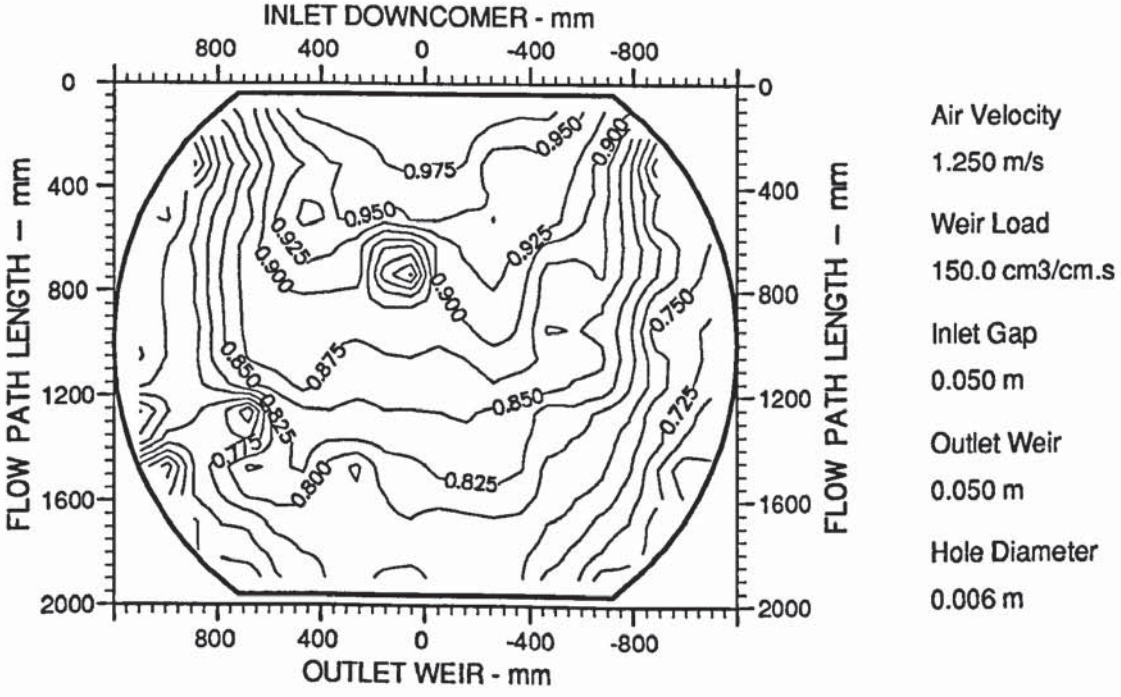

Figure A7.44 Two dimensional reduced temperature profiles showing straight and parallel isotherms (designation P).

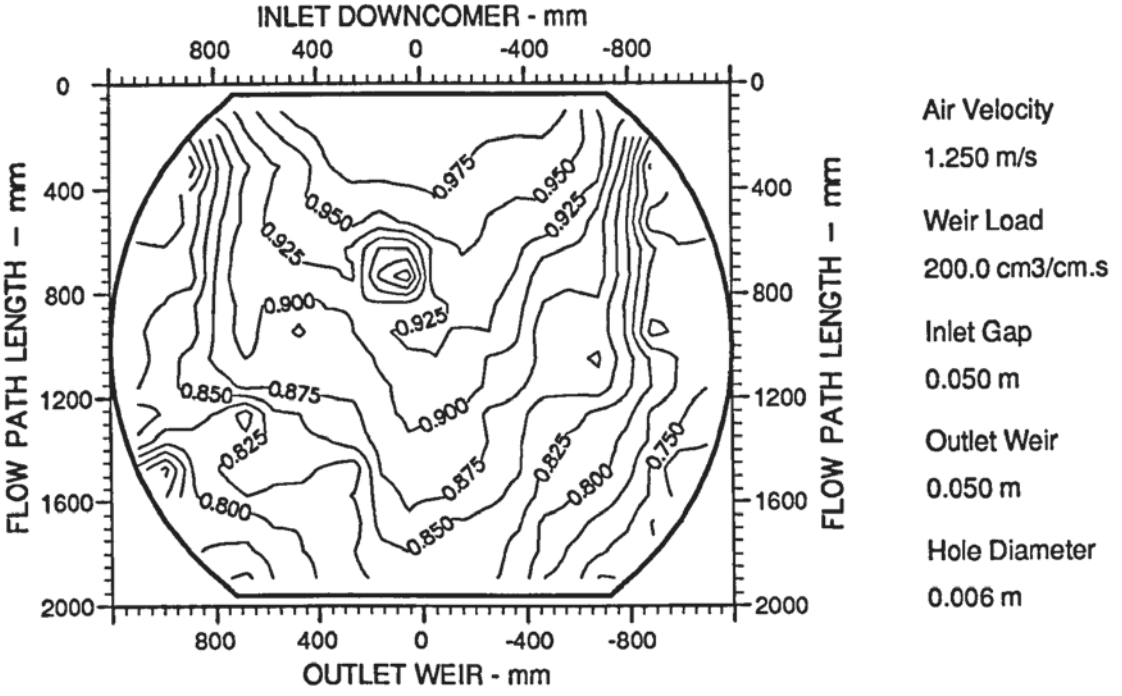

Figure A7.45 Two dimensional reduced temperature profiles showing a mixture of "U-shaped" and confused isotherms (designation U/M).

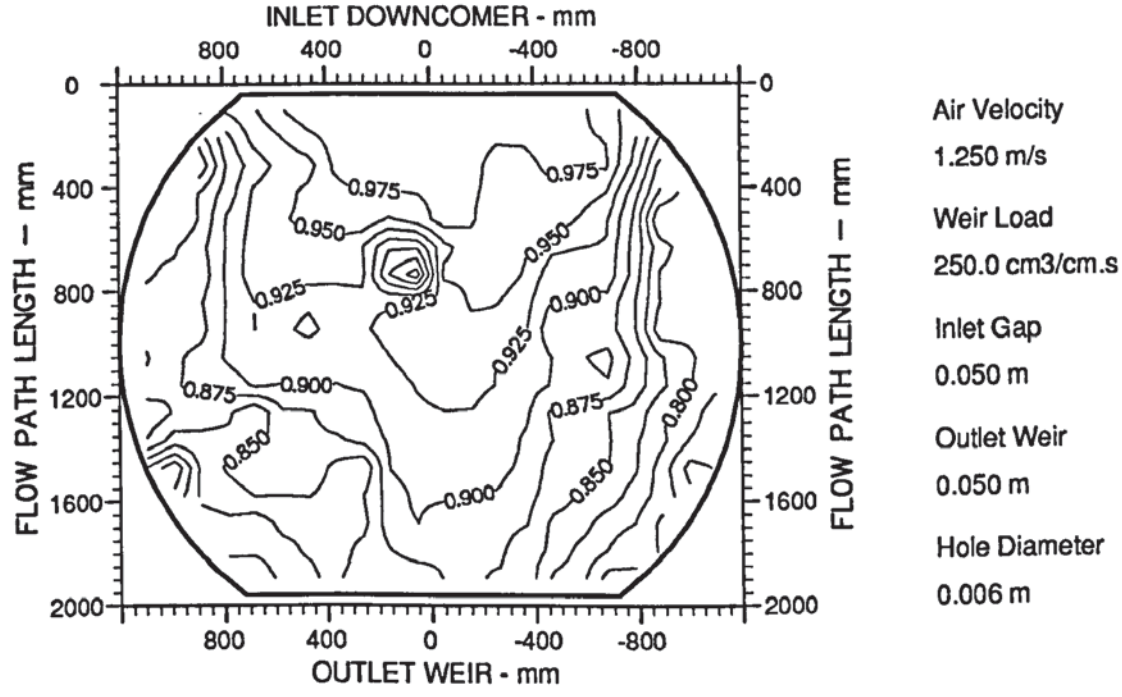

Figure A7.46 Two dimensional reduced temperature profiles showing distinctively "U-shaped" isotherms (designation U).

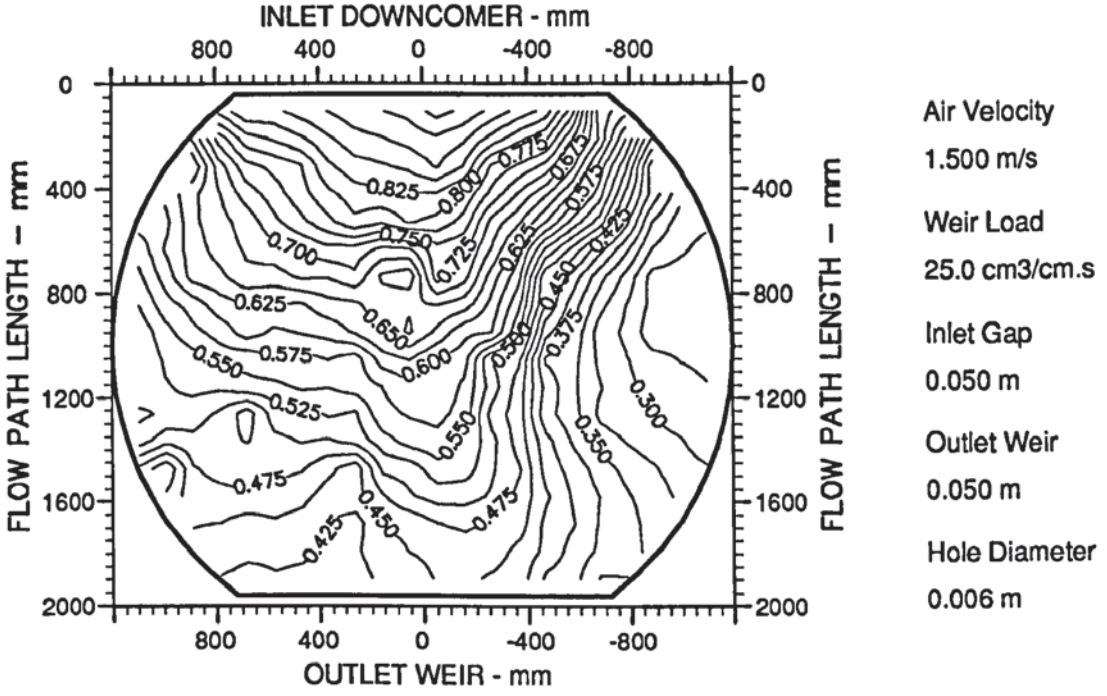

Figure A7.47 Two dimensional reduced temperature profiles showing a mixture of "U-shaped" and confused isotherms (designation U/M).

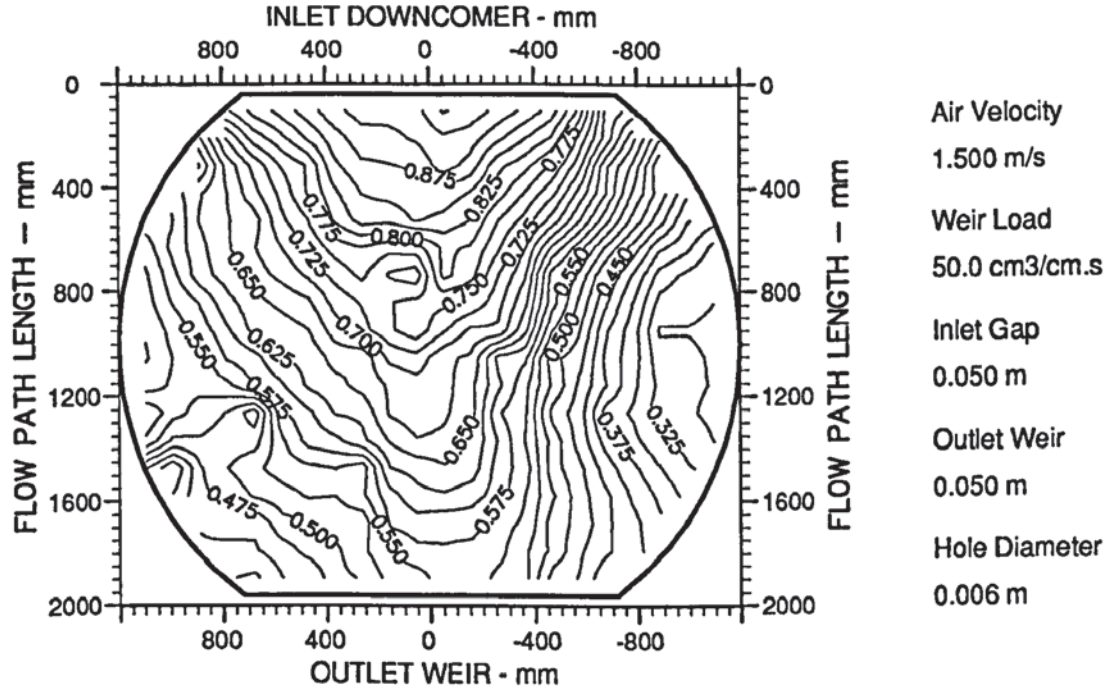

Figure A7.48 Two dimensional reduced temperature profiles showing straight and parallel isotherms (designation P).

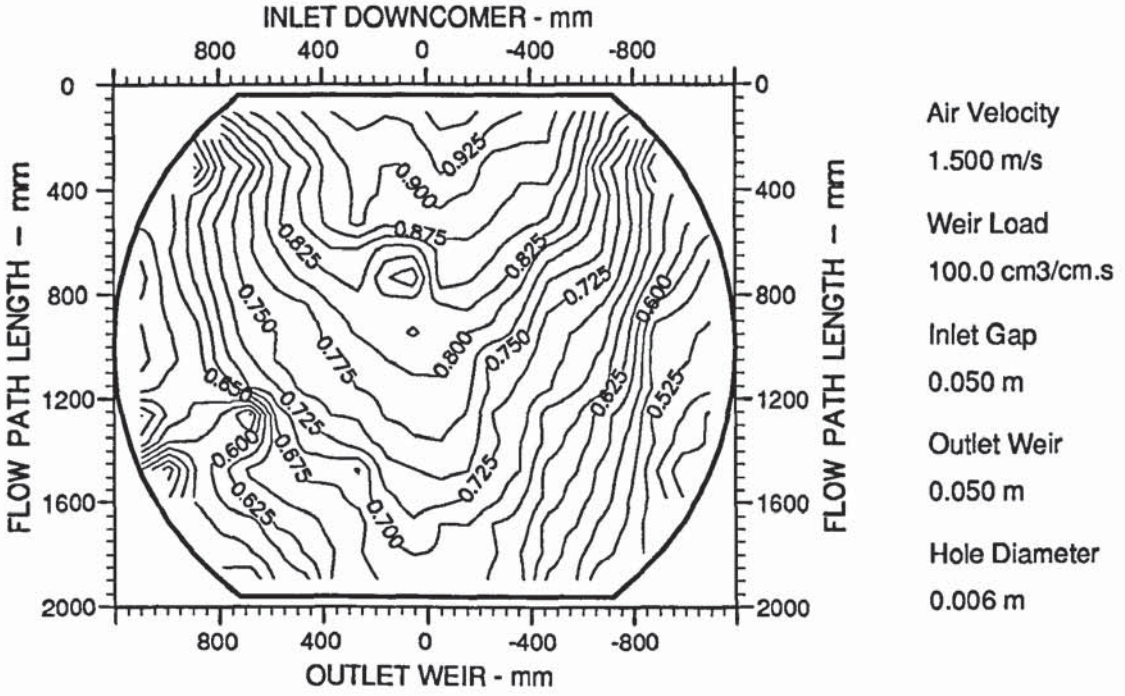

Figure A7.49 Two dimensional reduced temperature profiles showing distinctively "U-shaped" isotherms (designation U).

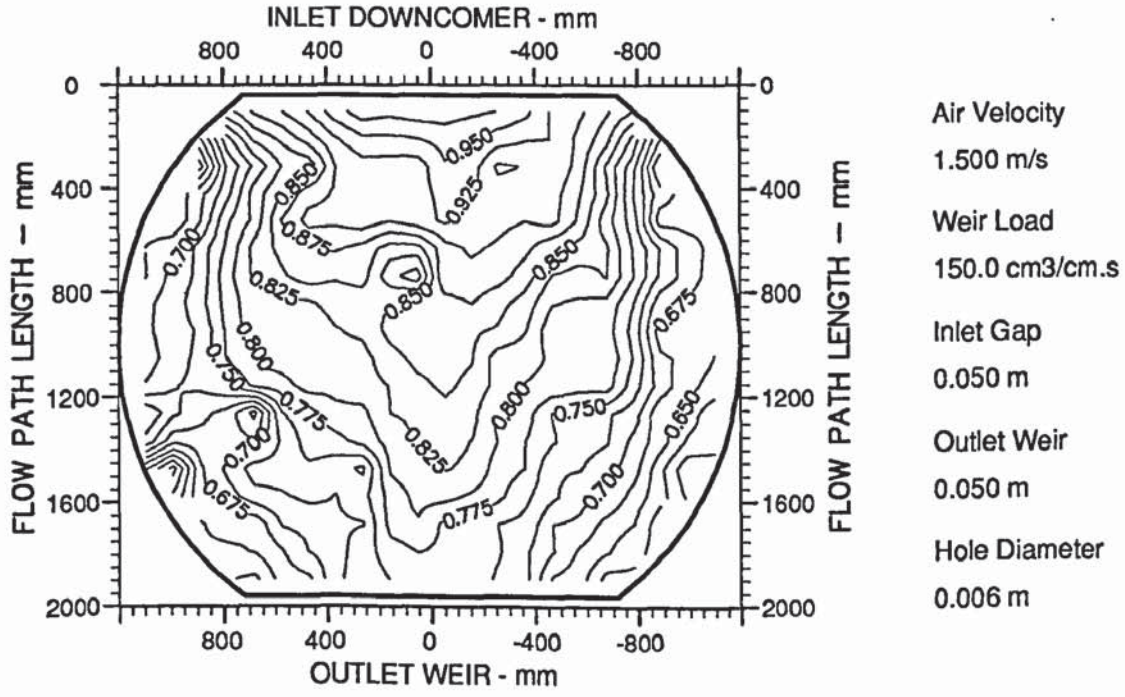

Figure A7.50 Two dimensional reduced temperature profiles showing distinctively "U-shaped" isotherms (designation U).

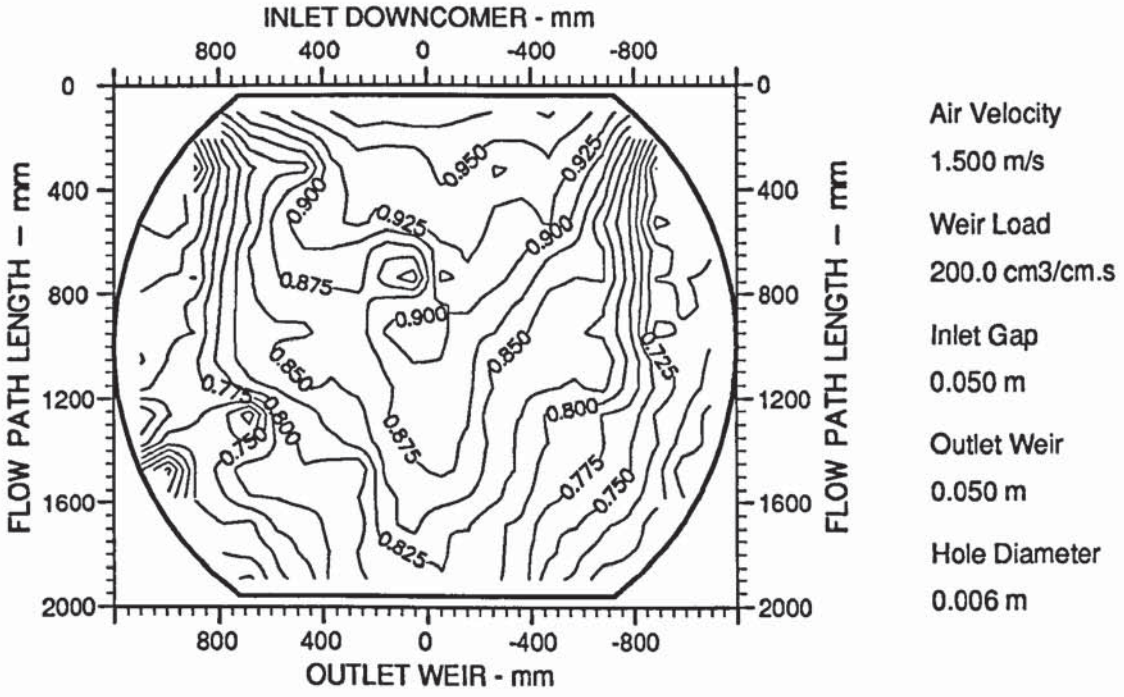

Figure A7.51 Two dimensional reduced temperature profiles showing distinctively "U-shaped" isotherms (designation U).

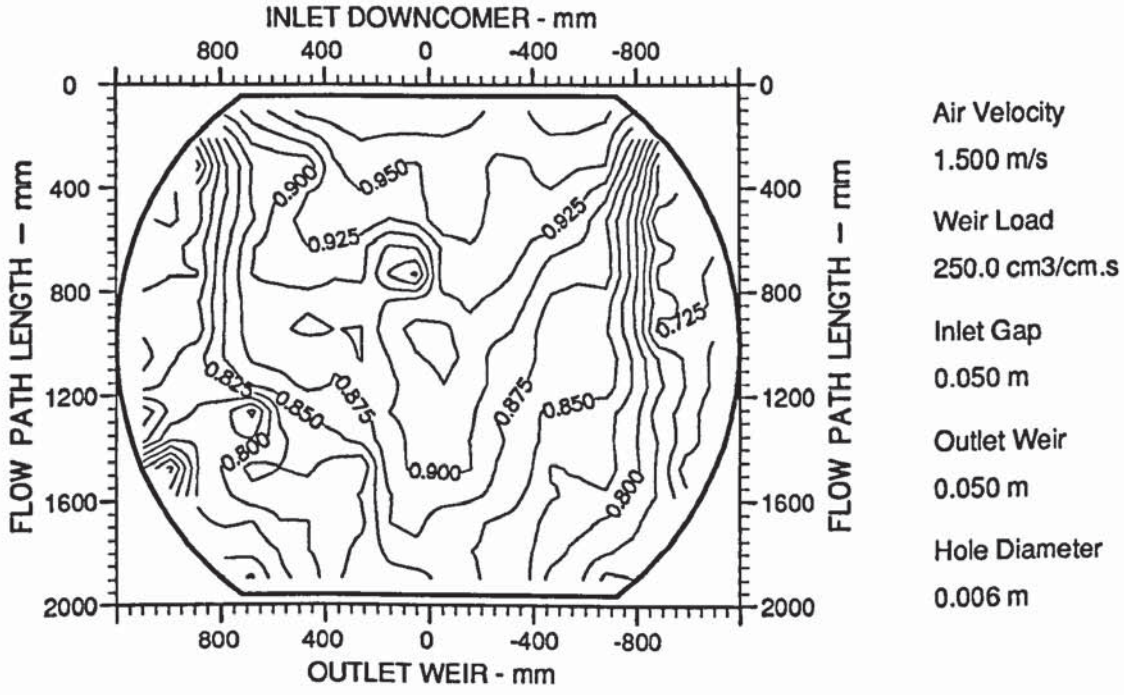

Figure A7.52 Two dimensional reduced temperature profiles showing shallow transverse "U-shaped" isotherms (designation hU).

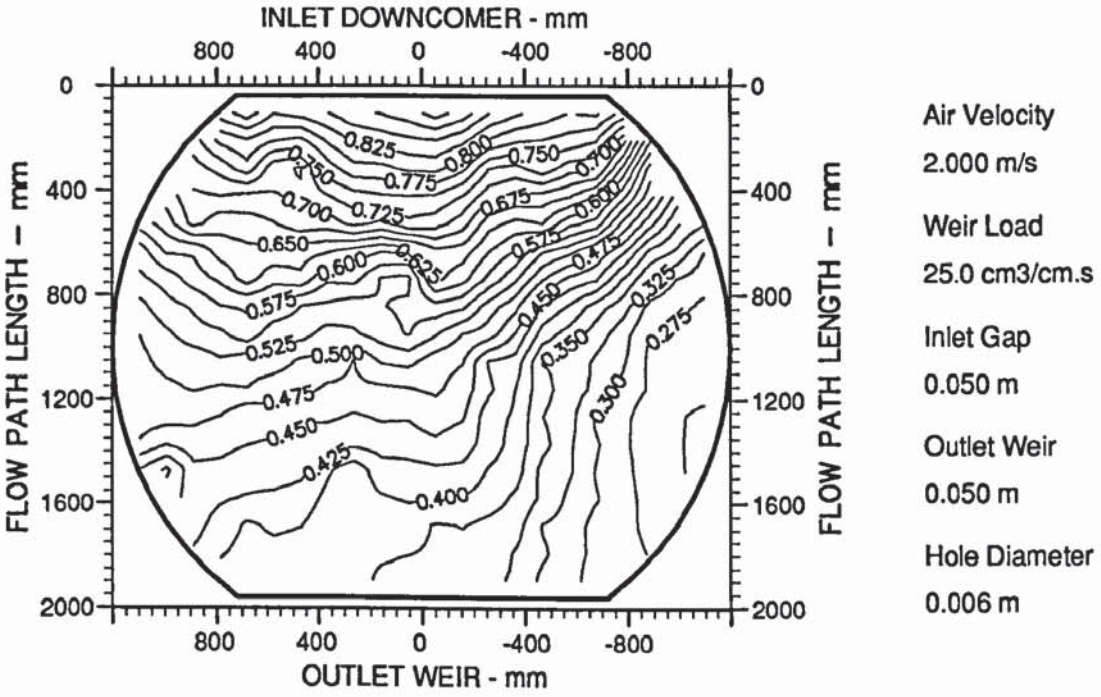

Figure A7.53 Two dimensional reduced temperature profiles showing severe transverse "U-shaped" isotherms (designation TU).

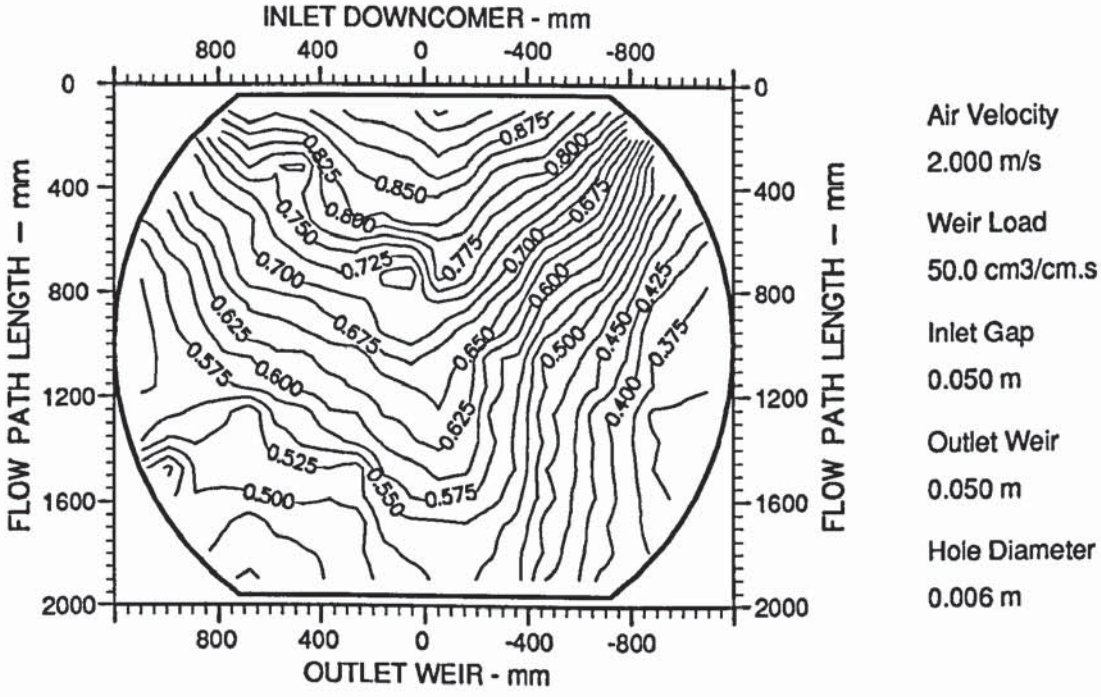

Figure A7.54 Two dimensional reduced temperature profiles showing distinctively "U-shaped" isotherms (designation U).

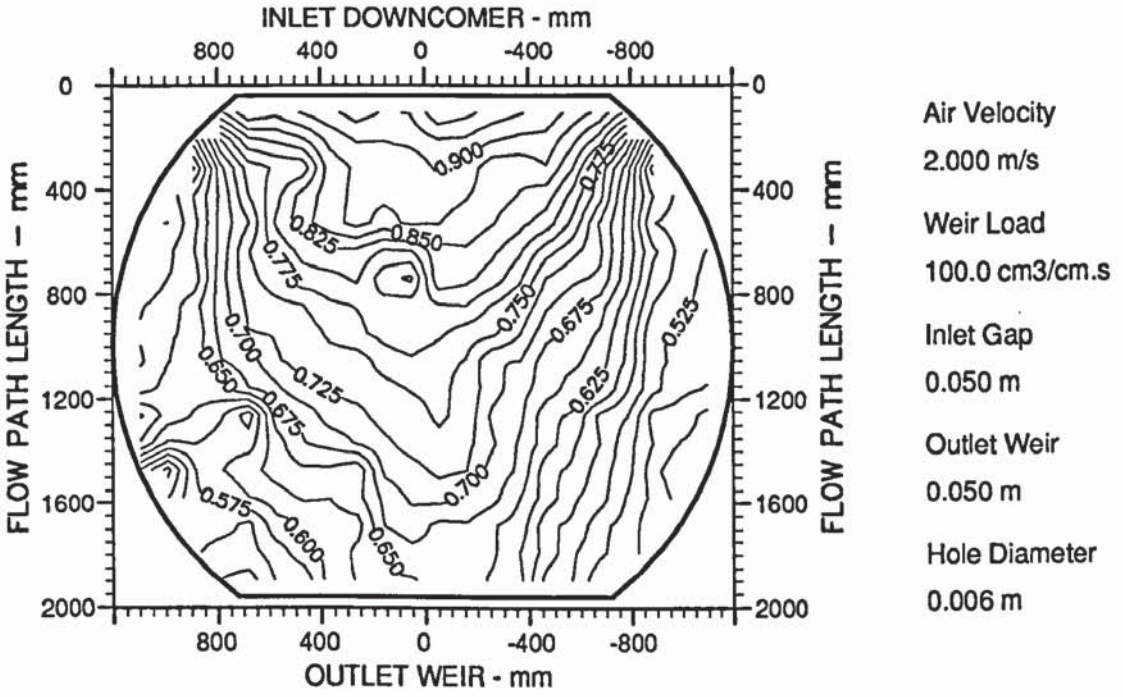

Figure A7.55 Two dimensional reduced temperature profiles showing distinctively "U-shaped" isotherms (designation U).

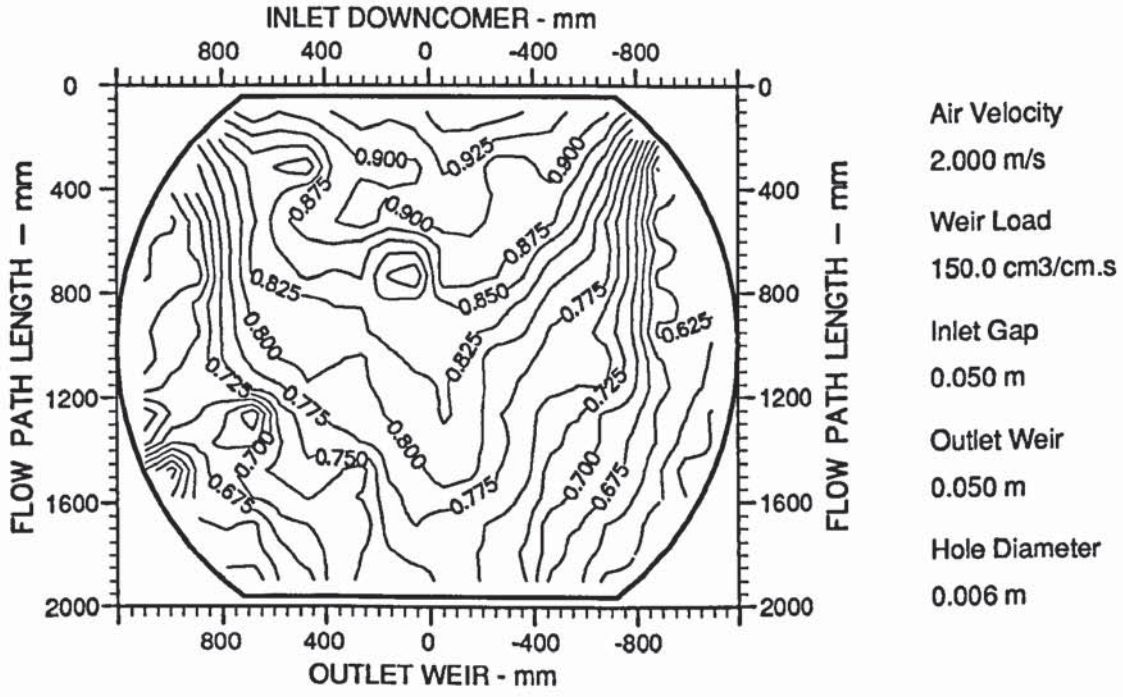

Figure A7.56 Two dimensional reduced temperature profiles showing a mixture of "U-shaped" and confused isotherms (designation U/M).

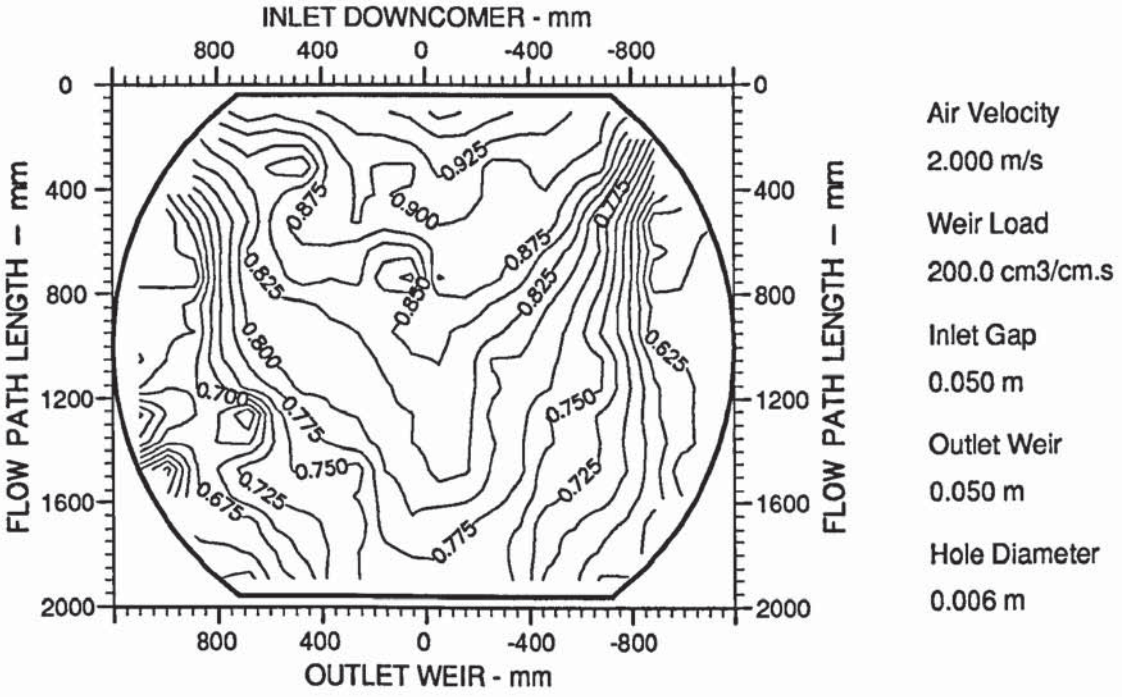

Figure A7.57 Two dimensional reduced temperature profiles showing severe transverse "U-shaped" isotherms (designation TU).

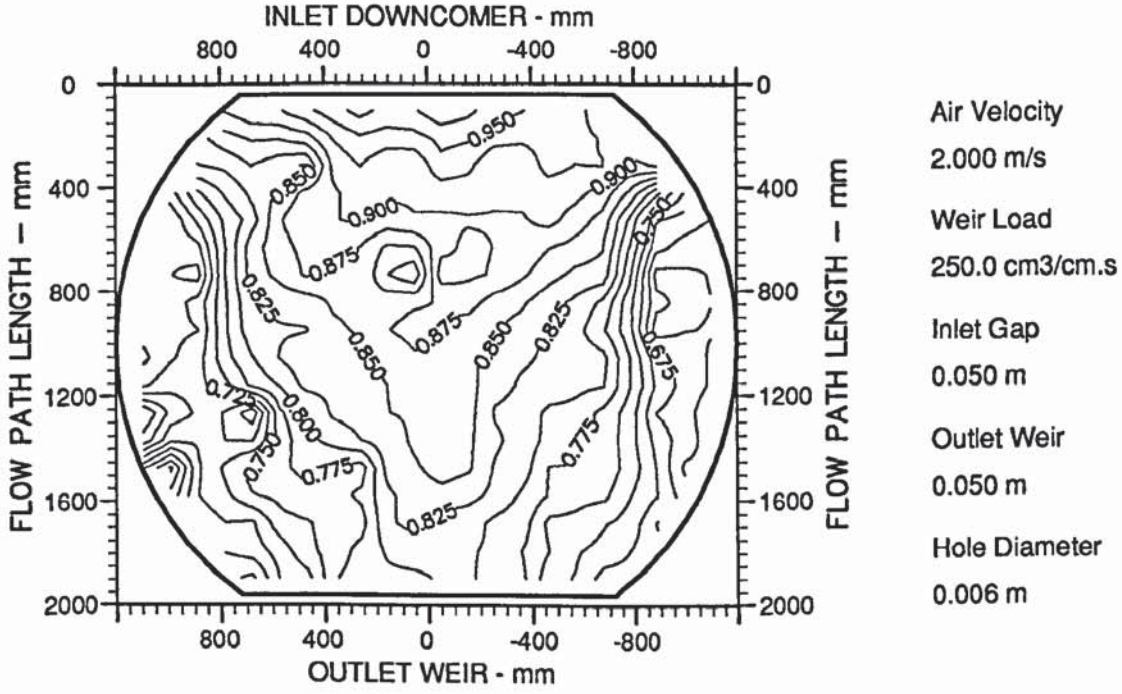

Figure A7.58 Two dimensional reduced temperature profiles showing distinctively "U-shaped" isotherms (designation U).

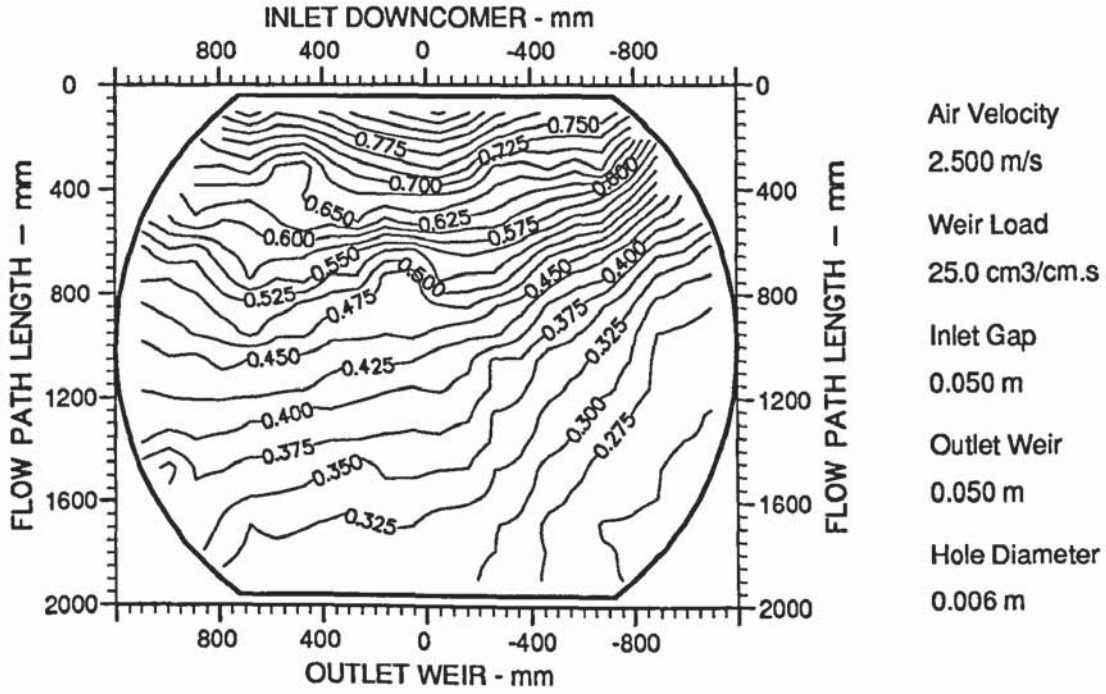

Figure A7.59 Two dimensional reduced temperature profiles showing distinctively "U-shaped" isotherms (designation U).

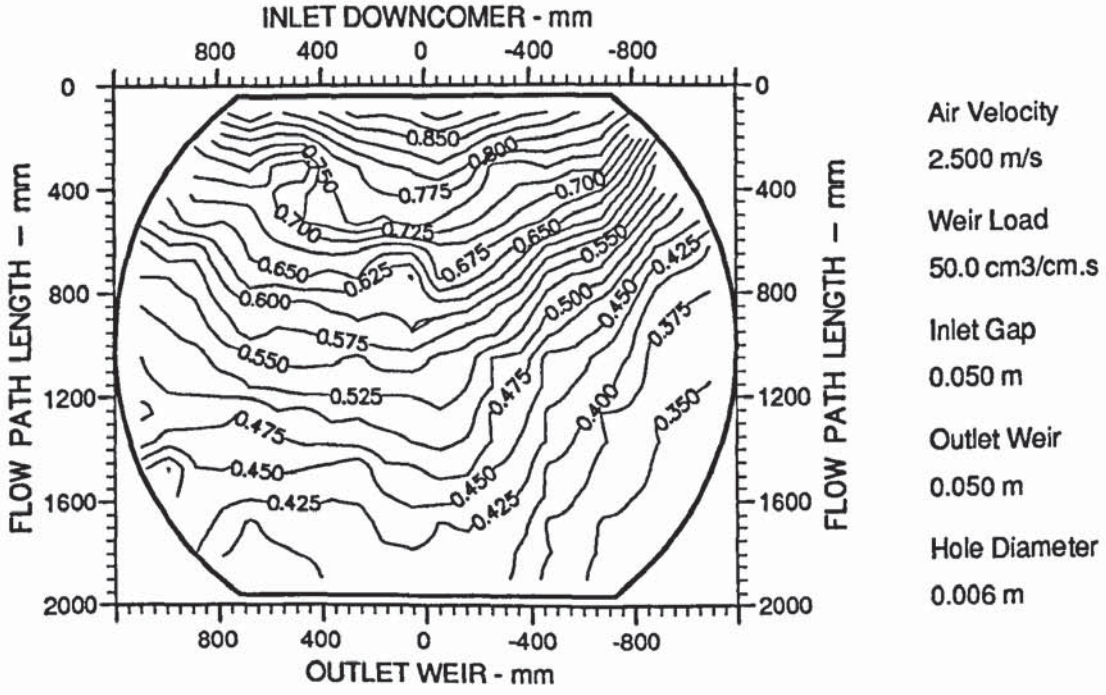

Figure A7.60 Two dimensional reduced temperature profiles showing a mixture of "U-shaped" and confused isotherms (designation U/M).

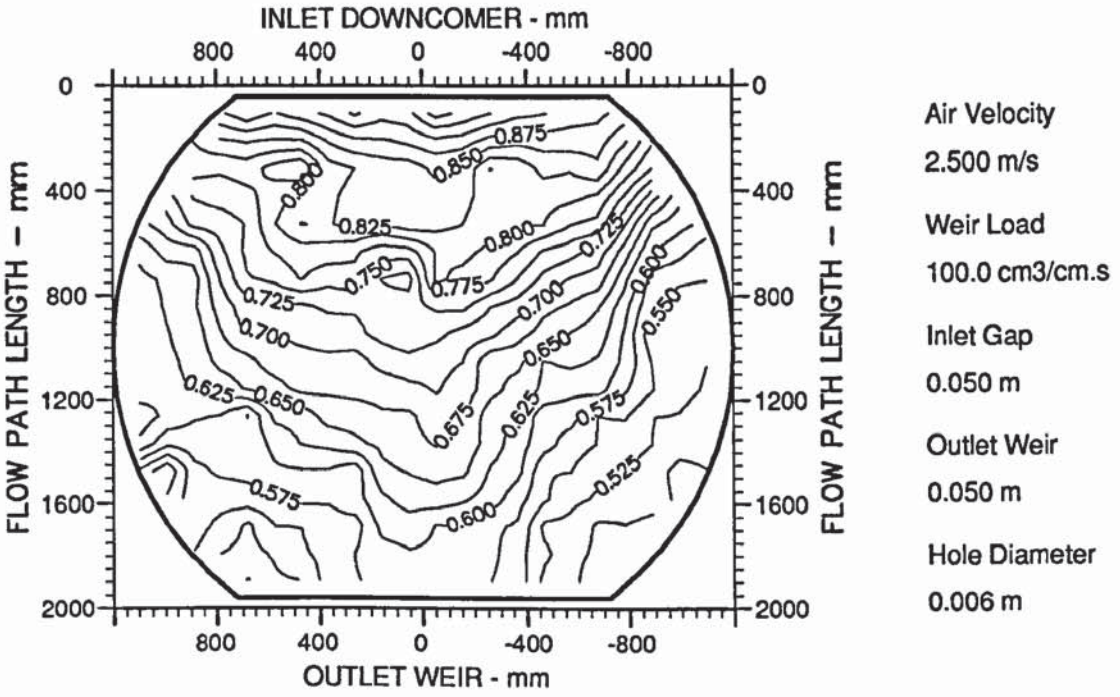

Figure A7.61 Two dimensional reduced temperature profiles showing confused and severe transverse "U-shaped" isotherms (designation M/TU).

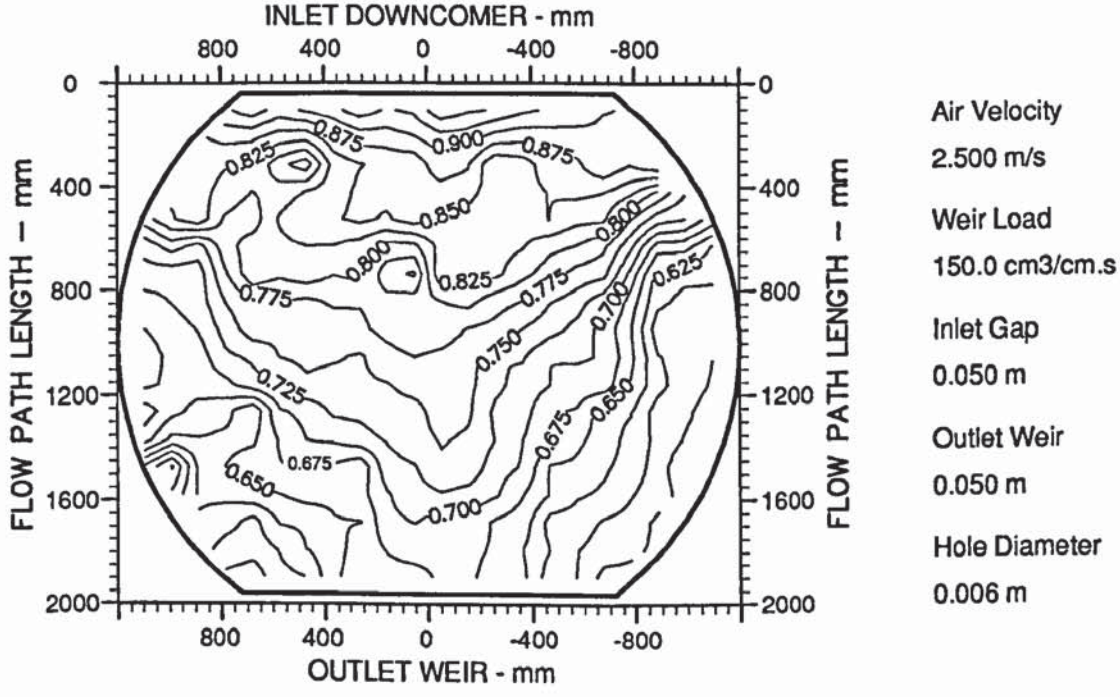

Figure A7.62 Two dimensional reduced temperature profiles showing confused and severe transverse "U-shaped" isotherms (designation M/TU).

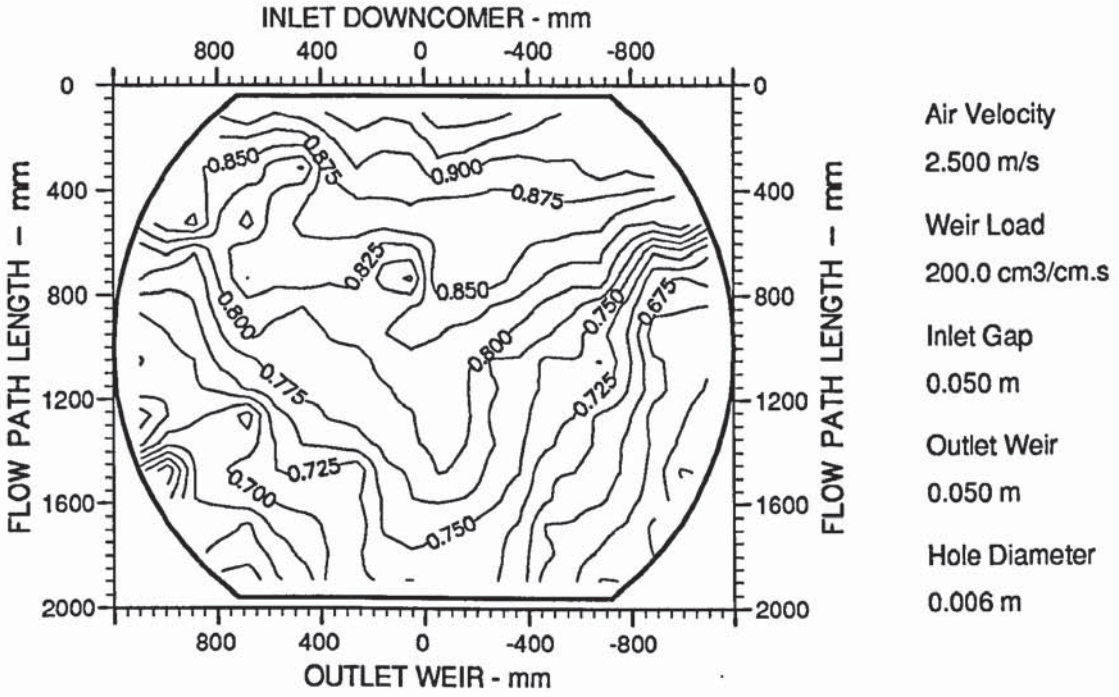

Figure A7.63 Two dimensional reduced temperature profiles showing distinctively "U-shaped" isotherms (designation U).

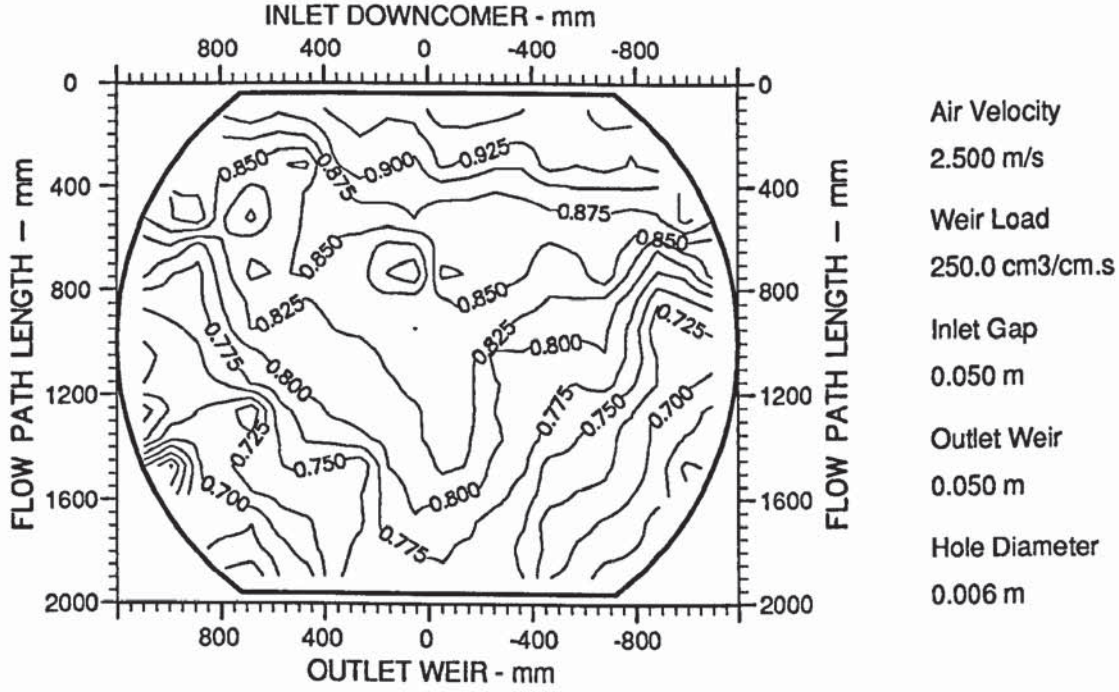

Figure A7.64 Two dimensional reduced temperature profiles showing distinctively "U-shaped" isotherms (designation U).

APPENDIX 8

Three-Dimensional Liquid Head Surface Profiles For The Separation of Flow Experiments

The three-dimensional black and white displays presented below are a full set of liquid head surface profiles to complement the results of the height of clear liquid experiments in Chapter 8. Measurement of the clear liquid height was used to show the effect of non-separated and separated liquid flow patterns on the liquid head across the tray. As with the water-cooling experiments, the water weir load was varied over a wide range for a fixed superficial air velocity at the equal inlet gap-outlet weir settings of 10 mm, 10 mm; 20 mm, 20 mm; and 50 mm, 50 mm. Flow rate information is presented in Table A7.1 in Appendix 7.

Note that the height of clear liquid profiles in all of the experiments are either horizontal, or contain an uneven surface at the inlet or the outlet, or both according to the extent of flow separation.

In addition, the designations assigned to each liquid head surface profile are included in the labelling of each diagram, and are summarised in Table A8.1.

Height of Clear Liquid Profile	Designation
Horizontal or flat profile	H
Uneven surface on tray inlet	NI
Uneven surface on tray outlet	NO
Uneven surface over the whole tray	N

Table A8.1 Summary of height of clear liquid profile designations.

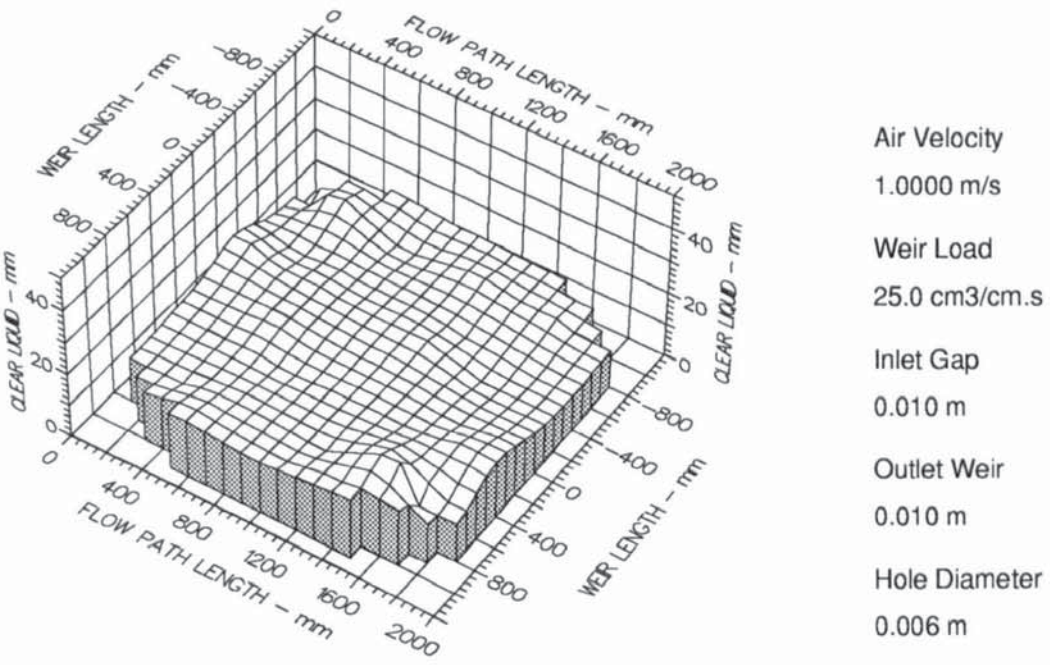

Figure A8.1 Three dimensional height of clear liquid profiles showing a comparatively horizontal or flat liquid surface (designation H).

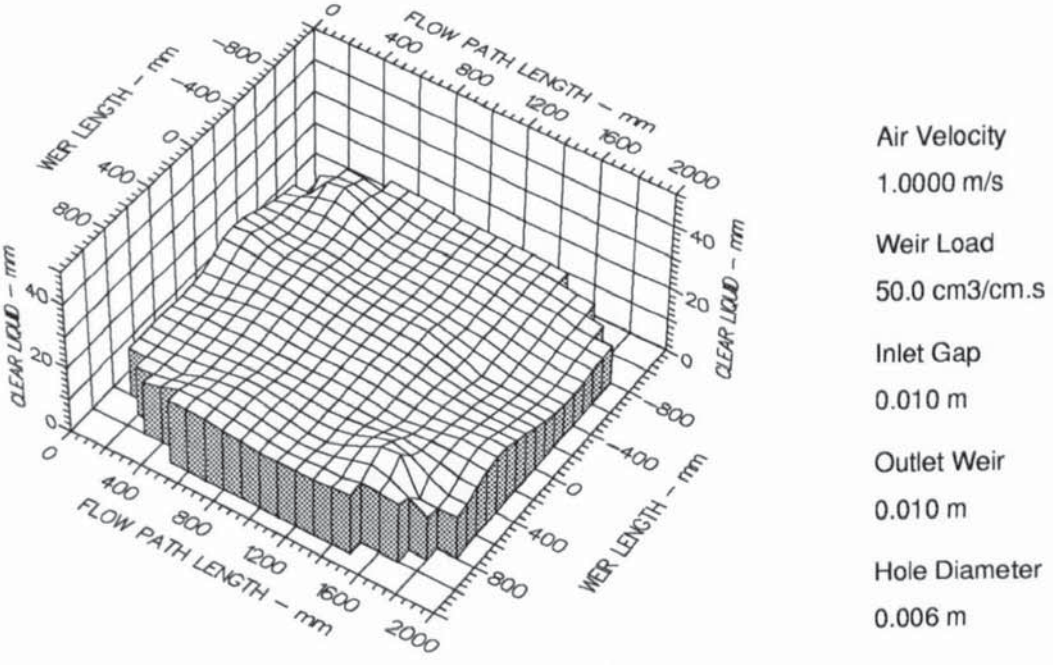

Figure A8.2 Three dimensional height of clear liquid profiles showing a comparatively horizontal or flat liquid surface (designation H).

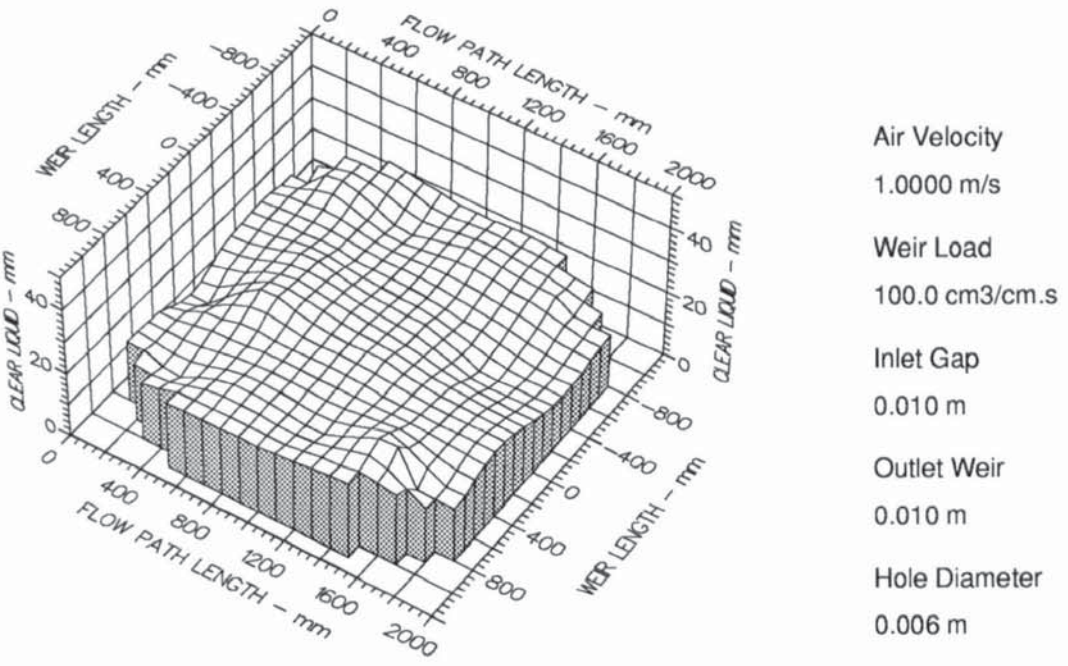

Figure A8.3 Three dimensional height of clear liquid profiles showing an uneven liquid surface at the tray inlet (designation NI).

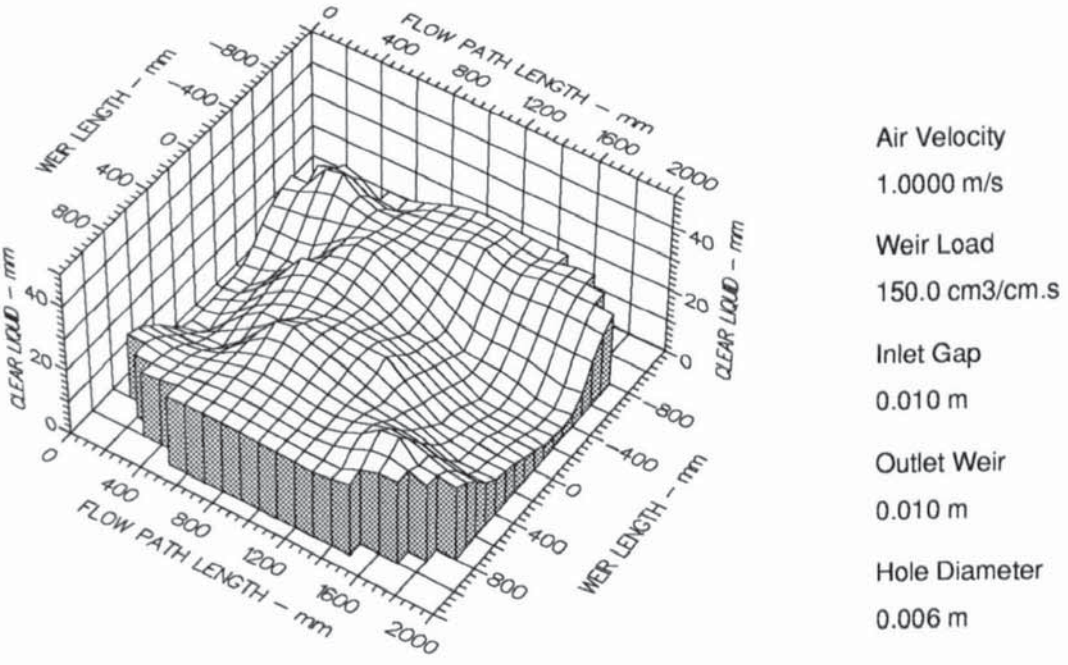

Figure A8.4 Three dimensional height of clear liquid profiles showing a comparatively horizontal or flat liquid surface (designation H).

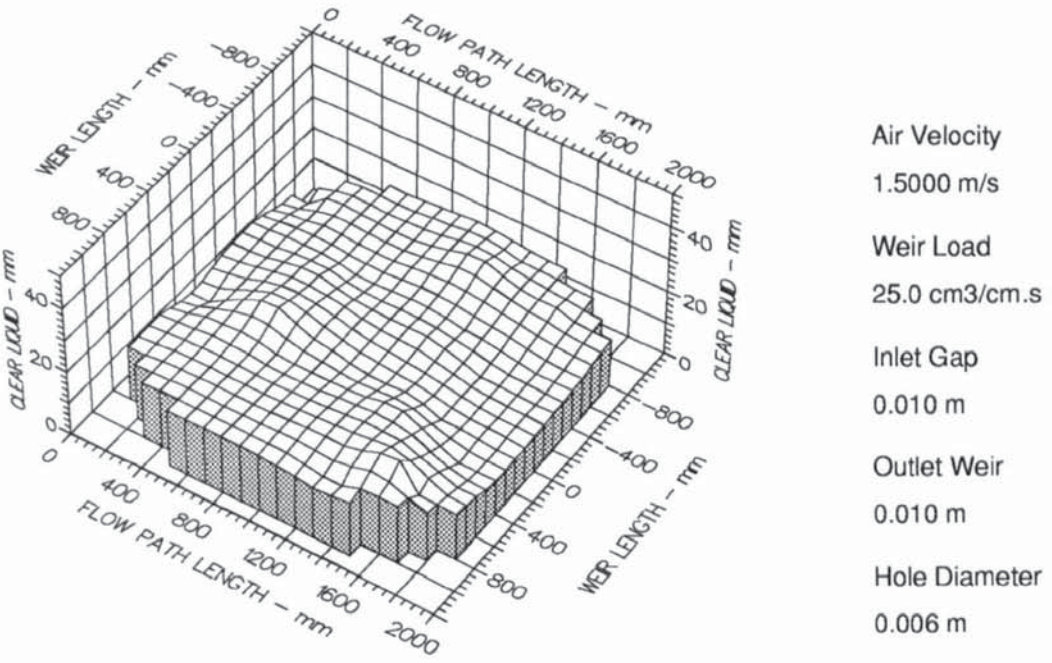

Figure A8.5 Three dimensional height of clear liquid profiles showing a comparatively horizontal or flat liquid surface (designation H).

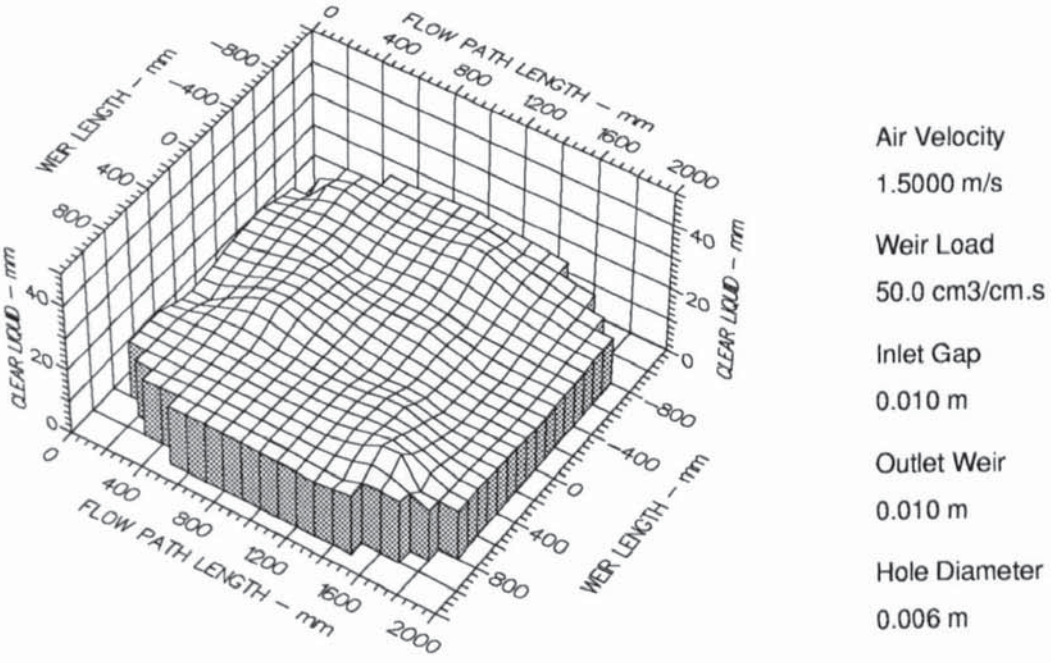

Figure A8.6 Three dimensional height of clear liquid profiles showing an uneven liquid surface at the tray inlet (designation NI).

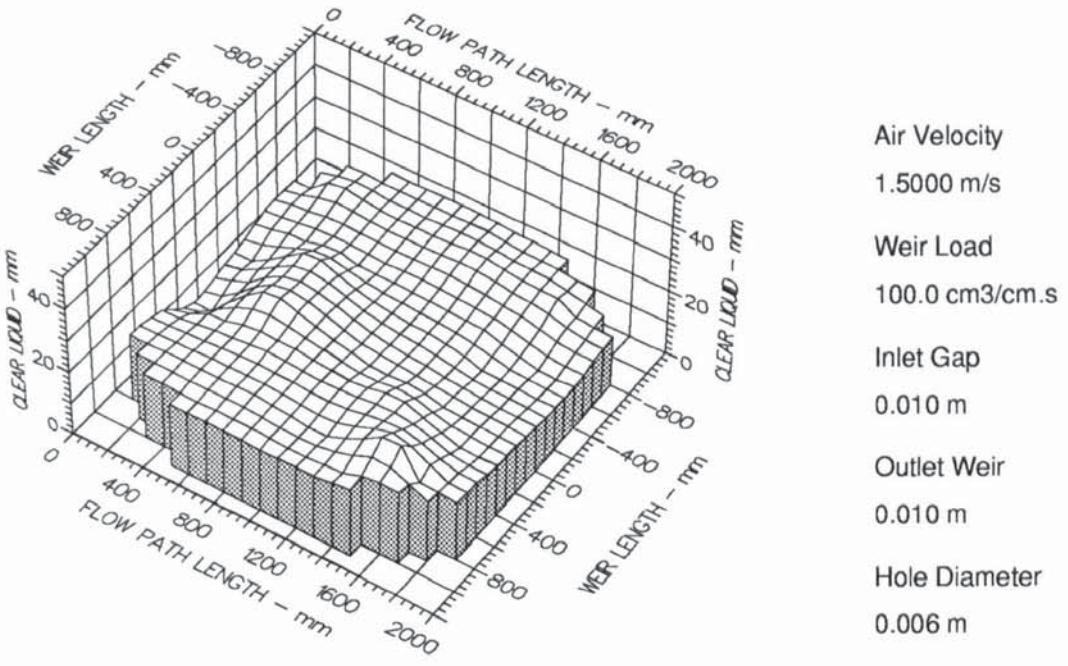

Figure A8.7 Three dimensional height of clear liquid profiles showing a comparatively horizontal or flat liquid surface (designation H).

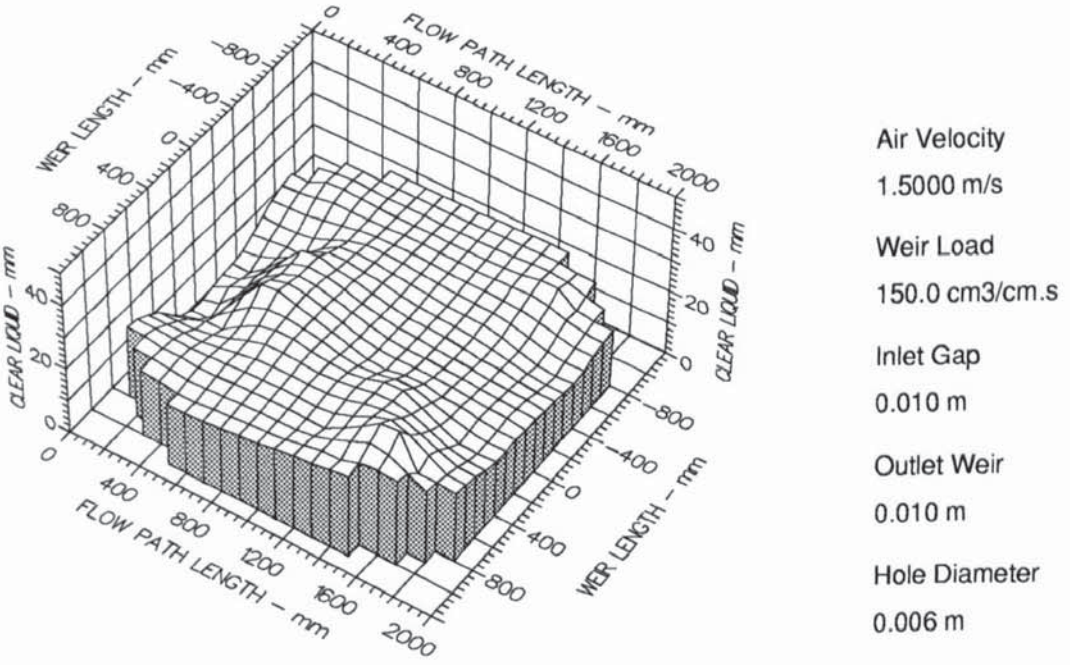

Figure A8.8 Three dimensional height of clear liquid profiles showing an uneven liquid surface at the tray inlet (designation NI).

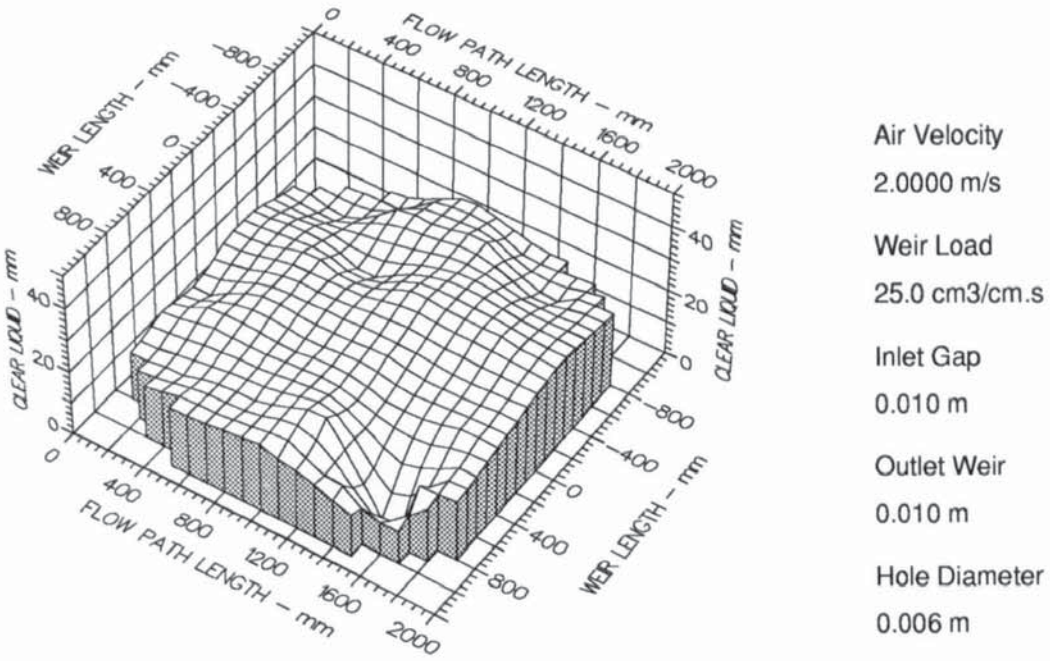

Figure A8.9 Three dimensional height of clear liquid profiles showing an uneven liquid surface at the tray inlet (designation NI).

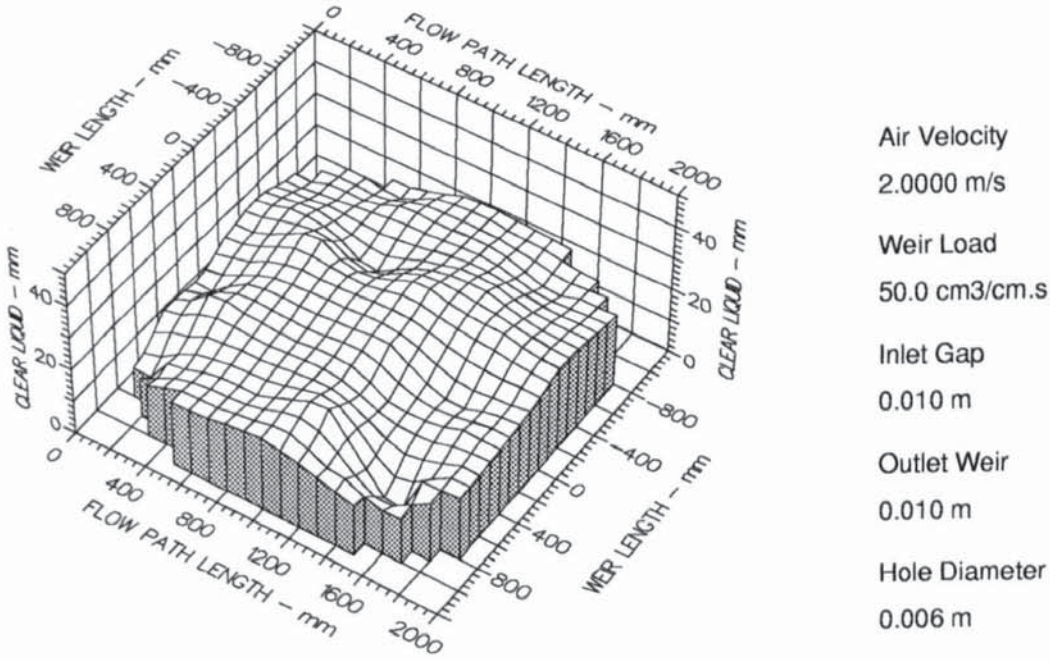

Figure A8.10 Three dimensional height of clear liquid profiles showing an uneven liquid surface over the whole tray (designation N).

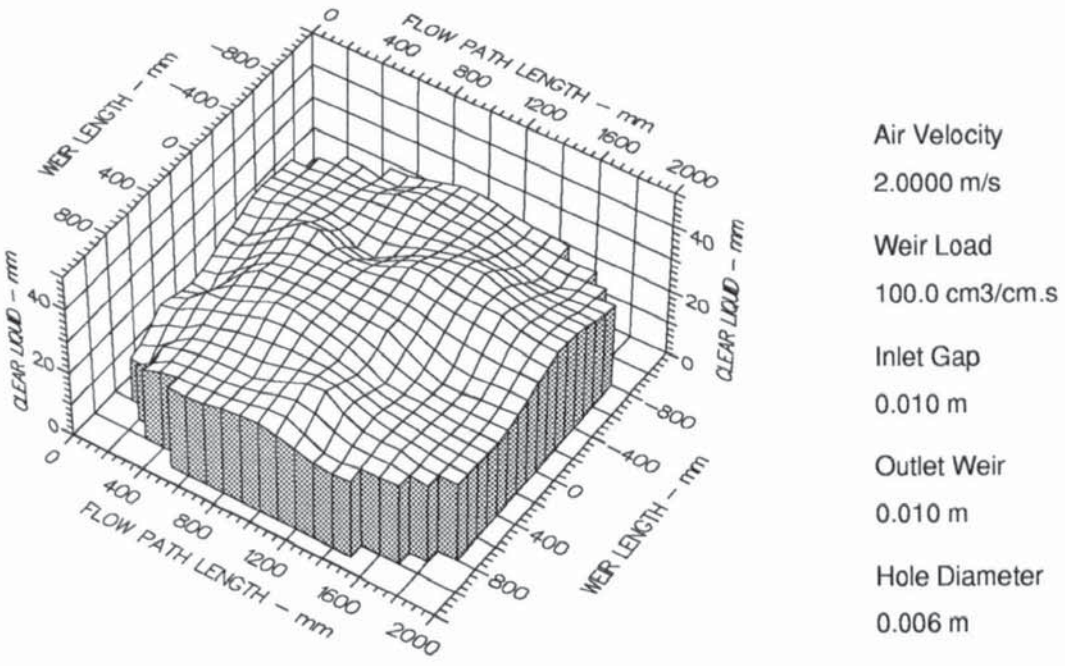

Figure A8.11 Three dimensional height of clear liquid profiles showing an uneven liquid surface at the tray inlet (designation NI).

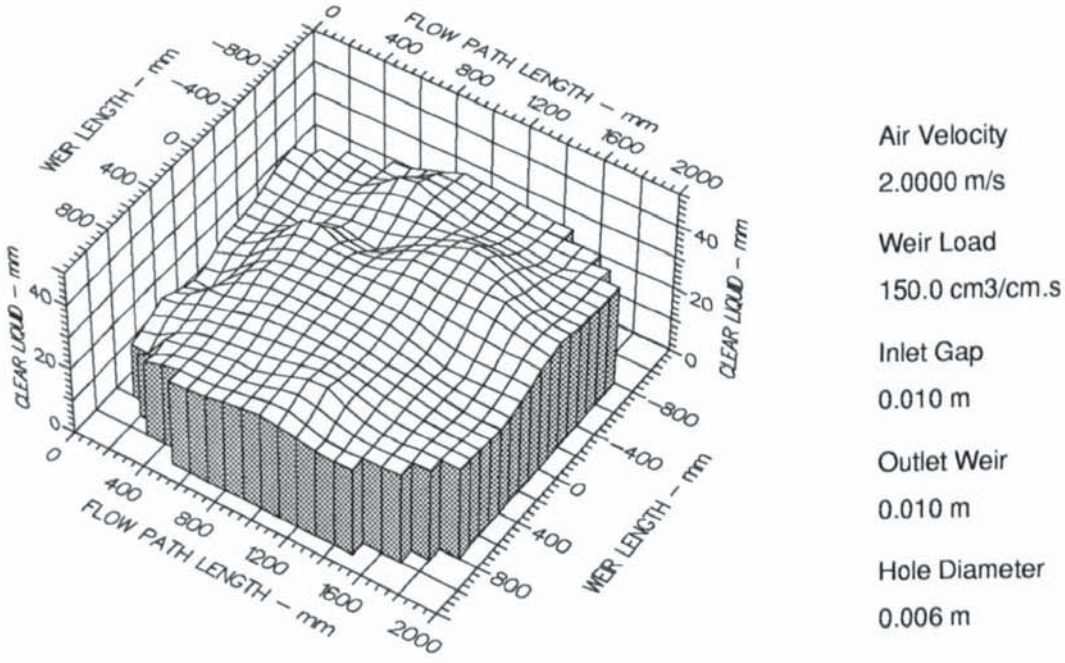

Figure A8.12 Three dimensional height of clear liquid profiles showing an uneven liquid surface at the tray inlet (designation NI).

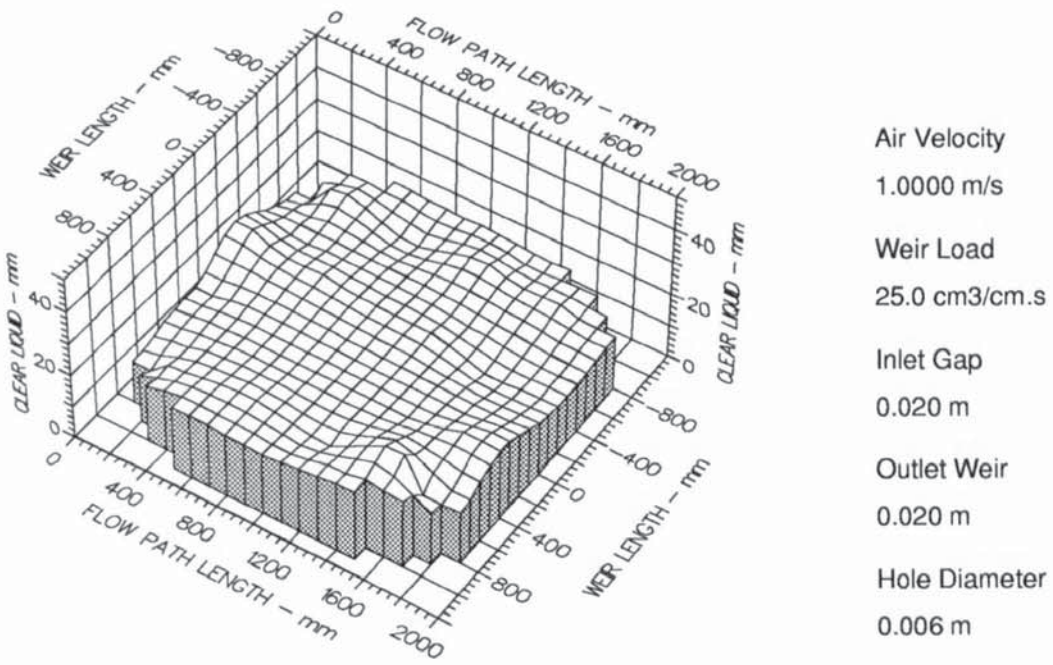

Figure A8.13 Three dimensional height of clear liquid profiles showing a comparatively horizontal or flat liquid surface (designation H).

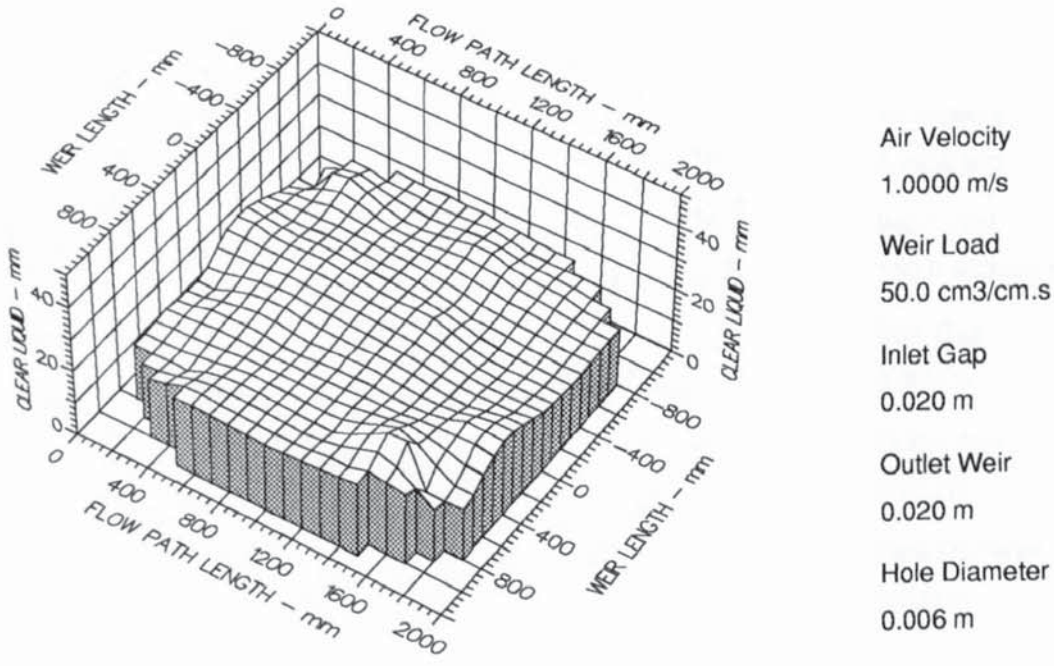

Figure A8.14 Three dimensional height of clear liquid profiles showing a comparatively horizontal or flat liquid surface (designation H).

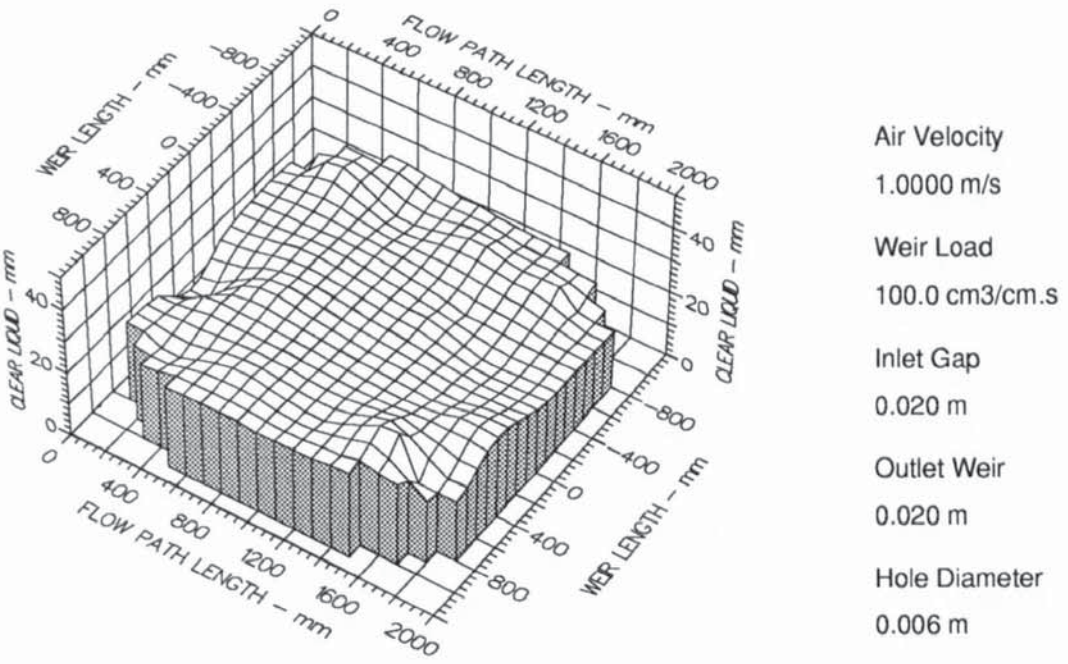

Figure A8.15 Three dimensional height of clear liquid profiles showing a mixture of horizontal and uneven liquid head profiles at the tray inlet (designation H/NI).

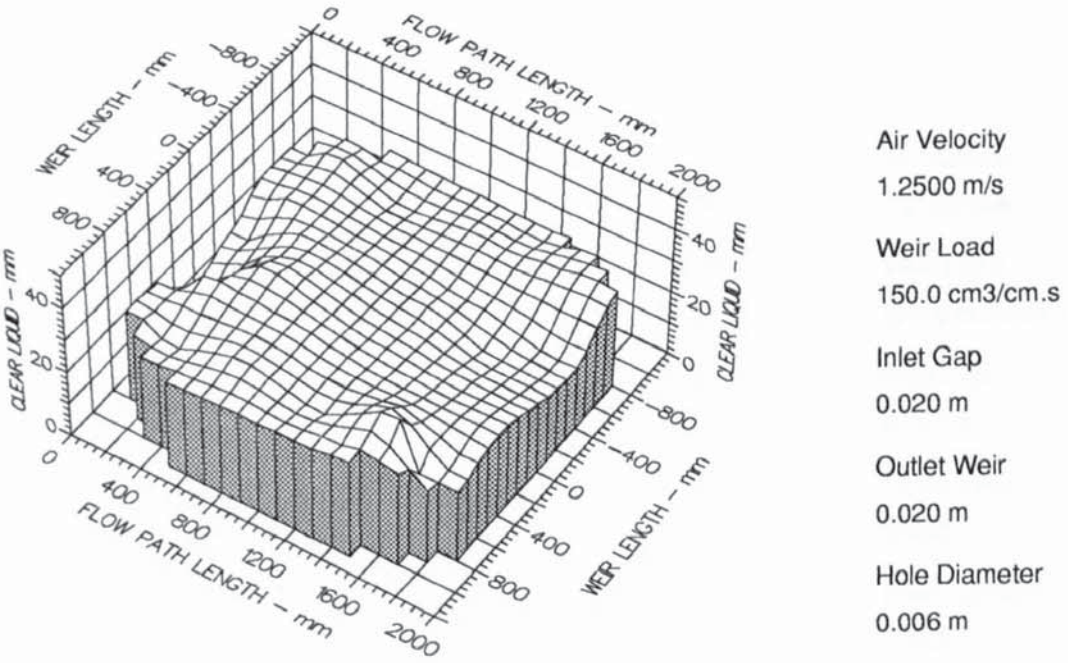

Figure A8.16 Three dimensional height of clear liquid profiles showing a comparatively horizontal or flat liquid surface (designation H).

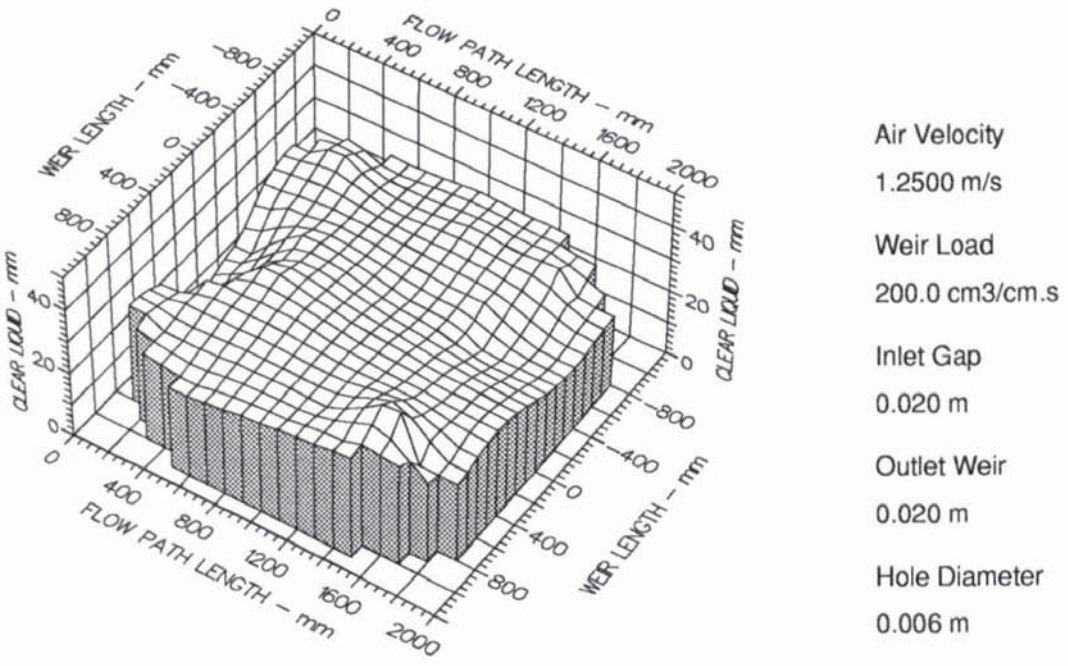

Figure A8.17 Three dimensional height of clear liquid profiles showing a comparatively horizontal or flat liquid surface (designation H).

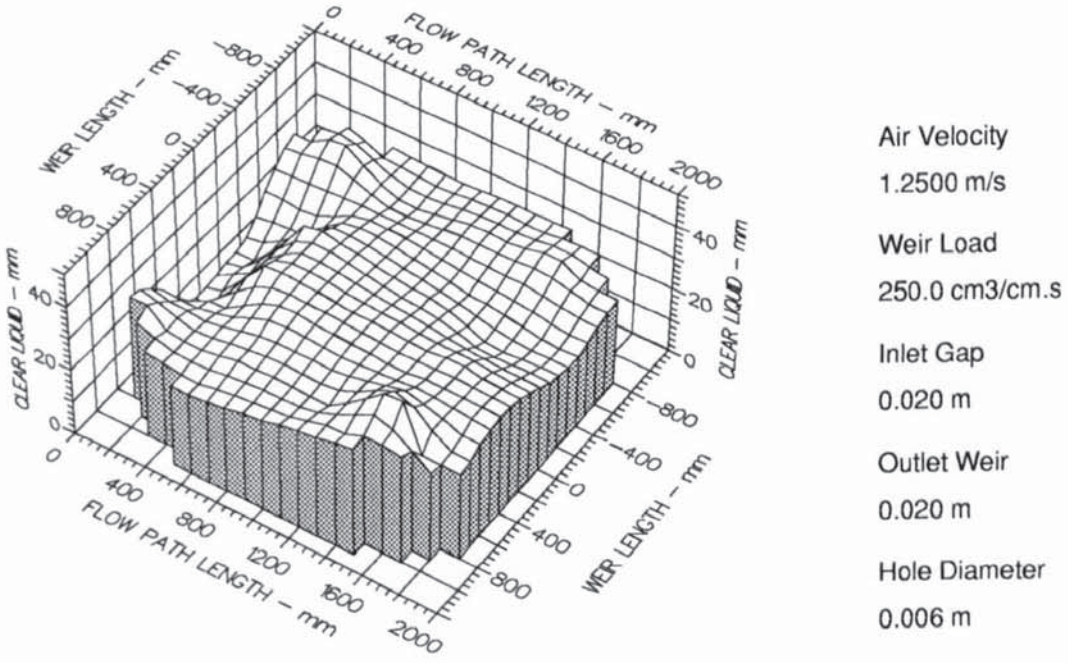

Figure A8.18 Three dimensional height of clear liquid profiles showing a mixture of horizontal and uneven liquid head profiles at the tray inlet (designation H/NI).

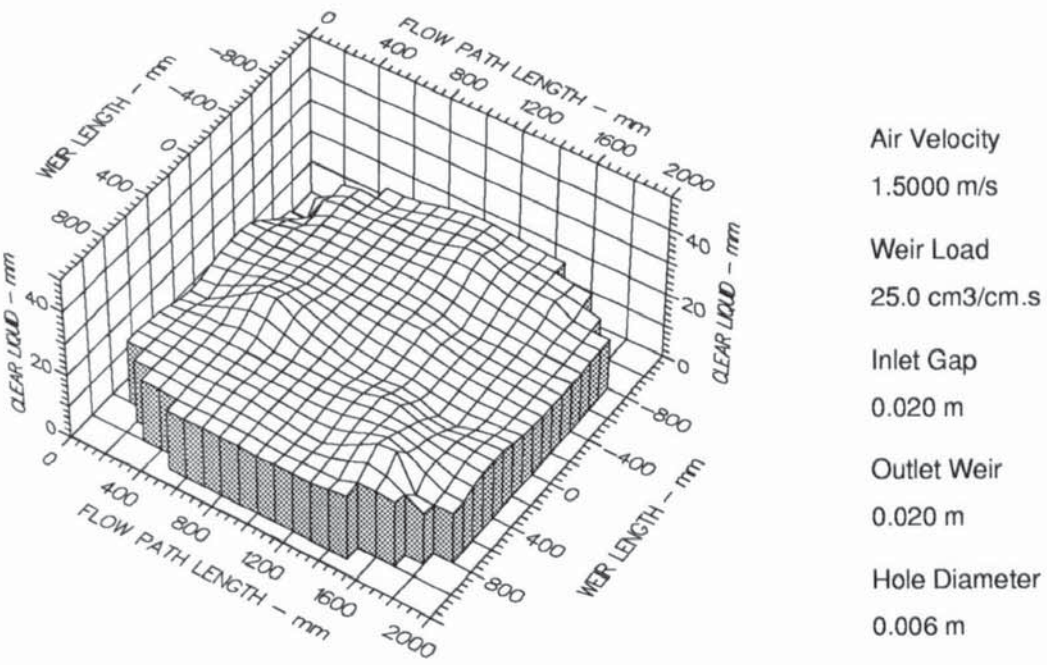

Figure A8.19 Three dimensional height of clear liquid profiles showing a comparatively horizontal or flat liquid surface (designation H).

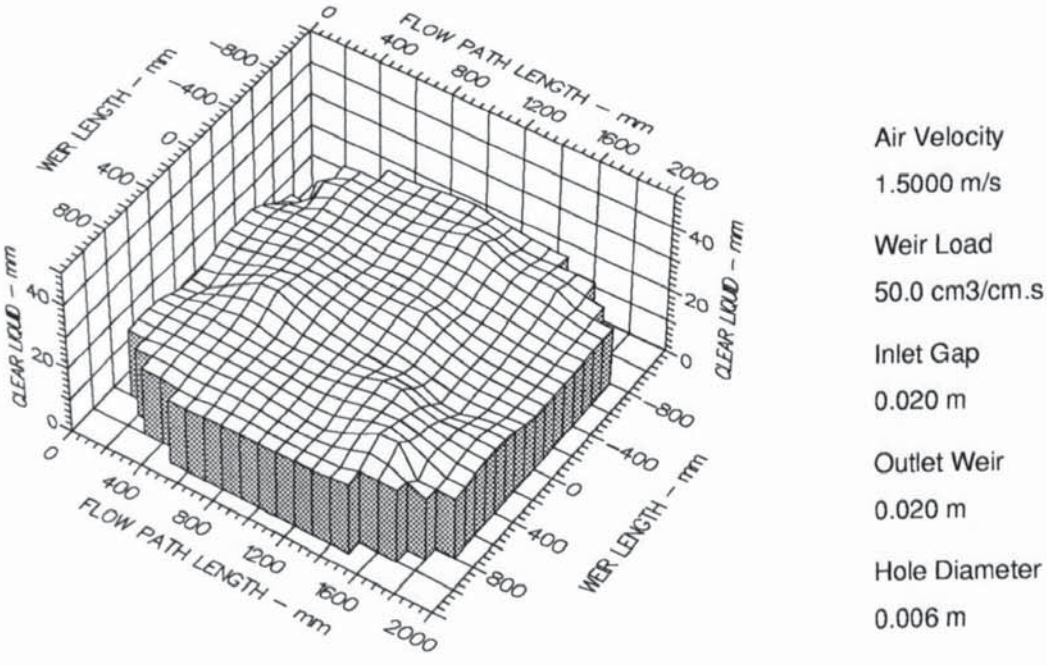

Figure A8.20 Three dimensional height of clear liquid profiles showing an uneven liquid surface at the tray inlet (designation NI).

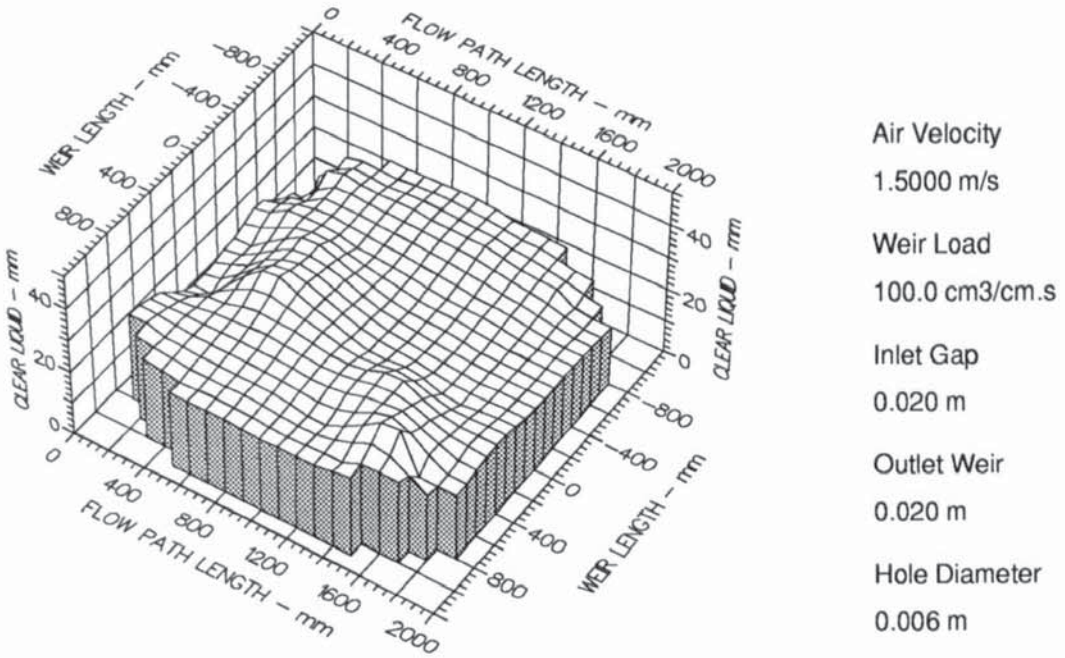

Figure A8.21 Three dimensional height of clear liquid profiles showing an uneven liquid surface at the tray inlet (designation NI).

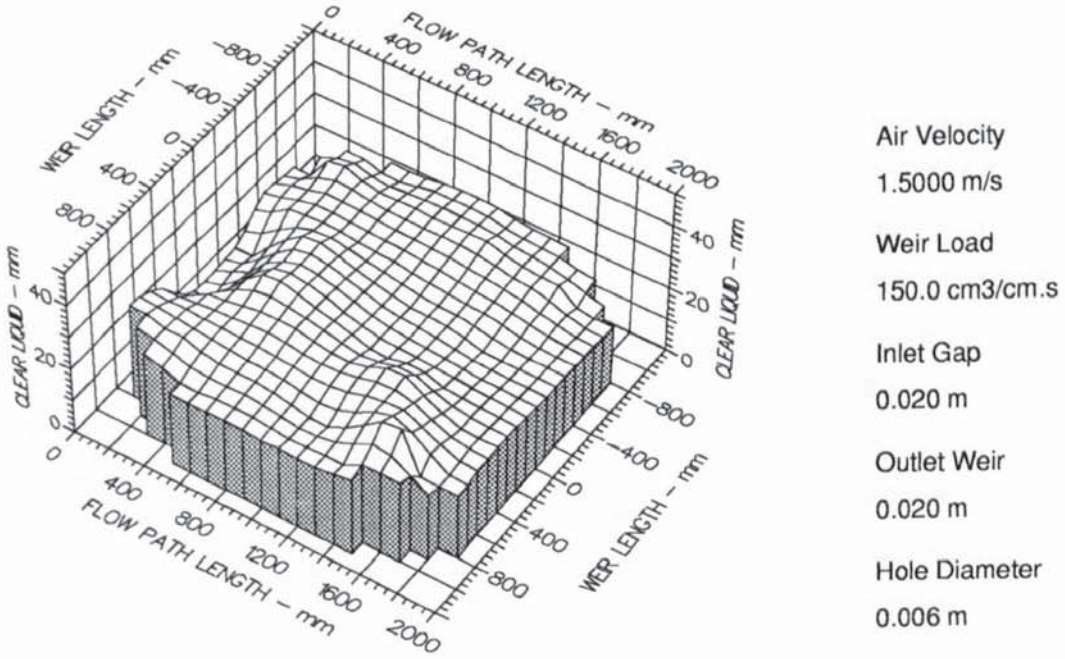

Figure A8.22 Three dimensional height of clear liquid profiles showing an uneven liquid surface at the tray inlet (designation NI).

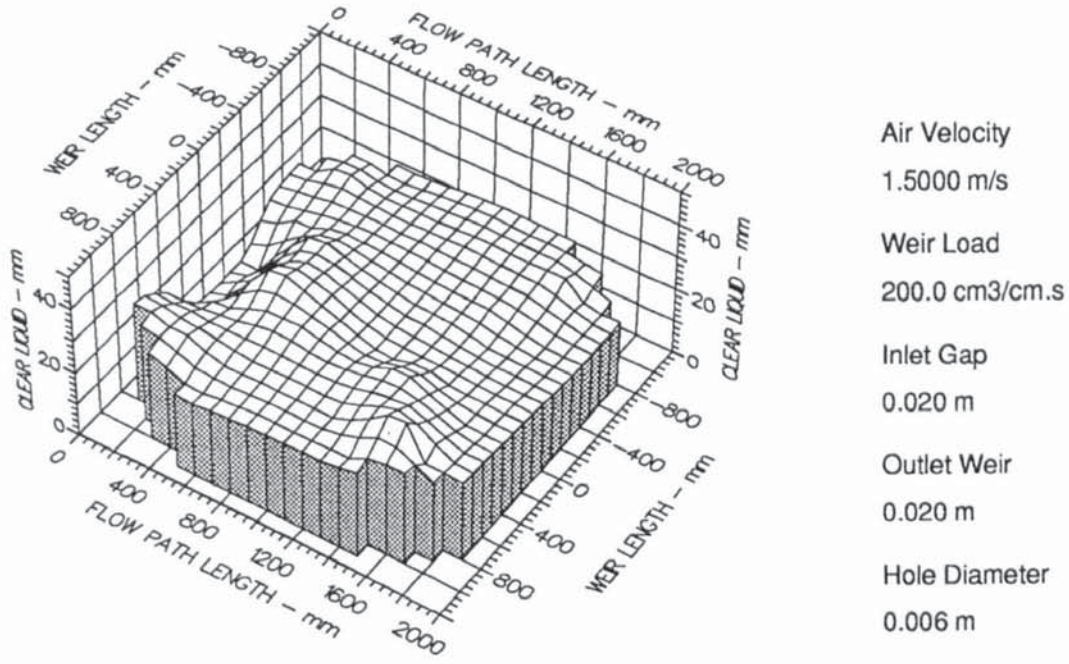

Figure A8.23 Three dimensional height of clear liquid profiles showing an uneven liquid surface at the tray inlet (designation NI).

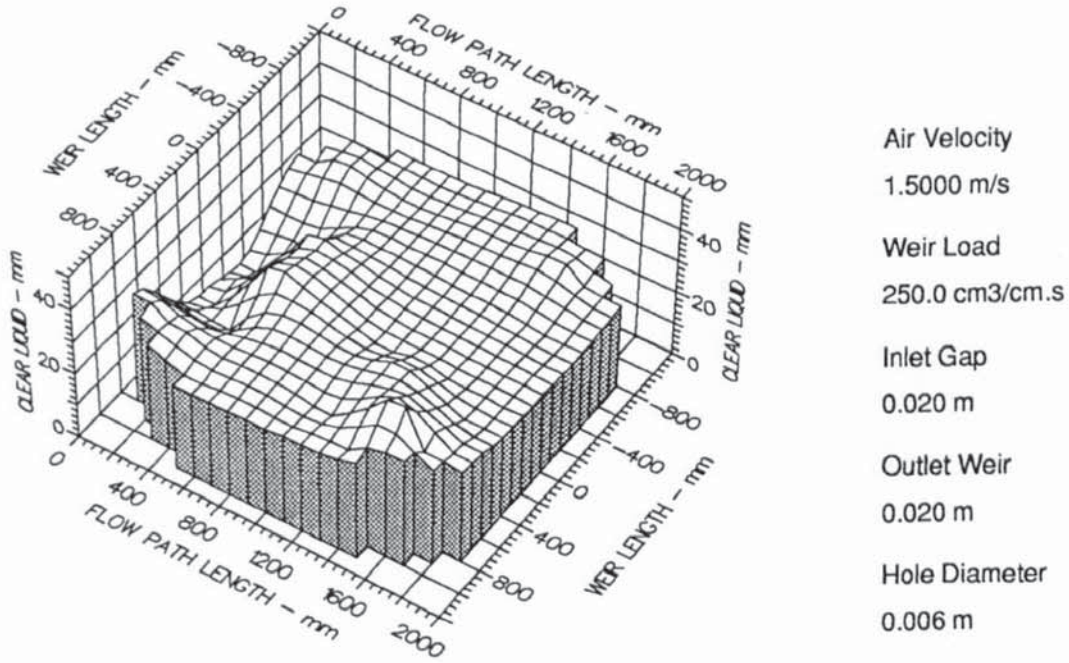

Figure A8.24 Three dimensional height of clear liquid profiles showing an uneven liquid surface at the tray inlet (designation NI).

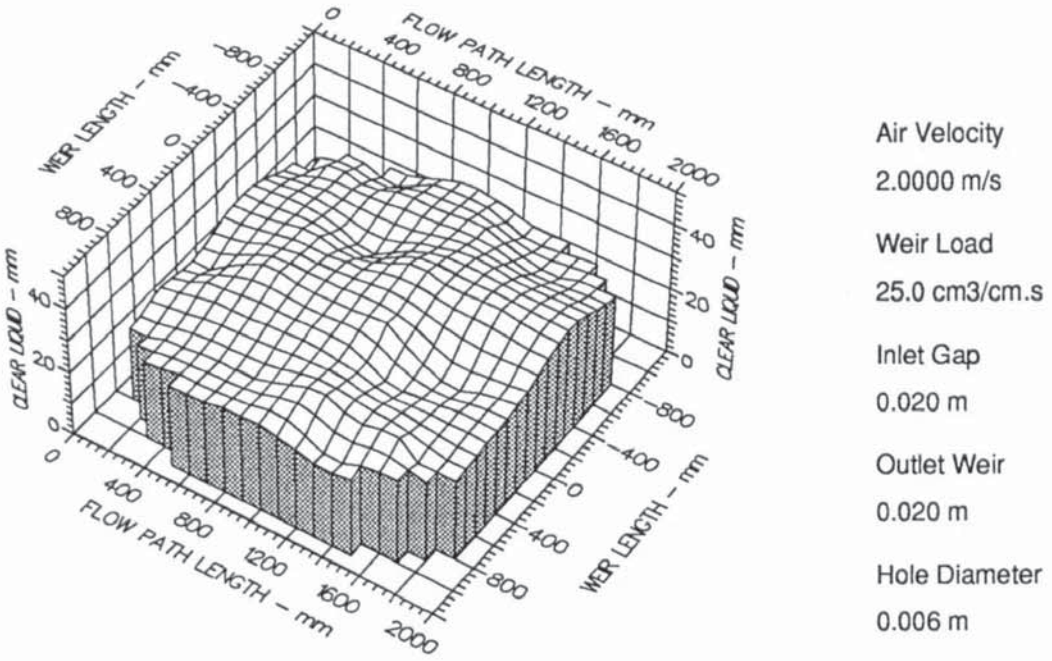

Figure A8.25 Three dimensional height of clear liquid profiles showing an uneven liquid surface at the tray inlet (designation NI).

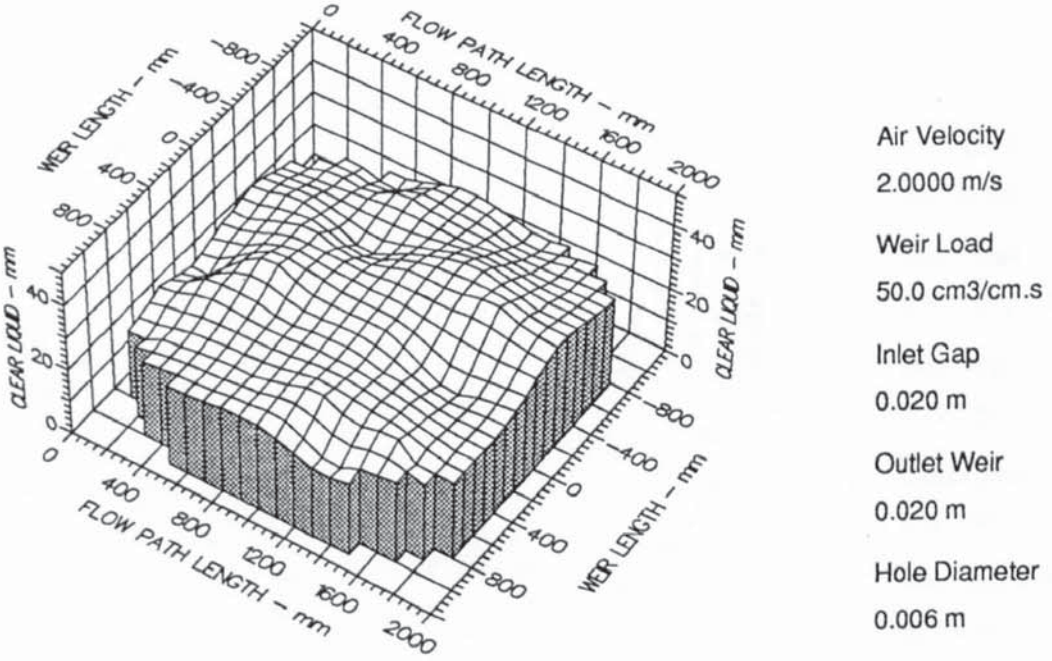

Figure A8.26 Three dimensional height of clear liquid profiles showing an uneven liquid surface at the tray inlet (designation NI).

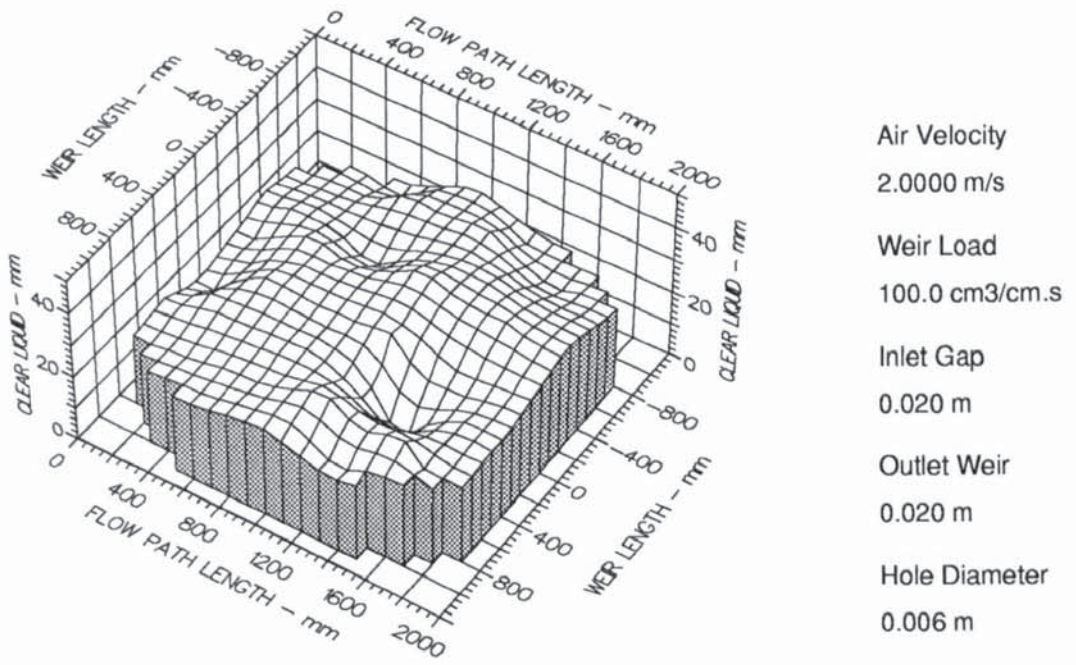

Figure A8.27 Three dimensional height of clear liquid profiles showing an uneven liquid surface over the whole tray (designation N).

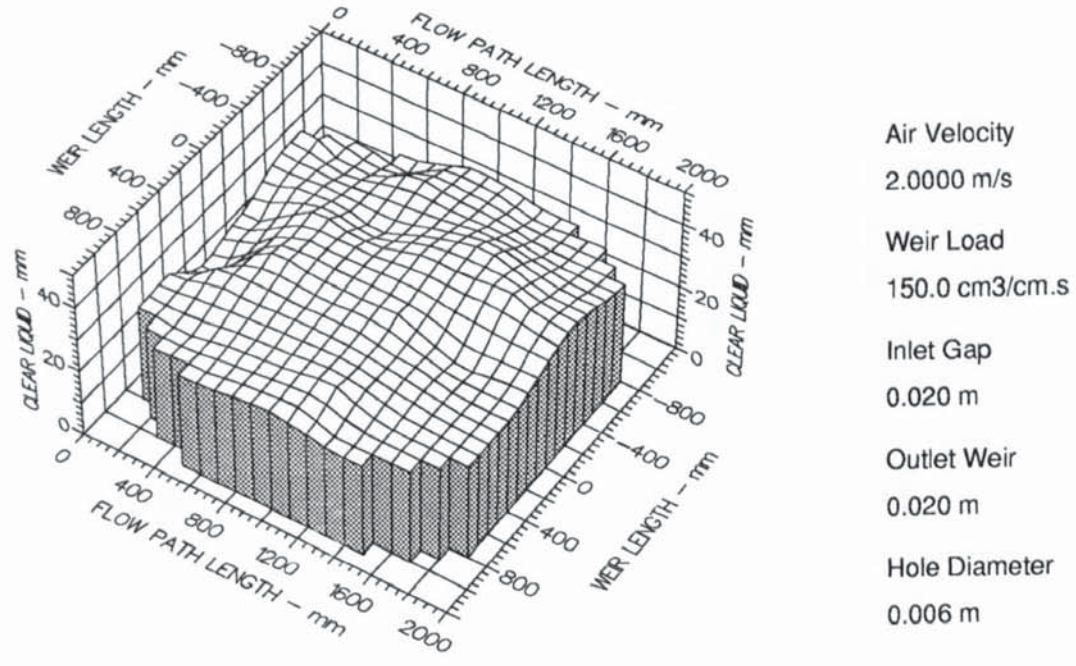

Figure A8.28 Three dimensional height of clear liquid profiles showing an uneven liquid surface at the tray inlet (designation NI).

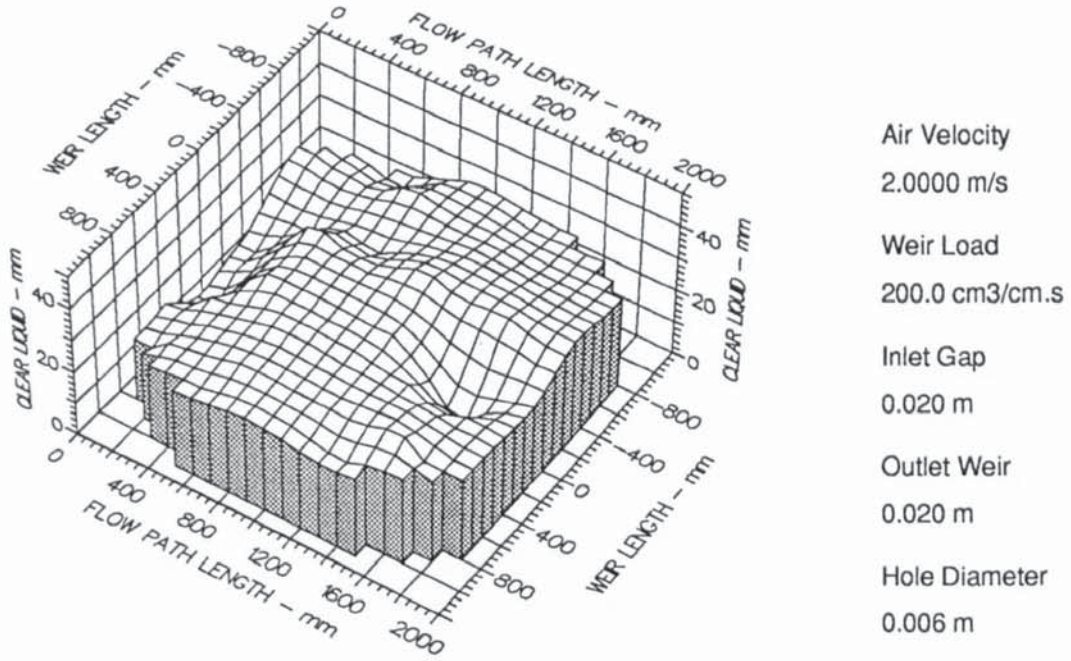

Figure A8.29 Three dimensional height of clear liquid profiles showing an uneven liquid surface at the tray inlet (designation NI).

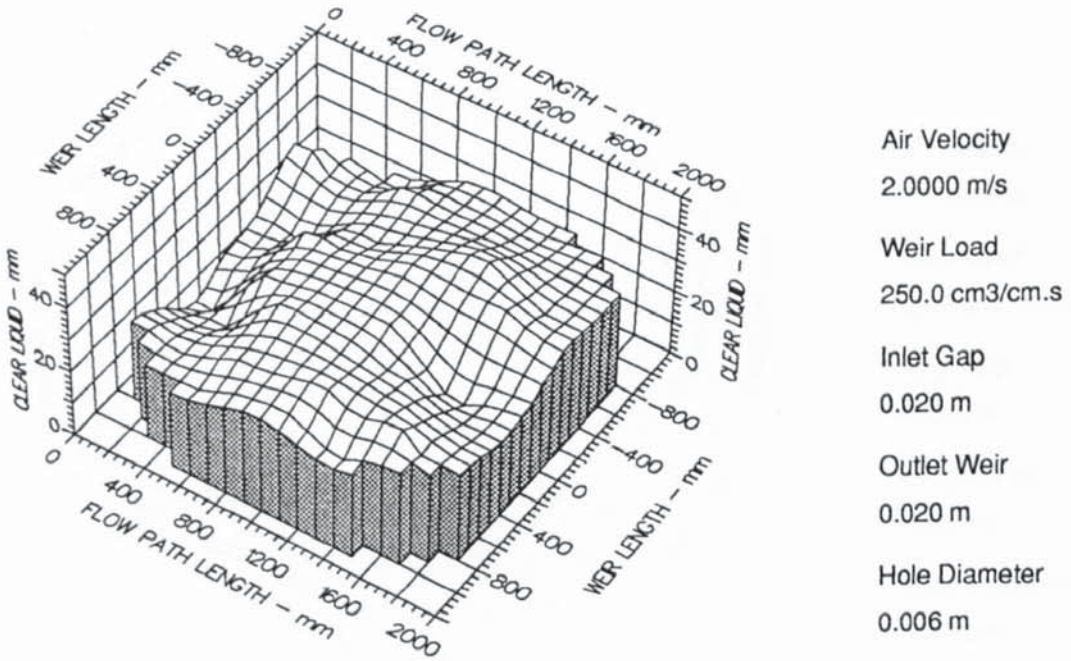

Figure A8.30 Three dimensional height of clear liquid profiles showing an uneven liquid surface over the whole tray (designation N).

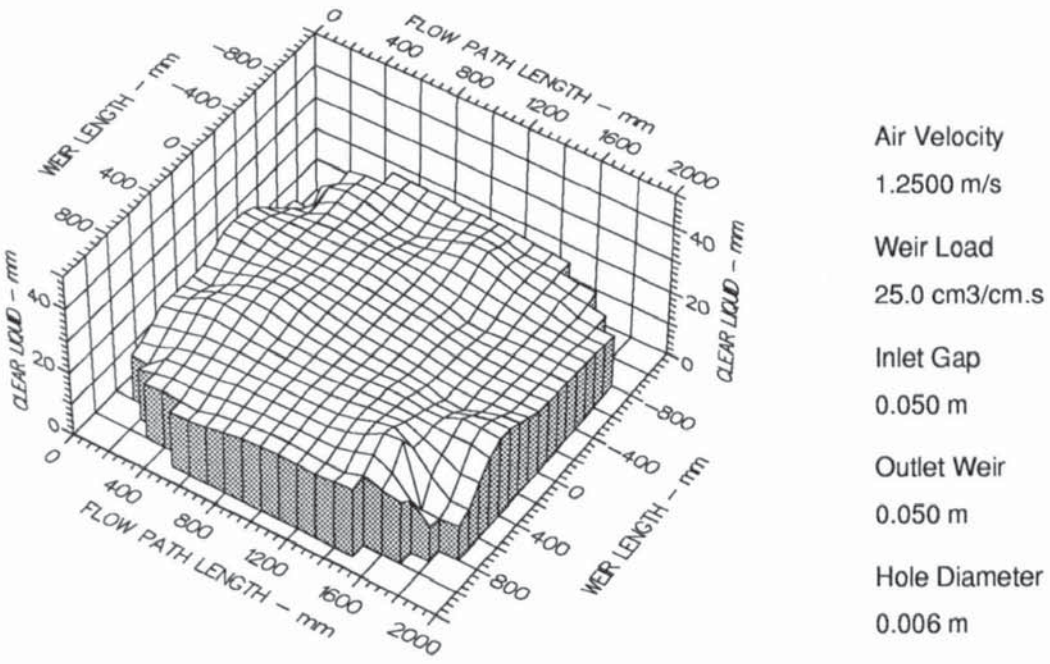

Figure A8.31 Three dimensional height of clear liquid profiles showing a mixture of horizontal and uneven liquid head profiles at the tray outlet (designation H/NO).

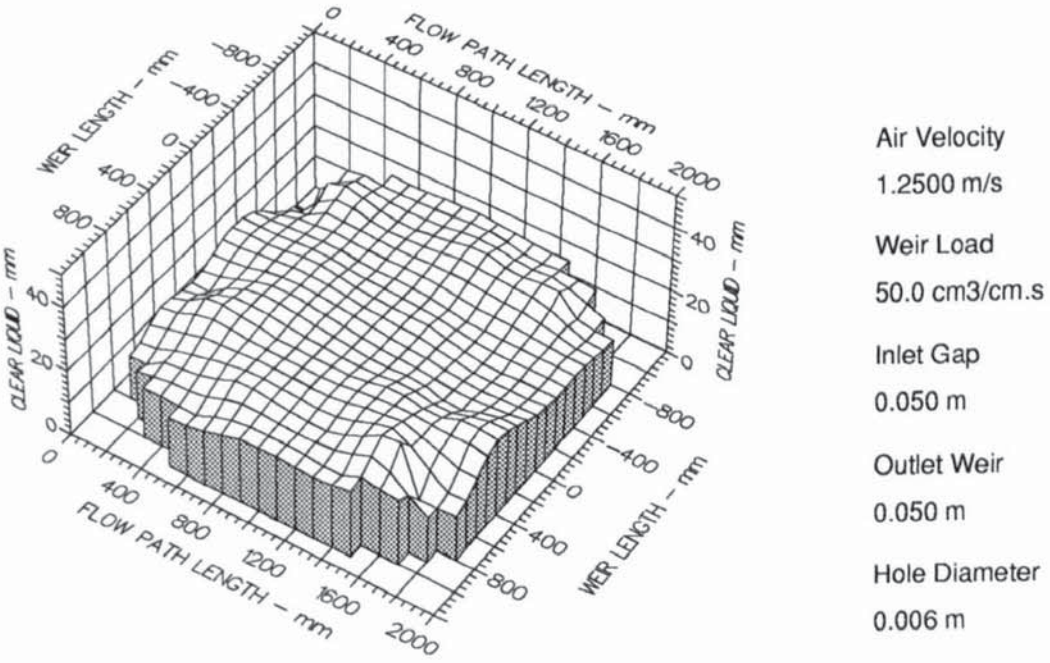

Figure A8.32 Three dimensional height of clear liquid profiles showing a mixture of horizontal and uneven liquid head profiles at the tray outlet (designation H/NO).

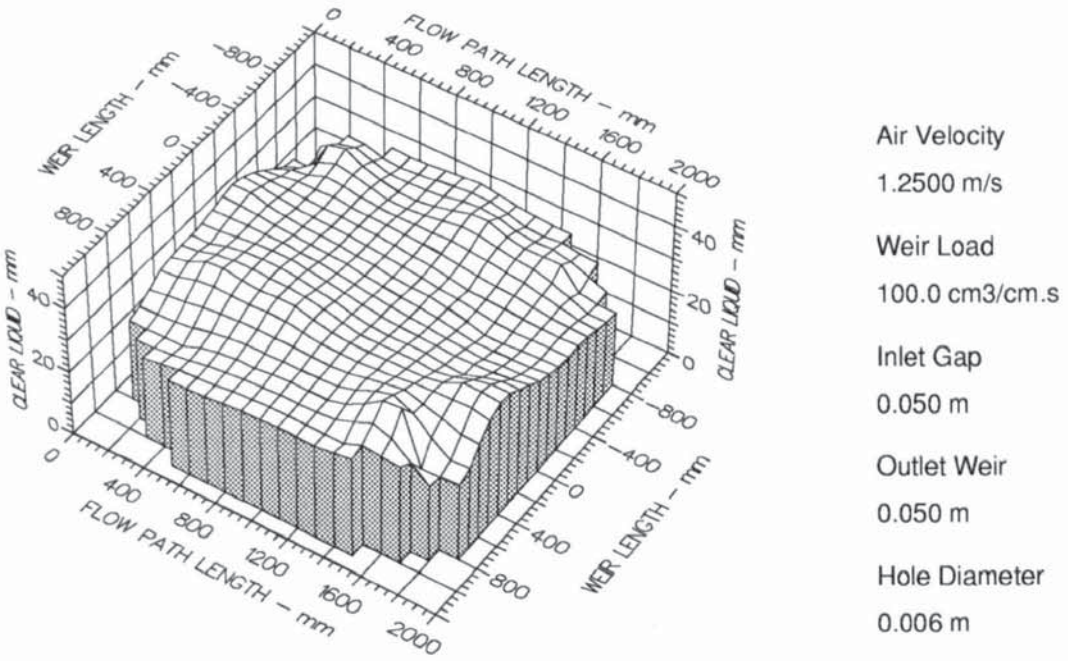

Figure A8.33 Three-dimensional height of clear liquid profiles showing an uneven liquid surface over the whole tray (designation N).

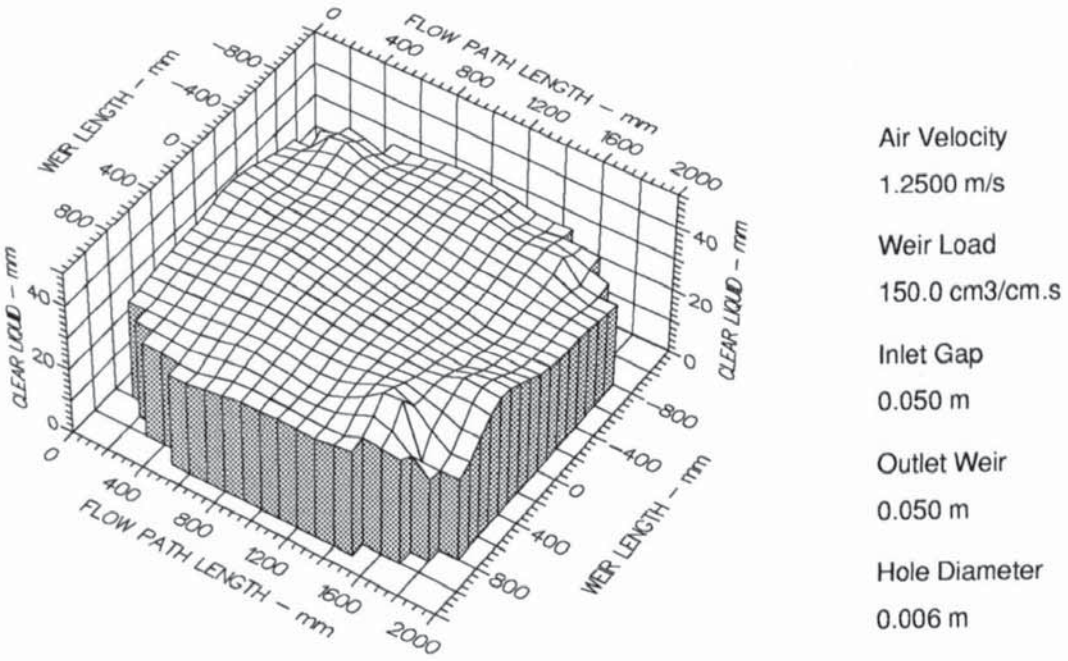

Figure A8.34 Three-dimensional height of clear liquid profiles showing a mixture of horizontal and uneven liquid head profiles at the tray outlet (designation H/NO).

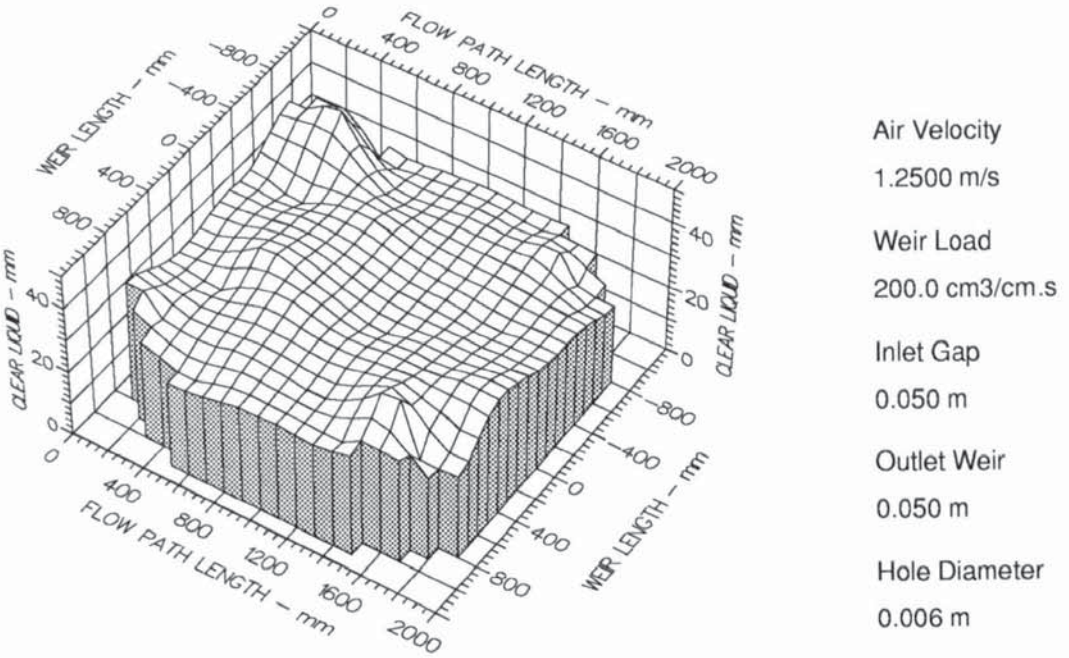

Figure A8.35 Three-dimensional height of clear liquid profiles showing a mixture of horizontal and uneven liquid head profiles at the tray outlet (designation H/NO).

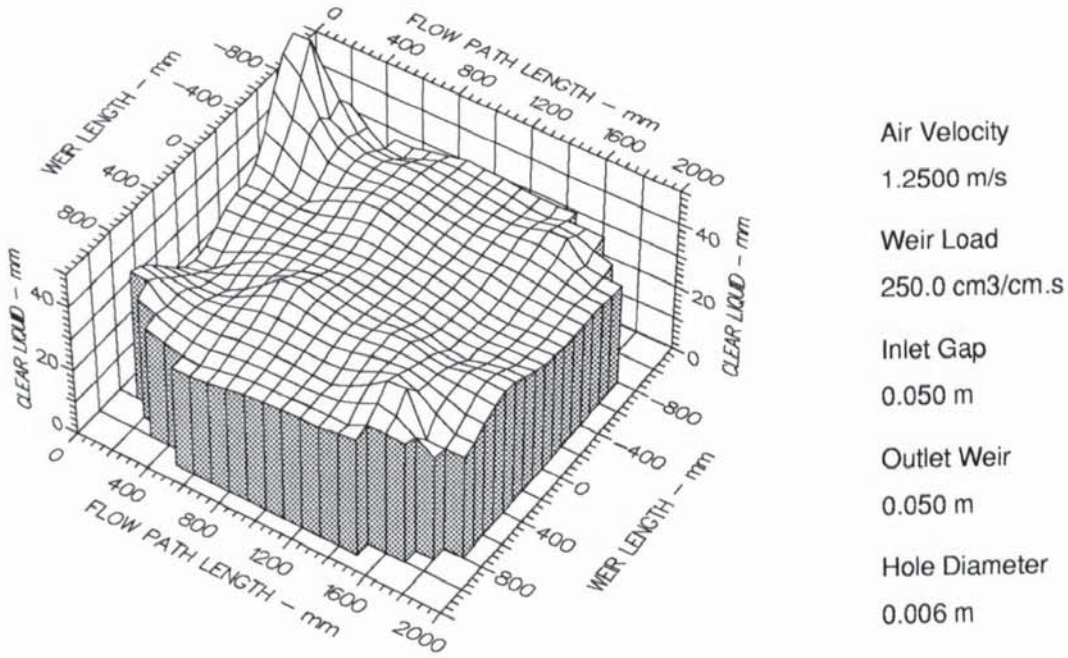

Figure A8.36 Three-dimensional height of clear liquid profiles showing an uneven liquid surface over the whole tray (designation N).

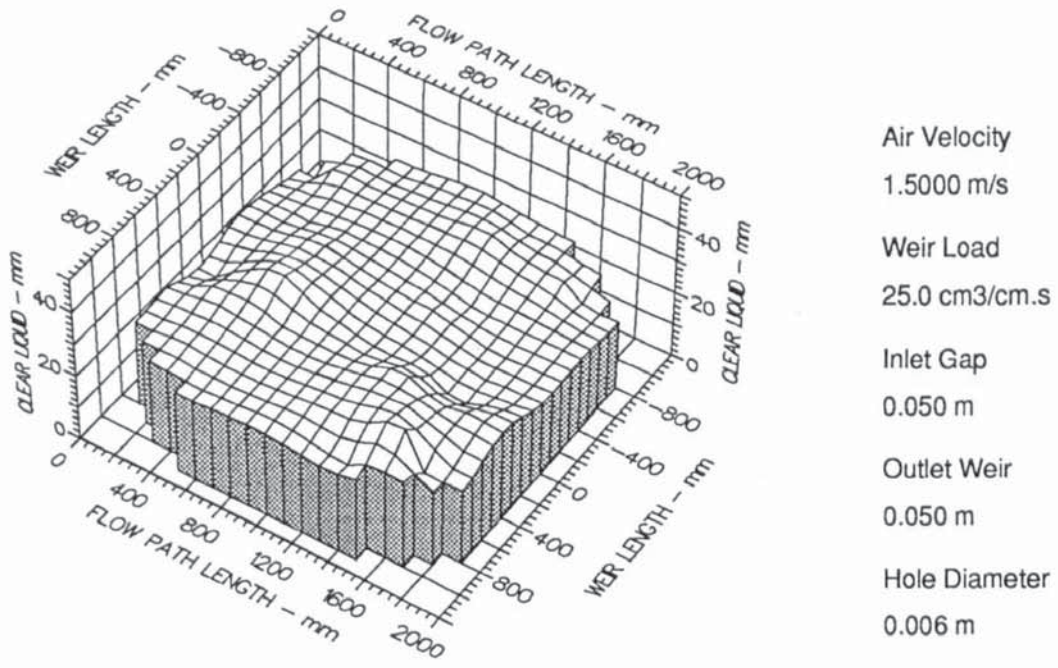

Figure A8.37 Three dimensional height of clear liquid profiles showing a mixture of horizontal and uneven liquid head profiles at the tray outlet (designation H/NO).

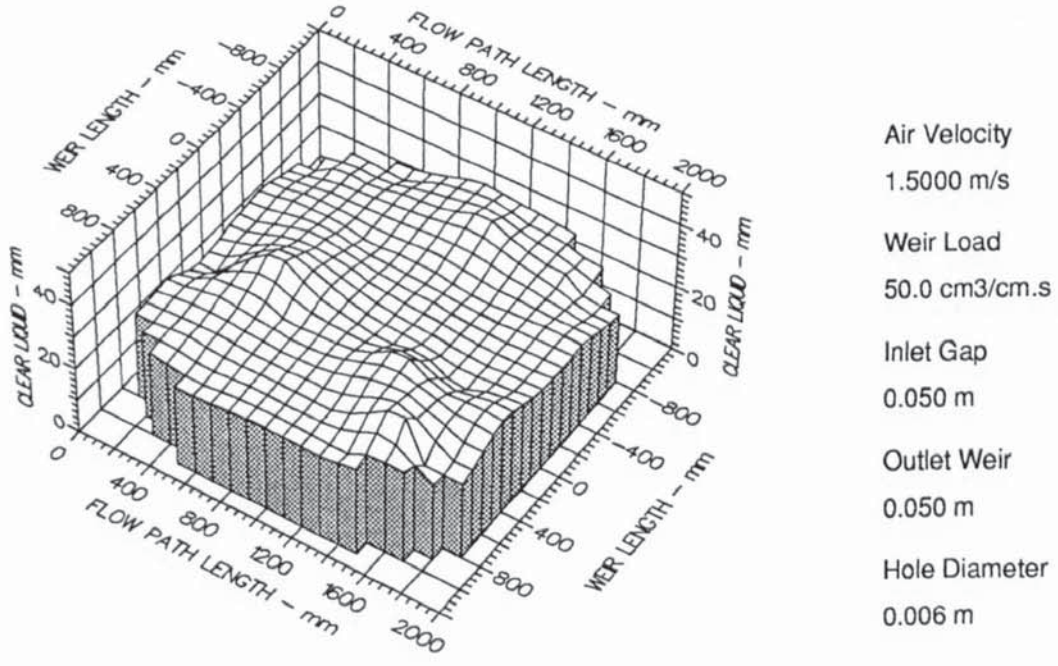

Figure A8.38 Three dimensional height of clear liquid profiles showing a mixture of horizontal and uneven liquid head profiles at the tray outlet (designation H/N).

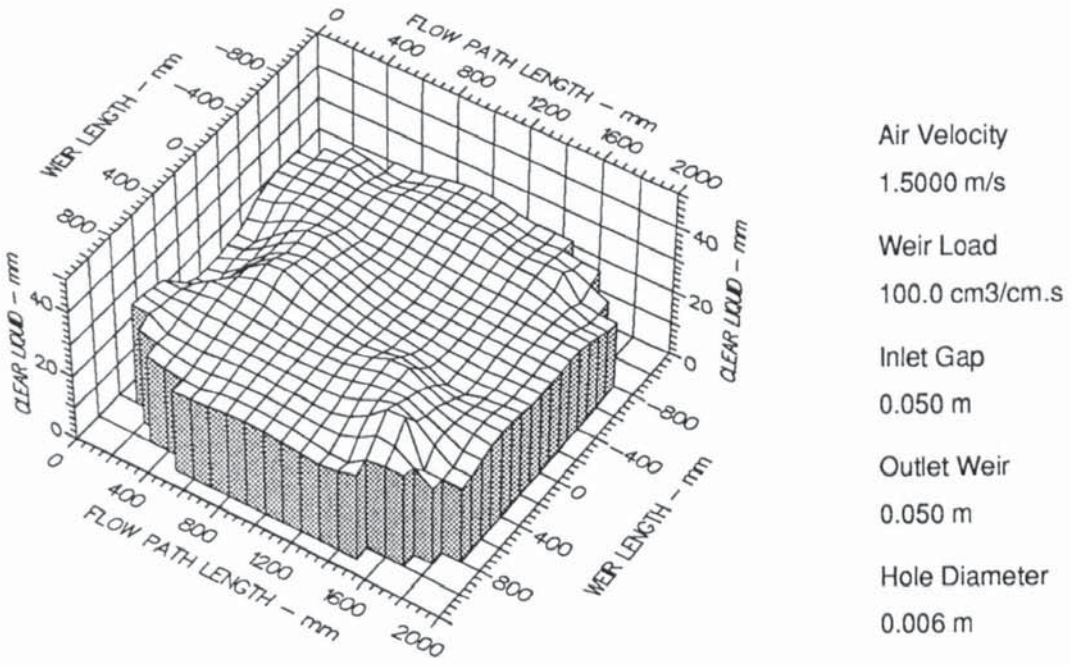

Figure A8.39 Three dimensional height of clear liquid profiles showing an uneven liquid surface over the whole tray (designation N).

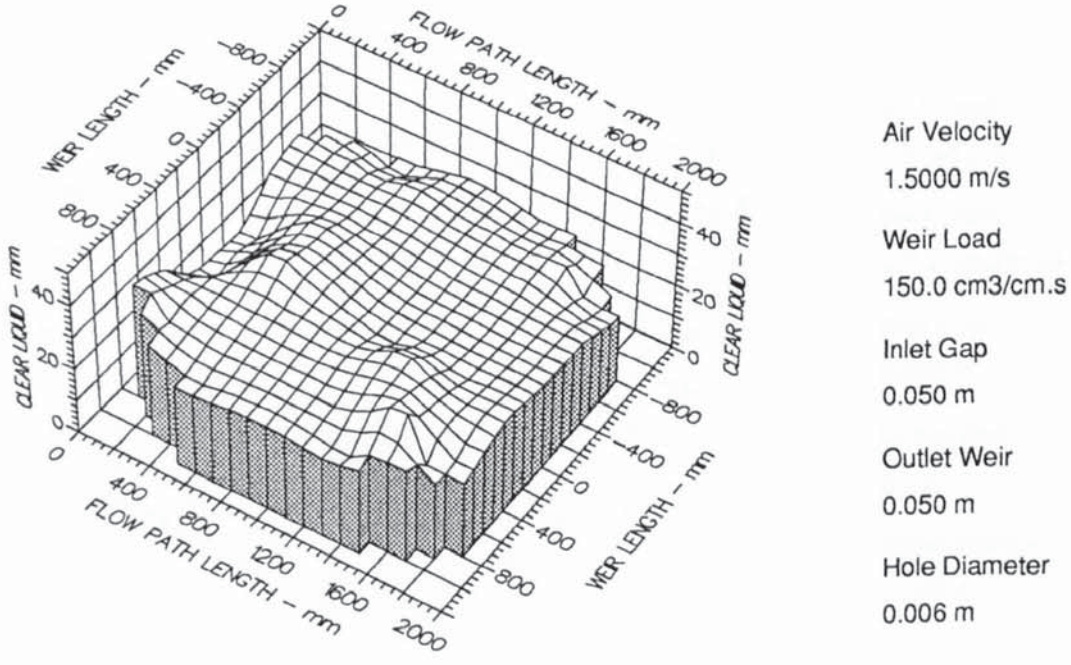

Figure A8.40 Three dimensional height of clear liquid profiles showing a mixture of horizontal and uneven liquid head profiles at the tray outlet (designation H/NO).

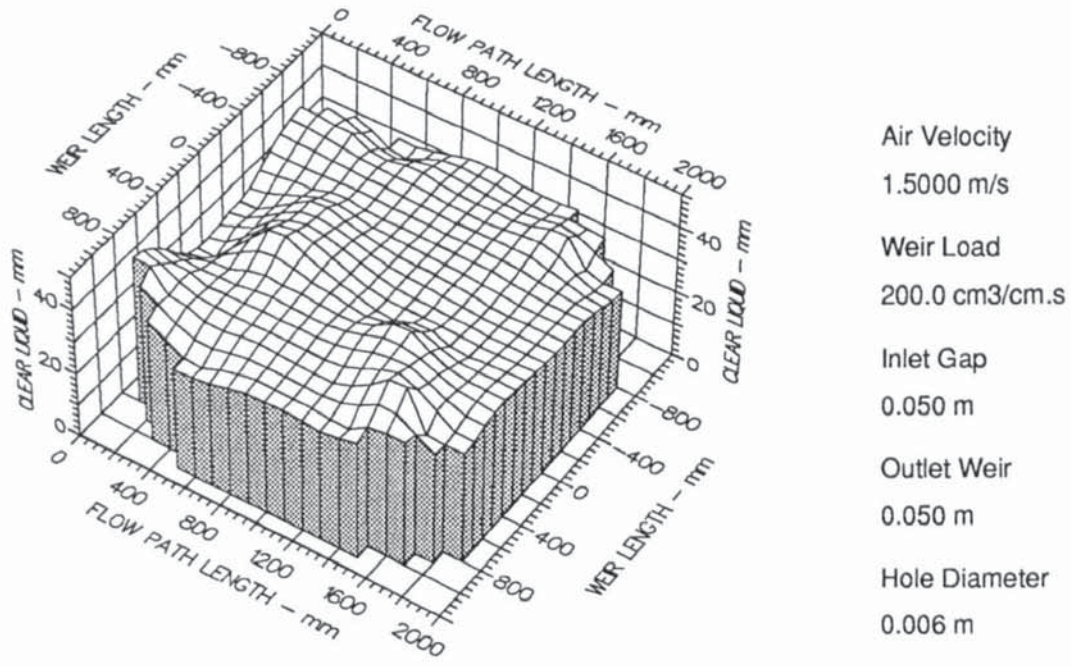

Figure A8.41 Three dimensional height of clear liquid profiles showing an uneven liquid surface over the whole tray (designation N).

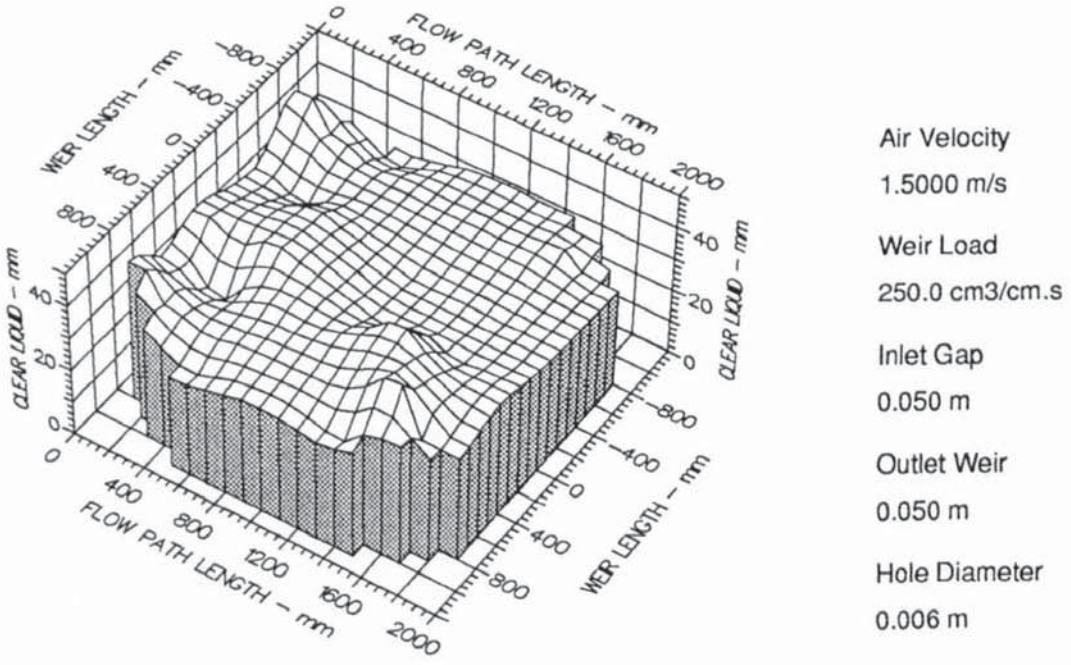

Figure A8.42 Three dimensional height of clear liquid profiles showing an uneven liquid surface over the whole tray (designation N).

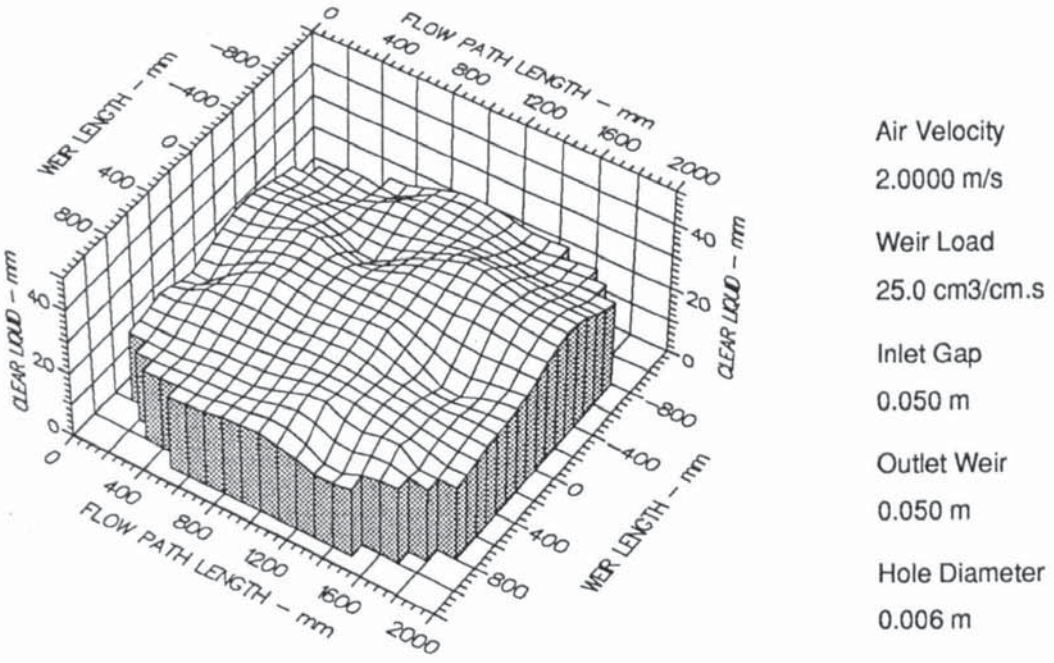

Figure A8.43 Three dimensional height of clear liquid profiles showing an uneven liquid surface at the tray inlet (designation NI).

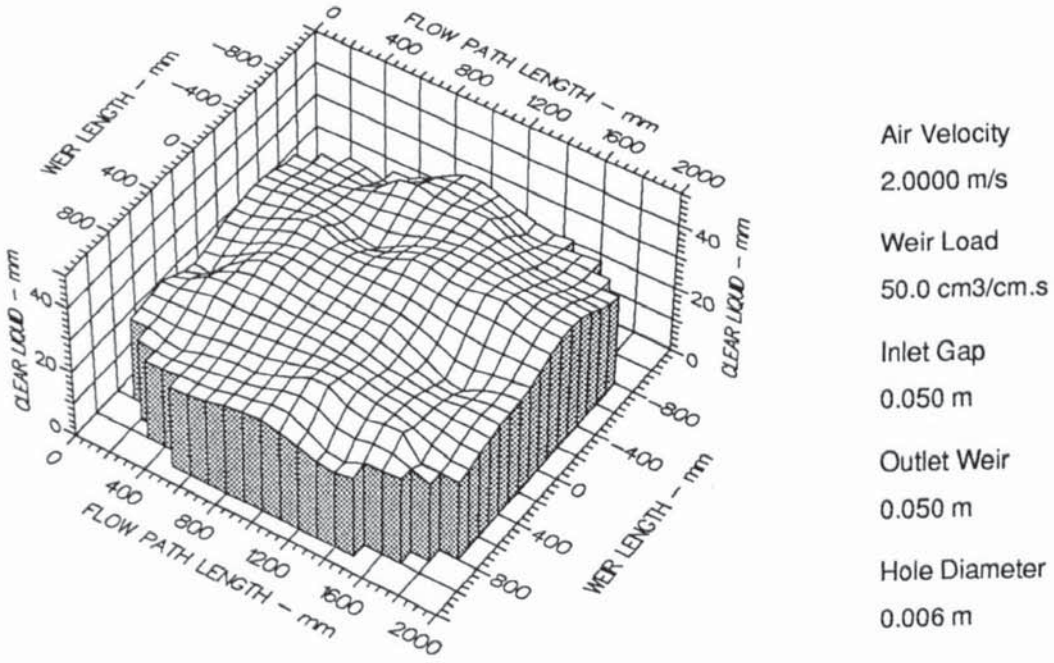

Figure A8.44 Three dimensional height of clear liquid profiles showing an uneven liquid surface over the whole tray (designation N).

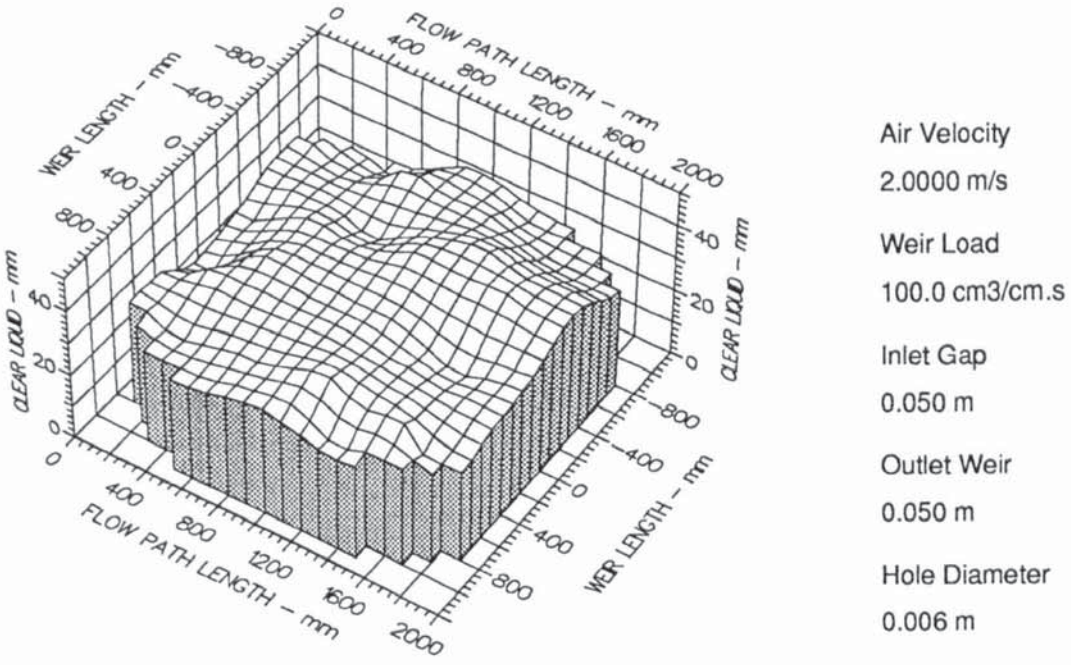

Figure A8.45 Three dimensional height of clear liquid profiles showing an uneven liquid surface over the whole tray (designation N).

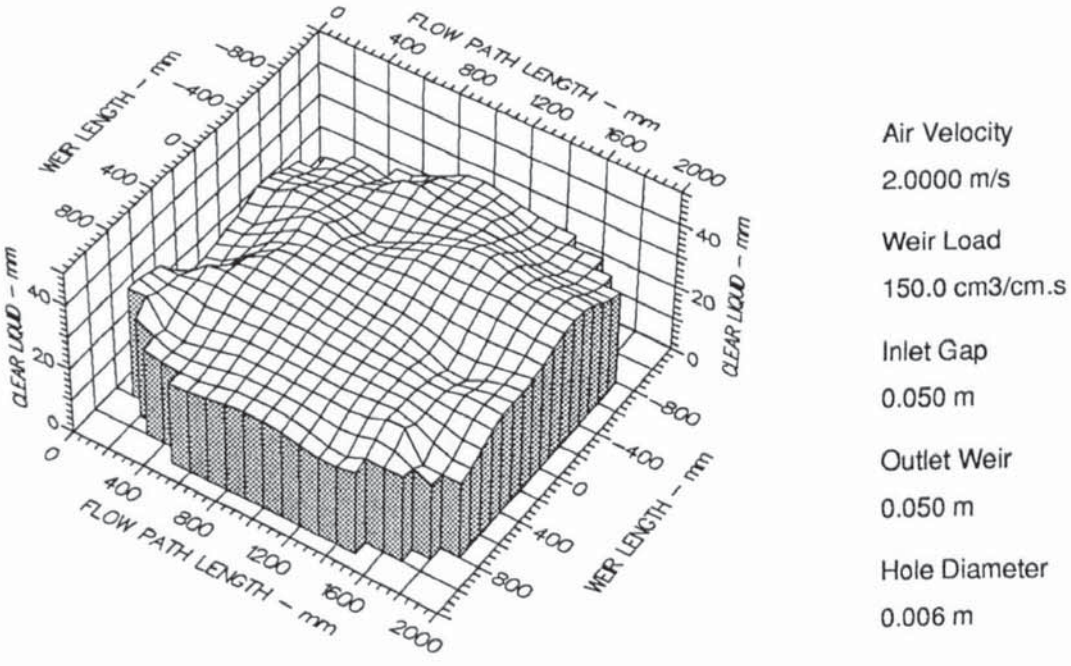

Figure A8.46 Three dimensional height of clear liquid profiles showing an uneven liquid surface at the tray inlet (designation NI).

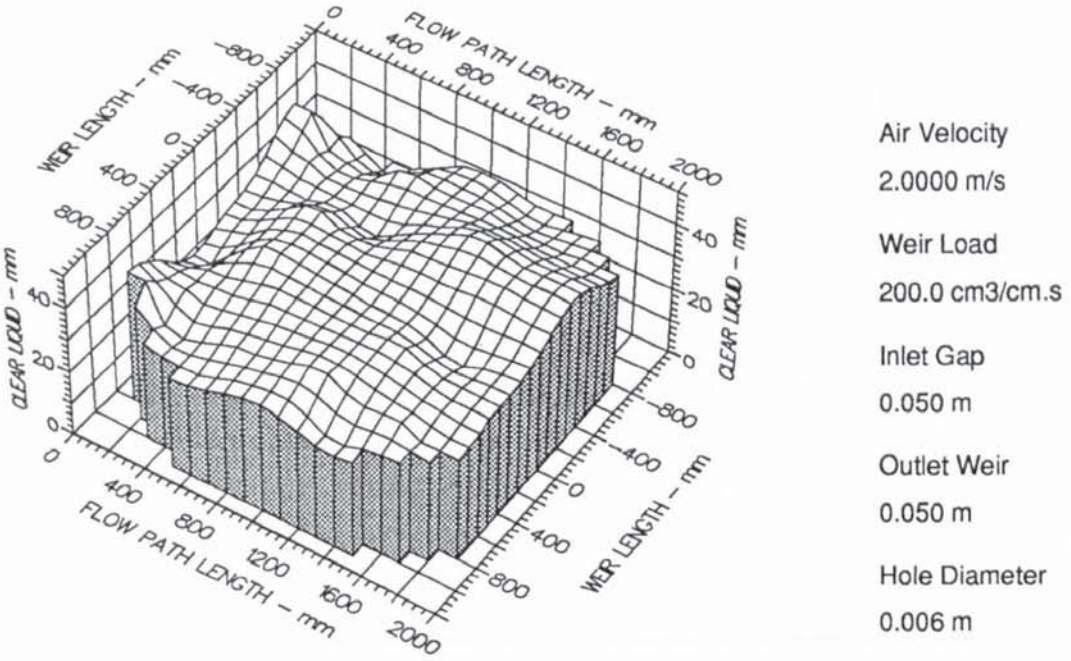

Figure A8.47 Three dimensional height of clear liquid profiles showing an uneven liquid surface over the whole tray (designation N).

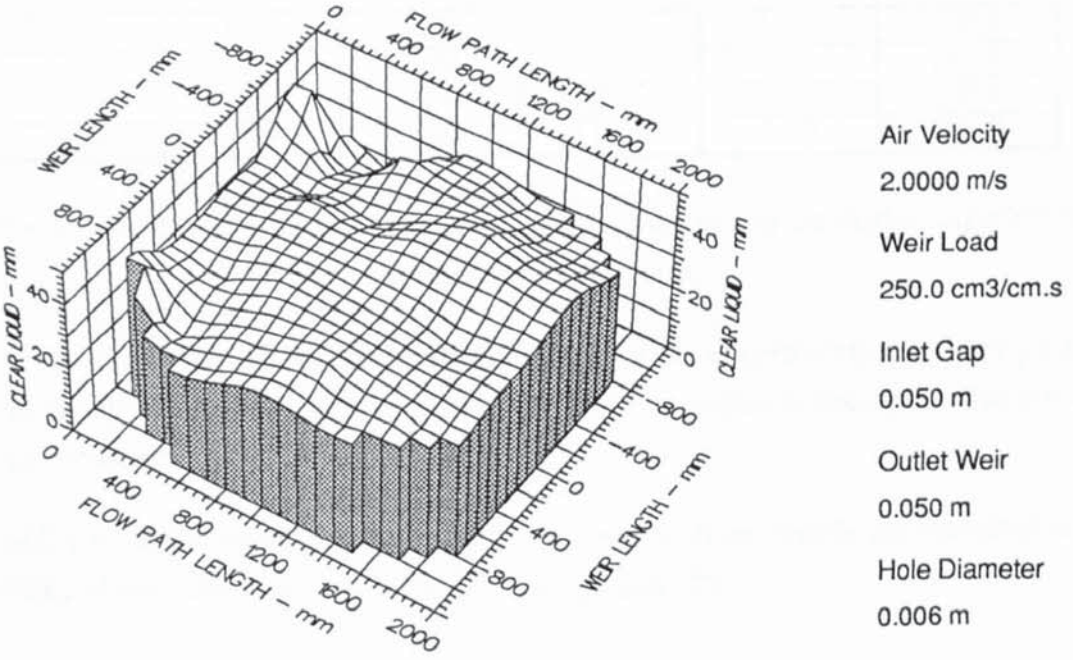

Figure A8.48 Three dimensional height of clear liquid profiles showing an uneven liquid surface over the whole tray (designation N).

APPENDIX 9

Two-Dimensional Reduced Temperatue Isotherm Displays For The Pressure Simulation Experiments

The two-dimensional black and white displays presented below are a full set of reduced temperature profiles to complement the results of the height of clear liquid experiments in Chapter 9. The water-cooling technique was used to show the effect of the liquid flow patterns for each simulated pressure on mass transfer. In these experiments, flow rates were varied at a fixed ratio of liquid flow to air velocity, and were chosen to represent distillation under vacuum, at atmospheric pressure, and at a moderate pressure. The flow rate and downcomer information for each simulated pressure is presented in Table A9.1.

Simulated Pressure					
Vacuum		Atmospheric Pressure		Moderate Pressure	
Inlet Gap = 10 mm Outlet Weir = 10 mm		Inlet Gap = 20 mm Outlet Weir = 20 mm		Inlet Gap = 50 mm Outlet Weir = 50 mm	
Air Velocity - ms^{-1}	Weir load - 10^4 $m^3/m.s$	Air Velocity - ms^{-1}	Weir load - 10^4 $m^3/m.s$	Air Velocity - ms^{-1}	Weir load - 10^4 $m^3/m.s$
1.00	12.5	1.00	60.0	1.25	100.0
1.50	18.5	1.50	90.0	1.50	150.0
2.00	25.0	2.00	120.0	2.00	200.0
2.50	31.0	2.50	150.0	2.50	250.0

Table A9.1 Summary of flow rates chosen for the simulation of distillation experiments at three different pressures.

Note that the reduced temperature profiles in all of the experiments are either parallel, distinctively "U-shaped", or a mixture of isotherms according to the distillation pressure being simulated.

In addition, the designations assigned to each temperature profile are included in the labelling of each diagram, (see Table A7.2 in Appendix 7).

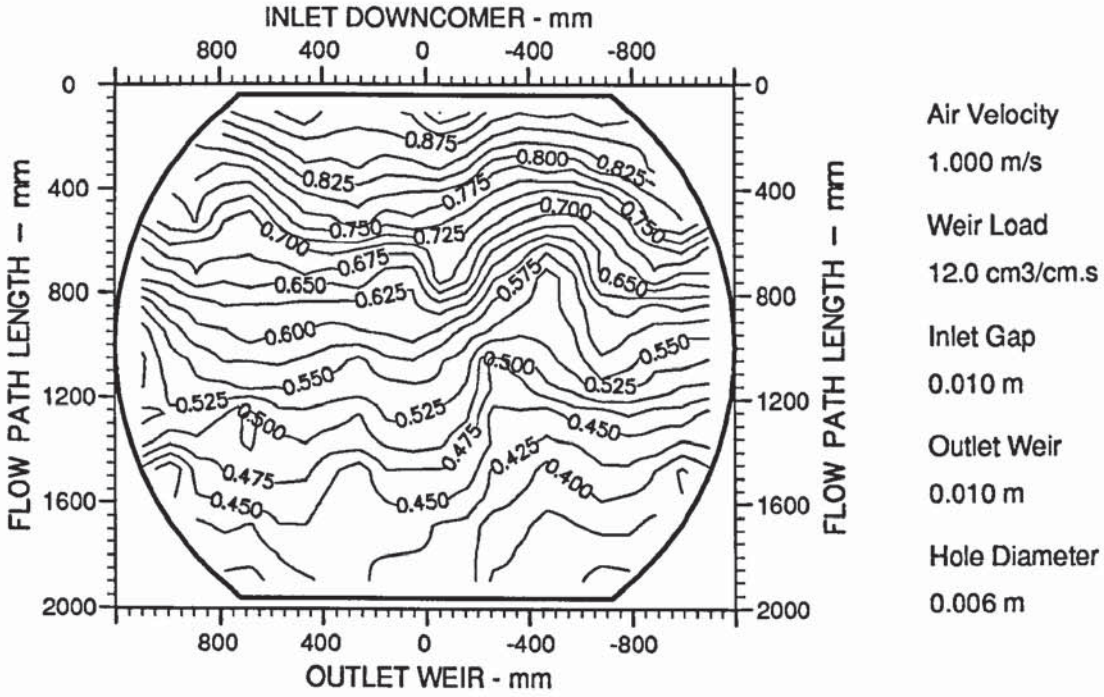

Figure A9.1 Two dimensional reduced temperature profiles showing straight and parallel isotherms (designation P).

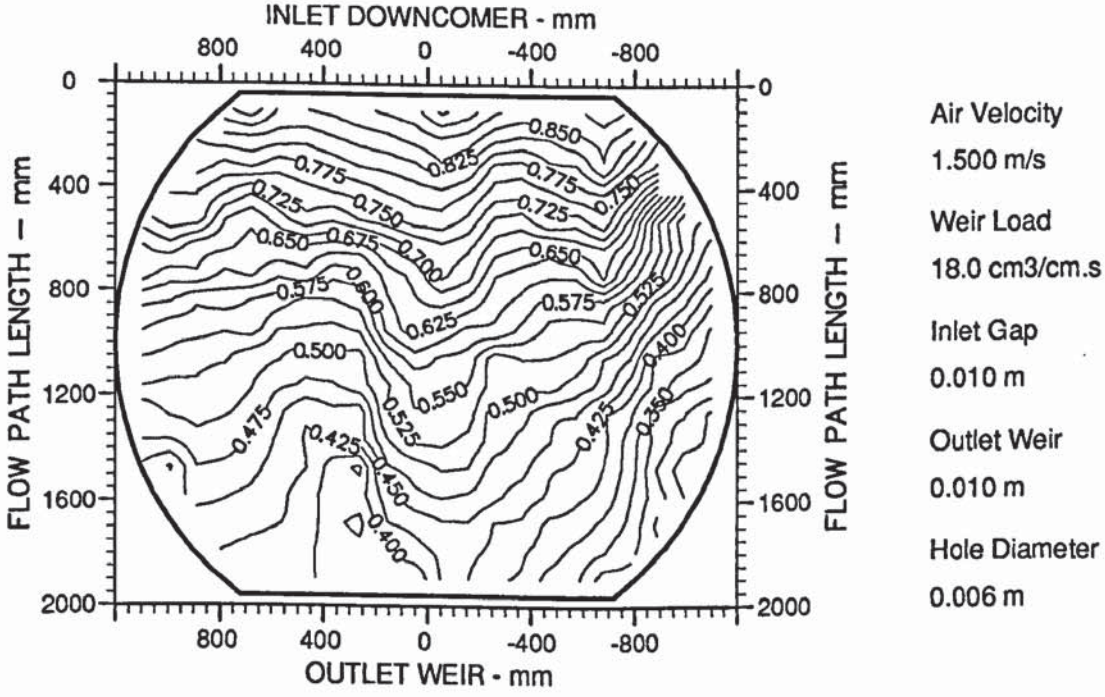

Figure A9.2 Two dimensional reduced temperature profiles showing straight and parallel isotherms (designation P).

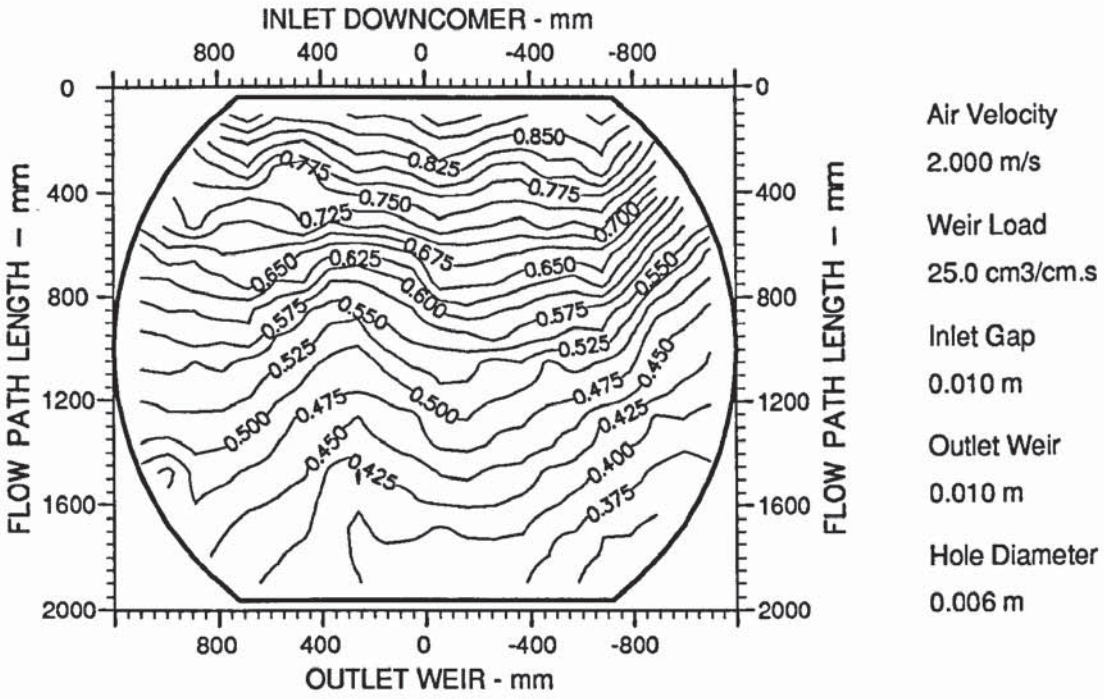

Figure A9.3 Two dimensional reduced temperature profiles showing straight and parallel isotherms (designation P).

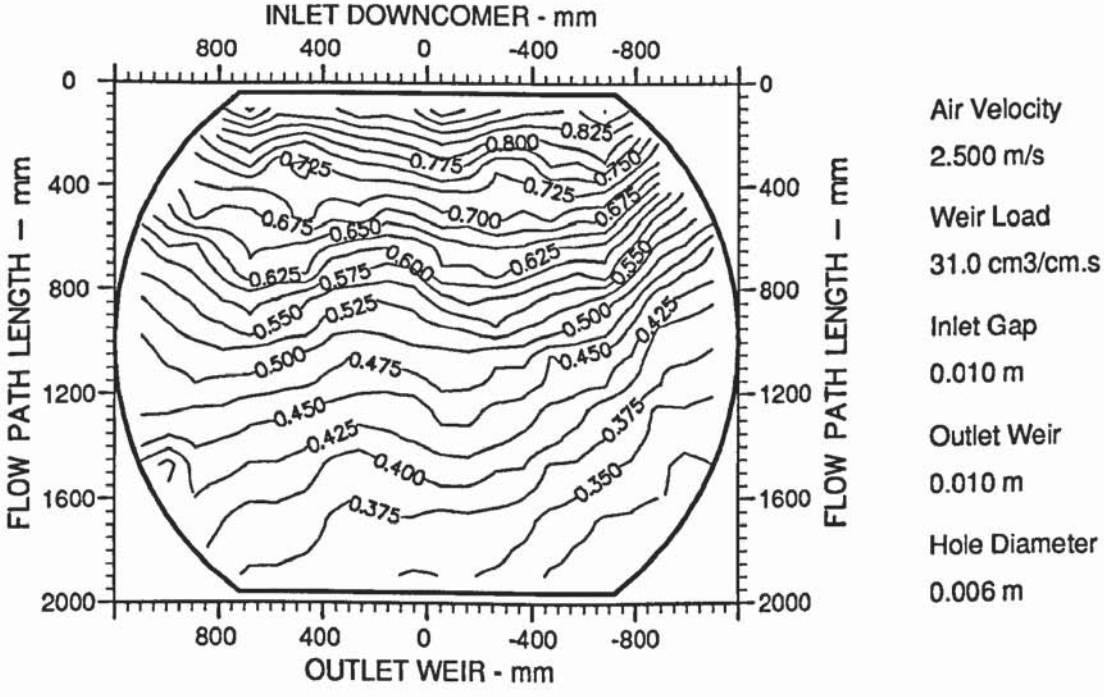

Figure A9.4 Two dimensional reduced temperature profiles showing straight and parallel isotherms (designation P).

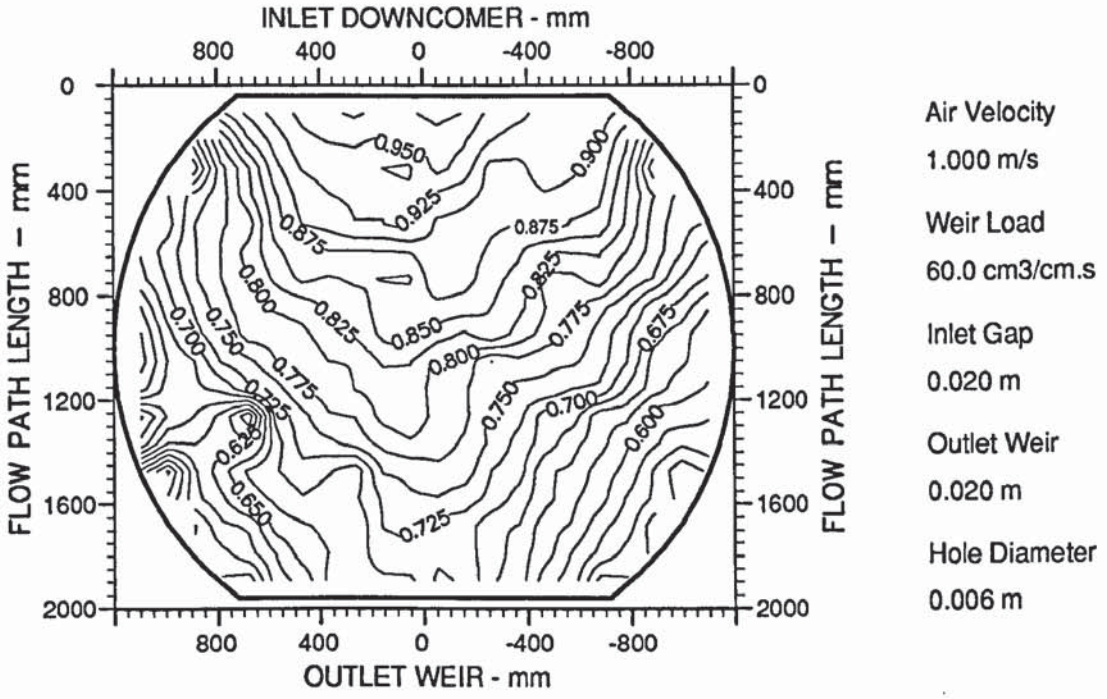

Figure A9.5 Two dimensional reduced temperature profiles showing distinctively "U-shaped" isotherms (designation U).

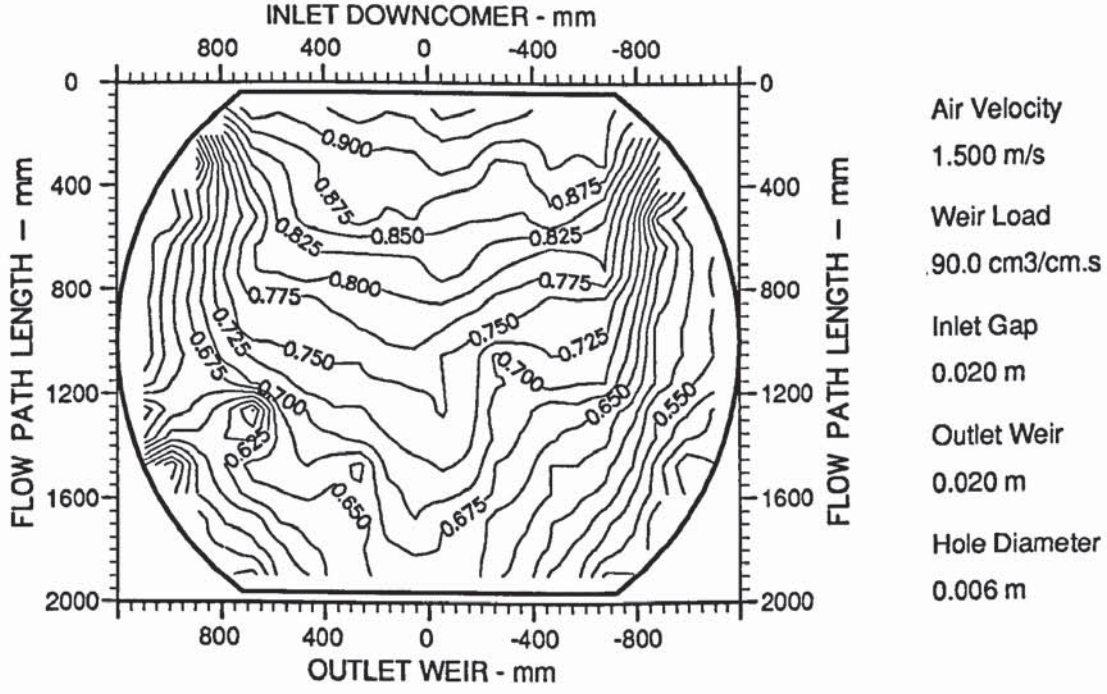

Figure A9.6 Two dimensional reduced temperature profiles showing shallow transverse "U-shaped" isotherms (designation hU).

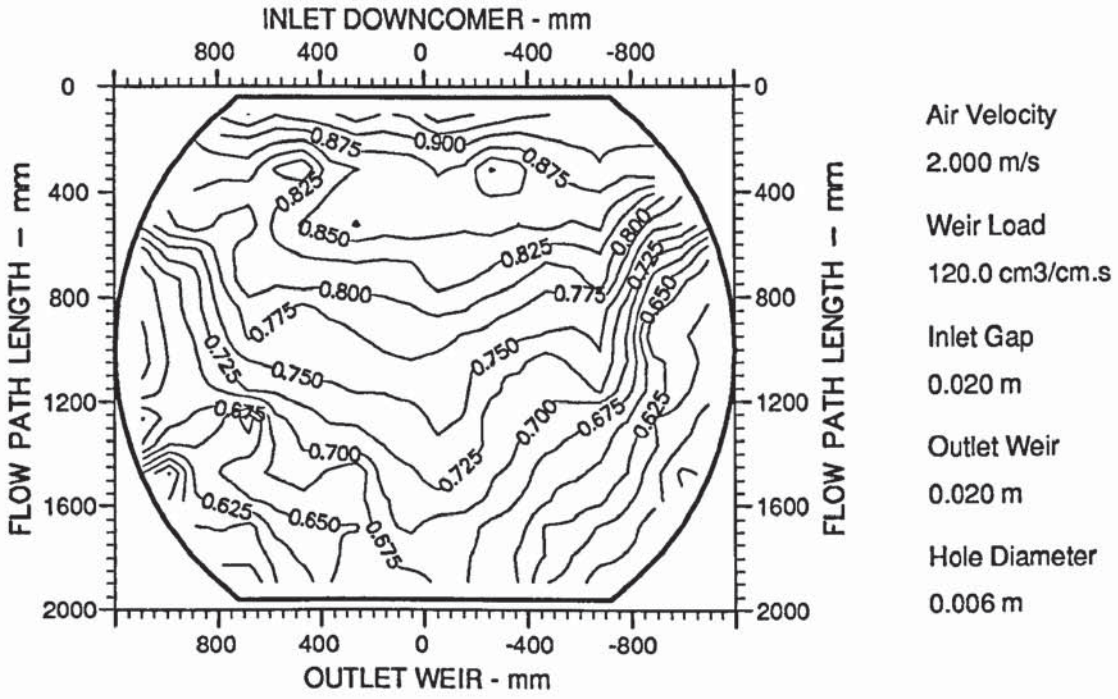

Figure A9.7 Two dimensional reduced temperature profiles showing shallow transverse "U-shaped" isotherms (designation hU).

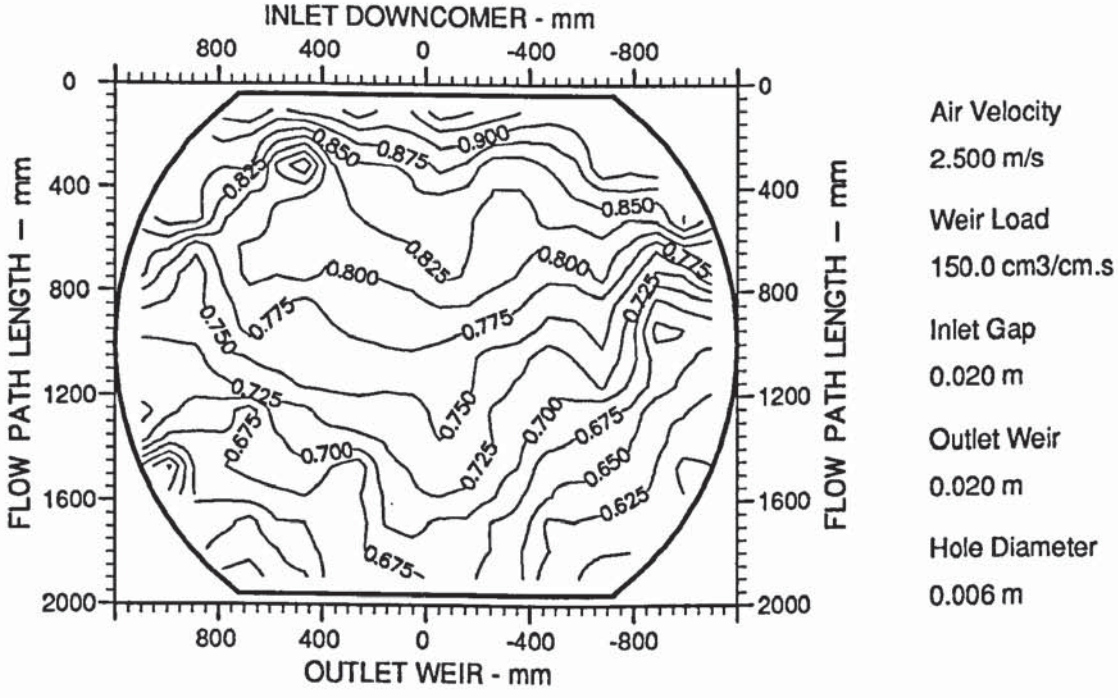

Figure A9.8 Two dimensional reduced temperature profiles showing shallow transverse "U-shaped" isotherms (designation hU).

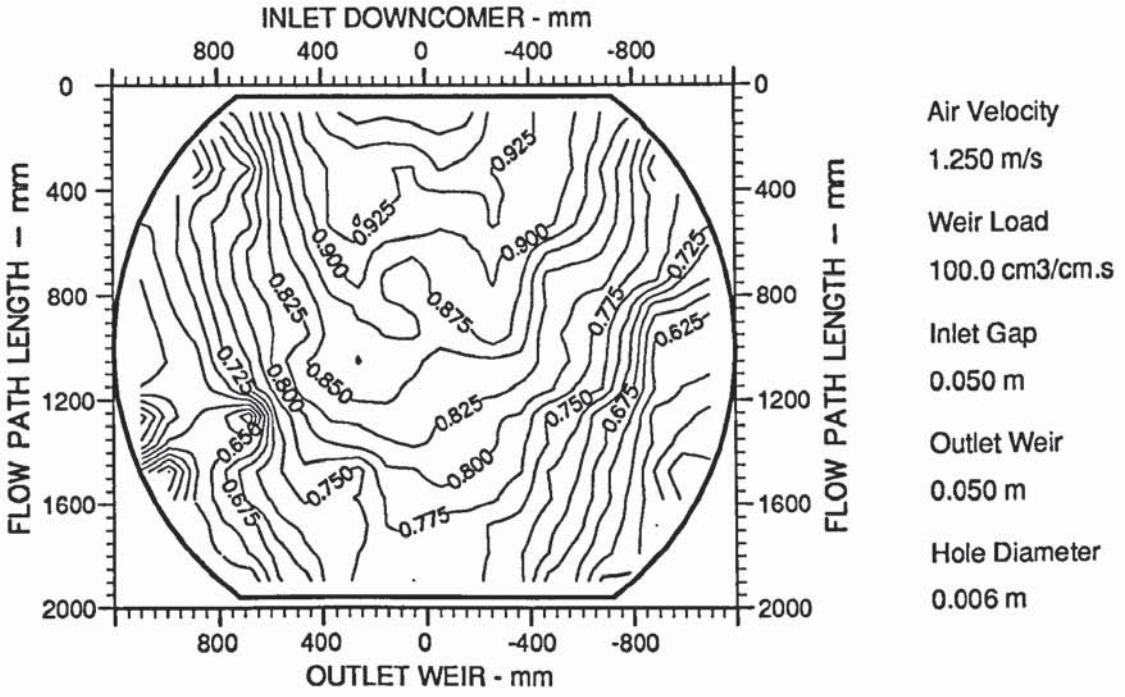

Figure A9.9 Two dimensional reduced temperature profiles showing distinctively "U-shaped" isotherms (designation U).

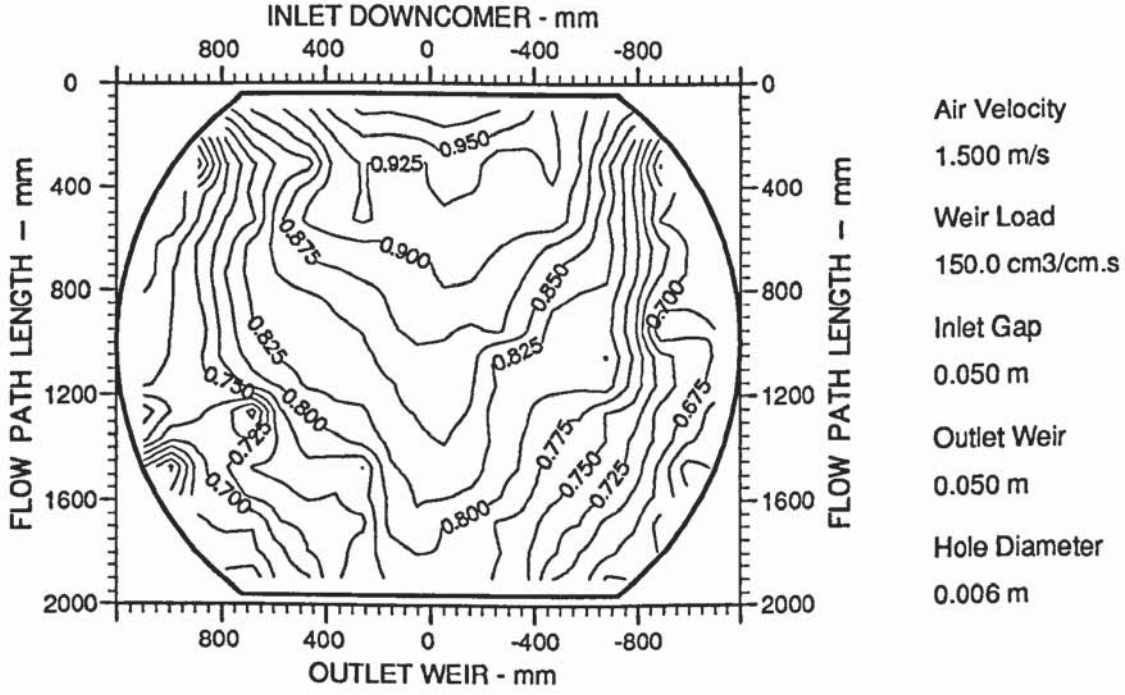

Figure A9.10 Two dimensional reduced temperature profiles showing distinctively "U-shaped" isotherms (designation U).

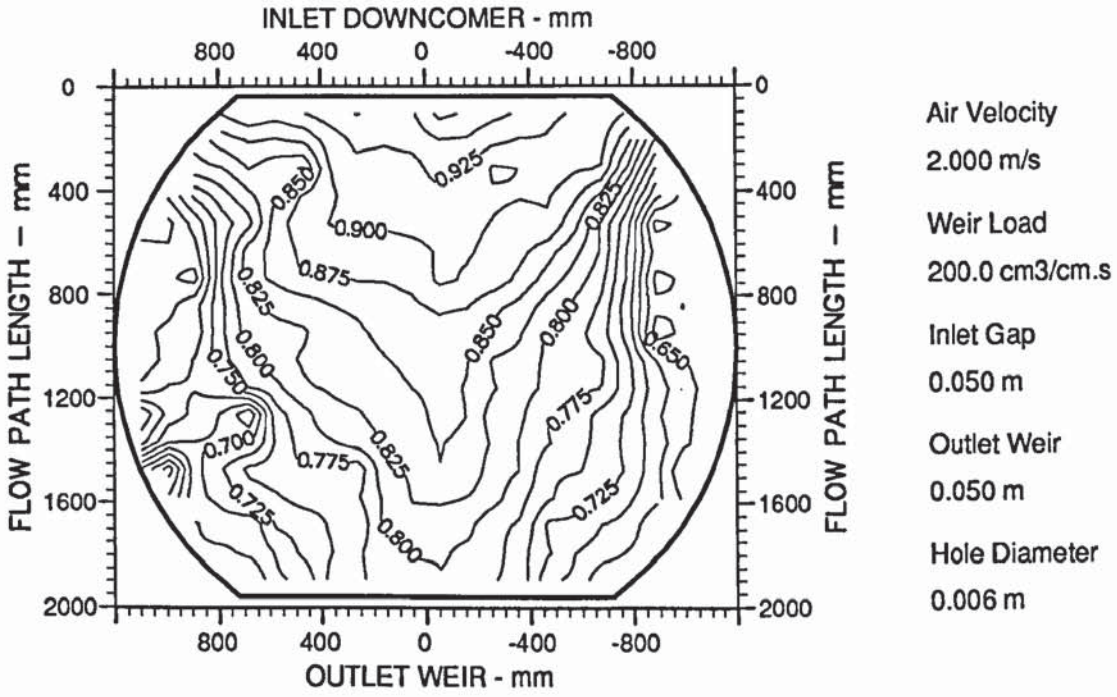

Figure A9.11 Two dimensional reduced temperature profiles showing distinctively "U-shaped" isotherms (designation U).

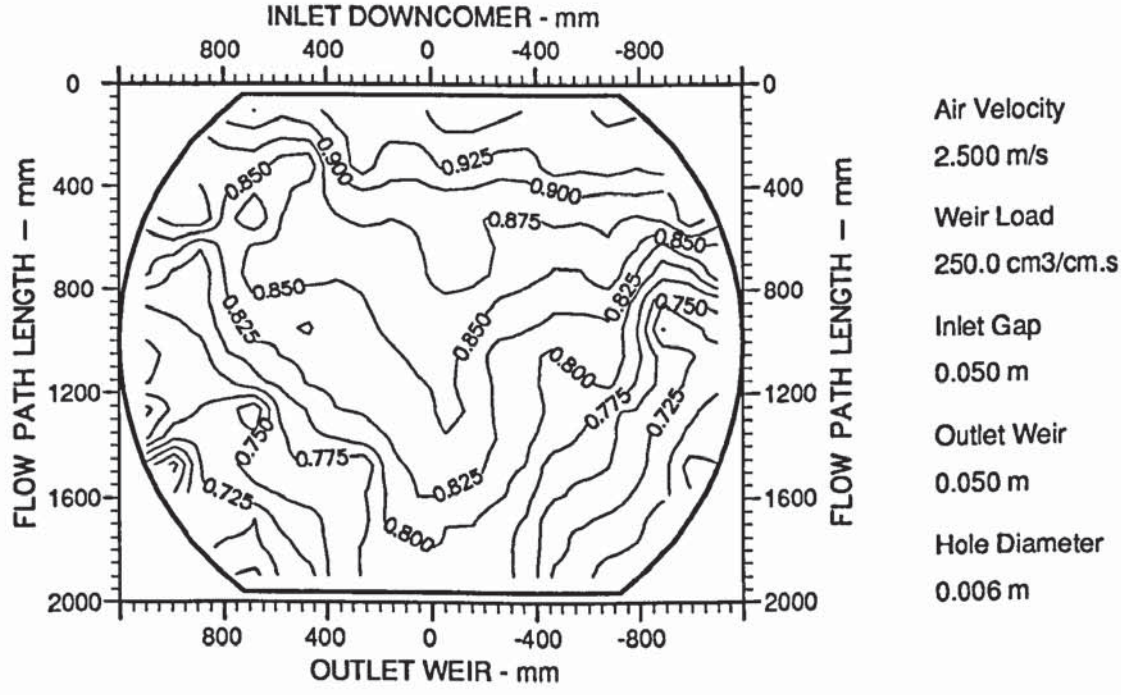

Figure A9.12 Two dimensional reduced temperature profiles showing distinctively "U-shaped" and mixed or confused isotherms (designation U/M).

PAGE
MISSING
IN
ORIGINAL

APPENDIX 10

Three-Dimensional Liquid Head Surface Profiles For The Pressure Simulation Experiments

The three-dimensional black and white displays presented below are a full set of liquid head surface profiles to complement the results of the height of clear liquid experiments in Chapter 9. Measurement of the clear liquid height profiles was used to show the effect of non-separated and separated liquid flow patterns on the liquid head across the tray. As with the water-cooling experiments, flow rates were varied at a fixed ratio of liquid flow to air velocity, and were chosen to represent distillation under vacuum, at atmospheric pressure, and at a moderate pressure. The flow rate information is presented in Table A9.1 in Appendix 9.

Note that the height of clear liquid profiles in all of the experiments are either horizontal, or contain an uneven surface at the inlet or the outlet, or both according to the distillation pressure being simulated.

A reminder of the designations assigned to each liquid head surface profile for the labelling of each diagram, are summarised in Table A10.1.

Height of Clear Liquid Profile	Designation
Horizontal or flat profile	H
Uneven surface on tray inlet	NI
Uneven surface on tray outlet	NO
Uneven surface over the whole tray	N

Table A10.1 Summary of height of clear liquid profile designations.

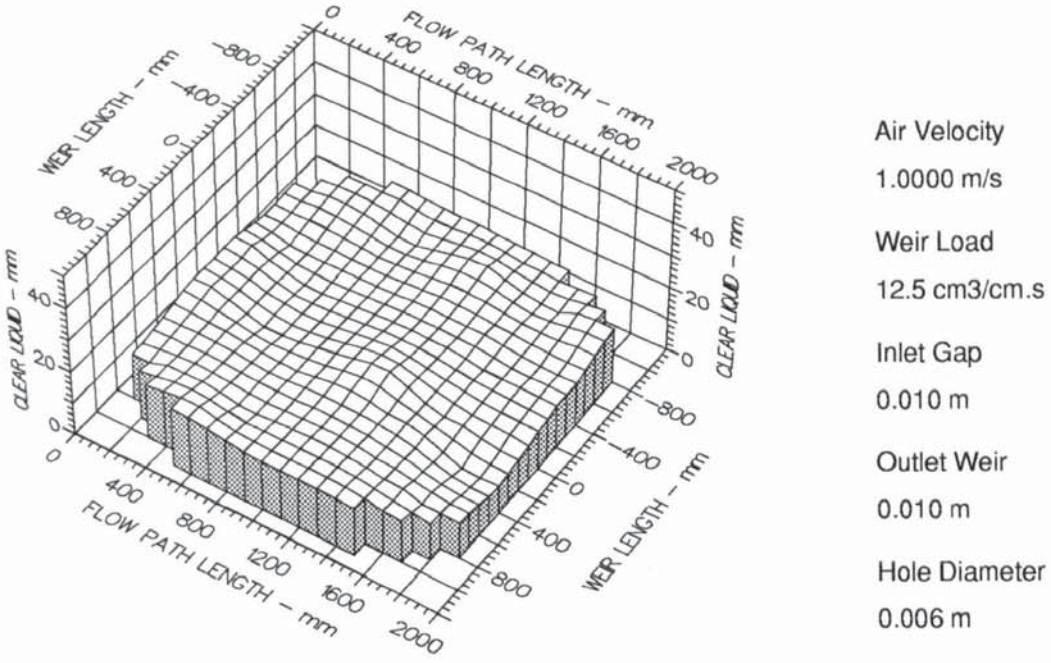

Figure A10.1 Three dimensional height of clear liquid profiles showing a comparatively horizontal or flat liquid surface (designation H).

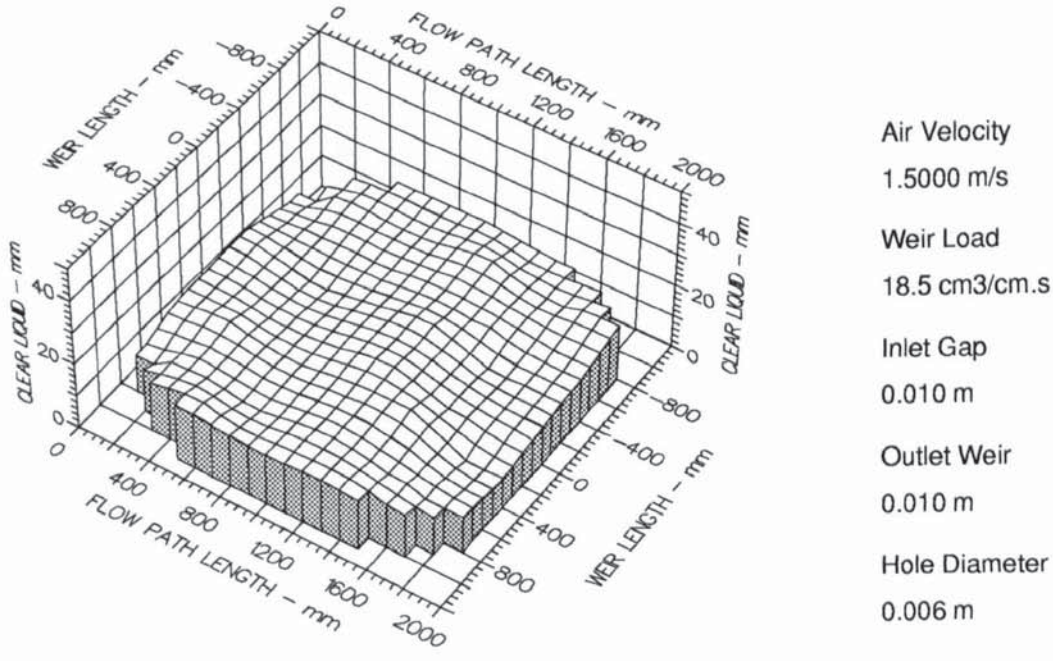

Figure A10.2 Three dimensional height of clear liquid profiles showing a comparatively horizontal or flat liquid surface (designation H).

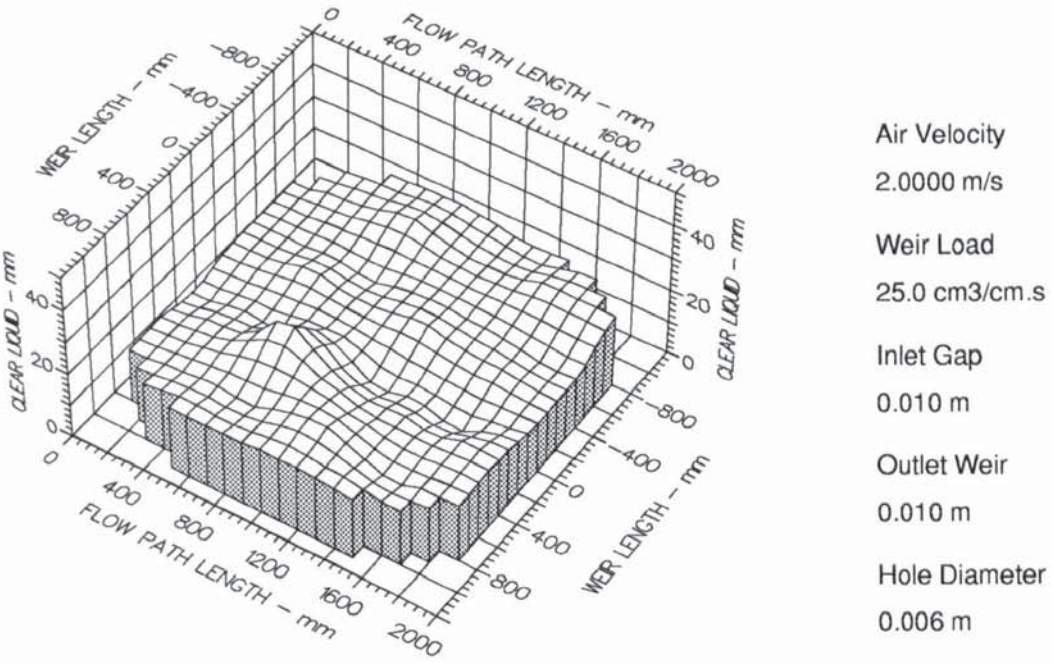

Figure A10.3 Three dimensional height of clear liquid profiles showing a comparatively horizontal or flat liquid surface (designation H).

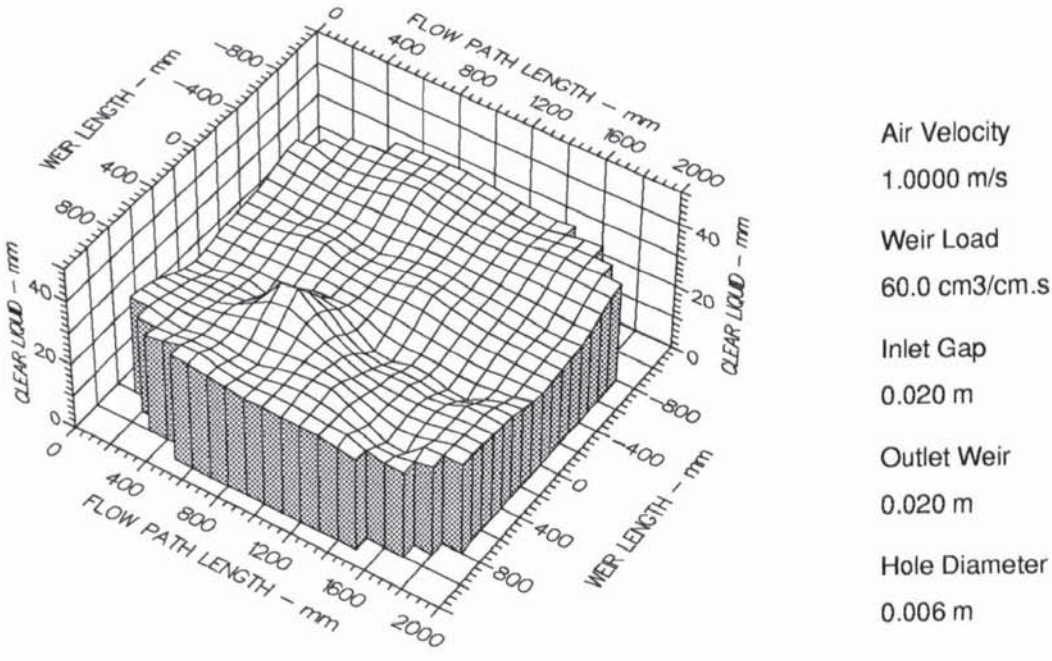

Figure A10.4 Three dimensional height of clear liquid profiles showing a comparatively horizontal or flat liquid surface (designation H).

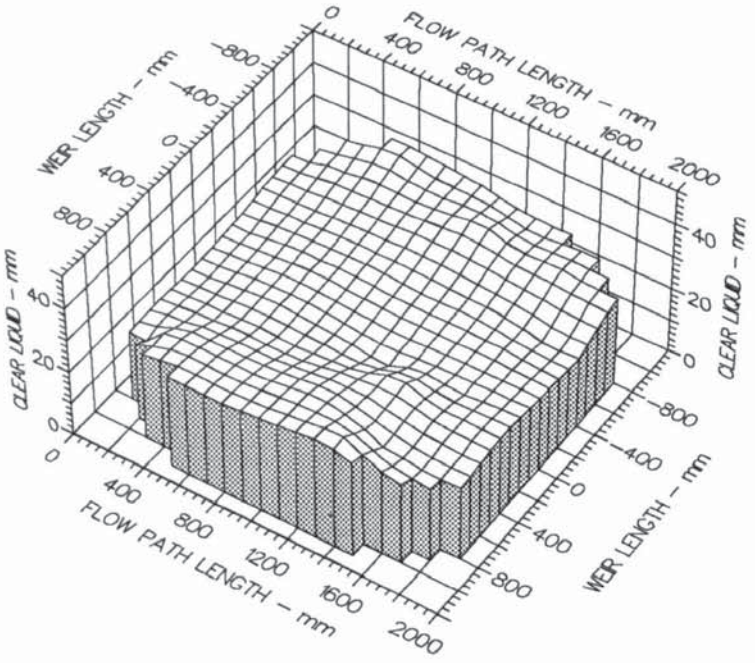

Figure A10.5 Three dimensional height of clear liquid profiles showing a comparatively horizontal or flat liquid surface (designation H).

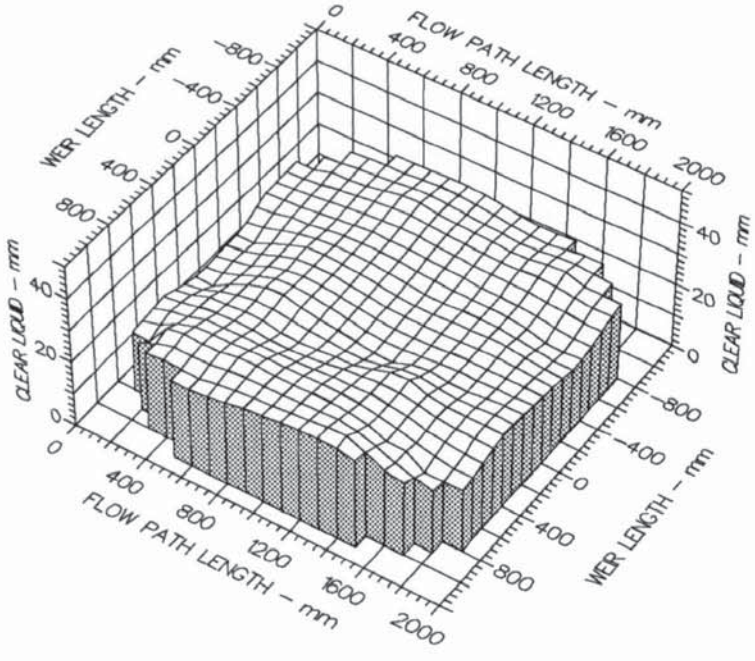

Figure A10.6 Three dimensional height of clear liquid profiles showing a mixture of horizontal and uneven liquid head profiles at the tray inlet (designation H/NI).

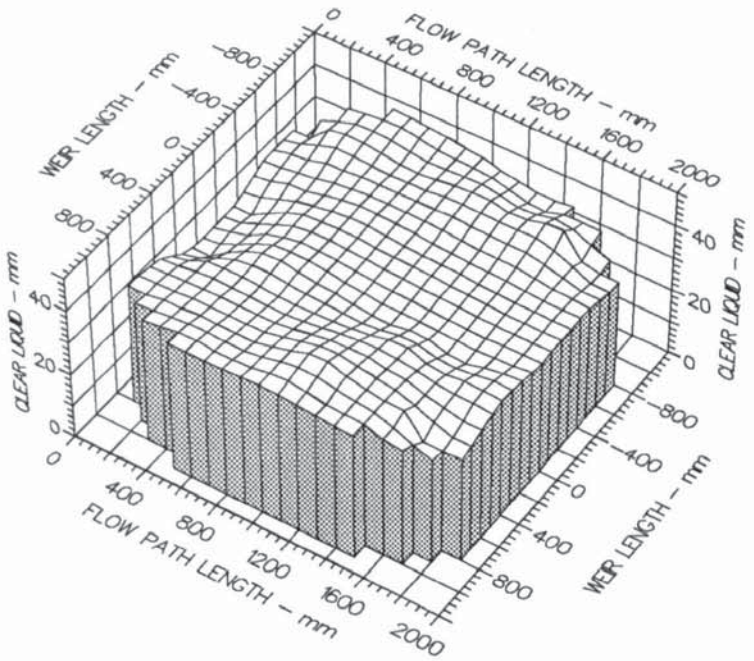

Figure A10.7 Three dimensional height of clear liquid profiles showing an uneven liquid surface at the tray inlet (designation NI).

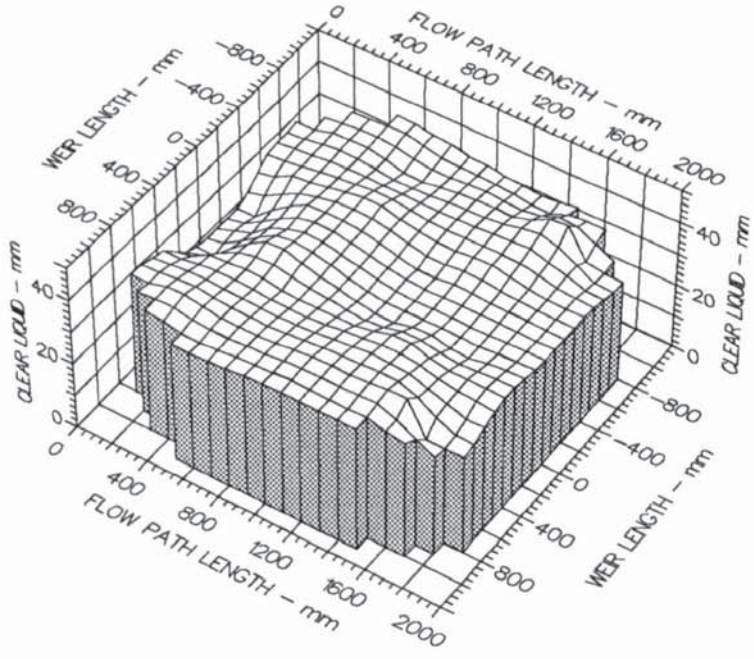

Figure A10.8 Three dimensional height of clear liquid profiles showing an uneven liquid surface at the tray inlet (designation NI).

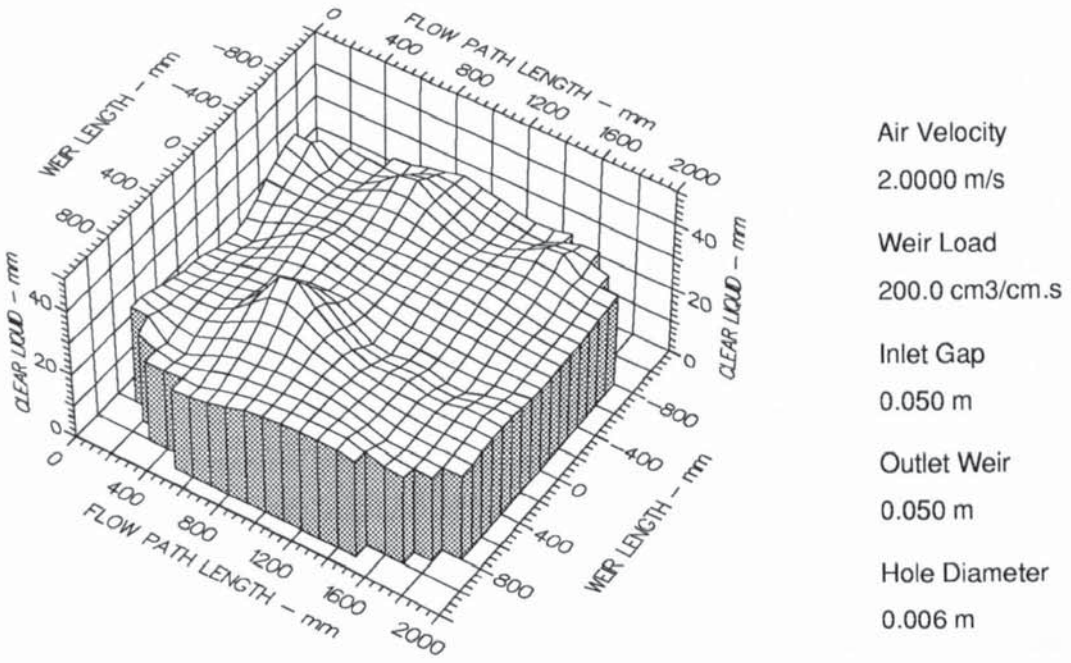

Figure A10.9 Three dimensional height of clear liquid profiles showing an uneven liquid surface over the whole tray (designation N).

APPENDIX 11

Predicted Two-Dimensional Reduced Concentration Profiles for the Pressure Simulation Experiments

The two-dimensional displays presented below are a full set of reduced concentration profiles predicted using the stagnant regions model (SRM) of Porter et al., (1972) by incorporating data from the water-cooling experiments into the model. Input parameters used in the SRM computer program included the tray dimensions and the froth properties. The tray data included the weir length, tray diameter, weir height, hole diameter, and the fractional free area of the tray. Data for the froth included the vapour and liquid flow rates, experimental λ, N_{Pe}, experimental E_{OG}, ρ_L, ρ_V, and the average height of clear liquid.

The results complement the representative examples for each pressure simulation in Chapter 9 which, in turn, were compared with corresponding experimental temperature isotherms for the same operating conditions. Concentration profiles show the effect of the liquid flow patterns for each pressure simulation on mass transfer. The flow rate and downcomer information for each simulated pressure are presented in Table A9.1 of Appendix 9.

Note that the reduced concentration profiles are "U-shaped" for each pressure simulated including vacuum distillation. It was shown in Chapter 9 that the SRM was not valid for vacuum simulation for the following reasons.

a) The concentration profiles were "U-shaped" as compared to the straight and parallel temperature isotherms.

b) The high air-rate to water-rate ratio for vacuum simulation meant that the tray was operating under a different flow mechanism as compared with the higher pressure simulations, i.e., spray regime operation.

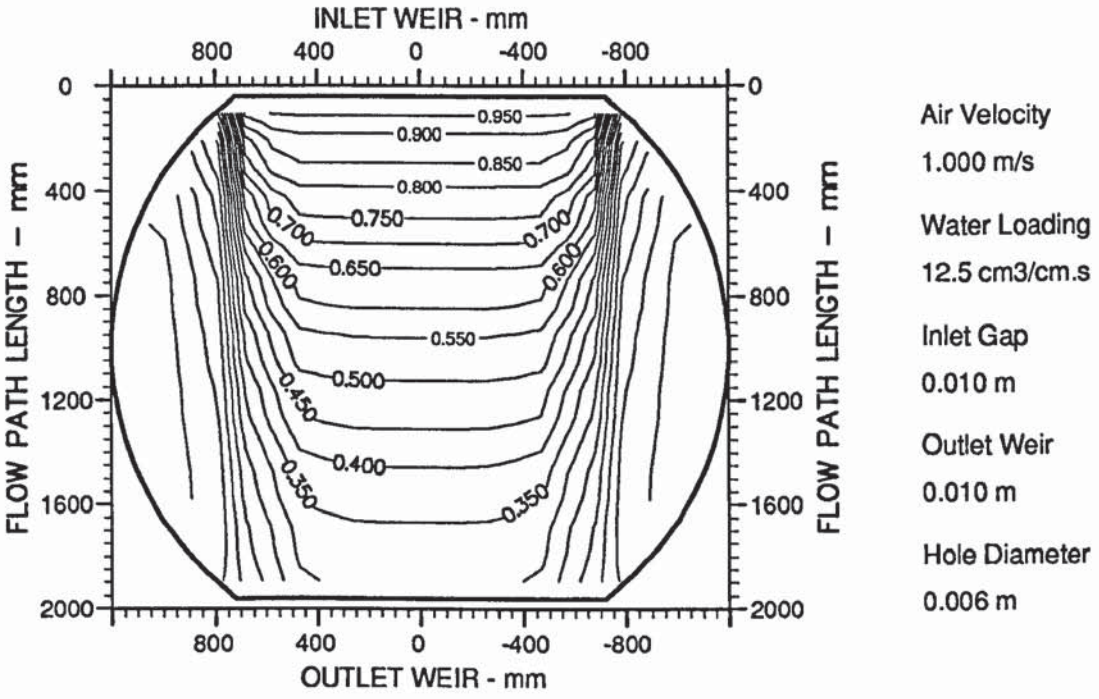

Figure A11.1 Two dimensional reduced concentration profiles showing shallow transverse "U-shaped" profiles during vacuum simulation.

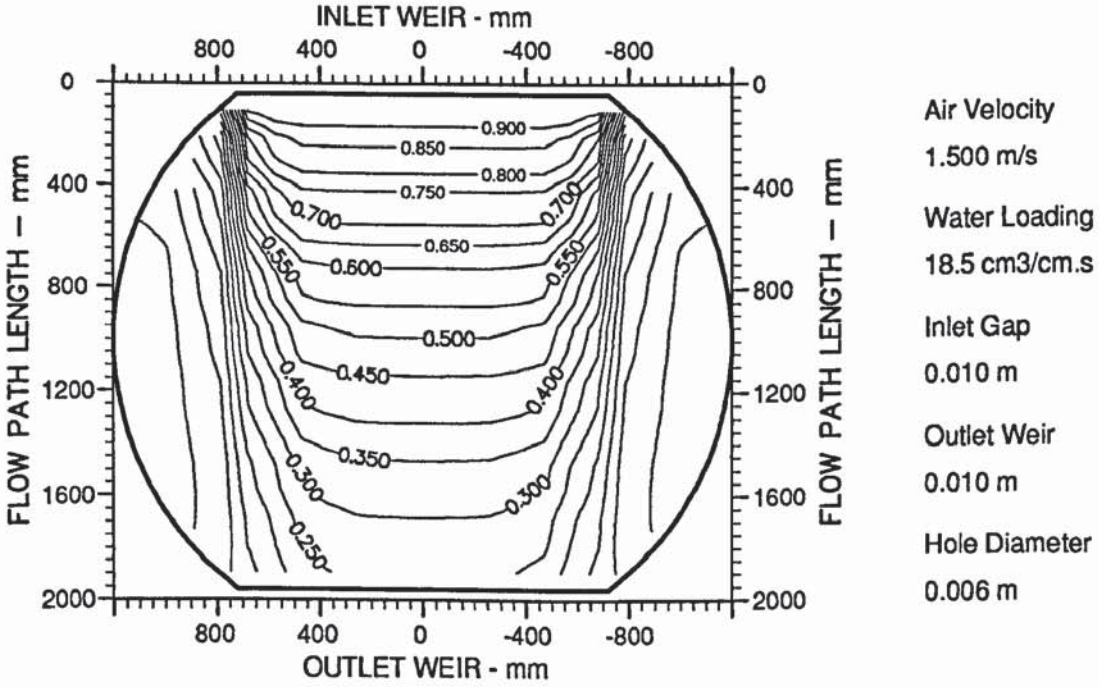

Figure A11.2 Two dimensional reduced concentration profiles showing shallow transverse "U-shaped" profiles during vacuum simulation.

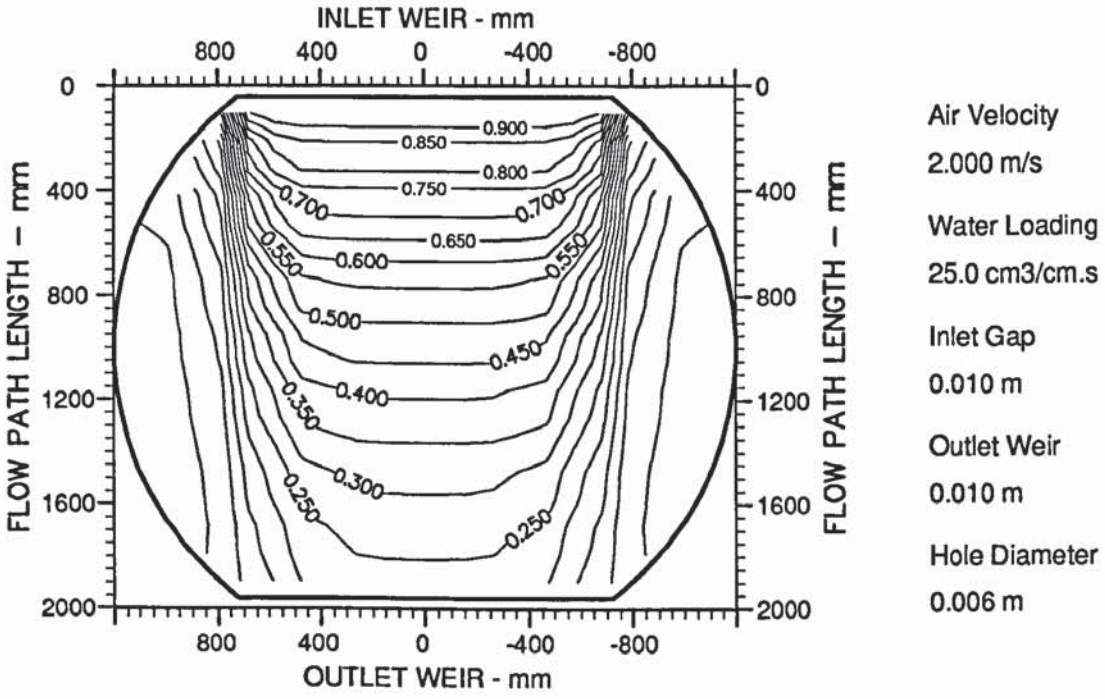

Figure A11.3 Two dimensional reduced concentration profiles showing shallow transverse "U-shaped" profiles during vacuum simulation.

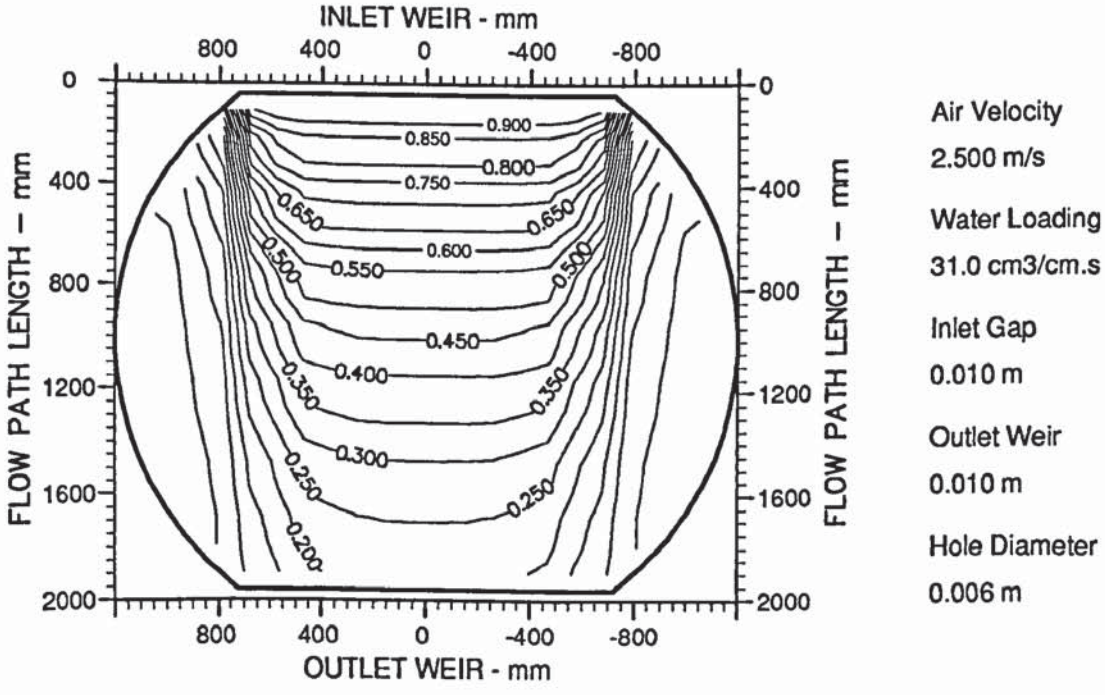

Figure A11.4 Two dimensional reduced concentration profiles showing shallow transverse "U-shaped" profiles during vacuum simulation.

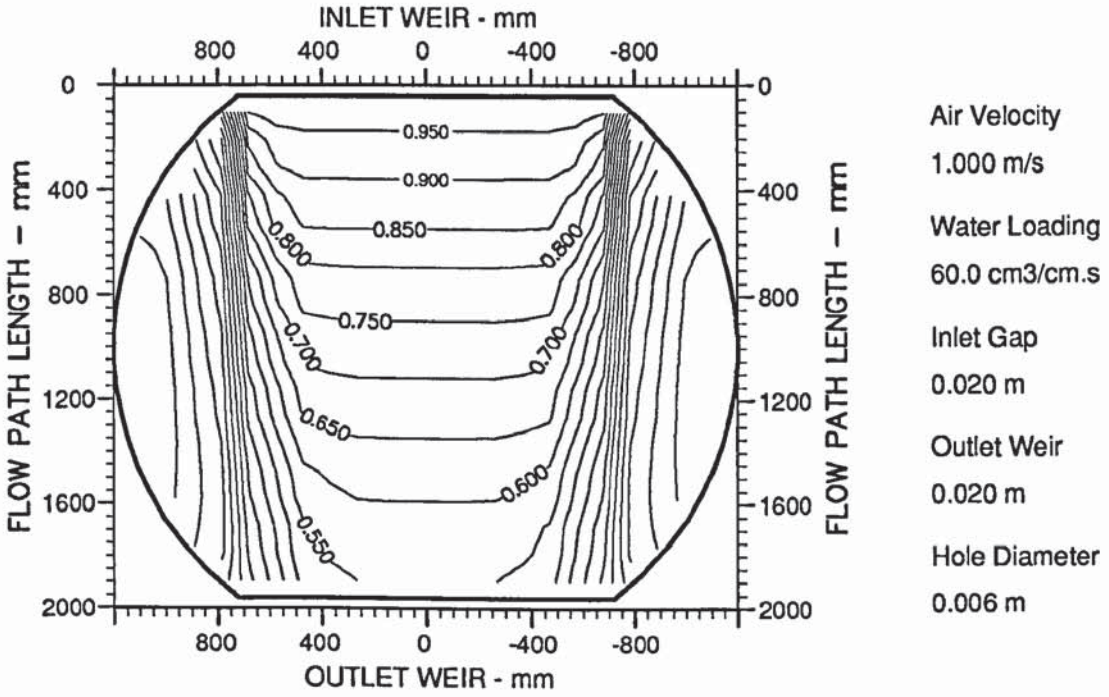

Figure A11.5 Two dimensional reduced concentration profiles showing transverse "U-shaped" profiles during atmospheric pressure simulation.

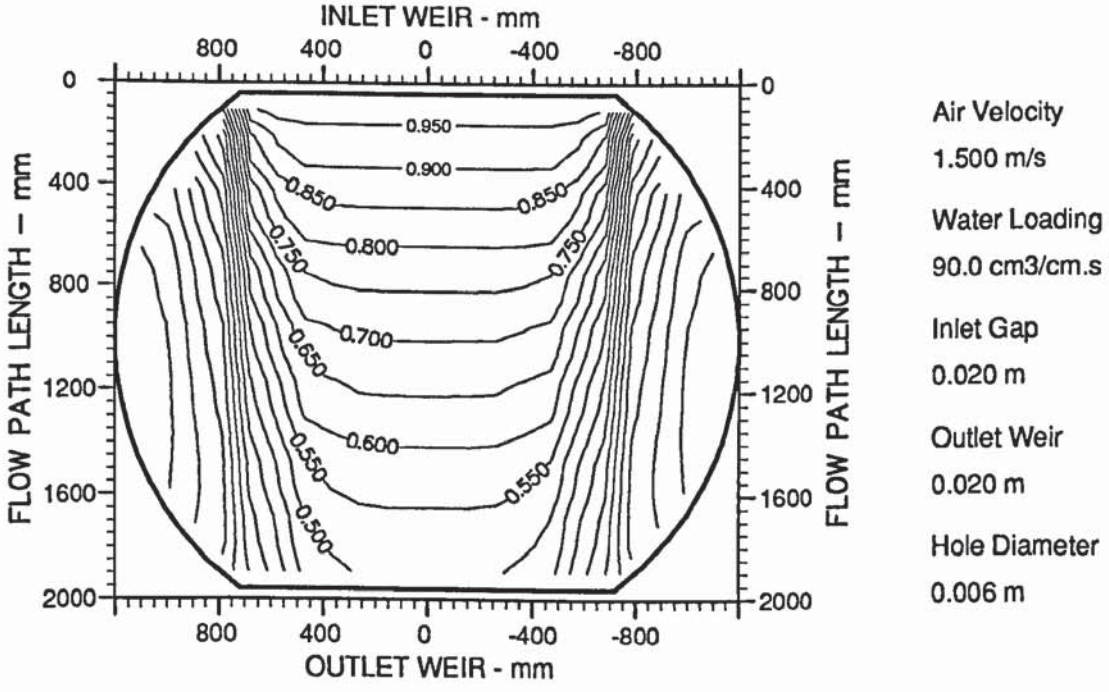

Figure A11.6 Two dimensional reduced concentration profiles showing transverse "U-shaped" profiles during atmospheric pressure simulation.

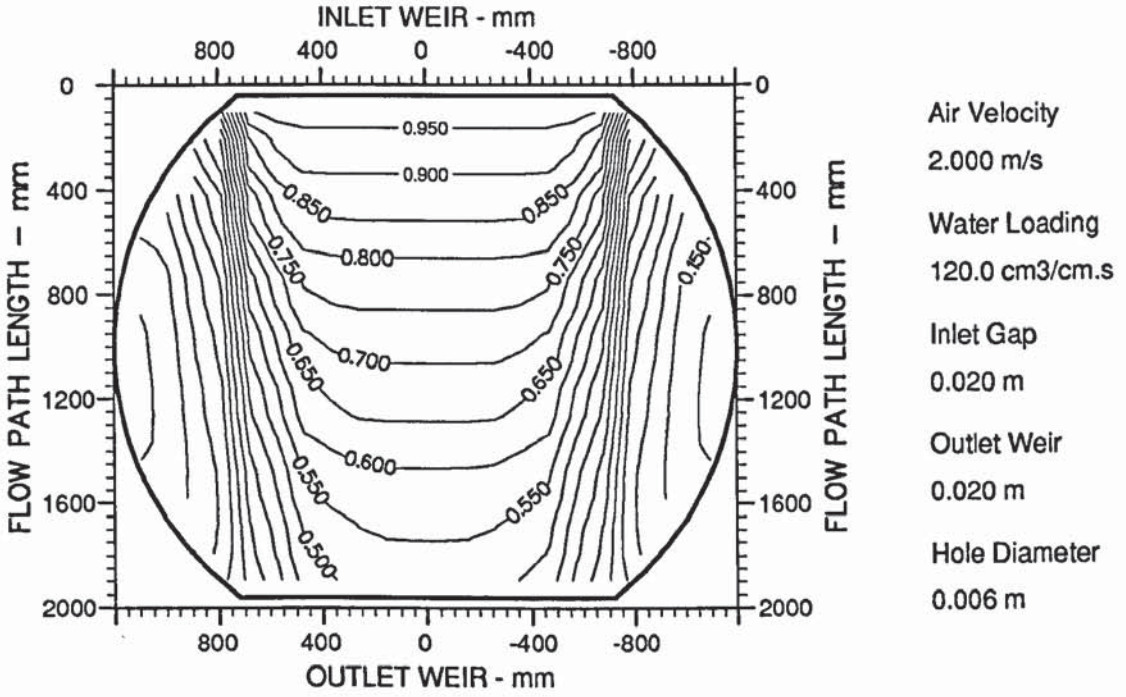

Figure A11.7 Two dimensional reduced concentration profiles showing transverse "U-shaped" profiles during atmospheric pressure simulation.

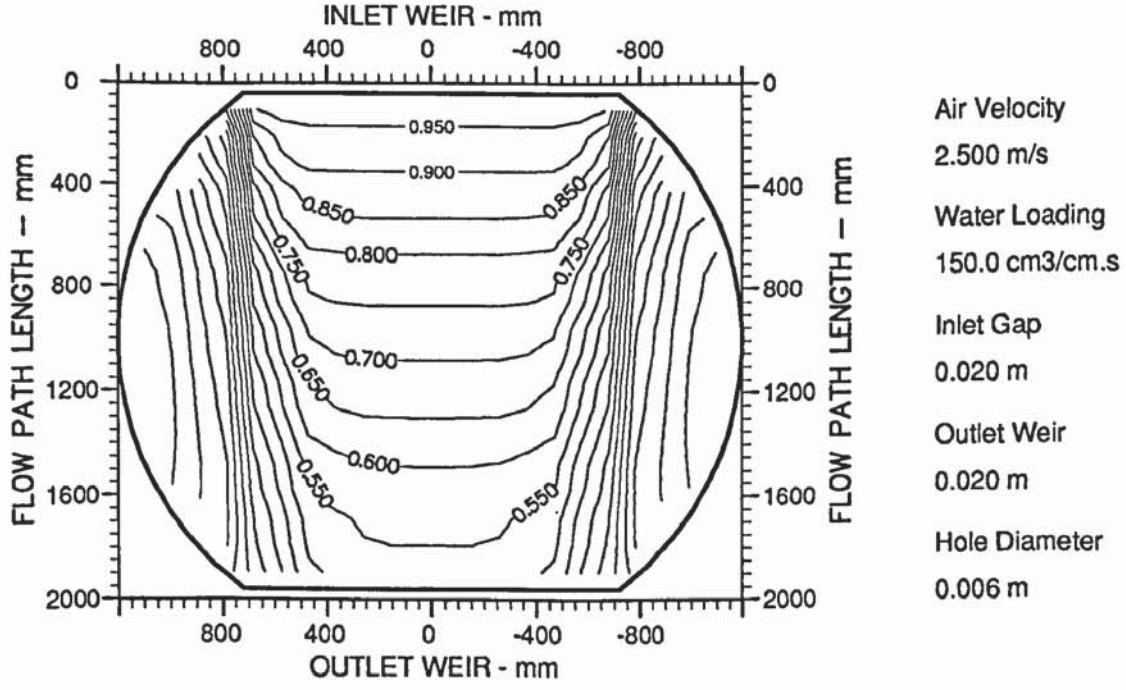

Figure A11.8 Two dimensional reduced concentration profiles showing transverse "U-shaped" profiles during atmospheric pressure simulation.

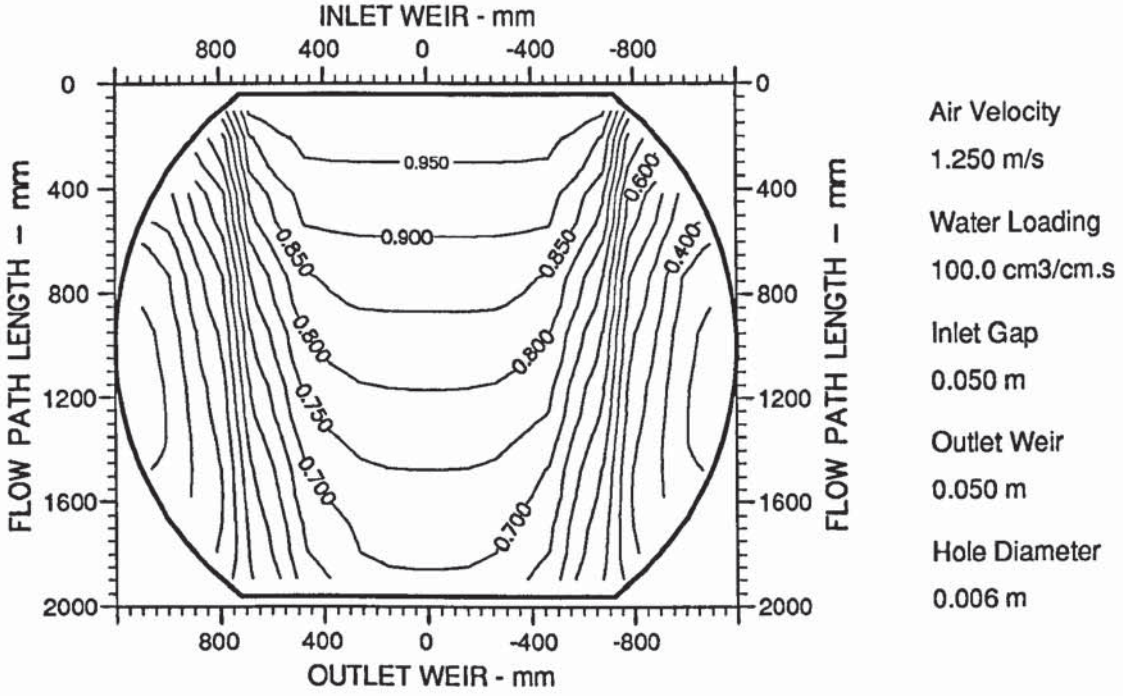

Figure A11.9 Two dimensional reduced concentration profiles showing distinctively "U-shaped" profiles during moderate pressure simulation.

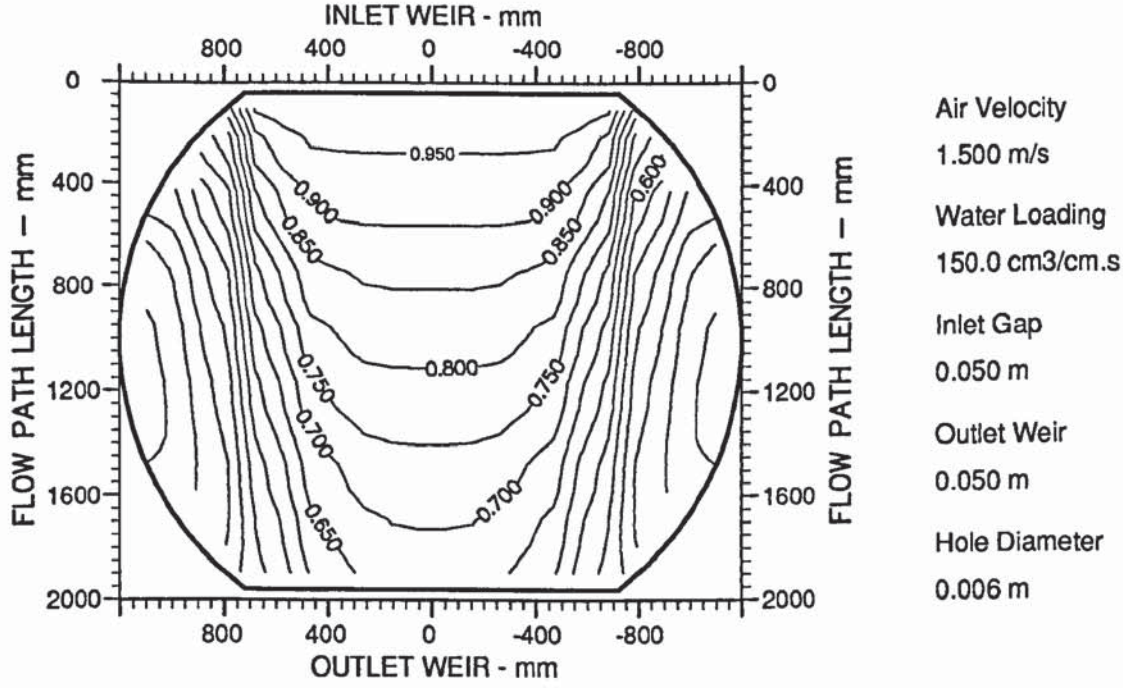

Figure A11.10 Two dimensional reduced concentration profiles showing distinctively "U-shaped" profiles during moderate pressure simulation.

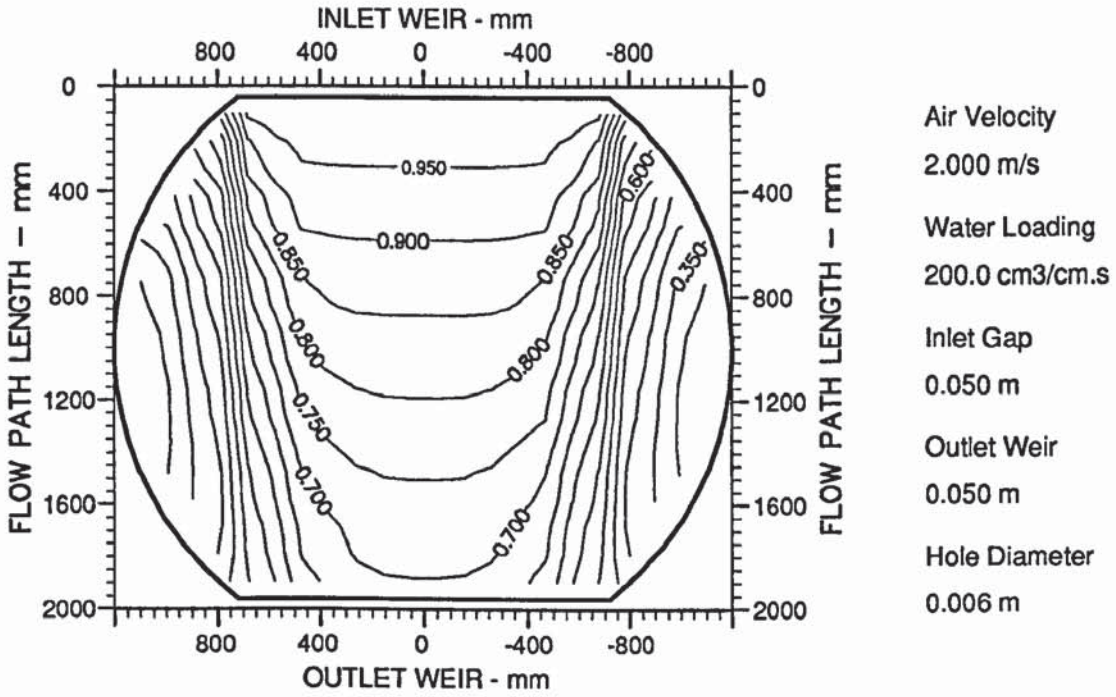

Figure A11.11 Two dimensional reduced concentration profiles showing distinctively "U-shaped" profiles during moderate pressure simulation.

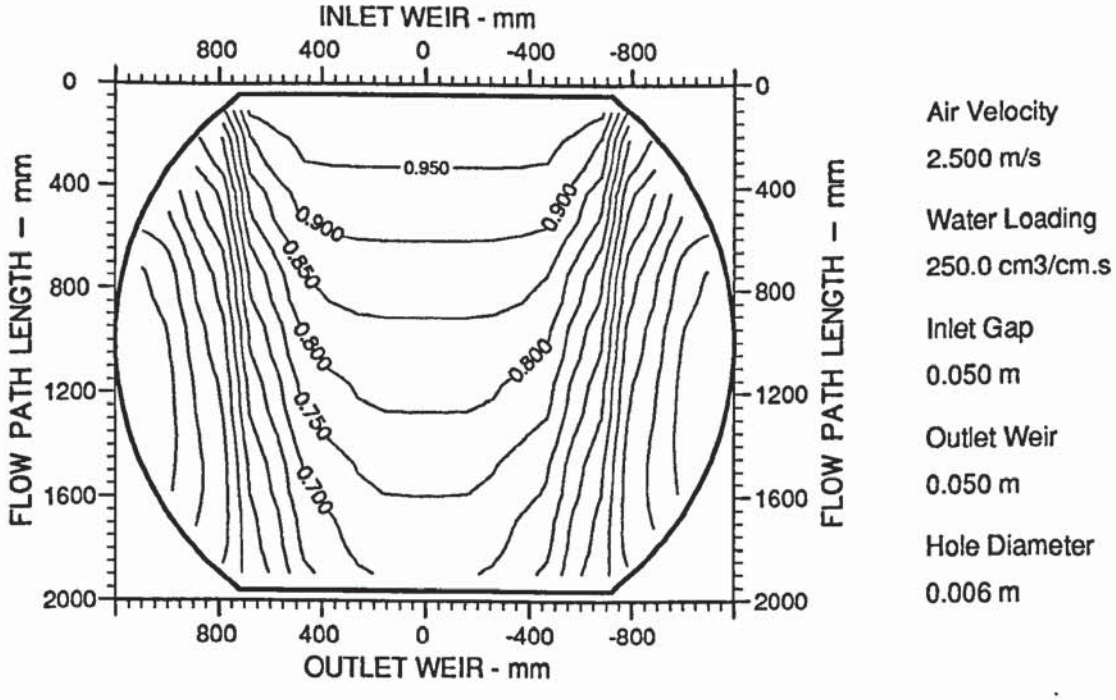

Figure A11.12 Two dimensional reduced concentration profiles showing distinctively "U-shaped" profiles during moderate pressure simulation.

APPENDIX 12

Three-Dimensional Liquid Head Surface Profiles For The Two Tray Experiments

All the measured height of clear liquid data to generate three-dimensional liquid head surface profiles, for the gas-liquid contacting experiments described in Chapter 10, including the simulation of distillation at different pressures, are contained on a 3.5 inch, 1.2Mbyte disk. The disk may be found in the rear cover of Volume 2 of the thesis, and was formatted using MSDOS version 4.0.

On insertion into a suitable disk drive, the directory HCL2TRAY is displayed on the screen. The designations assigned to the sub-directories contained within the HCL2TRAY directory may be defined as follows:-

G is the designation for the gap under the inlet downcomer.
50 the first figure is the size of the gap beneath the inlet downcomer in mm.
W is the designation for the outlet weir height.
50 the second figure is the outlet weir height in mm.
2T is the designation for the two tray experiments.

On moving into the HCL2TRAY directory, the following sub-directories may be found:-

G10W102T G20W202T G50W502T 2TDATUM 3DHCL2T

On using a suitable editor, or a 132 character screen, the individual files, containing the inlet gap and outlet weir settings, the datum (dry tray) readings, and the actual readings taken during gas-liquid contacting can be viewed. The positions of the manometer tappings are presented in Figure 5.16 of Chapter 5.

The 3DHCL2T sub-directory contains the program coding 3DHCL.FOR for generating the three-dimensional liquid head surface profiles using the UNIRAS suite of plotting routines, aswell as calculating the point height of clear liquid results. These values are recorded onto output data files. In addition the inlet gap/outlet weir heights of 10 mm, 10 mm; 20 mm, 20 mm; 50 mm, 50 mm, can be found in the data files CONF1.DAT, CONF2.DAT, and CONF3.DAT.

The datum (dry tray) files for all of the gas-liquid contacting experiments are contained within the sub-directory 2TDATUM. There are nine datum files, labelled

2TDATMn.DAT (where n = 1 to 9). These correspond to a different superficial air velocity containing one data set for each clear liquid height input set measured during the air -water contacting experiments. The actual clear liquid height readings can be found in the sub-directories G10W102T, G20W202T, and G50W502T respectively. The results are stored on data files labelled 2TMANn.DAT where n is defined as follows:-

n = 01 to 38 for the experiments at the inlet gap and outlet weir setting of 50 mm, 50 mm (i.e., 2TMAN01.DAT - 2TMAN38.DAT data files are stored in the G50W502T sub-directory).

n = 39 to 80 for the experiments at the inlet gap and outlet weir setting of 20 mm, 20 mm (i.e., 2TMAN39.DAT - 2TMAN80.DAT data files are stored in the G20W202T sub-directory).

n = 81 to 120 for the experiments at the inlet gap and outlet weir setting of 10 mm, 10 mm (i.e., 2TMAN81.DAT - 2TMAN120.DAT data files are stored in the G10W102T sub-directory).

To run the computer program 3DHCL.FOR, the following set of instructions must be carried out.

a) The datum file must contain one data set for each input data set from the air-water contacting experiments. During data processing, the 2TDATMn.DAT files must be renamed DATUM.DAT in order to satisfy the requirements of the computer program.

b) The data files containing the inlet gap and outlet weir heights are required. The CONF.DAT files must be renamed CONFIG.DAT in order to run the program 3DHCL.FOR.

c) The actual height of clear liquid data files, 2TMANn.DAT need to be renamed MANOM.DAT during each run of the computer program.

d) The coordinates of the manometer pressure tappings on the two trays, labelled MCOORD.DAT, must be used as input in the 3DHCL.FOR computer program..

e) The output data to produce three-dimensional liquid head surface profiles are stored in POST.DAT files, with point height of clear liquid values being written onto HCLOUT.DAT output files.

It is important to note that all the clear liquid height data contained on the disk were measured on two 6.35 mm hole sieve trays at tray spacing of 300 mm.

LIQUID DISTRIBUTION AND MASS TRANSFER ON A 2.4 M DIAMETER DISTILLATION TRAY

S Chambers and K E Porter
Separations Process Group
Department of Chemical Engineering & Applied Chemistry
Aston University

Introduction

It has been known for many years that in some circumstances tray efficiency is reduced by a non-uniform flow of liquid across the tray. In particular it has been observed that sometimes there are regions at the sides of the tray where the liquid circulates and which are bypassed by the main liquid stream which, (on single pass trays) flows straight across the tray from inlet downcomer to outlet weir. These side regions may contain liquid which approaches equilibrium with the rising vapour, and the vapour passes through them with a reduced concentration change. This leads to a loss in tray efficiency which might be recovered by means of flow control devices.

Several theoretical studies on the effect of liquid channelling on tray efficiency have been published but these are based either on hypothetical flow patterns or on those flow patterns observed in a limited number of experiments. There appears to be no previous experimental investigation in the causes of maldistributed flow and of its effect on mass transfer.

Description of the 2.4 m diameter column and test rig

Distillation is simulated by blowing air through water. Cooling hot water by the air provides a mass transfer analogy e.g. water temperature is analogous to liquid concentration. The effect of the liquid flow pattern on mass transfer is determined by measuring the water temperature at over 100 positions on the tray.

Air is supplied by a 150 HP fan and the water is circulated by a 125 kW pump. The maximum heat input for the water cooling experiments is 1.2 MW supplied by two gas fired water heaters each 0.5 MW supplement by a steam top-up supply for fine tuning of the water temperature. "Flow pointers" (similar in principle to weather vanes) are positioned all over the tray to show the direction of flow and the positions of the flow pointers is recorded by video camera.

Principle Conclusions

1. A large tray test rig incorporating a 2.44 diameter column, a 150 HP fan and 1.2 MW of water heating has been constructed. This unique facility has equipment for the experimental observations of liquid flow patterns, and an evaluation of the effect of the flow patterns on mass transfer by cooling water with air.

2. The water cooling experiment on which over 100 temperature measurements are processed has proved to be a convenient and sensitive test of the effect of the flow patterns on tray mass transfer.

3. Two single pass sieve trays have been tested, one perforated with 1 mm diameter holes and the other with 6.35 mm diameter holes. Liquid channelling associated with liquid circulation at the sides of the tray has been observed on both plates. Water cooling temperature profiles have confirmed the driving force for heat transfer is

reduced in the circulating regions.

4. The flow patterns formed on the perforated plates have been compared with those formed by water only flow over an unperforated plate of the same size.

5. In the water only experiments, except for extremely low weir loads, the flow separated at the ends of the inlet downcomer forming circulating regions at the sides of the tray, which, on a small increase in weir load, increased in size to fill the sides of the tray outside the downcomers.

6. The liquid flow patterns observed on the 1 mm diameter hole plate are similar to those observed in the water only experiments. The effect of the air flow is to delay the onset of separation and circulation which occurs at higher weir loads than in the water only experiments. The size of the circulating regions formed on the perforated plate with gas flow depends on the velocity of water entering the tray and thus on the size of the gap beneath the inlet downcomer as well as on the weir load.

7. Four regions of circulation were observed on the 6.35 mm diameter hole plate with one at each end of the outlet weir as well as one at each end of the inlet downcomer circulations near the end of the outlet weir depends on air velocity.

8. Increasing the air velocity through the 6.35 mm diameter hole tray causes the circulations near the outlet weir to increase in size and strength such that at high air velocities they reverse the direction of flow of the circulations near the inlet downcomer. This produces severe liquid channelling.

9. It is likely that different types of flow control devices (designed to prevent channelling and circulation) will be needed depending on whether the circulation is driven by liquid flow (as in the 1 mm diameter hole experiment) or by gas flow (as in the 6.35 mm diameter hole experiment).

FLOW PATTERNS AND TEMPERATURE PROFILES ON A 2.44M DIAMETER SIEVE TRAY

K.E. Porter*, K.T. Yu**, S. Chambers* and M.Q. Zhang**

* Department of Chemical Engineering and Applied Chemistry, Aston University, Birmingham B4 7ET, UK.

** Chemical Engineering Research Centre, Tianjin University, Tianjin, P.R. China.

Abstract

The liquid flow pattern was investigated by experiment on a 2.44 m diameter distillation simulator and by computational fluid dynamics. The effect of the gas flow on the liquid flow was determined by comparing the flow patterns produced by water only flow over an unperforated tray with those produced by air-water contacting on sieve trays. For most experiments with water only, the flow separated at the ends of the inlet downcomer producing large circulating regions at the sides of the tray. The effect of air flow is to inhibit circulating flow which only appeared at high water inlet velocities. In experiments to simulate distillation the liquid was in forward flow over most of the tray.

The water cooling experiment was used to show the effect of flow patterns on mass transfer. In most cases (including simulated distillation), there were colder regions at the sides of the tray where the slower moving liquid has a longer residence time.

The computed flow pattern was obtained from a turbulent two phase flow mathematical model which incorporates the resistance to the liquid flow of the rising gas through it. In general, the computed flow pattern revealed forward flow between the downcomers with very slow or non-moving liquid at the sides of the tray. In some cases the computed flow pattern contained reverse flow near the column wall.

INTRODUCTION

Several previous works support the view that the liquid flow pattern on distillation trays is of importance in determining tray efficiency. Of particular interest is the occurrence of liquid circulation in the horizontal plane, or a region on the tray in which there is very slow moving or stagnant liquid. The liquid in these regions soon comes close to equilibrium with the vapour passing through it , so that negligible changes in vapour concentration occur. This results in a reduction of tray efficiency and column efficiency (Porter et al, 1972, 1973 and 1974; Bell and Solari, 1974; Smith and Delnicki, 1975; Porter and Jenkins, 1979; Sohlo and Kouri, 1982; Solari et al, 1982; Kouri and Sohlo, 1985; and Yu et al, 1986).

There is little or no previous work which reports observations of the liquid flow pattern (Sohlo, 1982) on a tray of a commercially interesting size such that the ratio of depth of froth to flow path length is typical of that found in practice.

In part I of this paper, we present the results of experiments on sieve trays 2.44m in diameter using the air-water test system to simulate distillation flow patterns. In part II we present a mathematical model of two phase flow on a tray which allows for the resistance to the liquid flow of gas as it passes through it.

Part I EXPERIMENTAL OBSERVATION OF TRAY FLOW PATTERNS

Experimental Procedures

Investigations were carried out on the 2.44m diameter test facility at Aston University. This is an air-water simulator column which incorporates an overhead video camera to record flow patterns and a supply of hot water for water cooling experiments to measure tray efficiency. A short description of the test rig is provided in Appendix 1. The water cooling experiment and the calculation of point and tray efficiencies are described in appendices 2 and 3 respectively.

The approach used was to first observe single phase flow patterns obtained with water flowing over an unperforated tray. The effect of the gas flow on the liquid flow pattern was then observed by blowing air through water flowing across a sieve tray. Two sieve trays were used with hole diameters of 1.00mm and 6.35mm. The investigations involved the use of various air and water flowrates for different combinations of gaps under the inlet downcomer and outlet weir heights. These are shown in Table 1.0.

Particular attention was paid to the direction of flow at many positions across the tray. The direction of flow from the inlet downcomer towards the outlet downcomer is described as **"forward flow"**. Flow in the opposite direction is described as **"reverse"** flow. In some experiments a reverse flow resulting from the effect of liquid circulation was observed as shown in Figure 1.0. In these cases, the area of tray occupied by circulating liquid was estimated visually and recorded.

Single Phase Flow Patterns by means of a Dye Tracer

In the single phase, or water only experiments, the direction of flow and the size of circulating regions were observed by the movement of a coloured dye discharged from a solenoid controlled injection system attached across the length of the inlet downcomer.

Biphase Flow Patterns by means of Directional Flow Pointers

For two phase flow, the direction of flow was observed using Directional Flow Pointers partially submerged in the froth or spray, which behaved in a similar way to that of weather vanes used to show the direction of the wind. A description of a flow pointer is given in Appendix 4. Flow pointers were evenly spread across the tray at 34 positions as shown in Figure 2.0.

The experiments described above were followed by those in which hot water was fed onto the tray and cooled by the air forced through the sieve trays. When compared with distillation, air enthalpy is analogous to vapour concentration and variations in water temperature are analogous to variations in liquid concentration. In these experiments the water temperature was measured at 108 equally spaced positions on the tray as shown in Figure 3.0. Data processing of water temperature measurements by means of a MICROLINK data logger and the UNIRAS computer suite of plotting routines yielded two dimensional isothermal contour diagrams, and three dimensional surface temperature diagrams, as shown in Figures 8a, 8b, 9a, 9b and 10.

Programme of Experiments

The program of experiments was in three parts:

1. Observation of water only flow patterns using various combinations of inlet gap and outlet weir height.
2. Observation of flow patterns in air - water experiments. For each of the three combinations of inlet gap and outlet weir, (ie 10 mm,10 mm; 20 mm, 20 mm; and 50 mm, 50 mm), at several fixed air velocities, the water weir load was increased and the change in liquid flow pattern from forward flow to reverse and/or circulating flow was observed.

3. Simulation of distillation at different pressures. In these experiments, flow rates were varied at a fixed ratio of liquid flow to air velocity. Three flow rate ratios were chosen to represent distillation under vacuum, at atmospheric pressure, and at a moderate pressure (about 2 bar). The inlet gap and outlet weir height were set equal at 10mm for the vacuum simulation, 20mm for the atmospheric pressure simulation, and 50mm for the pressure distillation. These values were chosen to maintain a comparatively low liquid head (backup) in the inlet downcomer, representative of practical distillation.

EXPERIMENTAL RESULTS

Flow Patterns

In general, at low liquid flow rates the liquid flow was in the forward direction at all positions on the tray, but above some liquid flow rate , circulating regions appeared on the tray, near the ends of the inlet downcomer. The size of the circulating regions increased with liquid flow rate. Thus the results presented in Figures 4.0, 5.0 and 6.0 are a plot of the percent of the tray area occupied by regions of liquid circulation against weir load.

Water only Experiments

As shown in Figure 4.0, for the experiments with water only on the unperforated tray, liquid circulation started at very low weir loads and increased rapidly with weir load to reach a maximum area of 30 % of the tray. This corresponded to the situation where all of the segments at the side of the tray were covered with circulating liquid as shown in Figure 1.0. The effect of inlet gap and outlet weir on these flow patterns was small and all the results for single phase flow are within the shaded area of Figure 4.0.

Two Phase Flow Experiments

The passage of air through the water flowing over the perforated trays reduced the circulation. A similar pattern of results was obtained in that the circulating area increased with weir load, but the rate of increase was less than for the water only experiments and showed a strong dependence on the size of the gap beneath the inlet downcomer through which the liquid entered the tray. Figure 5.0 shows results obtained with the tray perforated with 1.0 mm diameter holes. The larger the inlet gap the smaller the velocity of the liquid entering the tray and the larger the weir load required to produce a given area of circulation.

The results with the 6.35 mm hole diameter sieve tray are shown in Figure 6.0. This shows a similar pattern except that the area covered by circulating liquid is reduced at the high air velocities of 2.0 and 2.5 ms^{-1}.

The results of the experiments to simulate distillation are shown in Figure 7.0 which is presented as a plot of air velocity against weir load for each of the simulations. The air velocity is also shown as load factor, C_s, to permit comparison with distillation. On the straight lines representing the three simulated pressures, are shown the percentages of tray area covered by circulating liquid. This shows that in the simulation of vacuum distillation a "forward flow" flow pattern was observed at all flow rates. For the atmospheric and pressure distillation, the area covered by circulation was in most cases 12% but not more than 15%.

Thus in the experiments which simulated distillation, most of the tray area was occupied by forward flow, i.e. in the direction from the inlet downcomer to the outlet weir. However, it was observed that particularly for the higher weir load simulations of atmospheric and pressure distillation, the velocity of flow near the column wall was less than that in the middle of the tray between the downcomers. This is important in interpreting the results of the water cooling experiments described below.

WATER COOLING EXPERIMENTS

Temperature Profiles

The longer the liquid stays on the tray the cooler it becomes. Thus parts of the tray where there are long liquid flow paths, or where the liquid moves more slowly will have a lower temperature than other parts. Figures 8.0a and 8.0b are typical of the temperature profiles obtained in experiments to simulate atmospheric and pressure distillation. The isotherms are U-shaped with colder liquid at the sides of the tray even in situations where most of the liquid is forward flow.

The temperature profiles obtained when a significant proportion of the tray area is covered by circulating liquid are also U-shaped and similar to those described above obtained with the forward flow patterns. However with liquid circulation and a reverse flow near the column wall, the coldest liquid is found near the ends of the inlet downcomer, whereas with a forward flow the coldest liquid is found at the sides of the tray near the ends of the outlet downcomer. These similarities and differences between the temperature profiles obtained for forward flow (associated with very small circulation) and large circulating flow are shown by comparing Figures 9.0a and 9.0b. The same air and water flowrates were used in these experiments, the difference being the size of the gap under the inlet downcomer.

The isotherms obtained at the flow rate ratio which simulated vacuum distillation are approximately straight and parallel to the downcomers (see figure 10.0). This implies that there may be a different flow mechanism for this flowrate ratio, (high gas rate and low liquid rate), which may be related to operation in the spray regime (Porter et al., 1977; Raper et al., 1984).

Heat Transfer and Tray Efficiencies

Values of point efficiency, E_{og}, and tray efficiency,E_{mv}, were calculated from the results of the water cooling experiments by the method outlined in Appendix 3.0. Table 2.0 presents the efficiency results for the experiments which simulated distillation at different pressures. The changes in the point efficiency,E_{og} , from an average of 42% for the simulation of vacuum distillation, to an average of 81.5% for atmospheric distillation and 88% for pressure distillation are similar to those found in practical distillation columns. The changes in tray efficiency, E_{mv} , from an average of 105% for atmospheric simulation to 99% for pressure simulation are opposite to that found in distillation owing to the changes in the flow rate ratio which results in changes in λ (=mG/L) and a reduction in the expected value of E_{mv}/E_{og}. The ratio of water rate to air rate is lower in the simulation of vacuum distillation than the ratio used to simulate pressure distillation. This means that the relative increase from point efficiency to tray efficiency is greater for the simulated vacuum distillation than for the simulated pressure distillation. This effect of air to water ratio change is greater than the change in point efficiency.

The efficiency results presented in Table 3.0 show that for the same operating conditions, the tray efficiencies obtained for the 1.0mm hole diameter tray were higher than those obtained with the 6.35mm hole diameter tray.

PART 2. THEORETICAL COMPUTATION OF A TWO DIMENSIONAL MODEL OF LIQUID PHASE FLOW ON A TRAY

The experimental results in part I are for one particular size and shape of distillation tray. Therefore it is desirable to obtain a mathematical model of the flow pattern on any tray and which may form the basis for a prediction of mass transfer throughout a distillation column.

In this paper, a turbulent liquid flow model is presented in which the rising vapour provides a resisting force to liquid flow. The resulting equations are solved by means of

In this paper, a turbulent liquid flow model is presented in which the rising vapour provides a resisting force to liquid flow. The resulting equations are solved by means of techniques developed in modern computational fluid dynamics for single phase flow. Further details may be found in M.Q. Zhang's PhD thesis (1991).

The Flow Equation

The basic equations representing the turbulent liquid flow on a tray are composed of the Reynolds equation which is derived from the Navier-Stokes equation, and the continuity equation as follows:

$$u_j \cdot \frac{\partial u_i}{\partial x_j} = \frac{1}{\rho} \cdot \frac{\partial}{\partial x_j} \cdot \left[-p\delta_{ij} + D \cdot \left(\frac{\partial u_i}{\partial x_j} + \frac{\partial u_j}{\partial x_i} \right) - \rho \overline{u_i u_j} \right] \tag{1.0}$$

$$\frac{\partial u_j}{\partial x_j} = 0 \tag{2.0}$$

In applying equation (1) to the flow of turbulent liquid on a tray, the vertically rising vapour may be regarded as a part of the resistance to the liquid flow, thus an additional term representing the resistance is added. This is obtained by assuming that, as a result of momentum transfer from the liquid to the vapour, the vapour leaving the top of the froth attains a horizontal velocity component, which in both magnitude and direction, is equal to that of the local liquid flow. Thus the resisting force to the liquid flow caused by the rising vapour is expressed as:

$$F_{vi} = \rho_g u_s u_i dxdy \tag{3.0}$$

By adding this resisting force into the Reynolds equation and rearranging, equation (1) becomes:

$$u_j \cdot \frac{\partial u_i}{\partial x_j} = \frac{1}{\rho} \cdot \frac{\partial}{\partial x_j} \cdot \left[-p\delta_{ij} + D \cdot \left(\frac{\partial u_i}{\partial x_j} + \frac{\partial u_j}{\partial x_i} \right) - \rho \overline{u_i u_j} \right] - \frac{\rho_g u_s}{\rho h} u_i \tag{4.0}$$

The Reynold's stress, $(-\rho \overline{u_i u_j})$ in equation (4) may be replaced by the multiple of an eddy viscosity D_e and a velocity gradient, that is:

$$-\rho \overline{u_i u_j} = D_e \cdot \left(\frac{\partial u_i}{\partial x_j} + \frac{\partial u_j}{\partial x_i} \right) \tag{5.0}$$

Substituting equation (5) into equation (4) and making the reasonable assumption that, $D << D_e$, the following equation of motion is obtained:

$$u_j \cdot \frac{\partial u_i}{\partial x_j} = \frac{1}{\rho} \cdot \frac{\partial}{\partial x_j} \cdot \left[-p\delta_{ij} + D_e \cdot \left(\frac{\partial u_i}{\partial x_j} + \frac{\partial u_j}{\partial x_i} \right) \right] - \frac{\rho_g u_s}{\rho h} u_i \tag{6.0}$$

Due to the vigorous agitation of the liquid by the rising vapour, it is assumed that any variation in liquid velocity with liquid depth may be neglected. The flow of liquid on the tray is considered to be two dimensional and the following equations apply:

$$u \cdot \frac{\partial u}{\partial x} + v \cdot \frac{\partial u}{\partial y} = -\frac{1}{\rho} \cdot \frac{\partial p}{\partial x} + \frac{\partial}{\partial x} \left(D_e \cdot \frac{\partial u}{\partial x} \right) + \frac{\partial}{\partial y} \left(D_e \cdot \frac{\partial u}{\partial y} \right) - \frac{\rho_g u_s}{\rho h} u \tag{7.0}$$

$$u\cdot\frac{\partial v}{\partial x}+v\cdot\frac{\partial v}{\partial y}=-\frac{1}{\rho}\cdot\frac{\partial p}{\partial y}+\frac{\partial}{\partial x}\left(D_e\cdot\frac{\partial v}{\partial x}\right)+\frac{\partial}{\partial y}\left(D_e\cdot\frac{\partial v}{\partial y}\right)-\frac{\rho_g u_s}{\rho h}v \qquad (8.0)$$

and the equation of continuity:

$$\frac{\partial u}{\partial x}+\frac{\partial v}{\partial y}=0 \qquad (9.0)$$

Additional relationships required to solve these equations are taken from those used in the computation of single phase flow patterns. A two equation flow model is chosen comprising of a transport equation for the kinetic energy of turbulence, k:

$$u_j\cdot\frac{\partial k}{\partial x_j}=\frac{\partial}{\partial x_j}\cdot\left(\frac{D_e}{\sigma_k}\frac{\partial k}{\partial x_j}\right)+G-\varepsilon \qquad (10.0)$$

where

$$G=D_e\cdot\left(\frac{\partial u_i}{\partial x_j}+\frac{\partial u_j}{\partial x_i}\right)\cdot\frac{\partial u_i}{\partial x_j} \qquad (10.0a)$$

and a transport equation for the dissipation rate of turbulence energy.

$$u_j\cdot\frac{\partial \varepsilon}{\partial x_j}=\frac{\partial}{\partial x_j}\cdot\left(\frac{D_e}{\sigma_s}\frac{\partial \varepsilon}{\partial x_j}\right)+(C_1G-C_2\varepsilon)\frac{\varepsilon}{k} \qquad (11.0)$$

In addition, the turbulent viscosity D_e is related by:-

$$D_e=C_\mu\cdot\frac{k^2}{\varepsilon} \qquad (12.0)$$

Launder et al (1972 and 74) proposed the following values for the constants based on a large amount of experimental work.

$$C_m=0.09 \quad C_1=1.44 \quad C_2=1.92 \quad \sigma_k=1.00 \quad \sigma_s=1.30 \qquad (13.0)$$

For the two dimensional model, equation (10) becomes:

$$u\frac{\partial k}{\partial x}+v\frac{\partial k}{\partial y}=\frac{\partial}{\partial x}\cdot\left(\frac{D_e}{\sigma_k}\cdot\frac{\partial k}{\partial x}\right)+\frac{\partial}{\partial y}\cdot\left(\frac{D_e}{\sigma_k}\cdot\frac{\partial k}{\partial y}\right)+G-\varepsilon \qquad (14.0)$$

and equation (11) becomes:

$$u\frac{\partial k}{\partial x}+v\frac{\partial k}{\partial y}=\frac{\partial}{\partial x}\cdot\left(\frac{D_e}{\sigma_k}\cdot\frac{\partial k}{\partial x}\right)+\frac{\partial}{\partial y}\cdot\left(\frac{D_e}{\sigma_k}\cdot\frac{\partial k}{\partial y}\right)+(C_1G-C_2\varepsilon)\frac{\varepsilon}{k} \qquad (15.0)$$

The velocity field is calculated by solving equations (7), (8), (9), (12), (14) and (15).

THE BOUNDARY CONDITIONS

1. Centreline Boundary

The theoretical liquid velocity field is symmetrical with respect to the centre line of the tray at right angles to the downcomers. Thus:

$$\frac{\partial u}{\partial y} = 0, \quad v = 0, \frac{\partial k}{\partial y} = 0, \quad \frac{\partial \varepsilon}{\partial y} = 0$$

2. Wall Boundary

Theoretically, we may set the boundary condition of no slip at the column wall, viz:

$$u = 0, \quad v = 0, \quad k = 0, \ \varepsilon \text{ is a finite value}$$

To simplify the computation in the wall region where the velocity gradient becomes very steep, a wall function taken from single phase flow theory was introduced.

3. Inlet Boundary

The inlet boundary condition was set at, $u_{in} = L/h$; $v_{in} = 0$. This implies that the liquid velocity entering the tray is equal to that of the froth near the inlet downcomer.

4. Outlet Boundary

The method of finite volume was chosen for the computation such that the results are practically not influenced by the outlet boundary condition, and the outlet flow conditions may be taken as if the flow is unidirectional.

THE COMPUTED FLOW PATTERN

A typical computed result is given graphically in Figure 11 in which the liquid velocities in the longitudinal direction are shown by a number of profiles. The reversed flow region in this specific case is estimated to be approximately 8.5% of the total bubbling area which is in fair agreement with the experimental result shown in Figures 5.0 and 6.0 under the same operating condition. However, in many cases the computed results do not show the existence of reverse flow, but instead, a region of almost zero velocity appears adjacent to the column wall. More details are given in Zhang's Ph.D thesis.

Figure 11 also shows that in the divergent section of the tray, the liquid velocity remains uniform in the main flow region between the downcomers but diminishes sharply in the segmental region, whilst in the convergent section the velocity distribution becomes parabolic owing to the mixing of the contracted current of liquid from the segmental region.

DISCUSSION

The results of the experiments have shown that the passage of the gas through the liquid has a significant effect on the liquid flow pattern. When, as a single phase, the liquid flows through the divergent / convergent channel formed by a single pass tray, except for very low weir loads, the flow separates at the ends of the inlet downcomer and forms circulating regions throughout the segments at the sides of the tray. The effect of forcing the gas through the liquid is to prevent flow separation which only occurs at much higher weir loads and with smaller gaps under the inlet downcomer (ie at high liquid inlet velocities).

For the conditions where the inlet velocity of the liquid is reduced in order to decrease the liquid backup in the downcomer to levels found in practical distillation, the liquid does not circulate in the segmental regions at the sides of the tray, but flows in the forward direction over most of the tray area. At the low weir loads typical of vacuum distillation,

it was found that temperature isotherms in water cooling are approximately straight and parallel to the downcomers which implies that liquid residence time profiles will be similar. This may be due to a different flow regime. Similar concentration profiles were predicted for the spray regime by Porter, Safekourdi, and Lockett (1977).

The temperature isotherms produced in the simulations of distillation at higher pressures (approximately 1 and 2 bar) are distinctively "U-shaped". This is caused by the longer length of flow path near the column wall and also the possible lower liquid velocity in this region. The U-shaped isotherms obtained with both forward flow and with a region of circulation at the sides of the tray are similar to the concentration profiles predicted by the theoretical model of Porter, Lockett, and Lim (1972). In this model it is assumed that the liquid at the sides of the tray is stagnant, ie in between slow forward flow at the sides of the tray and a circulating flow in which a reverse flow occurs near the column wall. This is significant because in other papers , by Porter et al (1972; Lockett et al,1973; Lim et al 1974), it was predicted that in a column of single pass trays placed one above the other, the effect of this type of maldistributed flow produces a much greater reduction in column efficiency than for a single tray.

The theoretical model of the flow pattern presented in part 2 provides a promising start for a new interpretation of tray and column efficiency based on the fluid mechanics of two phase flow across the tray. This branch of fluid mechanics might be described as Open Channel Two Phase Flow. It is a relatively unexplored field and the model presented here is , as far as we know, the first attempt at a theoretical description of the phenomena. It is based on the assumption that the gas enters the froth from the tray in a vertical direction and attains a horizontal velocity component equal to that of the liquid cross flow before leaving the froth. Thus the momentum required to accelerate the gas in the horizontal direction offers an additional resistance to the liquid flow which is much greater than the frictional drag resistance of the liquid along the tray floor. This has a significant effect on the liquid flow pattern. This assumption is reasonable for the conditions of the experiments described in Part I.

In order to complete this theoretical model of a distillation tray it was necessary to use relationships which are known to be valid for single phase turbulent flow but which are assumed to be applicable to a situation where turbulence and mixing is produced by a continuous stream of vapour passing through the liquid. These are defined above in equations (10) and (11) which refer to the kinetic energy of turbulence, its dissipation rate,and that describing the velocity profile near a boundary layer adjacent to the column wall. Their use permitted the calculation of the flow patterns to be based on procedures established in the computational fluid dynamics for single phase flow and for two phase flow in pipes (Murphy, 1974). An experimental investigation into the validity of this approach and the identification of an improved calculation procedure for Open Channel Two Phase Cross Flow is the subject of our present work.

References

A.I.ChemE., Bubble Tray Design Manual "Prediction of Fractionation Efficiency", AIChE, New York, (1958).

Bell, R. L. and Solari, R. B., "Effect of non-uniform velocity fields and retrograde flow on distillation plate efficiency", A I ChE J., **20** (4), 688, (1974)

Hine, C. J., "Effect of Liquid Flow Patterns on Distillation Trays", Ph.D.Thesis, Aston University, Birmingham, England, (1990).

Kouri, R. J. and Sohlo, J. J., "Effect of developing liquid flow patterns on distillation plate efficiency", Chem. Eng. Res. Des., **63** (2), 117, (1985).

Launder, B.E., Morse, A., Rodi, W., Spalding, D.B., Proceedings of NASA Conference on Free Shear Flow, Langley (1972).

Launder, B. E. and Spalding, D. B.," The numerical computation of turbulent flows ", Comp. Math. Appl. Mech. Engng., **3**,269 (1974).
Murphy, J.D., " Turbulence Modelling ", NASA. TM 8 5889 (1984).
Porter, K. E. and Jenkins, J. D., "The interrelationship between industrial practice and academic research in distillation and absorption", IChemE Symp. Ser., n56, 5.1/1, (1979).
Porter, K. E., Lockett, M. J. and Lim, C. T., "The effect of liquid channelling on distillation plate efficiency", Trans. IChemE, **50**, 91, (1972), **51**, 61 ,(1973),52, **52**, 193, (1974).
Porter, K.E., Lockett, M.J., Safekourdi, A., " Plate efficiency in the spray Regime", Trans.I ChemE 55 190, (1977).
Raper, J.A.,Hai, N.T., Pinczewski, W.V. and Fell,C.J.D.,"Liquid passage on sieve trays operating in the spray regime", Chem.Engng Sci, **62**, n2,111, (1984).
Smith, V.C. and Delnicki, W.V., " Optimum sieve tray design ", Chem.Engng Prog. **71** (8) 68, (1975).
Sohlo, J. and Kouri, R.J.,"An analysis of enhanced transverse dispersion on distillation plates", Chem. Engng Sci., **37**,n2,193, (1982).
Solari, R., Saez, E., D' Apollo,I. and Bellet, A.,"Velocity distribution and liquid flow patterns on industrial sieve trays", Chem. Engng Comm. **13**,369, (1982).
Yu, K. T., Huang, J. and Zhang, Z. T., "Residence time profile and plate efficiency for a large tray with single-pass or two-pass liquid flow", J. Chem. Ind. Engng (China), **2**, 151, (1986).
Zhang, M. Q., " ", Ph.D Thesis, Tianjin University, Tianjin, Peoples Republic of China, (1991).

Nomenclature

C_1, C_2, C_m	Constants	[-]
C_{air}, C_{wat}	Specific heat capacities of air and water vapour	[kJ/kg K]
Cp	Specific heat capacity	[kJ/kg K]
C_s	Capacity factor = $u_s / [\rho_V/(\rho_L - \rho_V)]$	[m/s]
D	Tray diameter	[m]
D	Kinematic viscosity (Eddy viscosity)	[m^2/s]
De	Eddy diffusion coefficient	[m^2/s]
E_{og}	Murphree point efficiency	[-]
E_{mv}	Murphree tray efficiency, based on vapour phase	[-]
G	Total Air (vapour) mass flowrate	[kg/s]
G	See Equation (10a)	[-]
h_w	Height of outlet weir	[m]
h_{cl}	Height of clear liquid	[m of H_2O]
H_{fg}	Latent heat of water	[kJ/kg]
$\overline{H_2}$	Average enthalpy of air leaving the froth	[kJ/kg]
H_1	Average inlet enthalpy of air	[kJ/kg]
H^*_{Tout}	Enthalpy of air in equilibrium with water at temperature T_{out}	[kJ/kg]
H^*_{Ti}	Enthalpy of air in equilibrium with water at temperature T_i	[kJ/kg]
H_{2i}	Outlet enthalpy of air from position i on a tray	[kJ/kg]
$Hum_{(Tdb,wb)}$	Humidity of air under dry/wet bulb conditions	[-]
IG	Height of gap under the inlet downcomer	[m]
K	Constant	[-]
k	Turbulent Kinetic Energy, $\frac{1}{2}\overline{u_i' u_j'}$	
L	Total Liquid mass flowrate	[kg/s]

m	Gradient of equilibrium line	[-]
OW	Outlet weir height	[m]
p	Pressure	[ ]
Pe	Peclet number, $Pe = Z^2 / De.t_L$	[ ]
t	Time	[s]
t_L	Average liquid contact time	[s]
$\overline{T_{in}}$	Average inlet water temperature entering the tray	[K]
$\overline{T_{out}}$	Average inlet water temperature leaving the tray	[K]
T_{db}	Air dry bulb temperature	[K]
T_{wb}	Air wet bulb temperature	[K]
T_r	Reduced temperature driving force	[-]
T_i	Temperature of water at position i on a tray	[K]
u	Mean componental velocity in x direction	[ms^{-1}]
u_i	Mean componental velocity in x_i direction	[ms^{-1}]
u_j	Mean componental velocity in x_j direction	[ms^{-1}]
u_i , u_j	Fluctuating componental velocity in x_i and x_j directions	[ms^{-1}]
U_s	Superficial column velocity	[m/s]
v	Mean componental velocity in y direction	[ms^{-1}]
W	Weir length	[m]
x	Cartesian coordinate of the tray in the main flow direction	[-]
y	Cartesian coordinate of the tray perpendicular to the x - direction	[-]
Z	Flow path length	[m]

Greek Letters

δ	Kroneeker function	
ε	Dissipation rate of turbulent energy	
ρ_l	Liquid density	[kg/m^3]
ρ_g	Vapour density	[kg/m^3]
σ_k , σ_s	Constants	[-]
λ	Ratio of gradient of equilibrium line to operatingline (= mG/L)	[-]

Subscripts

1,2	Pertaining to inlet and outlet conditions used in enthalpy balance	[-]
db	Dry Bulb	[-]
cl	Clear Liquid	[m]
g	Gas	[-]
in	Inlet	[-]
i,j	In part I, i defined as a point value In partII, i and j defined as the direction perpendicular and parallel to the inlet and outlet downcomers	[-]
l	Liquid	[-]
out	Outlet	[-]
wb	Wet bulb	[-]

Superscripts

*	Pertaining to equilibrium conditions	[-]

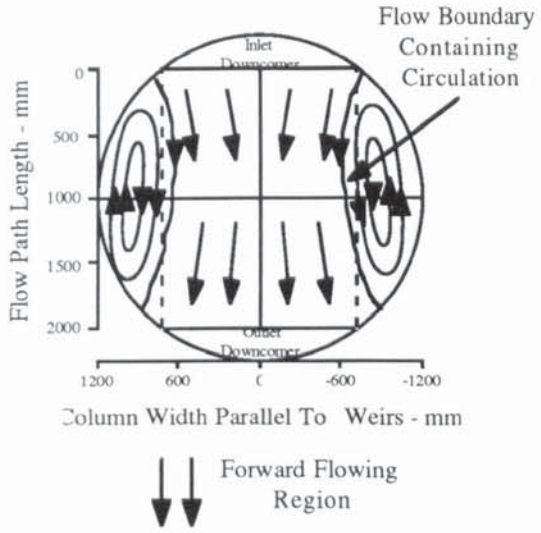

Fig. 1.0 Coloured dye injection water only experiment indicating 30% circulation

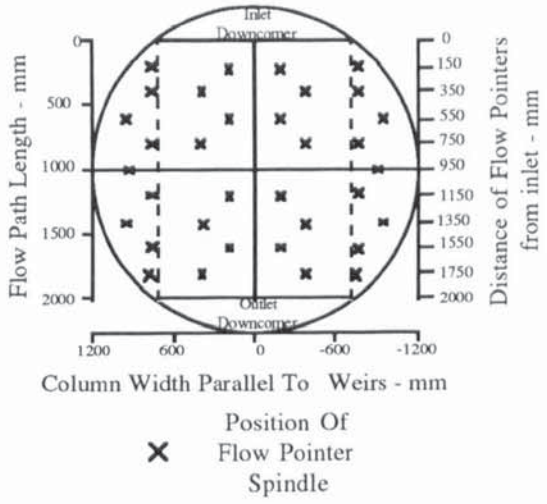

Fig. 2.0 Arrangement of the directional flow pointers on the perforated test trays

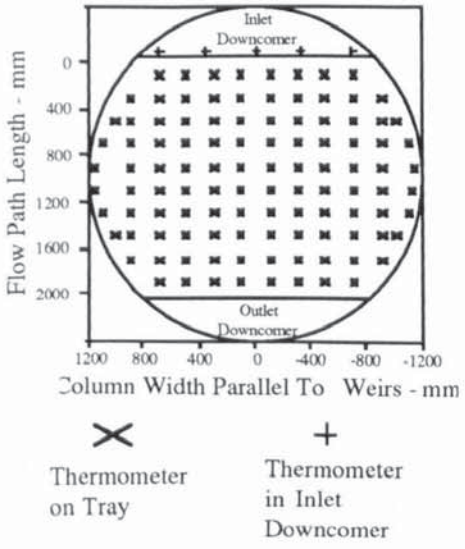

Fig.3.0 Arrangement of platinum resistance thermometers on the perforated test trays

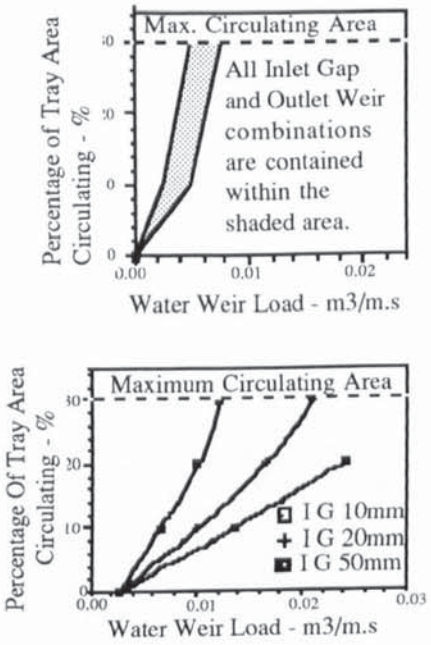

Figs. 4.0 and 5.0 Summary of circulation results for water only on the non perforated tray and the air- water biphase on the1.0mm hole tray respectively (Hine,1990)

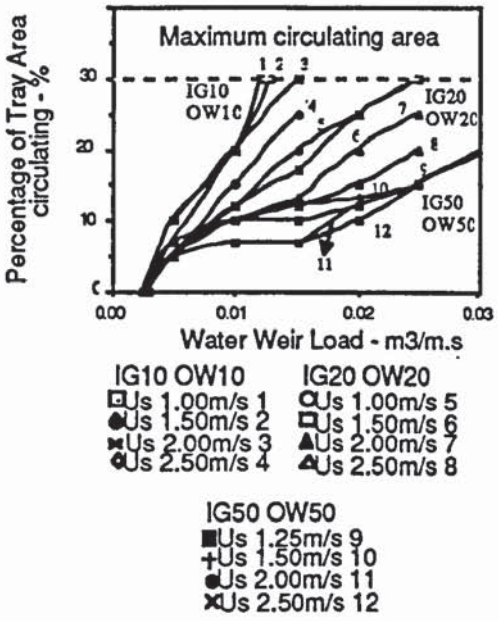

Fig. 6.0 Summary of biphase circulation on 6.35mm hole tray

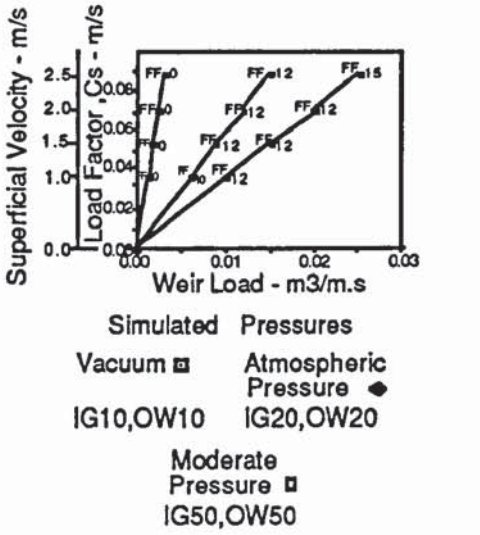

Fig. 7.0 Summary of liquid flow patterns for experiments which simulate distillation

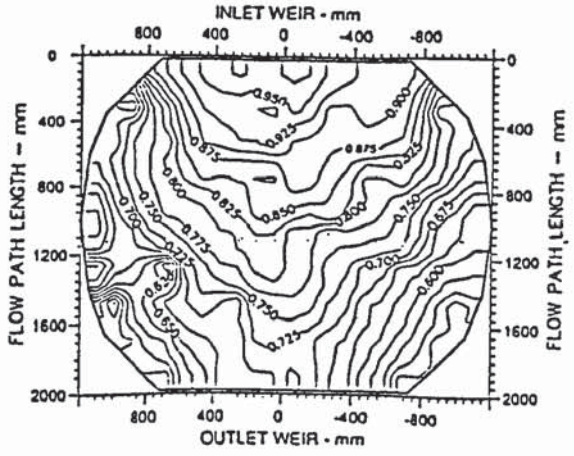

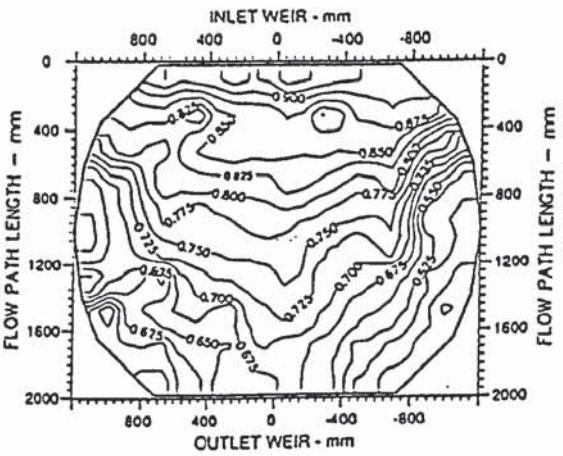

Superficial Velocity	=	1.00 ms^{-1}	Superficial Velocity	=	2.00 ms^{-1}
Weir Load	=	60.0 $cm^3/cm.s$	Weir Load	=	120.0 $cm^3/cm.s$

Inlet Gap / Outlet Weir Height = 20.0mm Hole Diameter = 6.35mm

Fig. 8a Two dimensional isothermal reduced temperature profiles for atmospheric pressure simulation

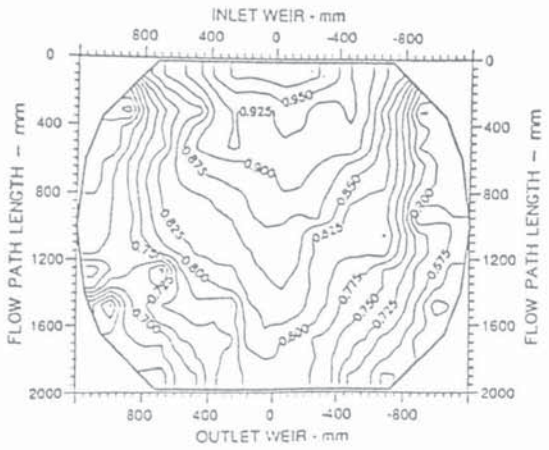

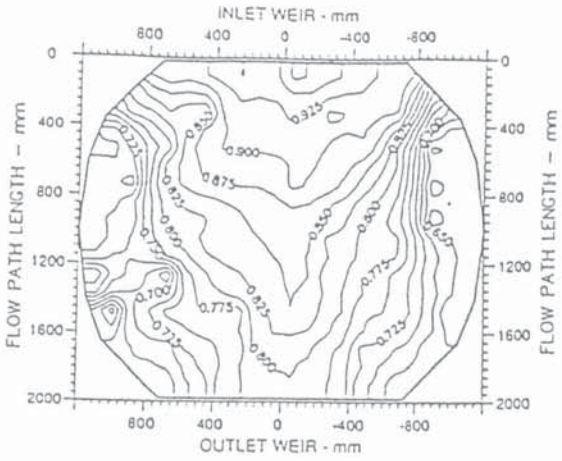

Superficial Velocity = 1.25 ms^{-1}
Weir Load = 100.0 $cm^3/cm.s$

Superficial Velocity = 2.00 ms^{-1}
Weir Load = 200.0 $cm^3/cm.s$

Inlet Gap / Outlet Weir Height = 50.0mm

Hole Diameter = 6.35mm

Fig. 8b Two dimensional isothermal reduced temperature profiles for moderate pressure simulation

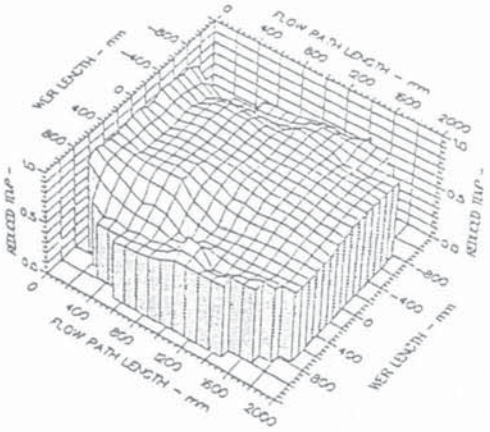

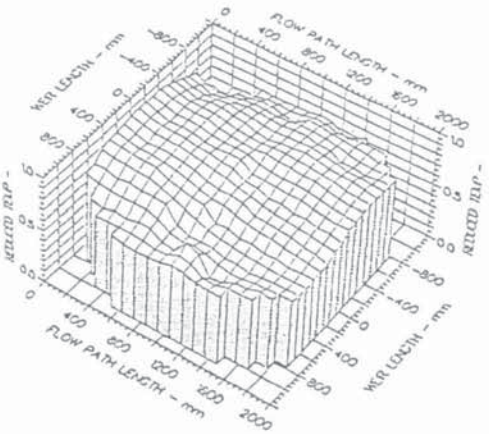

Inlet Gap = 50mm
Outlet Weir = 50mm

Inlet = 10mm
Oulet Weir = 10mm

Superficial Air Velocity = 1.50 m/s
Weir Load = 150.0 $cm^3/cm.s$

Fig. 9a Three dimensional reduced temperature profile diagram showing forward flow with negligible circulation

Fig.9b Three dimensional reduced temperature profile diagram showing circulating flow with 30% circulation

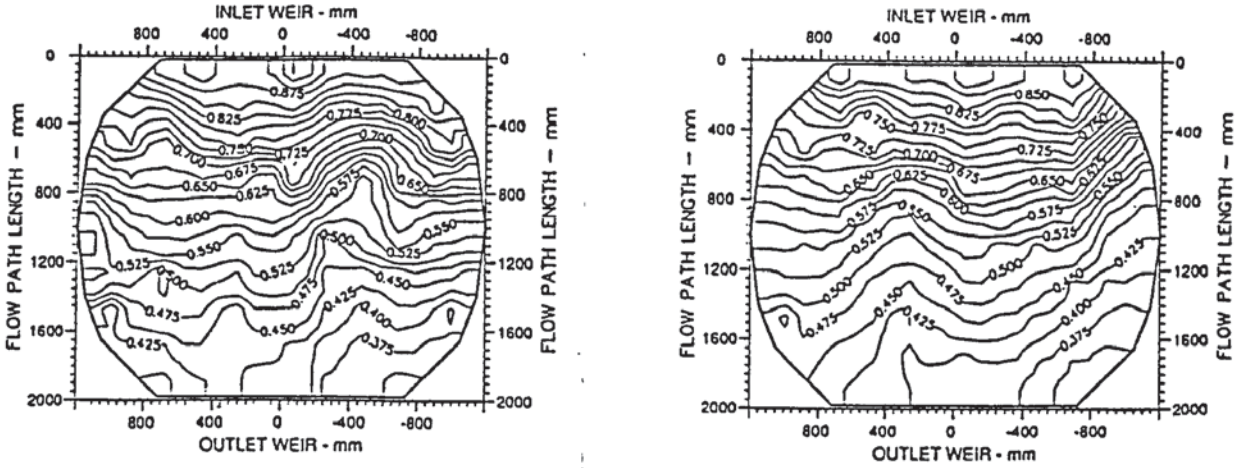

Superficial Velocity	= 1.00	ms^{-1}	Superficial Velocity	= 2.00	ms^{-1}
Weir Load	= 12.5	$cm^3/cm.s$	Weir Load	= 25.0	$cm^3/cm.s$

Inlet Gap / Outlet Weir Height = 10.0mm Hole Diameter = 6.35mm

Fig. 10 Two Dimensional Isothermal Reduced Temperature Profiles for Vacuum simulation

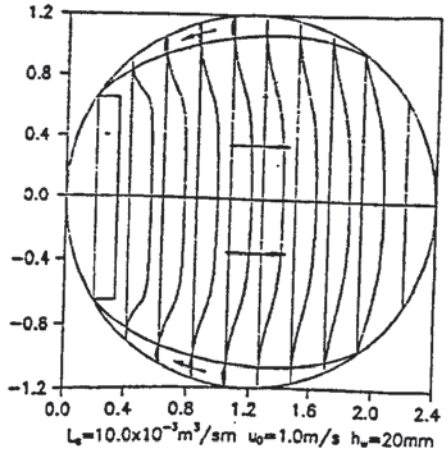

Superficial Velocity	= 1.00	ms^{-1}	Weir Load	= 100.0	$cm^3/cm.s$
Inlet Gap / Outlet Weir Height	= 20.0mm		Hole Diameters	= 1.0 and 6.35mm	

Fig.11 Computed Velocity Distribution showing Reversed Flow in the Segmental Tray Regions.

Design Specification of Test Trays			Study	Hole dia mm	Inlet gap mm	Outlet weir mm	Air velocity ms^{-1}	Weir Load cm3/cm.s
Test Column	Diameter	2.440m	Water only		10	10		25
	Weir Length	1.500m						50
	W/D ratio	0.615			20	20		100
	Width of Support Ring	0.050m						150
					50	50		200
	Flow Path Length	1.925m						250
Trays	Material	Aluminium	Air/ Water	1.00	10	10	1.00	25
	Free Area	10.0%					1.50	50
	Hole Diameter	0, 1, 6.35mm			20	20	2.00	100
	Thickness	1and1.8mm						150
	Edge of Hole	Sharp			50	50		200
	Pitch of Holes	Triangular						250
Areas	Downcomer Area	0.243m^2	Air/ Water	6.35	10	10	1.00	25
	Active Area	4.189m^2					1.25	50
	Total Hole Area	0.419m^2			20	20	1.50	100
Air Distributor Area	Active Area	4.189m^2					2.00	150
	Hole Diameter	1.80mm			50	50	2.50	200
	Thickness	1.80mm						250

Table 1.0 Tray Specifications, configurations and flow rates used in experiments

Simulated Pressure	Vacuum			Atmospheric Pressure			Moderate Pressure		
IG/OW-mm	10,10			20,20			50,50		
Superficial Air Velocity - ms^{-1}	Weir Load cm^3/cms	Efficiency - %		Weir Load cm^3/cms	Efficiency - %		Weir Load cm^3/cms	Efficiency - %	
1.00 (1.25 for M.P sim)	12.5	E_{OG}	36	60.0	E_{OG}	77	100.0	E_{OG}	88
		E_{MV}	68		E_{MV}	99		E_{MV}	103
		E_{MV}/E_{OG}	1.90		E_{MV}/E_{OG}	1.29		E_{MV}/E_{OG}	1.17
1.50	18.5	E_{OG}	41	90.0	E_{OG}	86	150.0	E_{OG}	94
		E_{MV}	75		E_{MV}	115		E_{MV}	106
		E_{MV}/E_{OG}	1.83		E_{MV}/E_{OG}	1.34		E_{MV}/E_{OG}	1.13
2.00	25.0	E_{OG}	45	120.0	E_{OG}	82	200.0	E_{OG}	87
		E_{MV}	80		E_{MV}	105		E_{MV}	95
		E_{MV}/E_{OG}	1.78		E_{MV}/E_{OG}	1.28		E_{MV}/E_{OG}	1.09
2.50	31.0	E_{OG}	47	150.0	E_{OG}	81	250.0	E_{OG}	83
		E_{MV}	93		E_{MV}	100		E_{MV}	92
		E_{MV}/E_{OG}	1.95		E_{MV}/E_{OG}	1.24		E_{MV}/E_{OG}	1.11

Table 2.0 Summary of measured Point and Tray Efficiencies on the 6.35mm tray at three simulated pressures.

Tray Hole Diameter-mm		1.00						6.35					
Superficial Velocity-m /s		1.50						1.50					
		Inlet Gap / Outlet Weir- mm						Inlet Gap / Outlet Weir- mm					
Weir Load $cm^3/cm.s$	Efficiency %	IG 10	OW 10	IG 20	OW 20	IG 50	OW 50	IG 10	OW 10	IG 20	OW 20	IG 50	OW 50
25.0	E_{OG}	48		51		53		38		52		56	
	E_{MV}	90		84		89		60		91		85	
	E_{MV}/E_{OG}	1.86		1.64		1.69		1.59		1.76		1.51	
50.0	E_{OG}	68		76		79		65		65		78	
	E_{MV}	110		121		124		97		92		105	
	E_{MV}/E_{OG}	1.62		1.59		1.57		1.48		1.43		1.34	
100.0	E_{OG}	76		82		88		76		72		87	
	E_{MV}	100		107		119		90		91		105	
	E_{MV}/E_{OG}	1.30		1.31		1.35		1.19		1.26		1.20	
150.0	E_{OG}	78		86		93		77		74		91	
	E_{MV}	86		99		113		78		84		102	
	E_{MV}/E_{OG}	1.09		1.15		1.21		1.01		1.14		1.13	

Table 3.0 Comparison of Point and Tray Efficiencies for 1.00 and 6.35mm hole diameter sieve trays.

APPENDIX 1.0 DESCRIPTION OF THE 2.44M DIAMETER AIR-WATER SIMULATOR

1.1 Overall Test Facility

The industrial scale tray distillation simulator, incorporating a 2.44m diameter column shell, a 150HP air fan and two 0.6MW water heating units is equipped for direct observation of the liquid flow patterns and investigations into the effect of liquid flow patterns on mass transfer by cooling hot water flowing across sieve trays by means of a rising air stream. A full description of the distillation simulator is given by C.J. Hine (1990) and is shown in Figure A1.0

The air-water simulator comprises of three principle units: a 3.05m diameter air distribution shell, the middle 2.44m diameter tray column shell and the top air exhaust ducting system.

1.2 Air Distribution

Unsaturated ambient air, from the air fan, enters the air inlet at the side of the distribution shell tangentially and is forced to swirl downwards inside an annulus between the outer and inner column shell before entering the central flow chamber. The swirling effect is eliminated by a system of radial baffles inside the annulus and central flow chamber. The air is then forced through a distributor plate before passing through the test tray and froth. Initially, using the original air distributor plate, it was found that the air flow pattern, particularly at high air flow rates and low liquid flow rates, forced the recirculation of liquid on the outlet tray section.

Hence, the gas distribution was adjusted, using a 10% free area 1.80mm hole diameter perforated plate (see figure A1.0), until the effect of the gas flow on the liquid flow pattern was shown to be negligible.

1.3 Liquid Distribution

The test tray with support framework and downcomers is housed in the middle column shell. A 1.0m packed bed of 25mm Pall Rings in the inlet downcomer is used to ensure a uniform distribution of liquid before entering the test tray. Rising air enters the test tray

which is supported on a lattice beam framework, situated 850mm above the air distribution plate, and becomes saturated when contacted with the crossflow of liquid. The saturated air, on leaving the froth, enters the exhaust ducting where it is subsequently vented to the atmosphere.

Water from two sump tanks is charged to the inlet downcomer where it is contacted with air across the active bubbling area before being discharged back to the sump tanks via the outlet downcomer and exit pipe. For water cooling experiments, heated water, in a closed loop cycle, from gas-fired tanks and a steam top-up supply preheat the water feed in a water-water double heat exchanger to a temperature of about 45 degC before entering the test tray.

1.4 Observation of Flow Patterns

There is a reducing section at the top of the column, with four windows for direct observations of liquid flow patterns. A video camera, supported on a platform 4.5m above the test tray, permits the flow patterns to be recorded or displayed on a monitor at ground level.

APPENDIX 2.0 TEMPERATURE DATA ACQUISITION AND GRAPHICAL REPRESENTATION OF THE TEMPERATURE PROFILES.

2.1 Temperature Data Collection and Processing

Water cooling involves the cooling of hot water as it crosses the test tray by evaporating a small fraction of water. Since water temperature is analagous to liquid concentration and heat transfer is analagous to mass transfer, the heat transfer process is monitored by measuring the temperature of the water as it is cooled by the air. This is carried out using 108 resistance thermometers spread evenly across the tray.

During water cooling, rapid temperature data acquisition was achieved using a MICROLINK data logging device whereby each resistance thermometer undergoes twenty complete scans every 1.2 seconds and the average temperature value is computed. This data is corrected using calibration data points and if steady state has been achieved and maintained during data sampling, the temperature data and averaged data are recorded onto computer data files.

2.2 Graphical Representation of Temperature Profiles

Temperature values, on conversion into interpolated temperature data, are used to generate two and three dimensional graphs thus making interpretations of the collected data much easier. The software package used to produce these graphs is the UNIRAS suite of plotting routines.

The two dimensional display is a temperature contour map which provides a summary of isotherms showing lines of constant temperature, and gradients indicated by the distance between adjacent isotherms. The isothermal contours show lines of equal temperature increments and include reduced temperature profiles in which the figures shown on each isotherm represent the reduced temperature, T_r, defined as;

$$T_r = \frac{T - T_{wb}}{T_{in} - T_{wb}} \qquad \text{(A2.1)}$$

in which T, T_{in}, and T_{wb} are the measured point water temperature, inlet water temperature, and the wet bulb temperature of the entering air respectively.

The three dimensional display is a surface temperature plot which shows the temperature variation across the tray area at the expense of showing no lines of equal temperature (isotherms). Again this form of diagram is a plot of reduced temperature profiles.

APPENDIX 3.0 METHOD OF CALCULATING POINT AND TRAY EFFICIENCY.

The cooling of hot water by rising air on an operating tray provides an analogy between heat and mass transfer. Therefore a heat balance can be constructed from which point and tray efficiency calculations can be made. (Fortran computer software was developed (Hine, 1990) in order to calculate the Murphree point and tray efficiencies.)

$\overline{T_{in}}$ represents the temperature of hot water entering the test tray whereas $\overline{T_{out}}$ represents the average temperature of water leaving the tray. Air rises upto the tray with a uniform enhalpy, H_1, whilst $\overline{H_2}$ represents the enthalpy of almost saturated air leaving the froth Hence, on the basis of air enthalpy, the Murphree tray efficiency, E_{mv}, may be defined as:

$$E_{MV} = \frac{\overline{H_2} - H_1}{H^*_{Tout} - H_1} \qquad \text{(A3.1)}$$

where H^*_{Tout} is the enthalpy of saturated air in equilibrium with the average temperature of the water leaving the tray. Similarly the Murphree point efficiency in terms of air enthalpy at position i is defined as:

$$E_{OG} = \frac{H_{2i} - H_1}{H^*_{Ti} - H_1} \qquad \text{(A3.2)}$$

where T_i is the local water temperature at position ion the tray, and H^*_{Ti} is the air enthalpy in equilibrium with T_i, H_1, H^*_{Tout}, and H^*_{Ti} were obtained from psychrometric data tables During water cooling, water temperature data acquisition is carried out at fixed air and water flowrates which permits the calculation of the overall saturated air enthalpy leaving the froth, $\overline{H_2}$, from the heat balance:

$$G\cdot(\overline{H_2} - H_1) = L\cdot Cp\,(\overline{T_{in}} - \overline{T_{out}}) \qquad \text{(A3.3)}$$

Substituting $(\overline{H_2} - H_1)$, from equation (A3.3) into (A3.1) will yield the Murphree tray efficiency. The determination of point efficiency is based on the assumption that it is constant at all points on the tray. The calculation is made easier by noting that the arrangement of the resistance thermometers (Figure 3.0) justifies the assumption that each P.R.T. is representative of the same amount of tray area and thus of the same gas flow rate. It then follows that :

$$\overline{H_2} = \frac{1}{n}\sum_{i=1}^{n} H_{2i} \qquad \text{(A3.4)}$$

where n is the number of working resistance thermometers and H_{2i} is the saturated air enthalpy above the froth at each resistance thermometer i.

$$\text{Now} \quad (H_{2i} - H_1) = E_{OG} \cdot (H^*_{Ti} - H_1) \tag{A3.5}$$

$$\text{and} \quad (\overline{H_2} - H_1) = \frac{1}{n}\sum_{i=1}^{n}(H_{2i} - H_1) = \frac{E_{OG}}{n}\sum_{i=1}^{n}(H^*_{Ti} - H_1) \tag{A3.6}$$

$$\text{Thus} \quad E_{OG} = \frac{\overline{H_2} - H_1}{\frac{1}{n}\sum_{i=1}^{n} H^*_{Ti} - H_1} = \frac{\frac{L}{G} C_p(\overline{T_{in}} - \overline{T_{out}})}{(\overline{H^*_{Ti}} - H_1)} \tag{A3.7}$$

APPENDIX 4.0 DESCRIPTION OF A DIRECTIONAL FLOW POINTER

A flow pointer, shown in Figure A2.0, consists of a thin aluminium sheet, with a painted arrow head indicator, loosely hinged on a vertical rod and is supported above the tray deck with a spacer so it can rotate freely and become aligned with the direction of flow. The flow pointers reveal the direction of flow only and not the flow velocity. Nevertheless they provide reliable information about the flow patterns and, in particular, permit the observation of biphase circulation revealed by a number of rotating flow pointers on the tray segments and/or flow pointers pointing backwards towards the inlet downcomer. All the observations were recorded using the overhead video camera.

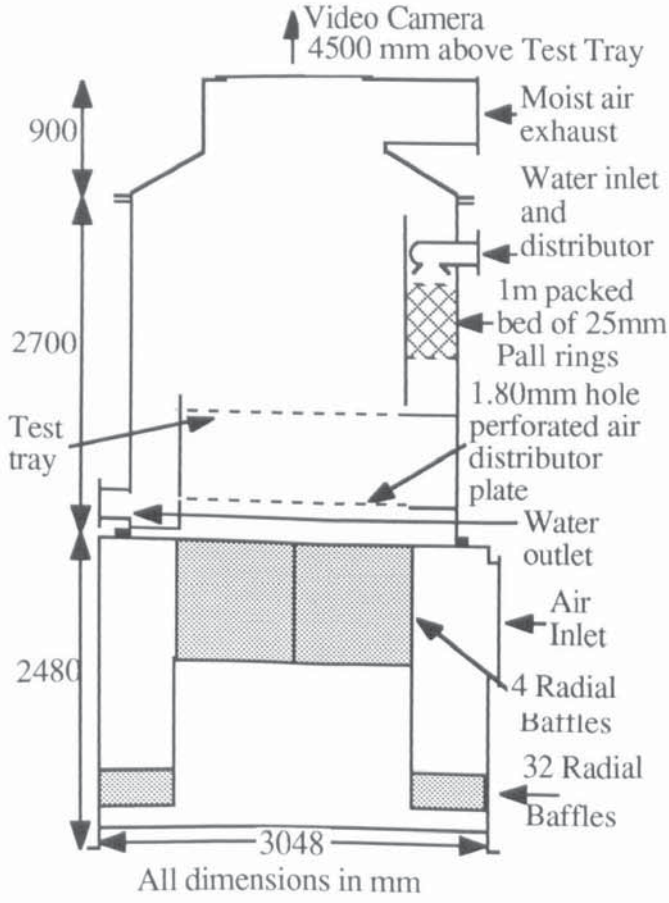

Fig. A1.0 Schematic diagram of the 2.44m diameter distillation simulator

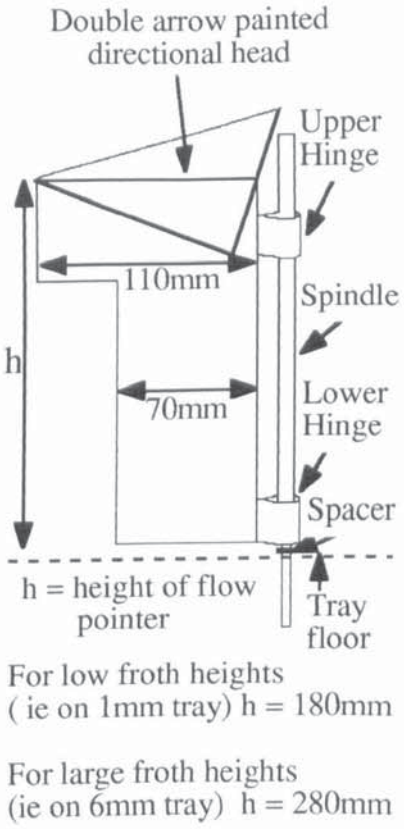

Fig.A2.0 Schematic diagram of a directional flow pointer